Macroseismic Characterization through Earthquake Environmental Effects: Dataset update and Grid-Based applications of the ESI-07 scale

Eliana Medea Muccignato Rodio

Università degli Studi dell' Insubria

- 2025 -

PhD Course in Chemical and Environmental Sciences

XXXVI Cycle

Università degli Studi dell' Insubria
Department of Science and High Technology

PhD Course in Chemical and Environmental Sciences XXXVI Cycle
Curriculum Environmental Sciences

PhD Thesis

Macroseismic Characterization through Earthquake Environmental Effects: Dataset update and Grid-Based applications of the ESI-07 scale

Supervisor Dra. Maria Francesca Ferrario
Candidate Eliana Medea Muccignato Rodio

accepted on the recommendation of
Dr. Christoph Grützner
Dr. Luca Guerrieri

Academic Year 2024/2025

Gnōthi sautón

TABLE OF CONTENT

LIST OF FIGURES

CHAPTER 1

CHAPTER 2

CHAPTER 4

CHAPTER 5

CHAPTER 6

LIST OF TABLES

CHAPTER 3

CHAPTER 4

CHAPTER 5

CHAPTER 6

INTRODUCTION

This research project is conducted under the GEOSCIENCES-IR project (geosciences-ir.it), funded by the PNRR (National Recovery and Resilience Plan). The program aims to establish a research infrastructure for the Italian Network of Geological Surveys (RISG), fostering collaboration between ISPRA, the Geological Survey of Italy, and Regional Geological Surveys. The project addresses several critical challenges, such as outdated geological knowledge, fragmentation of expertise, and the shortage of technical staff. Within this framework, my PhD activity is included in WP3 "Landslides and sinkholes", which focuses on applied research, new technologies, and knowledge transfer to support decision-making for risk reduction.

Earthquake Environmental Effects (EEEs) are physical manifestations of seismic activity that can leave permanent and measurable imprints on the landscape (Serva et al., 2015a; 2015b). They arise from the interaction between source processes (i.e., slip-induced vibrations and finite-fault deformation), seismic wave propagation, and local geological conditions (Michetti et al., 2004; Michetti et al., 2007). Their recognition is fundamental for hazard assessment and risk mitigation, as they document the environmental footprint of earthquakes, often preceding or accompanying structural damage and providing long-term evidence of seismic processes (Boulton et al., 2025; Naik et al., 2023; Ferrario, 2019; Comerci et al., 2015a. The Environmental Seismic Intensity scale (ESI-07), based exclusively on earthquake-induced environmental effects (EEEs) (Michetti et al., 2004; Michetti et al., 2007), was designed to offer an environment-based and reproducible framework for intensity assessment. Over the past two decades, the ESI-07 scale has gained increasing global recognition, supporting hundreds of applications worldwide (Ferrario et al., 2022a; 2022b; Vittori et al., 2021; Yang et al., 2023), and representing a bridge between geological evidence, engineering seismology, and risk management.

Within this framework, the present PhD dissertation pursues two complementary objectives:
a) to compile harmonized EEEs and ESI-07 datasets at multiple spatial scales; and
b) to develop and test a grid-based methodology capable of producing reproducible and agile ESI-07 intensity estimates from large and heterogeneous datasets.

To achieve the first goal, three datasets are created: a) a global ESI-07 events catalogue, developed by expanding the work of Ferrario et al. (2022b); b) a dataset of earthquake-induced landslides (EQUILs) compiled for integration into the national IFFI catalogue; and c) a dataset of 44 535 EEEs documenting the effects of the Mw 7.5 Noto Peninsula earthquake of 1 January 2024.

To achieve the second goal, a grid-based methodology is firstly applied to a set of 40 EQUILs inventories derived from US Geological Survey (USGS) and authors' datasets. Subsequently, the same methodology is extended to all categories of EEEs included in the ESI-07 scale and tested on the Mw 7.5 Noto Peninsula earthquake of 1 January 2024.

The research starts building upon the baseline dataset compiled by Ferrario et al. (2022b), expanding and harmonizing it into a comprehensive global catalogue of ESI-07 applications. The updated dataset

documents the temporal and geographical distribution of ESI-07 events, the approaches adopted for intensity evaluation, and the variety of ESI-07 outputs derived, ranging from descriptive EEEs inventories to advanced analytical and cartographic products such as ESI-07 shakemaps and ESI-07 attenuation maps. The analysis highlights a continuous methodological evolution in the use of the ESI-07 scale and points to the persistence of temporal and regional gaps, underlining the need for systematic documentation and broader application of ESI-07 methodologies worldwide.

At the national scale, the research focuses on EQUILs. Within the framework of the GEOSCIENCES-IR WP3 "Landslides and Sinkholes", a harmonized dataset of EQUILs is compiled to contribute to the enhancement of the national *Inventario dei Fenomeni Franosi in Italia* (IFFI) (Di Paola et al., 2024; ISPRA, 2025). The catalogue integrates multiple independent archives, including the Italian Catalogue of Earthquake-Induced Ground Failures (CEDIT) (Martino et al., 2020), CFTI (Zei et al., 2024), the Earthquake-induced Environmental Effects Catalogue (EEE), historical maps (Govi and Sorzana, 1977), and works of the University of Insubria (Pizza et al., 2023; Paganini, 2023; Lazzati, 2020; Camarda, 2021). The dataset, fully compatible with the IFFI structure and aligned with FAIR principles, provides a comprehensive national overview of EQUILs. The analysis conducted investigates the spatial and temporal distribution of data, as well as the potential application of ESI-07 volumetric thresholds to assess their suitability for intensity estimation.

Confirming the usefulness of the EQUILs inventories for the estimation of the intensity, a grid-based workflow, firstly applied in Ferrario (2022), is refined and applied to derive ESI-07 intensities, Landslide Number Density (LND) and Landslide Area Percentage (LAP) from 40 inventories from 33 global earthquakes, mainly derived from the USGS global landslide repository (Schmitt et al., 2017; Tanyas et al., 2017) and from previous ESI-07 studies (Ferrario, 2022a; Ferrario et al., 2024). The analysis investigates the relationships between landslide metrics and ESI-07 intensities, examining the fitting of different predictors and the factors influencing the variability of results such as kinematics, magnitude and the choice of inventory. Cross-comparisons with independent ESI-07 datasets and published ESI-07 isoseismals are conducted to evaluate the robustness and transferability of the approach across diverse tectonic and climatic environments. The study provides the methodological basis for the subsequent application of the grid framework to other categories of EEEs and its validation on recent large-scale seismic events.

To validate and extend the approach, the ESI-07 grid methodology is applied to the Mw 7.5 Noto Peninsula earthquake (Japan, 1 January 2024). A comprehensive multi-source dataset is compiled, covering the affected area and including multiple categories of EEEs derived from different sources, such as aerial imagery, remote sensing data, field observations, and press and social-media sources.
The grid-based workflow is used to estimate ESI-07 intensities at different spatial resolutions, producing two different resolution ESI-07 grid maps that delineate clear patterns of variation across the peninsula. Coseismic landslides mapped after the Noto peninsula earthquakes are used to test the predictive power of the equations developed by Muccignato & Ferrario (2025), which provide an ESI-07 estimate based on LND and LAP values. The accuracy of the resulting grid-based intensity field is also assessed through a comparison

with ESI-07 isoseismal compiled for the Noto event, showing a coherent spatial correspondence between the two representations.

The outcomes of this dissertation confirm that EEEs can serve as a robust, reproducible, and scalable foundation for macroseismic characterization, providing measurable parameters directly linked to earthquake magnitude and impact. The study consolidates the role of EEEs as quantitative indicators, demonstrating their capacity to capture objectively and with consistency the environmental footprint of seismic events. In this context, the compilation of harmonized and interoperable resources represents a significant step toward the creation of FAIR-compliant datasets that support both scientific investigation and operational implementation. Building upon these foundations, the proposed ESI-07 grid-based workflow introduces a tool that allows for an agile and reproducible assignment of ESI-07 intensities, facilitates the integration of heterogeneous data sources, and produces accurate outputs, such as the derivation of empirical regression for LND-LAP-ESI and ESI-07 grid intensity maps, which enable systematic comparison across events and spatial contexts.

Future developments emerging from this research point toward several complementary directions. Firstly, the harmonization of inventories and the systematic re-evaluation of historical datasets represent a fundamental step to enhance the spatial and temporal completeness of macroseismic analyses and for the application of ESI-07 Intensity scale. Building on this foundation, the ESI-07 grid methodology provides a pathway for extending quantitative applications to other case studies, thus expanding the descriptive and analytical potential of the ESI-07 scale. Another perspective involves the development of participatory reporting platforms, in which citizen-contributed observations can be integrated with standard data sources (e.g., reconnaissance field surveys, remote sensing) under controlled validation procedures, improving the completeness, accessibility, and timeliness of post-event information. Moreover, the comparison of grid-based ESI-07 outputs with seismological and engineering datasets offers new opportunities for cross-validation with shake maps, ground-motion models, and attenuation relationships, bridging geological evidence with quantitative seismic modelling. From an operational standpoint, the workflow demonstrates strong potential for rapid post-event assessment, as semi-automatic ESI-07 grid maps can complement conventional shakemaps by providing immediate, spatially explicit visualizations of environmental impacts and supporting both emergency response and field reconnaissance activities.

In conclusion, this work highlights how the natural environment can serve as both a witness and a measure of seismic activity and macroseismic analysis. By interpreting the landscape as a physical record of earthquake processes, the ESI-07 scale provides a consistent and reproducible framework that enriches conventional approaches and deepens our understanding of seismic intensity. Ultimately, the study reaffirms the importance of viewing environmental effects not as secondary consequences, but as fundamental expressions of earthquake impact, capable of linking past and present events through a measurable and enduring imprint on the Earth's surface.

THESIS STRUCTURE

The thesis is organized into six main chapters:

- Chapter 1 – Introduction and Theoretical Framework: Contextualization of EEEs and the ESI-07 scale, evolution of macroseismic approaches, and motivation for the study.
- Chapter 2 – Global ESI-07 Catalogue: Compilation and analysis of 218 ESI-07 events, trends in data sources, outputs, and applications.
- Chapter 3 – EQUILs in Italy: Harmonization of the IFFI-compatible EQUILs dataset (3,483 records), spatial patterns and ESI-07 intensity estimation.
- Chapter 4 – Development of a Grid-Based Methodology: Definition of LND and LAP parameters, empirical regressions with ESI-07, and uncertainty analysis over 40 EQUILs inventories.
- Chapter 5 – The Mw 7.5 Noto 2024 Case Study: Application of the grid workflow to 44,491 EEEs, spatial validation, and integration of participatory data for the 1 January 2024 Mw 7.5 Noto event.
- Chapter 6 – Discussion and Conclusions: Comparative evaluation of traditional vs grid-based ESI approaches, role of heterogeneous and social data, epistemic uncertainties, and future research perspectives.

CHAPTER 1

THE ESI-07 INTENSITY SCALE

INTRODUCTION

Environmental effects are commonly produced by moderate to large earthquakes and can leave permanent imprints in the physical environment (Serva et al., 2015a; Serva et al., 2015b). These phenomena are generated from the combined action of event source processes (i.e., slip-induced vibrations and finite fault deformation), the propagation of seismic waves, and different local site conditions (Michetti et al., 2004; Michetti et al., 2007). Due to their widespread occurrence and magnitude, environmental effects can generate significant damage at both regional and local scales, affecting infrastructure and human settlement (Boulton et al., 2025; Comerci et al., 2015a; Ferrario, 2019; Naik et al., 2023; Velázquez-Bucio et al., 2021), making their recognition and evaluation essential for reliable hazard and risk assessment (Serva, 2019; Serva et al., 2015b). Environmental effects are documented across different timescales: they are recorded in instrumental and modern events, described in historical sources, and preserved in geological and stratigraphic records. Seeing this, the landscape becomes a readable archive of seismic processes (Michetti et al., 2004).

Seismic intensity refers to the characterization of earthquake effects on people, built structures, and natural environment, and is typically expressed using twelve-degree macroseismic scales (Musson and Cecić 2012). Macroseismic intensity studies allow for the reconstruction of the spatial distribution of shaking and direct effects on physical environment, providing constraints on the identification of the seismogenic source and enabling the construction of isoseismal fields (Michetti et al., 2004; Michetti et al., 2007). The use of traditional intensity scales (e.g., MCS scale, MSK scale, and MM scale) based solely or primarily on damage to people and man-made structures (Michetti et al., 2015), may yield to results biased by socioeconomic conditions, rather than reflecting the intrinsic characteristics of the event itself. This limitation becomes particularly evident in rural or sparsely populated areas, or in societies characterized by non-permanent architecture or nomadic populations, where structural damage is absent, limited or non-diagnostic (Michetti et al., 2004; Michetti et al., 2007). Environmental effects have historically been included as diagnostic indicators in most classical macroseismic scales (e.g., MCS, MM, and MSK) reflecting the original formulation of seismic intensity proposed in the early XX century (Mercalli G., 1902). The exclusion of such effects in more recent scales, and particularly in the EMS-98, represents a methodological break with this tradition, limiting the comparability between historical and modern intensity estimates. In this context, environmental effects, due to their permanent, observable, and scalable nature, are crucial for assessing earthquake intensity, especially at higher degrees (XI–XII), where structural damage typically saturates and loses resolution (Michetti et al., 2004; Michetti et al., 2007).

The Environmental Seismic Intensity scale (ESI-07) is a scale based solely on the categorization, measurement and mapping of earthquake-induced environmental effects (EEEs) (Michetti et al., 2004; Michetti et al., 2007; Ferrario et al., 2022b). Its adoption improves the capacity to evaluate the size of seismic events based on objective evidence of environmental impacts, and thereby providing valuable data for seismic hazard assessments, and support planning strategies within broader disaster risk management framework (Michetti et al., 2004; Michetti et al., 2007).

1.1 DEVELOPMENT OF THE ESI-07 SCALE

Environmental effects have historically been included in traditional macroseismic scales such as the Mercalli–Cancani–Sieberg (MCS) scale (Sieberg, 1930), the Medvedev–Sponheuer–Karnik (MSK) scale (Medvedev et al., 1964), the Modified Mercalli scale (Wood and Neumann, 1931; Dowrick, 1996; Hancox et al., 2002), and the Japanese JMA scale (Koto, 2000). Despite that, with the advent of instrumental seismology, intensity studies increasingly focused on damage to built structures, and environmental effects became underrepresented. To address this gap, a multidisciplinary working group was established within the INQUA Subcommission on Paleoseismicity and the Italian Agency for Environmental Protection (APAT, now ISPRA), in order to systematize earthquake environmental effects and define reproducible diagnostic criteria for intensity assessment (Michetti et al., 2004; 2007).

Initial efforts included the review and comparison of the MCS, MSK, and MM scales (Serva L., 1994; Esposito et al., 1996) and the formulation of a preliminary version (i.e., INQUA scale). The first formal version was presented at the XVI INQUA Congress in 2003 (Reno, USA) and adopted provisionally. Following international testing, the Environmental Seismic Intensity scale (i.e., ESI-07 Scale) was officially released and adopted in 2007 (Michetti et al., 2004; 2007).

1.2 ESI-07 INTENSITY SCALE: THE CHARACTERISTICS

1.2.1 ESI-07 SCALE INTENSITY DEGREES AND TYPES OF EEES

The ESI-07 scale is characterized by twelve distinct degrees, which span from I to XII. Each of them is associated with specific diagnostic EEEs, with increasing severity and spatial extent (Fig.1.1) (Serva L., 2019; Michetti et al., 2015; Michetti et al., 2004; Michetti et al., 2007). The scale can be used autonomously, particularly in contexts where effects on human and built structures are absent or saturated, or associated with traditional scales (e.g., MCS, MSK, MM, EMS), allowing a more comprehensive intensity assessment (Serva L., 2019; Michetti et al., 2015).

The ESI-07 scale defines two distinct categories of EEEs: primary effects, which represent the direct surface expression of the seismogenic fault, and secondary effects, which are induced by seismic shaking. EEEs are controlled by hypocentral depth, magnitude, frequency of shaking, duration and level of ground motion (i.e., velocity, displacement and acceleration) and modulated by local geological and geomorphological context, which together represent the environmental sensitivity (Michetti et al., 2004; Michetti et al., 2007). EEEs can be permanent (e.g., surface faulting, tectonic uplift and subsidence) or transient (e.g., hydrological anomalies, tree shaking) (Michetti et al., 2007; Serva, 2019). Near-field damage associated with EEEs is dependent on high-frequency shaking, while far-field effects often are the result of long-period surface waves (Michetti et al., 2004; Michetti et al., 2007). EEEs are characterized by diagnostic thresholds and saturation levels, which are empirically defined across the twelve degrees of the scale (Michetti et al., 2004; Michetti et

al., 2007). ESI-07 guidelines and characterization of different EEEs are reported in Appendix for a deeper consultation (App.1.1).

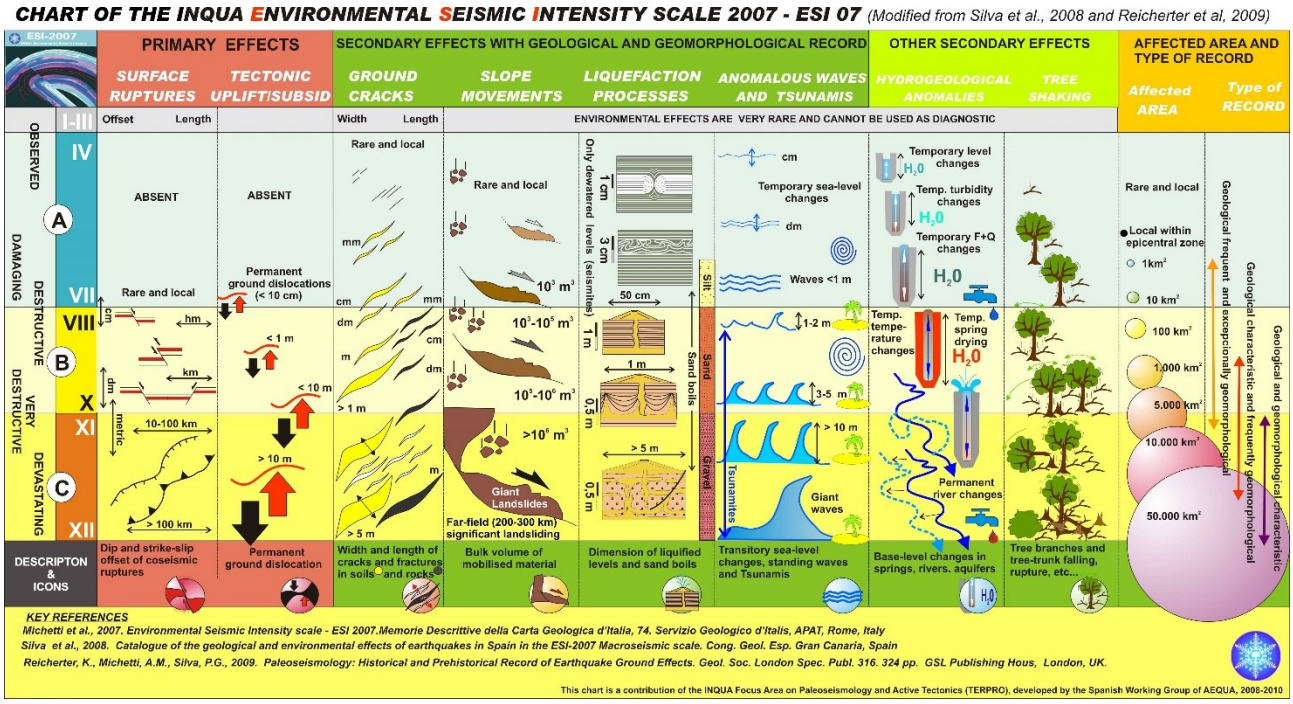

Figure 4.1 – Chart of the ESI-07 Intensity scale. EEEs intensities are visually explained, with quantitative characteristics and associated grades of intensity. Available at http://tierra.rediris.es/aequa/paleoinqua.html.

Primary effects

Primary EEEs are directly related to the surface rupture and permanent deformation caused by the earthquake source. Their occurrence reflects the size and energy of the event and, unlike damage to buildings or secondary effects, they do not suffer from saturation. These effects typically become diagnostic from intensity degree VIII, except in case of very shallow earthquakes in volcanic areas (Michetti et al., 2007).

Surface faulting and tectonic deformation

This category includes surface ruptures and tectonic uplift and subsidence. Their size is described through parameters such as Total Surface Rupture Length (SRL) and Maximum Displacement (MD), which may be correlated with earthquake magnitude. These effects provide critical input for estimating epicentral intensity (I_0) and are among the most reliable indicators, especially for higher intensity degrees (Michetti et al., 2004; Michetti et al., 2007).

Secondary effects

Secondary environmental effects are induced by ground shaking and are strongly influenced by the physical, geological and geomorphological properties of the affected area. Their occurrence and spatial distribution depend on factors such as topography, geology and hydrology. Some of these effects can appear even at

low intensity degrees but they acquire diagnostic value only within specific ranges different between the categories. The ESI-07 scale groups secondary effects into eight main categories (Michetti et al., 2007).

Ground cracks

Ground fractures unrelated to surface faulting are classified by their length and width. They may range from superficial hairline cracks to more substantial ruptures, extending hundreds of meters. The category also includes cracks in paved roads and pressure undulation. Ground cracks typically appear at intensity IV and tend to saturate at intensity IX (Michetti et al., 2015; Michetti et al., 2004; Michetti et al., 2007).

Slope movements

This class includes rockfalls, landslides, ruptures, slides and falls in riverbanks, submarine landslides and dams. Slope movements are considered diagnostic from intensity IV and saturate from intensity X (Michetti et al., 2015; Michetti et al., 2004; Michetti et al., 2007).

Liquefaction phenomena

Liquefaction includes manifestations such as sand boils and sand volcanoes, water-sand fountains, liquefaction, lateral spreading, fissuring and subsidence. These effects are typically associated with saturated loose sediments, but also can affect, if stronger, competent sediments. They are considered diagnostic in the range from intensity V to XII (Michetti et al., 2015; Michetti et al., 2004; Michetti et al., 2007).

Anomalous waves and tsunamis

These effects encompass seiches in closed basins, sudden swing or overflow from pools or reservoirs, and tsunami waves, accompanied by erosion and dumping of waste and eradication and movements of vegetation. These effects may initiate at intensity IV but are most relevant for intensity degrees IX to XII (Michetti et al., 2015; Michetti et al., 2004; Michetti et al., 2007).

Hydrological anomalies

This category includes changes in the discharge of watercourse, as well as variations in water levels, flow, temperature, turbidity, color, or chemical-physical properties. They are considered diagnostically relevant from intensity IV to XII (Michetti et al., 2015; Michetti et al., 2004; Michetti et al., 2007).

Tree shaking

This transient class involves the visible shaking, breaking and falling of trees due to ground motion. Tree shaking is observable from intensity IV to XII and can serve as a key indicator in forested areas or urban parks (Michetti et al., 2015; Michetti et al., 2004; Michetti et al., 2007; Dengler and McPherson, 1993).

Dust clouds

Dust clouds are transient atmospheric phenomena produced by ground shaking, typically in arid or semi-arid regions. They are associated with slope movements or surface collapses and are considered diagnostic from intensity VIII onward (Michetti et al., 2015; Michetti et al., 2004; Michetti et al., 2007).

Jumping stones

This effect involves the upward or lateral displacement of rocks of different dimensions and boulders due to seismic acceleration exceeding gravitational force. Jumping stones are observable from intensity VIII to XII and indicate very high to extreme ground motion conditions (Michetti et al., 2015; Michetti et al., 2004; Michetti et al., 2007).

1.2.2 EVALUATION CRITERIA AND APPLICATIONS OF THE ESI-07 SCALE

Macroseismic intensity assessment using the ESI-07 scale relies on two key parameters, which serve as independent tools for estimating the epicentral intensity (I_0), which is the intensity of shaking in correspondence to epicenter. They are defined as: a) size of primary faulting, quantified through Total Surface Rupture Length (SRL) and/or Maximum Displacement (MD), and b) total area affected by secondary EEEs. In cases where surface faulting parameters lie at the threshold between two different ESI-07 degrees, the ESI-07 assignment is guided by the overall distribution and characteristics of secondary EEEs. To avoid overestimation, isolated EEEs in the far field should be excluded (Michetti et al., 2015; Serva et al., 2015b).

Local intensity is defined by the identification of individual sites, each corresponding to a specific EEE observation: if different intensities are found in the same area (e.g. town), and the scale of representation does not allow the display of all ESI-07 values, the highest intensity grade could be retained, if the focus is on worst-case scenarios (Serva et al., 2015b); conversely, other choices may be applied (e.g., range of intensities). The aggregation of multiple sites then defines a Locality, which is defined by a single ESI-07 value, provided that the variability between different sites is not excessive. The spatial scale of a Locality is context-dependent: it must be sufficiently large to contain a representative set of effects, and small enough to refrain from the overlapping of areas with different seismic response (Serva et al., 2015b; Michetti et al., 2015).

If a systematic field survey is performed, it is recommended to perform a regular grid approach, dividing the territory into defined cells, with a cell size which is dependent on the scale of the investigation (Michetti et al., 2007). Each cell must be assigned with a local intensity based on observed EEEs, to enable the construction of an isoseismal map. Careful considerations must be taken into account to avoid incongruence when comparing or integrating results with standard macroseismic scales (Michetti et al., 2007).

Since its publication in 2007, the ESI-07 intensity scale has been used for the characterization of more than 150 historical and recent earthquakes, spanning from 300 AD to 2020 (e.g., Dretaki et al., 2022; Caccavale et al., 2019; Colón et al., 2019; Huayong et al., 2019; Ahmad et al., 2014; Fountoulis et al., 2013; Berzhinskii et al., 2010). Recently, Ferrario et al., (2022) has produced empirical regressions linking ESI I_0 values to moment magnitude and the total area affected by secondary EEEs, in order to support the integration of the ESI-07 intensity scale into contemporary seismic hazard assessment frameworks. A complete overview of the application of the ESI-07 scale is described in chapter 2.

1.3 ESI-07 INTENSITY SCALE APPLICATIONS: THE EEE CATALOGUE

Within the GEOSCIENCES-IR project, one of the specific objectives of WP4 is to provide interoperable and FAIR-compliant data and tools. In this context, the thesis includes the analysis and partial restructuring of the Earthquake Environmental Effects (EEE) Catalogue, a database developed to collect and systematize EEEs from earthquakes worldwide. The present section introduces the structure of the original version 1.0 of the EEE catalogue, as it constitutes an extensive application of the ESI-07 scale and a source of data for the analyses performed during the doctoral research, and in particular: a) source of data for compiling an updated global dataset of ESI-07 events (Chapter 2), and; b) source of data for extracting and validating earthquake-induced landslides (EQUILs), used to support the implementation of the Italian Landslide Inventory (IFFI) (Chapter 3). A consequent substantial effort is being conducted by ISPRA and WP4 in order to construct a dataset compliant with INSPIRE standards, by developing the data container in the form of a geopackage with standardized dictionaries and metadata and with the addition of new seismic events. A new version of the catalogue (version 2.0) is being developed and will be uploaded to address the limitations of the previous structure and improve user accessibility.

1.3.1 ORIGIN OF THE EEE CATALOGUE

The Earthquake Environmental Effects (EEE) Catalogue (EEE - Earthquake Environmental Effects Catalogue) is a catalogue designed to collect, standardize, and archive EEEs from recent, historical, and paleoevents. The catalogue aims to provide a coherent and accessible dataset to support the application and refinement of the ESI-07 intensity scale and for SHA (Guerrieri et al., 2015a, 2015b; Guerrieri L., 2011; Audemard et al., 2015). In this regards after the Mw 9.0 2011 Tohoku event (Mori et al., 2011a, 2011b) the IAEA (International Atomic Energy Agency) has explicitly recommended the inclusion of earthquake ground effects and paleoseismological data in seismic hazard assessments, especially in areas hosting critical infrastructure such as nuclear implants and facilities, reinforcing the relevance of this catalogue (Serva L., 2019).

The initiative originated within the project #0811 of the International Union for Quaternary Research (INQUA), with the technical support and development of the web infrastructure led by ISPRA (Geological Survey of Italy). The first online version of the catalogue, containing information on approximately 20 events, was presented at the XVIII INQUA Congress in Bern (2011) (Serva L., 2019).

1.3.2 EEE CATALOGUE STRUCTURE AND CHARACTERISTICS

The EEE Catalogue is defined by a multiscale approach, based on a relational database structure, which is organized into three hierarchical levels of detail: Earthquake, Locality, and Site, each corresponding to a specific data table with distinct fields (Guerrieri et al., 2015a, 2015b, 2011, 2009b, 2007). The Earthquake level contains general information about the seismic event (i.e., date, magnitude, epicentral area, and references). The Locality level describes the characteristic of the locality where EEEs have been documented

and includes local intensity assessments from either the ESI-07 or other traditional scales. The Site level contains detailed descriptions of individual EEEs, (i.e., typology, geometry, dimensions, site-specific information and multimedia documentation). All the cited tables are linked by the Earthquake code, which serves as a primary key. The quality and resolution of the data and the compilation of each hierarchical level are expected to vary significantly with the age of the earthquake (Guerrieri et al., 2015a).

The EEE Catalogue is accessible online through the ISPRA platform and is defined by a Google Earth-based public webmap interface for visualization and exploration (Fig. 1.2). Different buttons and tools are also present for interaction and deeper consultation. Events, localities and EEEs are represented by a definite symbology. Further information is displayed by a pop-up window if clicked.

***Figure 1.2 - EEE Catalogue web interface**. The web map allows visualization and consultation of the EEE catalogue database, displaying events, localities and sites information. Page extracted from EEE - Earthquake Environmental Effects Catalogue*

EEE catalogue can be updated with a new event by authorized compilers. To contribute, a new user must register on the ISPRA platform. The online interface allows compilers to interact with structured forms for each of the three data levels. Once data entry is completed, a validation request must be submitted. A scientific committee then reviews the information for both technical standardization and scientific accuracy before publication (Guerrieri et al., 2015b).

The version 1.0 of the EEE catalogue includes information of 202 events globally, of which 51 are located in Italy. A total of 4850 EEEs are collected, distributed in 4605 different sites.

CONCLUSION

The ESI-07 Intensity scale represents a robust tool for the evaluation of macroseismic intensity, used in conjunction to traditional macroseismic scales. Based exclusively on EEEs, the ESI-07 intensity scale captures a broad spectrum of geological, hydrological and physical phenomena. The classification and evaluation of the EEEs is structured across twelve intensity degrees, spanning from I to XII in accordance with traditional intensity scales. In particular, the ESI-07 scale proves especially effective when used with high-intensity events (ESI-07 XI–XII), where buildings or human-damage indicators saturate, in contexts where human exposure is limited or absent, for historical events and for paleoseismic reconstructions. The definition of epicentral and local intensity is based on measurable parameters like surface rupture length (SRL), maximum displacement (MD), and total area of secondary EEEs. The utility of the ESI-07 intensity scale has already been proved via the integration of extensive empirical datasets, threshold studies, and catalogues, which further strengthens its methodological foundation. Among the product available, the EEE Catalogue represents a structured database for the collection and consultation of EEEs worldwide. Designed to support the application of the ESI-07 intensity scale, version 1.0 offers a multi-level data structure that, despite limitations in usability and accessibility, has been employed as the foundational baseline for this study and for GEOSCIENCES-IR update products. As increasing attention is being paid to effects of earthquakes in the physical environment, the ESI-07 Intensity Scale emerges as a valuable tool for the comprehensive characterization of seismic events. Its exclusive focus on EEEs, and its proven applicability across diverse geographical and temporal contexts, suggest the potential for future applications aimed at re-evaluating past earthquakes and characterizing new events on a global scale. In this perspective, the development of standardized workflows and new practical methodologies for the implementation of the ESI-07 scale can significantly enhance its usability in both scientific and operational settings.

CHAPTER 2

ESI-07 APPLICATIONS AND TRENDS: UPDATING THE GLOBAL CATALOGUE

INTRODUCTION

The Environmental Seismic Intensity scale (ESI-07) has become an increasingly recognized tool for macroseismic characterization, providing robust and reproducible intensity indicators (Michetti et al., 2004; Michetti et al., 2007; Ferrario et al., 2022a; 2022b). Globally, an extensive number of earthquakes have been studied through the ESI-07 framework (Yang et al., 2023; Vittori et al., 2021; Tovar and Sánchez, 2020; Boulton et al., 2025; Mäntyniemi et al., 2021; Guerrieri et al., 2015; Audemard et al., 2015). A standardized catalogue of 157 seismic events analyzed through the ESI-07 was compiled by Ferrario et al. (2022).

Building on these foundations, the present work expands and updates the dataset, producing a harmonized catalogue up to 2025. The present study is conducted with two main objective: a) to provide a present-time overview of ESI-07 applications, and; b) to expand and update the previous ESI-07 events dataset in order to provide a harmonized catalogue up to 2025. A systematic bibliographic review, critical case study analysis, and harmonization of sources are performed, resulting in a final dataset of 218 seismic events distributed across 46 countries and spanning from 426 BC to 2024. The dataset highlights a marked spatial and temporal heterogeneity, with Southern Europe and the instrumental period events dominating. Three categories of data sources are identified: bibliography data, reconnaissance field surveys data, and remote sensing data. 10 different categories of ESI-07 outputs are extracted, from EEEs characterization and ESI-07 assignation to older events, to advanced products such as ESI-07 isoseismals, ESI-07 attenuation maps, and, more recently, ESI-07grid-based analyses and ESI-07 shakemaps. Furthermore, a focus is given to the 2022 Mw 7.7 Michoacán earthquake, which is included in the dataset, as a representative case study. Thanks to its diversified dataset, this event not only confirmed the potential of ESI-07 application for producing diversified outputs but also provided the first opportunity within this PhD research to explore grid-based approaches. While the concept of applying grid methodologies to EEEs has already been discussed in the literature (e.g., Ota et al., 2009; Ferrario M.F., 2022; Sridharan et al., 2023), the Michoacán dataset provided a theoretical basis for reflecting on the extensibility and validation of a grid-based methodology, setting the basis for further methodological development presented in the following chapters.

MATERIALS AND METHODS

The ESI-07 events final dataset compiled in this study is designed to document the applications of the ESI-07 Intensity Scale and quantify a) how many seismic events have been analyzed; b) which types of and how many EEEs have been identified for each study; c) the source of data and; d) what outputs have been produced through time. To achieve this, two complementary approaches are integrated in the dataset.

- Publication-based approach: As in Ferrario et al. (2022), each ESI-07 event is represented by a single record, obtained through the integration of different studies and covering all categories of EEEs.
- Inventory-based approach: EQUILs datasets from the USGS repository (e.g., Muccignato and Ferrario, 2025; see Chapter 4) are included by keeping the individual inventories of different authors separate.

By combining these two approaches, the dataset maximizes the amount of available information.

1.1 ESI-07 EVENT BASE DATASET

The base for the study and the base structure of the dataset is defined by the end-2023 ESI-07 event catalogue, developed by Ferrario et al., (2022) includes 157 events, distributed from 300 AD to 2020. The baseline fields are as follows:

- ID: unique identifier for each ESI-07 event
- Date: date of the event
- Epicenter: epicentral location of the event (name of the region or epicenter place name)
- Country: country affected by the earthquake
- Latitude and Longitude: geographic coordinates of the epicenter, expressed in geographic coordinates (WGS84)
- Faulting style: kinematic characterization of the seismic source (i.e., strike-slip, normal, reverse)
- Depth: focal depth, expressed in km
- I_0 ESI: epicentral ESI-07 intensity
- MDPs ESI: macroseismic data points representing measured EEEs
- Isoseismals ESI: isoseismal lines derived from EEE-based intensity distribution
- Other intensity scales: additional macroseismic scales applied in the study (e.g., EMS, MSK, MM)
- Imax (other scales): maximum intensity observed using alternative scales
- Affected area: total area affected by EEEs (km^2)
- SRL: surface rupture length (km)
- Setting: geographical setting of the epicenter (i.e., coastal, inland)
- References: bibliographic sources documenting the event

1.2 WORKFLOW FOR ESI-07 2025 EVENTS DATASET REALIZATION

The implementation of the 2025 updated ESI-07 dataset is performed following a five-step workflow, from base dataset definition to data characterization (Fig.2.1).

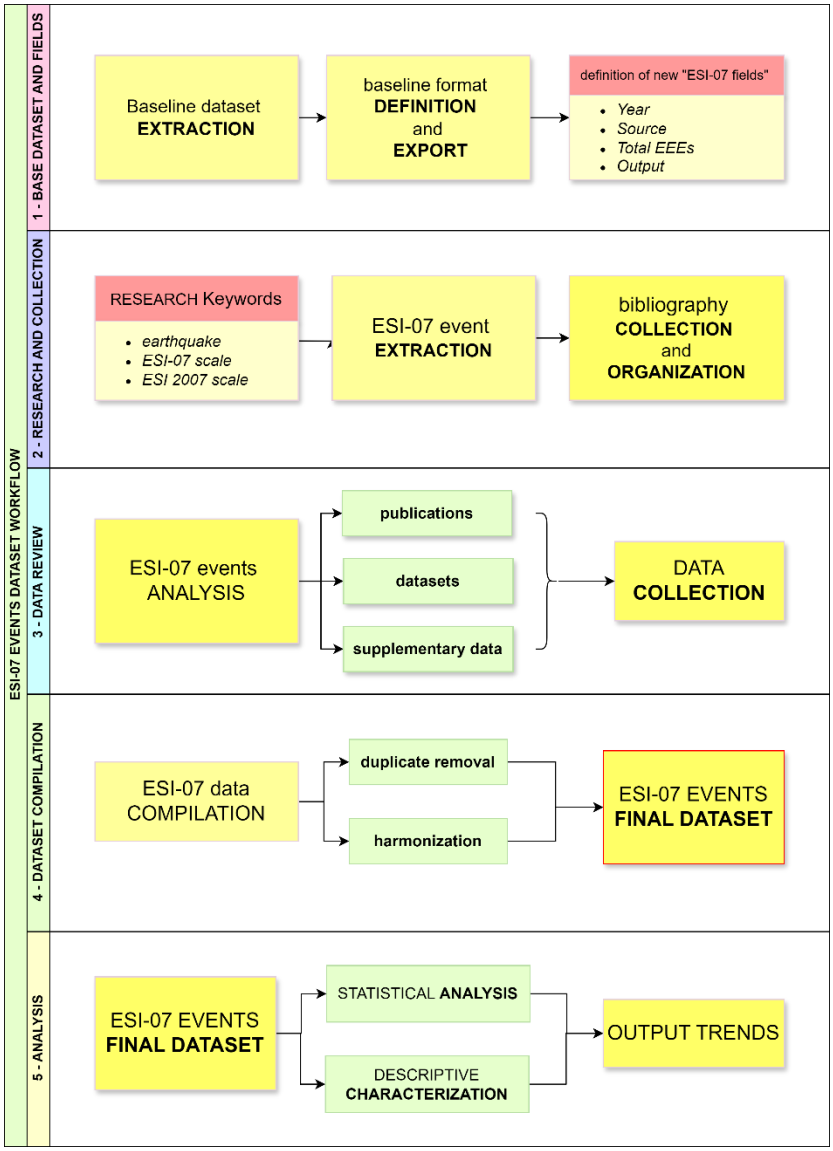

Figure 2.1 – ESI-07 event dataset workflow. *The workflow consists in five main steps which include: 1) base dataset selection and creation of field of interest; 2) research via keywords and bibliographic collection; 3) analysis of the bibliographic collection and data retainment; 4) ESI-07 data compilation and harmonization, which leads to ESI-07 events final dataset and; 5) statistical and descriptive analysis to visualize trends of the data*

Baseline Dataset and fields definition

The first step is defined by the extraction of the 2023 ESI-07 baseline dataset, constituted by 157 ESI-07 events, in order to provide a structural backbone and ensure continuity. The baseline dataset is analyzed and characterized, in order to define the structure and format, which will be applied to the updated version. Consequently, new fields of interest are defined:

- Year: reference year of the event
- Source: methodology applied to acquire data. This is a controlled field with predefined options, including *bibliography*, *reconnaissance field survey*, and *remote sensing data*.
- Total EEEs: total number of EEEs documented in the ESI-07 study consulted.
- Output: typology of outputs produced by the study.

Research of new ESI-07 case studies

In the second step an extensive bibliographic research is conducted, using international scientific repositories (e.g., ResearchGate, Scopus, Google Scholar). The keywords "*earthquake*", "*ESI-07*", and "*ESI 2007 scale*" are employed. Bibliographic sources are collected and organized.

Systematic ESI-07 events Review

In the third step each ESI-07 event and associated literature is carefully reviewed, in order to extract relevant information about the events analyzed. The necessary information is collected using the base format defined in step 1. Critical attention is given to identifying the number of EEEs collected and output of the publication. The review is performed both on publications already associated with the original baseline ESI-07 dataset and on newly identified works.

Data compilation and harmonization

In the fourth step data collected are implemented in the dataset in corresponding specific fields, and the ESI-07 events final dataset is compiled. During the integration process consistency of formats (e.g., outputs, date representation, coordinates) and harmonization of terminology across different sources is performed. Ambiguities and incomplete records are flagged, and in cases where bibliographic data are inconclusive, the corresponding attributes are set as n.a. After this step the ESI-07 events final dataset is obtained.

Statistical Analysis

In the fifth step, the ESI-07 events final dataset is subjected to descriptive characterization and statistical analysis. This includes analysis of temporal and geographical distribution of ESI-07 events, and relative abundance of different study outputs and EEEs datasets, all associated with relative trends.

RESULTS

2.1 DATASET OVERVIEW

The ESI-07 events final dataset compiled for this study includes a total of 218 earthquakes. Compared to the baseline ESI-07 event catalogue of 157 events, 61 new case studies are added. In particular, 40 events included derive from the study of Muccignato and Ferrario (2025) and 1 event is from the dataset compiled in 2025 for Mw 7.5 Noto Earthquake (Muccignato E., 2025). These latter represent the first systematic application of a grid-based methodology to large inventories of EQUILs, exposed in chapter 4 and 5. Although these inventories here included anticipates topics introduced later in the present thesis, these data are introduced here for the sake of completeness and to provide an updated repository covering the period of the doctoral research (2022–2025).

2.2 GEOGRAPHIC DISTRIBUTION

The ESI-07 events final dataset characterizes a total of 218 seismic events, distributed across 6 continents and 46 different countries (Fig. 2.2).

Europe emerges as the continent with the highest representation, with 97 events corresponding to 44.5% of the total. Asia is the second continent, with 59 events (27.1%), while South America accounts for 35 events (16.1%). The remaining continents are less represented, with 16 events in Oceania (7.3%), 10 in North America (4.6%), and a single event in Africa (0.5%).

The country with the largest number of documented ESI-07 events is Greece, with 42 cases, reflecting both the high seismicity of the Hellenic arc and the extensive application of ESI-07 studies in this area (e.g., Mavroulis et al., 2019; Papanikolau et al., 2009, 2017). Italy, with 23 events, and Spain, with 21, also show significant representation, which is consistent with their long historical documentation of earthquakes (e.g., Huayong et al., 2019; Valente et al., 2018; Guerrieri et al., 2009a, 2007; Silva et al., 2014, 2019). Other relevant countries are Peru, with 12 events, and China and Australia, with 10 events each. Colombia, Indonesia, Japan, and the United States all contribute with 8 events, while Russia 6, Taiwan 5, and Mexico 4 events. The remaining countries included in the ESI-07 events final dataset are represented by 1 to 3 earthquakes.

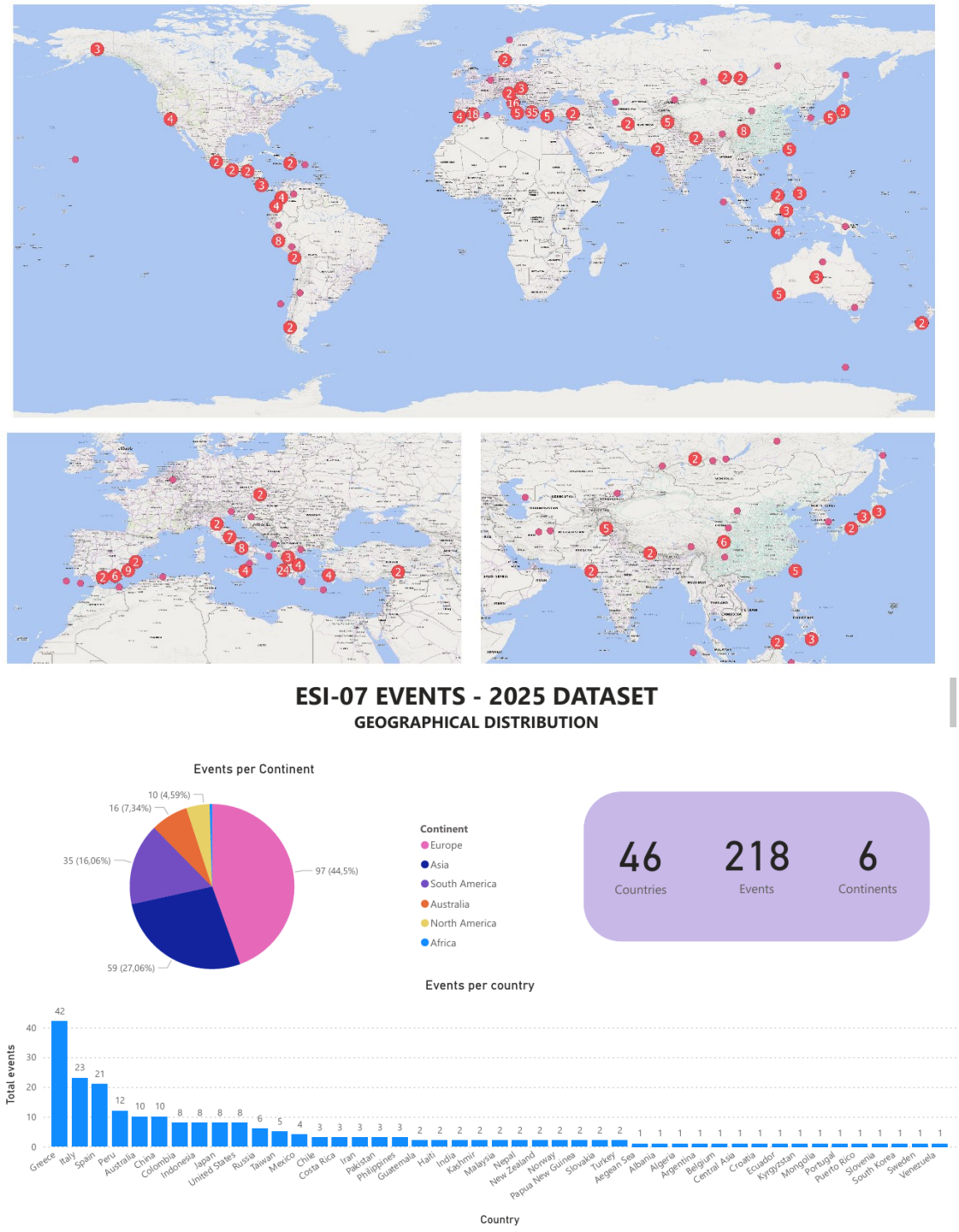

Figure 2.2 - Geographic distribution of the ESI-07 events. *The ESI-07 events final dataset contains 218 events distributed across 6 continents and 46 countries. Europe is the most represented continent with 97 events (44.5%), followed by Asia with 59 events (27.1%) and South America with 35 events (16.1%). Greece is the single country with the largest number of events (42), followed by Italy (23) and Spain (21).*

2.3 TEMPORAL DISTRIBUTION

The ESI-07 events included in the final dataset are distributed across a temporal window of two millennia, and specifically from 426 BC to 2024, across 119 distinct years (Fig. 2.3). The temporal trend is uneven, reflecting the heterogeneity of available sources. While ancient and medieval earthquakes are sparsely documented and often reconstructed indirectly from written narrative or paleoseismological evidence (Silva et al., 2014; Torabi et al., 2020), a progressive increase in the number of events is evident from the XVII century onwards. From the early modern period, and particularly after the middle XIX century, the growth in documented cases becomes more pronounced, corresponding to the expansion of systematic studies on historical seismicity. A marked increase is observed during the instrumental period, especially after the middle XX century, when field surveys, seismological networks, and, lastly, remote sensing technologies greatly enhanced the capacity to document EEEs.

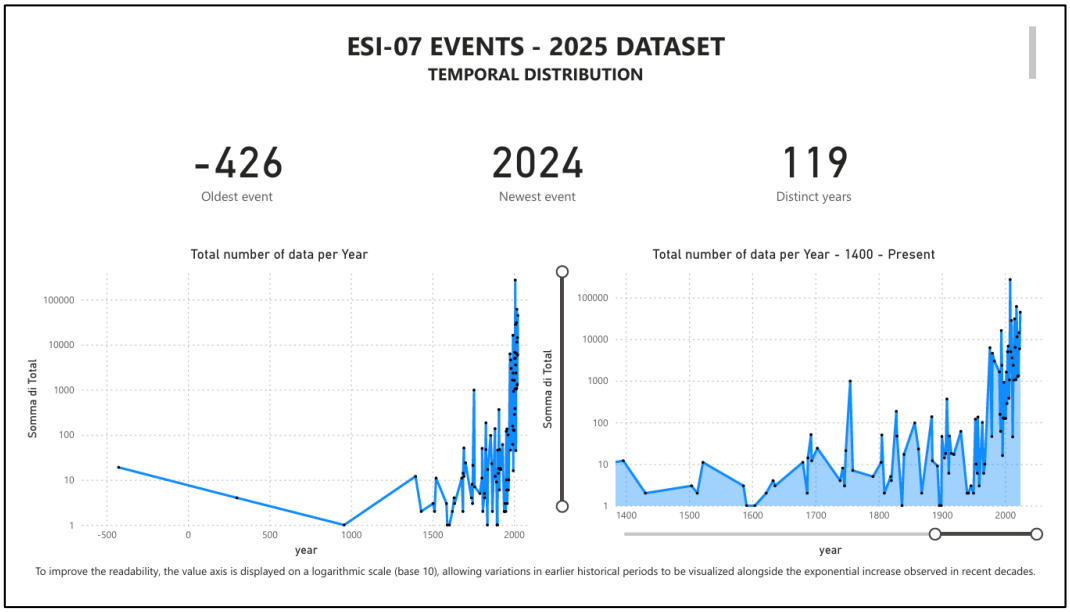

Figure 2.3 - Temporal distribution of the ESI-07 events. *The ESI-07 events final dataset covers a period from 426 BC to 2024, with 218 events distributed across 119 different years. A significant increase in documented events is observed from the XVII century onwards, with a sharp rise during the instrumental era.*

2.4 DATA TYPES AND ACQUISITION METHODS

The events included in the dataset are characterized by three categories of data sources: bibliography data, remote sensing data, and reconnaissance field surveys data (Fig. 2.4). Bibliography data constitute the majority, with 151 cases, corresponding to 67.1% of the total, while 55 events, equal to 25.2% of the total, are characterized by remote sensing data. Lastly, 30 events, representing 13.8% of the total, are documented through direct field surveys data (Fig.2.4).

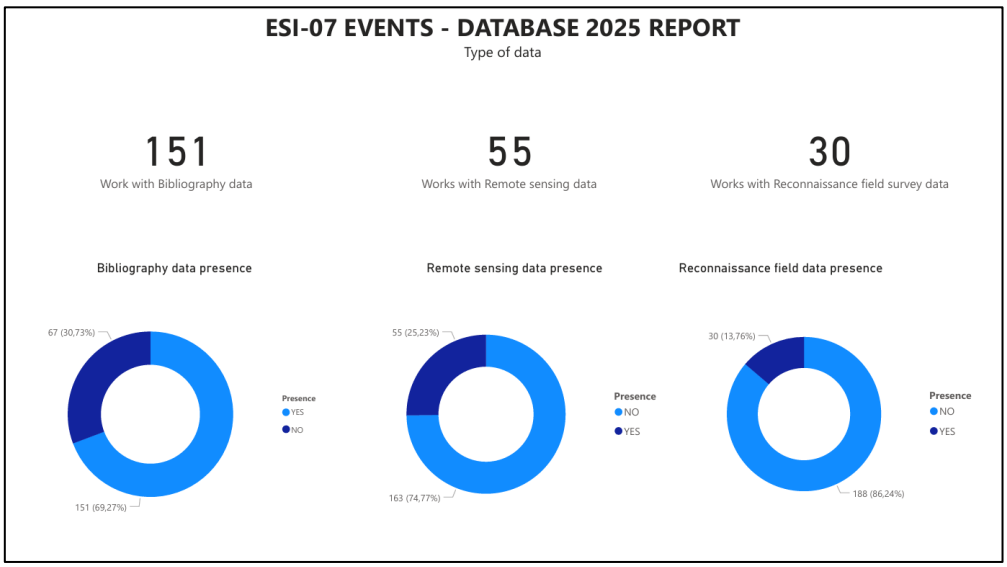

Figure 2.4 - Data type in the ESI-07 event dataset. *The ESI-07 events final dataset includes 3 categories of data sources: bibliography data (151 events, 67.1%), remote sensing data (55 events, 25.2%), and reconnaissance field data (30 events, 13.8%).*

The relative frequency of the three acquisition methods exhibits a marked temporal variation. Bibliography data remains a constant reference throughout the dataset, with an increase from middle XX century. Reconnaissance field surveys data, absent for older time periods, become increasingly common in the late XX and present time. Remote sensing data appear from the 1970s onwards, showing a marked and continuous increase, reflecting the technological advances in satellite imagery and aerial photography (Fig.2.5).

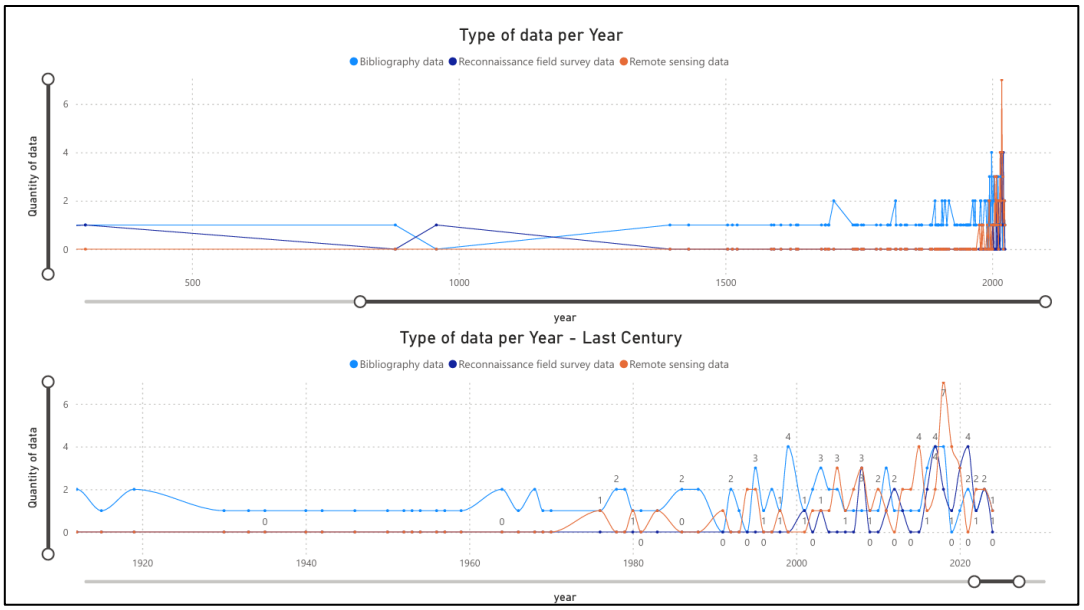

Figure 2.5 - Temporal distribution of data types. *Bibliography data are present throughout the entire temporal span. Reconnaissance field surveys increase from the late XX century onwards, while remote sensing data show a sharp increase after the 1970s, corresponding to the expansion of satellite and aerial survey technologies.*

2.5 SCIENTIFIC OUTPUTS

The examined studies provide a variety of outputs, which were categorized into 10 different classes (Fig. 8). The categories identified follow the original denomination adopted in each study consulted. A description of the ESI-07 output characteristics is reported when explicitly detailed by the authors. In some cases, different outputs may present similar characteristics, but the original naming is retained in order to respect the terminology used in the primary sources. The categories are defined as follows:

- *ESI-07 Assignation*: whether an ESI-07 intensity is assigned to an event, either at epicentral or regional scale, based on EEEs registered
- *EEEs Characterization*: presence of a qualitative and\or quantitative description of EEEs observed for an event
- ESI-07 Grid analysis: Quantitative approach which involves the subdivision of an area into grid cells of a specific dimension, which provide the display of the ESI-07 intensity field
- *ESI-07 Isoseismals*: contour lines indicating areas of equal ESI-07 intensities, derived from spatial interpolation of EEEs points
- *EEEs maps*: cartographic representation of the EEEs
- *ESI-07 Scale maps*: similar to ESI-07 grid analysis output, workflow is not specified
- *ESI-07 Shakemaps*: cartographic representation similar to instrumental shakemaps, based on ESI-07 intensities registered
- *ESI-07 Shock Intensity maps*: cartographic representation of shock zones characterized by higher ESI-07 intensities
- *ESI-07 Attenuation maps*: cartographic representation of the decay of ESI-07 intensities with distance

- *ESI-07 Intensity maps*: cartographic representation of the distribution of ESI-07 intensities

Among these outputs, "*ESI-07 assignation*" output is the most frequent, with 211 records. "*EEEs characterization*" output follows with 137 cases. "*ESI-07 Grid analysis*" is also significant, present 42 studies: for this category, is again worth noting that 40 out 42 studies are from Muccignato and Ferrario, 2025, and therefore represent a preview of the work that will be presented in the following chapters (Chapter 4 and 5).

Less frequent are outputs such as "*ESI-07 Isoseismal maps*", which are present in 30 studies, and "*EEEs distribution maps*", present in 28 studies. "*ESI-07 scale maps*" (17), "*ESI-07 Shakemaps*" (7), and "*ESI-07 Shock intensity maps*" (4) are moderately-low present in the dataset, while "*ESI-07 Attenuation maps*" and "*ESI-07 Intensity maps*" are extremely rare, each appearing in only a single study (Fig. 2.6).

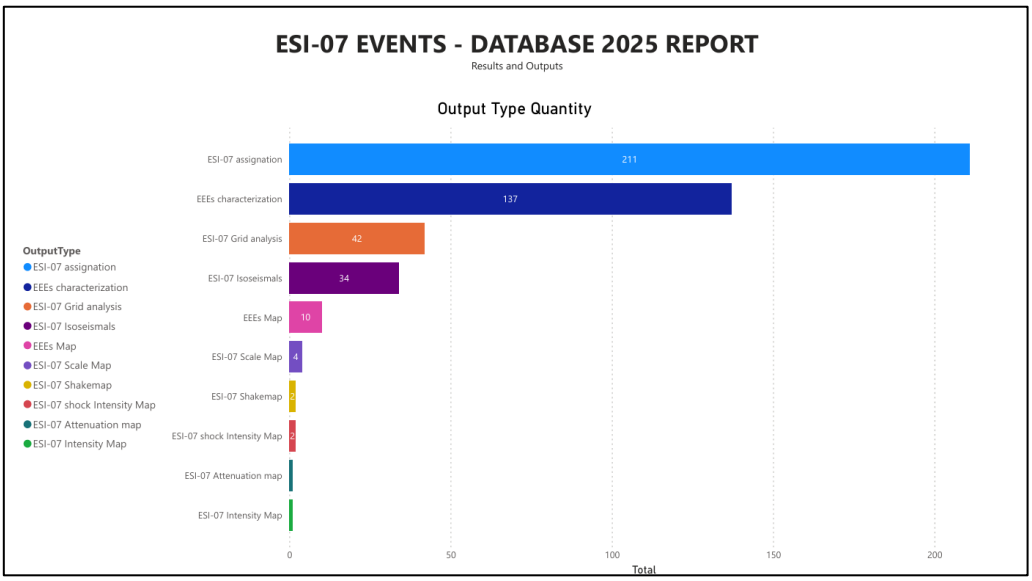

Figure 2.6 - Outputs of the ESI-07 event studies. *The dataset reveals ten categories of scientific products: ESI-07 assignation, EEEs characterization, ESI-07 grid analysis, ESI-07 isoseismals, EEEs maps, ESI-07 scale maps, ESI-07 shakemaps, ESI-07 shock intensity maps, ESI-07 attenuation maps, and ESI-07 intensity maps. The most frequent output is the ESI-07 assignation (211 records), followed by EEEs characterization (137) and ESI-07 grid analysis (42). The rarest outputs are attenuation and intensity maps, each documented in only one case.*

DISCUSSION

3.1 DATA AVALIABILITY AND DISTRIBUTION

The construction of the ESI-07 events final dataset relies fundamentally on the availability of structured datasets of EEEs and explicit outputs. For this reason, a key aspect is the possibility to quantify the number of EEEs reported for each event. Out of the 218 ESI-07 events included, 52 studies (23.9%) did not provide an explicit enumeration of the documented EEEs, reporting only descriptive information and\or generalized observations, making it impossible to reconstruct a precise numerical dataset of EEEs for those cases, and thus representing a critical issue for potential future applications and revision of data (e.g., multi-dataset grid-based ESI-07 analysis). Since EQUILs are among the most impacting and destructive geological risks (Keefer, 1984; Rodriguez et al., 1999), future steps could focus on the enrichment and integration of such data, particularly for Italian earthquakes, where extensive documentation already exists. A systematic revision of national catalogues such as IFFI catalogue could provide new data to be incorporated into the present dataset. Although these EQUILs records would not yet be associated with ESI-07 applications and ESI-07 outputs, they could be retrospectively included as case studies analyzed with the ESI-07 scale. Such integration would allow testing whether the addition of new EQUIL datasets influence temporal trends and outputs and can contribute to a more complete picture of the use of ESI-07 for macroseismic characterization.

The geographical and temporal distribution of the ESI-07 events in the final dataset clearly highlights a strong heterogeneity. Certain regions, particularly Southern Europe, are heavily represented, reflecting the systematic use of the ESI-07 scale supported by extensive historical sources (e.g., Silva et al., 2014; Papazachos et al., 2000, 2010; Kolyva, 1997; Guidoboni, 1994, 2019; Boschi et al., 1997) and the presence of active research communities. In contrast, areas such as Africa and the Middle East remain almost absent, potentially for scarcity of studies applying the ESI-07 scale in these contexts. A similar imbalance emerges in the temporal dimension. While a few ESI-07 events from antiquity and the medieval period are included, the majority of the dataset is composed of modern and instrumental earthquakes. The exponential growth observed with time is directly linked to the increasing availability of: a) scientific literature; b) growth of reconnaissance surveys and remote sensing technologies, and; c) the progressive adoption of EEEs and ESI-07 intensity scale as a reliable tool for macroseismic analysis.

These results underline how the distribution of ESI-07 events is primarily determined by the availability of published research rather than the actual occurrence of earthquakes. Addressing these gaps requires expanding the application of the ESI-07 scale both backwards, by revisiting historical and paleoseismological evidence, and forwards, by ensuring that large contemporary earthquakes are systematically characterized. Such efforts would strengthen the temporal and spatial continuity of the dataset and reinforce the role of ESI-07 as a unifying framework for the analysis of seismic environmental effects.

3.2 EVOLUTION OF ESI-07 OUTPUTS OVER TIME

To investigate the evolution of the application of the ESI-07 scale, the ESI-07 events final dataset was analyzed correlating type and number of ESI-07 outputs produced and different time intervals. This comparison reveals an exponential growth in both the quantity and diversity of ESI-07 outputs through time, and especially with a clear concentration from the late XIV century onwards and a systematic increase from the early XX century (Fig. 9).

For the oldest historical events, only EEEs characterization and ESI-07 assignation are available. For XIX century events, the first *ESI-07 isoseismals* output appear. From the middle XX century onwards, outputs diversify further with the introduction of *ESI-07 scale maps* and the first *ESI-07 attenuation maps*. In recent decades, and particularly since the late XX century, advanced products such as *ESI-07 grid analyses*, *EEEs maps*, *ESI-07 shock intensity maps*, *ESI-07 intensity maps*, and *ESI-07 shakemaps* are included in studies (Fig. 2.7).

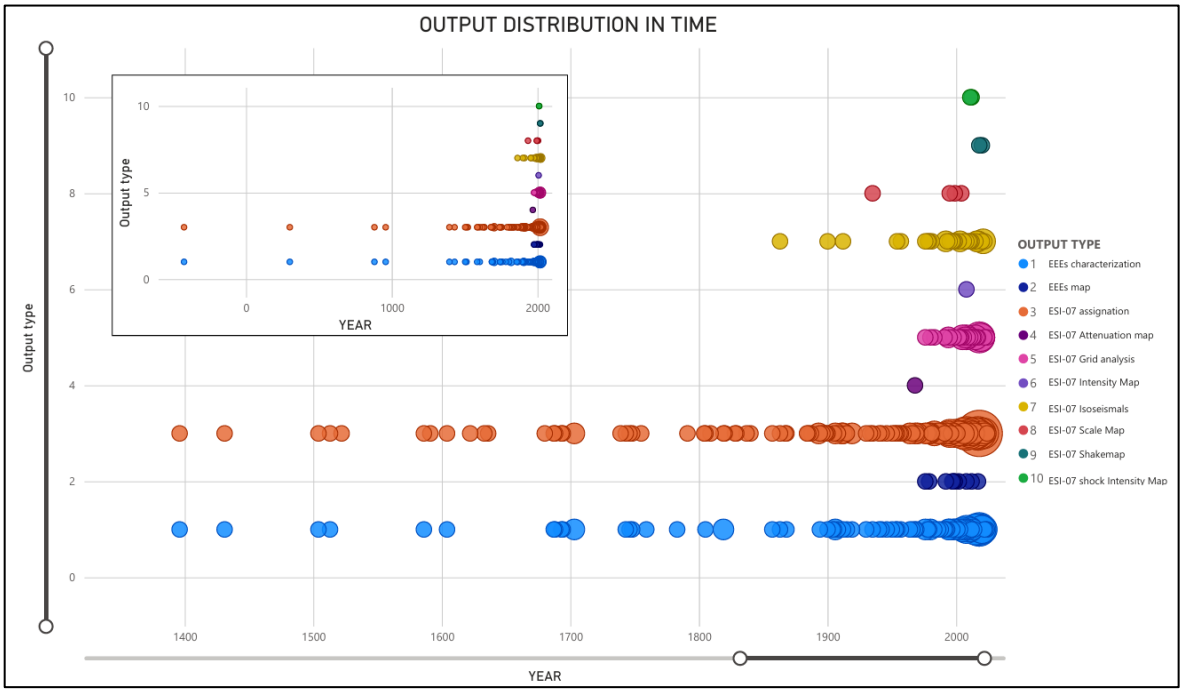

Figure 2.7 - Data distribution over time. *EEEs characterization and ESI-07 assignation are the only products available until the middle XIX century. ESI-07 isoseismals appear for studies of events of 1800s, while ESI-07 scale and ESI-07 attenuation maps become available from the middle XX century. More advanced outputs are associated with late XX century and present-day events.*

A closer focus on the 1900-2000 time period shows a steady increase in the number of ESI-07 outputs per event. While in the early 1900s their number rarely exceeded 1 to 5 per study, for events from the middle to late XX century the trend rises, reaching a maximum of 16 outputs for the 2008 Mw 7.9 Wenchuan (China) earthquake (Lekkas et al., 2010; Xu et al., 2014a; Li et al., 2014). In recent years, the number of ESI-07 outputs per event has stabilized between 10 and 15. A peak is observed in 2017, when several major earthquakes occurred in the same year, producing multiple studies and outputs (Triantafyllou et al., 2020; Huayong et al.,

2019; Nappi et al., 2021; Velázquez-Bucio et al., 2021; Naik et al., 2020; Papathanassiou et al., 2019; Hu et al., 2019) (Fig. 2.8).

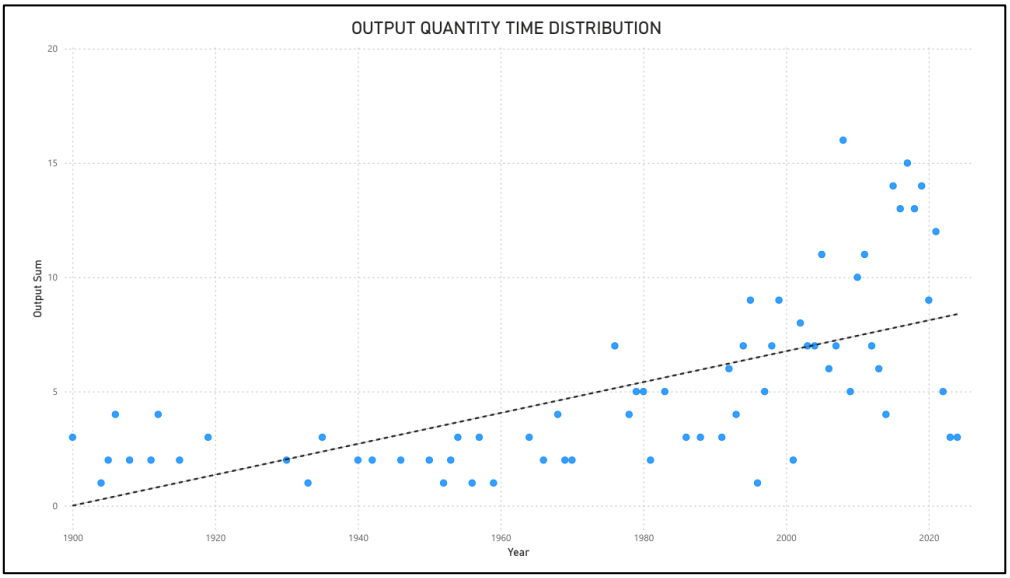

Figure 2.8 - Number of outputs per event through time. *The time trend of 1900-2000 shows an exponential increase, from 1–5 outputs in the early XX century to more than 10 outputs in recent decades, with a maximum of 16 for the Wenchuan earthquake (2008).*

The diversification of outputs observed in temporal trends, confirms the growing relevance of EEEs and ESI-07 Intensity Scale as macroseismic indicators, as the latter can provide a neutral tool respect to human and infrastructure damage-based intensity scales and indicators (Michetti et al., 2004; Michetti et al., 2007; Guerrieri et al., 2009a, 2009b; Lekkas et al., 2010; Papanikolaou et al., 2017; Naik et al., 2020). Nevertheless, some limitations remain evident: the application of the ESI-07 scale is dependent on the availability and quality of EEEs data and documentation, which result to be geographically and temporally heterogeneous, and in several cases lacks explicit quantification. In addition, the diversity of methodological approaches and the variability in the definition of ESI-07 outputs may hinder direct comparability across different studies. These factors highlight the need for continued efforts in harmonizing datasets and methodologies, in order to fully exploit the potential of the ESI-07 scale.

A further factor influencing the increase of the quantity of ESI-07 outputs per event is the improvement and spread of technologies and data acquisition methodologies (e.g., remote sensing techniques, GIS-environment analyses, technological devices).

3.3 THE 2022 MICHOACÁN EARTHQUAKE: A KEY CASE STUDY FOR ADVANCING ESI-07 METHODOLOGY

Within the ESI-07 events final dataset, the Mw 7.7 Michoacán (Mexico) earthquake represents the first case examined during the PhD research. Although the methodologies applied to this event were already consolidated in literature, its value lies in the heterogeneous dataset available in terms of sources (e.g., field

survey data, press data, remote sensing data) and EEEs type. In particular, the inclusion of a large EQUILs and the extent and diversity of EEEs dataset provided the opportunity to explore the theoretical foundation for the development and validation of an ESI-07 grid-based methodology.

The Michoacán earthquake hit Mexico on September 19th, 2022, and triggered a wide range of EEEs (e.g., slope movements, liquefaction processes, and anomalous waves and tsunamis). For this study, a work group was established, and, in its framework, I contributed to the collection and integration of a wide variety of EEEs data sources, including scientific papers, official reports, news articles, and social media content, in addition to validating georeferenced observations gathered in the field. My contribution also included the construction of the ESI-07 isoseismals, which were derived from more than 8000 georeferenced EEEs data (Fig. 2.9).

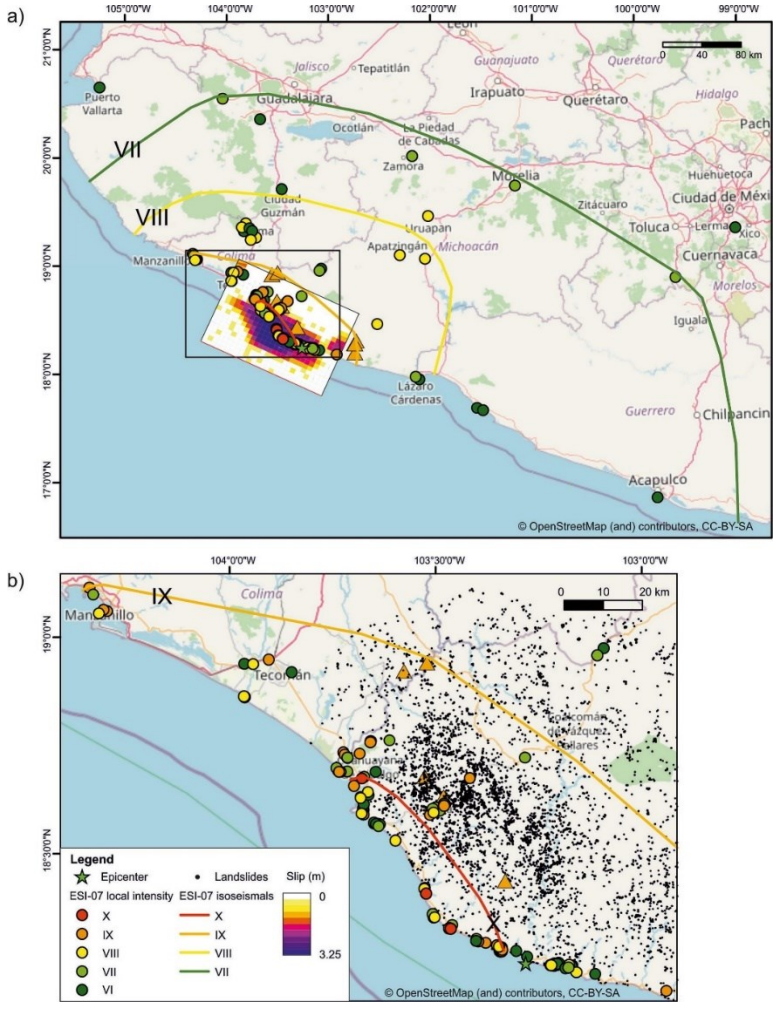

Figure 2.9 - ESI-07 isoseismals of the Michoacán earthquake. *ESI-07 Isoseismals derived from the integration of more than 8000 EEE data are shown, with intensity values ranging from ESI-07 X (red) to ESI-07 VI (green). A gradient background illustrates coseismic slip distribution. Modified after Velázquez-Bucio et al., 2024.*

A further part of the study was dedicated to the mapping and analysis of EQUILs, conducted through remote sensing methodology. The latter were analyzed using grid-based methodology which involved the computation of Landslide Number Density (LND) and Landslide Area Percentage (LAP) (Fig. 2.10).

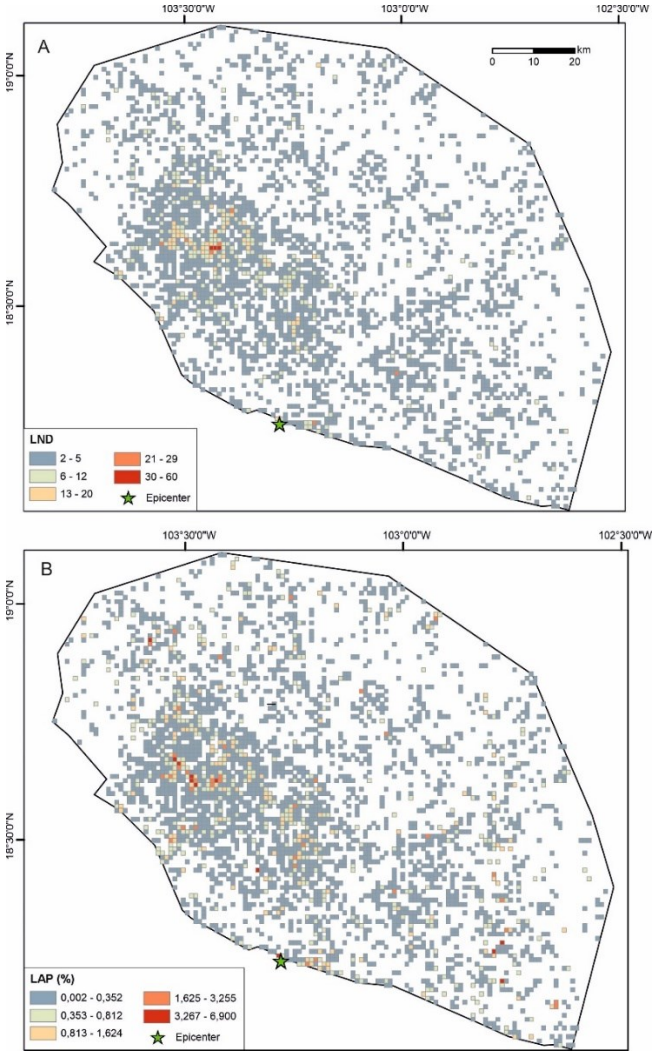

Figure 2.10 - Landslides mapped from satellite imagery and analyzed by a grid methodology. *A) Landslide Number Density (LND); B) Landslide Area Percentage (LAP). These standard descriptors define EQUILs distribution and, in this study, provided the theoretical baseline for exploring their role as validators for ESI-07 intensity computation. Modified after Velázquez-Bucio et al., 2024.*

The Michoacán earthquake case underline the value of a multi-source and data approach, where reconnaissance field surveys, remote sensing, press reports, and social data were integrated into a heterogeneous and extensive dataset. This plurality of sources enabled a comprehensive ESI-07 characterization and provided a theoretical baseline for reflecting how traditional landslide metrics (e.g., LND, LAP), when applied in a grid-based framework, can be compared with and potentially serve as validators for an ESI-07 intensity metric. At the same time, the inclusion of non-traditional data (i.e., social data) offers an opportunity to reflect on how these sources might be critically evaluated, particularly in terms of spatial accuracy and resolution.

CONCLUSION

In this study, a dataset of ESI-07 seismic events is constructed, in order to provide a present-time overview of ESI-07 applications and to construct an updated and harmonized dataset of ESI-07 seismic events. The ESI-07 events final dataset is compiled through a systematic review and harmonization of multiple sources, utilizing as baseline the ESI-07 catalogue constructed by Ferrario et al. (2022). A total of 218 ESI-07 events is included, distributed across 6 continents and 46 countries worldwide. Europe emerges as the continent with the highest number of documented events, with Greece, Italy, and Spain as the countries with most cases, while other regions such as Africa and the Middle East remain only marginally represented. The ESI-07 events final dataset covers a time span from 426 BC to 2024. The temporal distribution highlights a sharp increase in documented cases from the XVII century onwards, and an exponential growth during the instrumental period, reflecting both improved data availability and acquisition techniques and the progressive adoption of the ESI-07 Intensity scale. The ESI-07 events final dataset also captures the diversification of scientific outputs across time, ranging from assignations of *ESI-07 intensity and EEEs characterization* for earliest events, to more advanced products such as *ESI-07 Isoseismals*, *ESI-07 Scale maps, ESI-07 Attenuation maps*, and most recently ESI-07 grid-based analyses and *ESI-07 Shakemaps* for latest events.

The presence of innovative outputs is closely linked to technological advances and to the increasing recognition of EEEs, and more directly ESI-07 Intensity Scale, as reliable indicators for macroseismic intensity. The utility of the study lies in the systematic revision, integration and standardization of heterogeneous sources, ensuring potential compatibility and implementation of the dataset in the international EEE Catalogue while providing a robust foundation for future applications of agile methodologies for ESI-07 Intensity estimation.

CHAPTER 3

DOCUMENTING EEEs THROUGH LANDSLIDE INVENTORIES: IMPLEMENTING EQUILS IN THE IFFI CATALOGUE

INTRODUCTION

Updated and comprehensive EQUILs catalogues represent a critical tool for macroseismic characterization, as they provide quantitative information on the geographic location and dimensional attributes of EQUILs, which are evidence of seismic shaking and one of the most significant categories of EEEs for the application of the ESI-07 scale (Keefer, 1984; Michetti et al., 2007; Harp et al., 2011; Xu, 2015a, 2015b; Ferrario, 2022a).

In Italy, the Inventario dei Fenomeni Franosi in Italia (IFFI), managed by ISPRA in collaboration with regional authorities, is the official national catalogue of landslides (Di Paola et al., 2024; ISPRA, 2025a, 2025b). Although IFFI currently documents more than 630,000 landslides, the specific component of EQUILs has not been systematically emphasized, despite its strategic importance for macroseismic characterization. Addressing this gap requires updated and harmonized datasets consistent with FAIR principles (Findability, Accessibility, Interoperability, and Reuse).

Within the framework of the GEOSCIENCES-IR project, and specifically under Work Package 3 "Landslide and Sinkholes" (WP3), this study focuses on compiling and harmonizing an updated EQUILs dataset, aimed at supporting the systematic integration of EQUILs into the IFFI catalogue. The sources analyzed include the CEDIT catalogue (Martino et al., 2020), the CFTI (Zei et al., 2024), the EEE Catalogue (Guerrieri et al., 2015; Audemard et al., 2015), the historical dataset of Govi (1977) for the 1976 Friuli earthquake (Govi, 1977; Govi and Sorzana, 1977), and original datasets developed by the University of Insubria (Pizza et al., 2023; Camarda, 2021; Paganini, 2023; Lazzati, 2020). The resulting standardized dataset comprises 3483 records covering the entire Italian territory and spanning a wide temporal range. The dataset highlights recurrent clustering of landslides in seismically active regions, particularly along the Apennines and in correspondence with large historical earthquakes. The integration of heterogeneous sources reveals both strong consistency in the geographic distribution of records and gaps in spatial coverage and EQUILs characterization, underlining the importance of continued archival work and improved documentation strategies. The final dataset represents the first harmonized national archive of EQUILs fully compatible with the IFFI framework. It provides new insights into the spatial distribution and characteristics of EQUILs in Italy and constitutes a potential basis for further methodological developments aimed at macroseismic characterization through the ESI-07 scale.

The content of this chapter is largely based on the technical report IO-68, developed to achieve the intermediate objective 3.12 of the GEOSCIENCES-IR project.

MATERIALS AND METHODS

1.1 IFFI CATALOGUE

The Inventario dei Fenomeni Franosi in Italia (IFFI) represents the official national landslide inventory. It is developed and maintained by Istituto Superiore per la Protezione e la Ricerca Ambientale (ISPRA), in collaboration with Regional and Autonomous Province administrations (Di Paola et al., 2024; ISPRA, 2025a, 2025b). The catalogue record over 620 000 landslides, which cover approximately an area of 25 000 km^2, corresponding to the 8,3% of the national territory (Di Paola et al., 2024; ISPRA, 2025a, 2025b). Data are distributed across a period which spans from 1116 AD to 2025, with varying local updates (ISPRA, 2025a; Di Paola et al., 2024; Trigila et al., 2010; Iadanza et al., 2021). Landslides included in IFFI catalogue are characterized by data collected by different acquisition method such as research of historical records, interpretation of aerial photos and field surveys (Di Paola et al., 2024; ISPRA 2025a).

After the 5 May 1998, which caused severe damage in different municipalities of Campania region (e.g., Sarno, Siano, Quindici, Barcigliano and S. Felice a Cancello), the need for an updated landslide national inventory became evident. From this essential requirement, IFFI catalogue is ideated in 1999, and progressively evolved into a national standard repository, thanks to the collaboration between ISPRA, regional geological agencies and Regional Environmental Protection Agencies (ARPA) (Trigila et al.,2010). The first version of the IFFI catalogue was published in 2005 (Ispra, 2025b). Its implementation is mandated by Art.6, Law 132/2016 of Italian environmental legislation (ISPRA, 2025a, 2025b; Iadanza et al., 2021).

The base data model on which the catalogue is built, is defined by a "*Landslide form*", defined by three different entities:

- *Landslide report*: metadata associated with the event report (e.g., source of data, observation date and agency)
- *Landslide event*: individual landslide, defined with location and triggering cause
- *IFFI landslide*: vector geometries which represent spatial extent and typology

Each record encompasses up to 144 fields distributed across 19 thematic categories, including: movement type, activity state, damage reports and morphological context (Trigila et al., 2010; Iadanza et al., 2016). Each landslide is geolocated as a vector (i.e., point, polygon or line), depending on its scale and survey detail (Di Paola et al., 2024). In particular:

- PIFF data (Punto identificativo del Fenomeno Franoso), posed in correspondence of landslide crown
- Line, posed if the phenomena are characterized by an elongated shape
- Polygon: if landslide is cartographical and characterized by a distinct area

IFFI catalogue and data are accessible through the IdroGEO platform, with a Web application built with Progressive Web Application (PWA), FREST Application Programming Interface (API) services and FAIR standards (Iadanza et al., 2021). The online interface enables map-based interaction, data querying and

management, exporting in different format (e.g., CSV, GeoJSON) and sharing (Fig. 3.1). Registered users can update IFFI catalogue using API-based workflows and web editor.

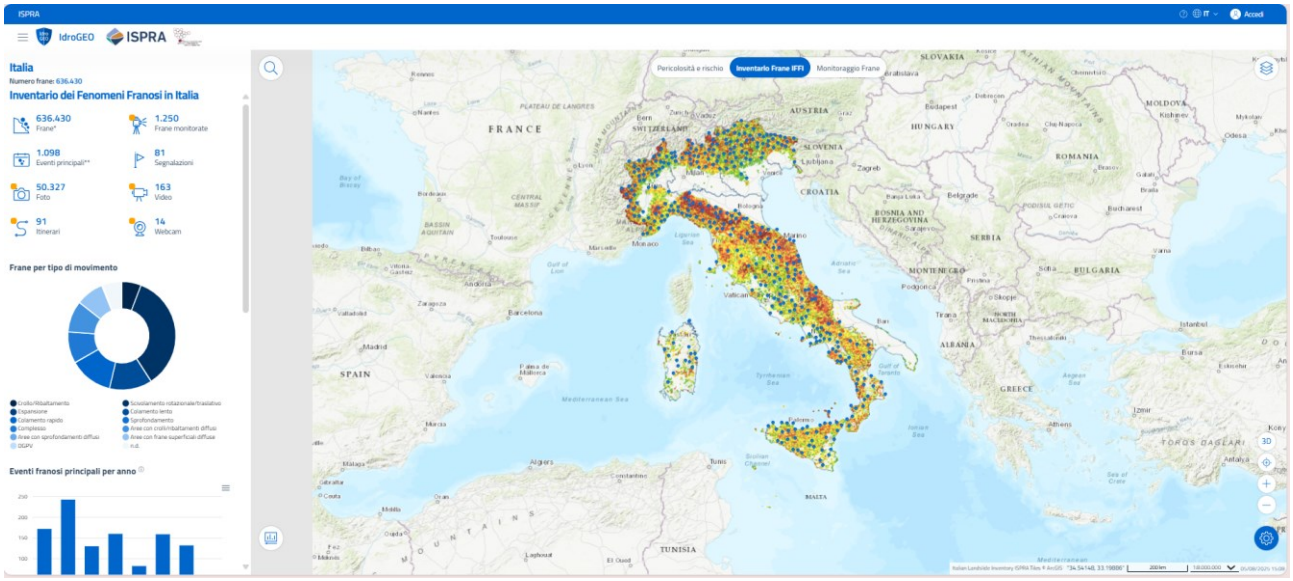

Figure 3.1 - Web interface of the IFFI catalogue. *The portal provides a GIS-based visualization of over 600 000 mapped landslides across Italy, shown as colored points overlaid on a topographic basemap. The web service includes a window for summary statistics (e.g., number of monitored landslides, principal events, landslide monitored, multimedia reference), interactive charts showing landslide types and temporal frequency, tools for filtering and layer selection. Image retrieved from IdroGEO - Inventario Frane IFFI.*

1.2 INPUT DATA

Input data are acquired from available official catalogues and academic products that document EQUILs for historical, instrumental, and post-event field investigations. After a preliminary research of potential useful input data, CEDIT (Martino et al., 2020), EEE (Guerrieri et al., 2015a, 2015; Audemard et al., 2015), CFTI Landslide (Zei et al., 2024) catalogues, specific case studies from University of Insubria (Pizza et al., 2023; Paganini, 2023; Camarda, 2021; Lazzati, 2020) and1976 Friuli earthquake map of Govi and Sorzana (1977), are selected.

1.2.1 EQUILS CATALOGUES

CEDIT CATALOGUE

The Italian Catalogue of Earthquake-Induced Ground Failures (CEDIT) (Martino et al., 2020) is a national repository of earthquake-induced ground effects (i.e. landslides, liquefaction phenomena, ground cracks). It was first conceived by Delfino and Romeo, in 1997 (Delfino and Romeo, 1997), with the main aim to document seismic induced effects on the natural environment and associate them with seismic parameters

(e.g., magnitude and macroseismic intensity). Since 2010 the catalogue has been managed by the Research Centre for Geological Risks (CERI; Sapienza University) (Martino et al., 2014, 2020; Caprari et al., 2018).

Data present in the catalogue are collected by historical data compilation, literature review and seismic databases (e.g. CFTI5Med and CPTI15) and post-event field surveys (Martino et al., 2020). Each earthquake-induced ground effect is correlated to a causative effect, and includes metadata as location, type of effect, intensity, geographic accuracy level (from metric to tens-kilometric) and references. These data are structured in five different and interrelated tables as follows: earthquake, effects, phase, bibliography and survey (Caprari et al., 2018; Martino et al., 2020).

CEDIT catalogue is accessible through an interactive WebGIS interface, which is updated through time (Martino et al., 2014; Caprari et al., 2018; Martino et al., 2020). On web interface users can query the earthquake-induced ground effects by searching by earthquake, effect type and geographic area (Fig.3.2).

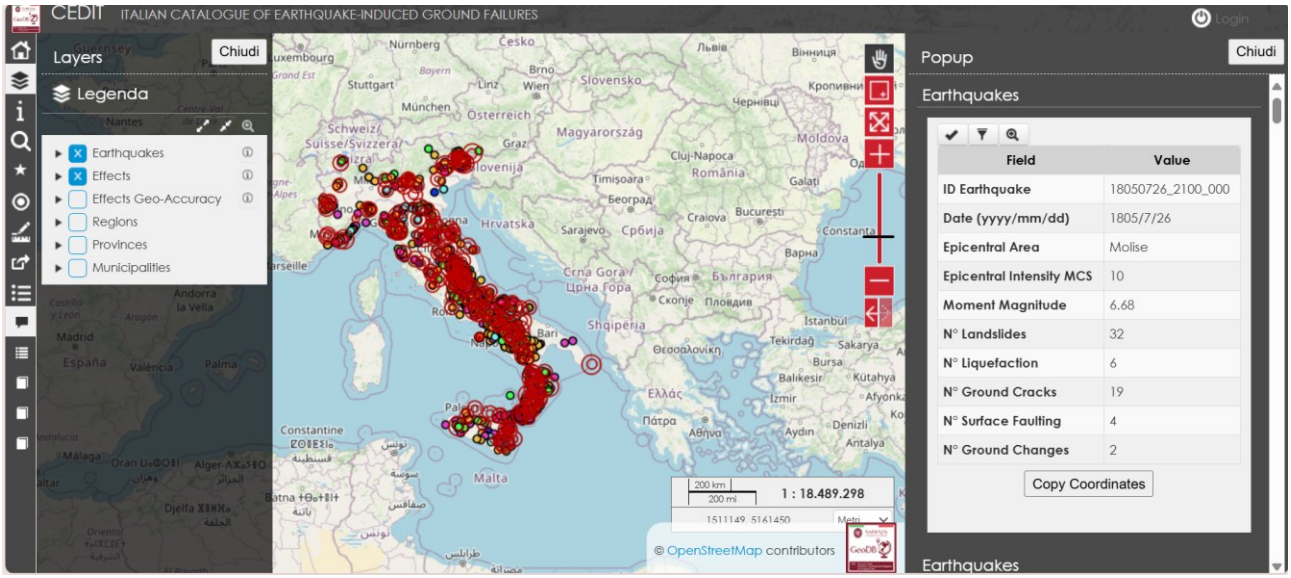

Figure 3.2 - WebGIS interface of the CEDIT catalogue . *The CEDIT WebGIS interface is characterized by a basemap, a layer panel and different tools to manage them. Each earthquake is symbolized, and ground effects are associated with different symbology. Each one can be filtered and queried individually. When an event is selected a popup window appears, providing detailed metadata. Image retrieved from Cedit - Italian Catalogue of Earthquake-Induced Ground Failures - GeoDB.*

From CEDIT catalogue 2084 points, labeled in "total effects" field either as "landslides", "rockfall", "earth spread" or "ground cracks related to slides", are extracted.

EEE CATALOGUE

The Earthquake Environmental Effects (EEE) Catalogue (Guerrieri et al., 2007; Ferrario et al., 2022) is an international database which compiles and standardize earthquake-induced environmental effects (EEEs). Its complete characterization is reported in chapter 1 (Ch. 1 – par. 1.3).From EEE catalogue, a total of 669 EQUILs points are extracted.

CFTI LANDSLIDES CATALOGUE

The CFTI Landslide Catalogue (Zei et al., 2024), linked to the broader Catalogo dei Forti Terremoti in Italia (CFTIMed), is a catalogue focused on historical earthquake-induced landslides (HEILs). The dataset was compiled in the framework of INGV, for the project "Multi-scale, integrated approach for the definition of earthquake-induced landslide hazard in Italy" funded by the Italian Ministry for the Environment, completed in 2022 and published in early 2024 (Zei et al., 2024).

Data are collected by reviewing historical sources, scientific articles and technical records and cross-comparison with other catalogues (i.e., CEDIT and EEE catalogue) (Zei et al., 2024). Data are also characterized by accuracy classes, from A to C, based on known localization. Furthermore, when CFTI landslides correspond to IFFI landslides, they are labeled as class AI or BI depending on original accuracy class and matching status.

The catalogue is available online with a WebGIS interface, for visualization, exploration and management of the data. The WebGIS interface is based on OpenLayers framework, integrating geospatial data visualization tools with real-time querying and multi-format (e.g., shapefile, KML, CSV) export functions (Zei et al., 2024). The interface displays a satellite basemap with overlayable layers, the menu allows for management of different layers (e.g., earthquakes, landslides). A search bar also presents for filtering data of interest. When clicked, any landslide opens a pop-up panel with all available information as: id and classification, coordinates, accuracy classes, location, event associated, references and corresponding IFFI Id if matched (Fig. 3.3).

The catalogue contains a total of about 1000 landslides. All the data points are retained for the present study.

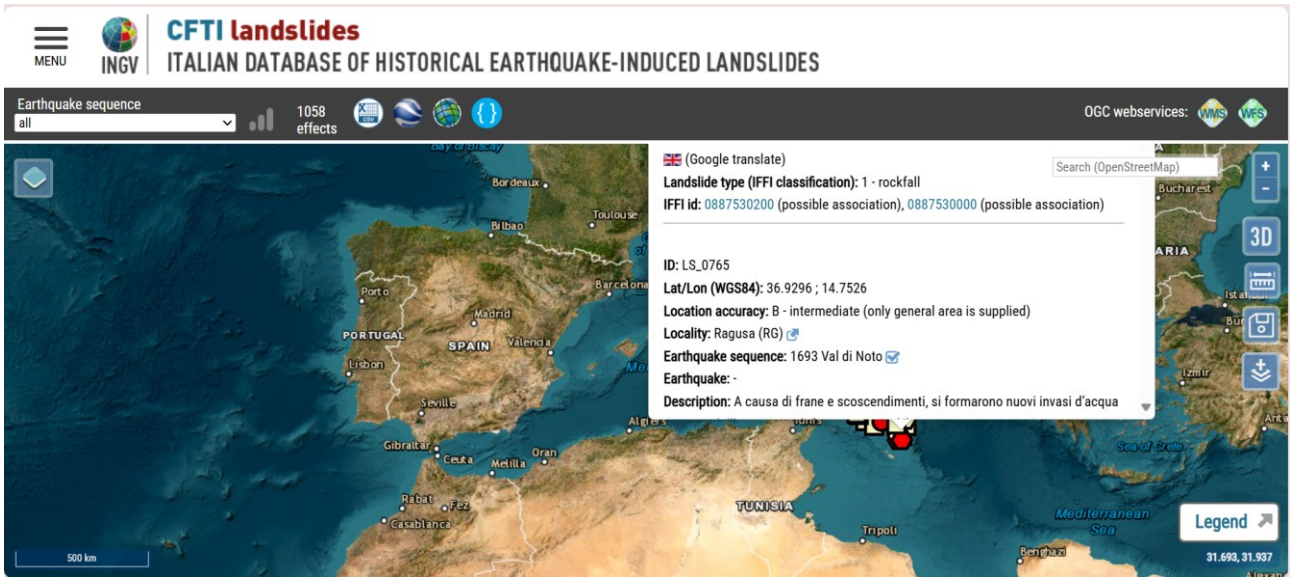

Figure 3.3 - WebGIS interface of the CFTI Landslides catalogue. *The platform displays georeferenced historical earthquake-induced landslides across Italy. When clicked, a selected entry displays information about the landslides as: id, coordinates, locality, location accuracy, earthquake and description. The pop-up window also shows the IFFI-compatible classification. The web interface also allows interactive visualization, search and tools selection. Image retrieved from CFTIlandslides*

1.2.2 OTHER INPUT DATA

UNIVERSITY OF INSUBRIA CASE-SPECIFIC DATASETS

Further data are collected from recent works from Insubria University, and particularly Bachelors, Masters and PhD theses focused on ESI-07 events and related EEEs effects. A total of four events are selected: Irpinia, 1980 (Pizza et al., 2023), Mt. Etna, 1971 (Camarda, 2021), Ischia, 2017 (Paganini, 2023, and Mt Etna, 2018 (Lazzati, 2020) events. These records are curated and digitized into GIS format.

1976 FRIULI INVENTORY (GOVI and SORZANA, 1977)

A geomorphological map, in both 1:25 000 and 1: 50 000 scale was compiled by Govi and Sorzana in 1977, after the 1976 Friuli Venezia Giulia seismic sequence (Govi M., 1977; Govi and Sorzana, 1977). The map is digitalized and a point/linear inventory in .shp format is constructed, in accordance with IFFI structure.

1.3 GENERAL WORKFLOW

To ensure methodological reproducibility, optimal management of data and harmonization to IFFI structure, a four-step workflow is implemented, based on collection, extraction, analysis and harmonization of EQUILs data (Fig. 3.4). The workflow is based on GIS environment (QGIS version 3.38.1) and .xls databases.

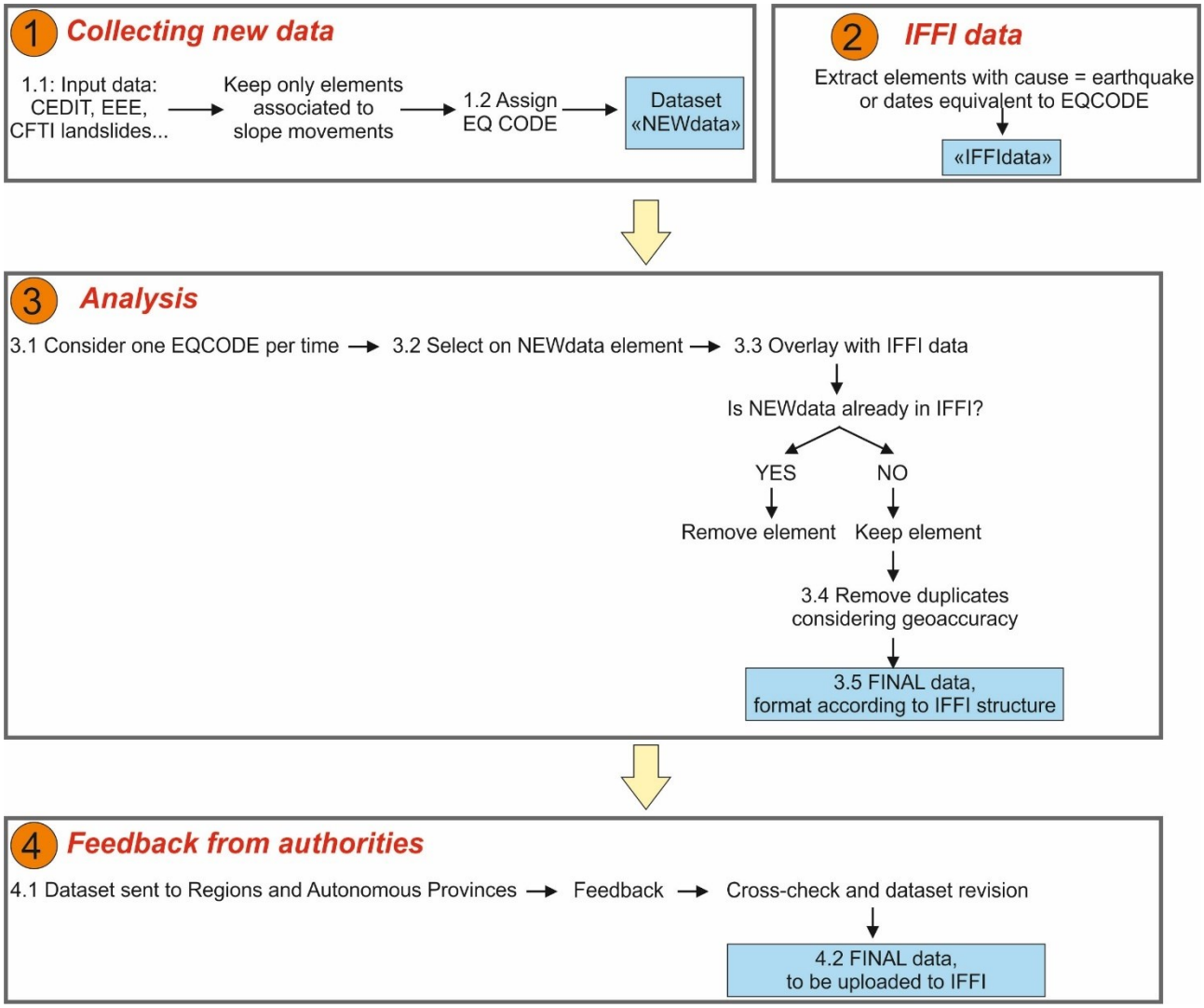

***Figure 3.4 - Workflow for the integration of EQUILs into the IFFI catalogue**. The diagram illustrates the four-step workflow adopted to harmonize external datasets (e.g., CEDIT, EEE, CFTI Landslides) with the IFFI structure. After collecting and characterizing preliminary EQUILs data (Step 1), corresponding IFFI entries are extracted (Step 2). A comparative analysis follows to eliminate duplicates and retain unique records based on spatial accuracy (Step 3). The final dataset is then validated with input from authorities prior to upload (Step 4).*

In step 1, all candidate entries from different sources (e.g., CFTI, CEDIT, Insubria works) pertaining to EQUILs are extracted. For each entry, a field named "EQCODE" is compiled, in order to assign the causative event or seismic sequence associated with the effect. The final output of the workflow is a temporary dataset "NEWData".

In step 2 the existing and updated IFFI catalogue is queried for records with matching or overlapping temporal references (same EQCODE) and classified as "earthquake-triggered" (i.e., cause = earthquake).

These entries are extracted from IFFI catalogue in order to assess redundancy and overlap with NEWdata extracted in step 1.

In step 3 each entry is analyzed individually to avoid duplication: this is done by selecting one "EQCODE" and one particular "NEWdata" element at a time. The entry is then compared with the IFFI data. A first deletion is done by considering if the "NEWdata" element is already included in the IFFI catalogue. The second deletion is based on location accuracy, source and description fields. In particular, when two entries from different datasets have a distance comparable to location accuracy, and no detailed description clarifies the presence of different slope movements or geomorphological settings, only one point is retained.

In step 4, the final harmonized dataset is submitted to regional geological authorities and ISPRA personnel for a complete review. Regional feedback serves as a final refinement of selected records and as a correction of administrative fields. Only after this ultimate validation process, is the final dataset approved and considered suitable for integration into the national IFFI catalogue.

RESULTS

2.1 EQUILS DATABASE HARMONIZATION

To ensure full interoperability IFFI catalogue, all EQUILs records from the final dataset are organized according to the official IFFI catalogue guidelines, which are characterized by 144 fields distributed across 19 thematic categories (Iadanza et al., 2021). These include both primitive (e.g., string, integer, date) and complex (e.g., coded lists, relational attributes) data types.

All mandatory fields are systematically compiled for each entry. Optional fields are filled when sufficient and reliable information are available from original sources. In agreement with ISPRA recommendations, particular emphasis is given to populating fields considered as critical factors for hazard analysis, traceability, and temporal discrimination.

In particular, the following key fields are compiled:

- Unique Identifiers: each record is assigned to an automatically generated "Landslide ID", as well as a "Sigle" field, which referred to the original dataset (e.g., CEDIT, EEE, CFTI).
- Date Fields: for each record, "date of activation" and "date of observation" are compiled, corresponding to the causative event, unless otherwise specified. "Date of compilation" for each record is uniformly assigned to 22/04/2024
- Institution and compiler: "Università dell'Insubria" is always inserted.
- Geolocation: administrative fields, and in particular "Region", "Province" and "Municipality", are extracted based on official ISTAT codes present in shapefiles. "Toponym" is extracted based on the original database (e.g., field "site" in CEDIT catalogue), while "Basin authority" is extracted from River Basin District Authority layer.
- Accuracy: "accuracy" field is classified into four standardized categories (i.e., Exact, 100 m, 1000 m, 10 000 m), based on source metadata and description of the EQUIL (tab. 3.1). This information is crucial during data merging, as we retained only records whose spatial difference fell within the defined geo-accuracy range. In older events, landslide locations often refer to nearby settlements or geomorphological features described in original historical sources.

Table 3.1 – Conversion table for accuracy field. *To harmonize different catalogue for IFFI "accuracy" field, related to geographic position, field descriptor are compared and listed, according to IFFI guidelines.*

IFFI "accuracy" field	CEDIT "class georef" field	CFTI Landslides	Irpinia 1980 (Pizza et al., 2023)
Exact	Site (GPS measurement): no error or negligible.		
100 m		A: excellent	A: high precision, metric accuracy
1000 m	Village (area extent of square km): average error 1 km. Town (area extent of tens of square km): average error 3 km.	B: intermediate	B: intermediate precision (100 m to 1 km)
10000m	City (area extent of hundreds of square km): average error 10 km. Province (area extent of thousands of square km, comparable to US county or England shire): average error 30 km	C: poor	C: indicative localization, km accuracy

- Description: field "description" is compiled referring to the input data sources
- Morphological and Geological Attributes "Type of movement" field is compiled whenever the information is available and extractable from relative fields in the original dataset or derived from the original description. Data are harmonized through a conversion table linking source definitions (e.g., CEDIT terms) to IFFI codes (e.g., slide, topple, flow, spread) (tab. 3.2). "Geology" is sporadically compiled, converting the definitions from CEDIT catalogue to IFFI codelist (e.g., limestone, marl, flysch, debris) (tab. 3.3).

Table 3.4 - Conversion table for type of slope movements. *CEDIT fields for type of slope movements are compared to description of IFFI guidelines and assigned to a specific id number.*

IFFI "type of movement" field	Description	CEDIT fields
0	n.d.	Landslides; fractures related to slides; ground changes; ground cracks; ground cracks related to slides
1	Fall/topple	Debris fall; earth fall; rock fall; rock topple; rock wedge slide
2	Rotational/translational slide	Debris slide; debris slump; earth slide; earth slump; rock slide; rock slump
3	Lateral spread	Earth spread
4	Slow earth flow	Earth flow
5	Rapid debris flow	Debris flow; mud flow
6	Sinkhole	
7	Complex	Rock avalanche
8	Deep-seated gravitational slope deformation	
9	Area affected by numerous rockfalls/topples	
10	Area affected by numerous sinkholes	
11	Area affected by numerous shallow landslides	

Table 5.3 - Conversion table related to geological unit. *CEDIT fields are compared to IFFI field description and then assigned to a specific ID number.*

IFFI "geology"	Description	CEDIT fields
1	Limestone	calcari pelagici, marne e travertini; calcari, dolomie
3	Marl	argille, argille e marne
4	Limestone-marly flysch	flysch calacreo marnosi
5	sandstone, sandstone flysch	flysch arenaceo-marnosi; Formazioni prevalentemente arenacee
6	shale, siltstone, pelitic flysch	argilliti, argilloscisti e complessi caotici; flysch pelitici
12	foliated metamorphic rock	Metamorfiti di medio grado
13	weakly foliated metamorphic rock	Metamorfiti di basso grado; Metamorfiti di vario grado; rocce metamorfiche
14	evaporite	Gessoso-solfifera, evaporiti; rocce gessose, anidridiche saline
16	conglomerate or breccia	Sabbie e conglomerati; sabbie, arenarie e conglomerati
17	debris	alluvioni, detriti e depositi glaciali
21	clay	Argille
22	mixed soil	Alluvioni e terreni misti

- State and Activity: The field "*Activity state"* is uniformly compiled with "active/reactivated/suspended" category (code 100), as all mapped landslides are coseismic, and, in consequence, active during the date of the seismic event. "Date of activation" is derived from "ID Earthquake" or "Earthquake code" fields. If referring to a seismic sequence, time interval is provided. This is particularly true for the 1783 Calabria sequence and data obtained from Govi map of the 1976 Friuli sequence (Govi and Sorzana, 1977; Govi, 1977).

- Observation and method: "Date of observation" is compiled referring to the date of the most recent observation of the landslide, here referred as the date of the event. Field "Method" is consistently compiled with "Historical data/Archive", referred to code 4. "Date source" is systematically filled with "archive\publications" categories. "Damaged elements" is systematically filled with "nd" category.

- Causative Process: the "*Causes"* field is always compiled with "earthquake" (code 22), which is categorized under physical processes.

- References and multimedia: "References" is compiled with bibliography when information derived from published works, while "Multimedia\Link info landslides" are compiled with URL derived from the original source

2.2 EQUILS FINAL DATASET

The final EQUILs dataset obtained for IFFI catalogue implementation contains 3483 point features (Fig. 3.5) and 1056 linear features (Fig.3.6), referring to 118 distinct historical, modern and instrumental seismic events, 19 Italian regions, and 1505 sites (Fig. 3.7). The dataset has been harmonized according to official IFFI structure (Iadanza et al., 2021), as outlined in paragraph 2.1. Spatially, EQUILs occurrences are widespread across the Italian territory, and particularly along mountainous area as the Apennine chain, the Alpine arc, and several seismically active areas distributed in central and southern Italy. Sardinia is the only region without any recorded events (Fig.3.5).

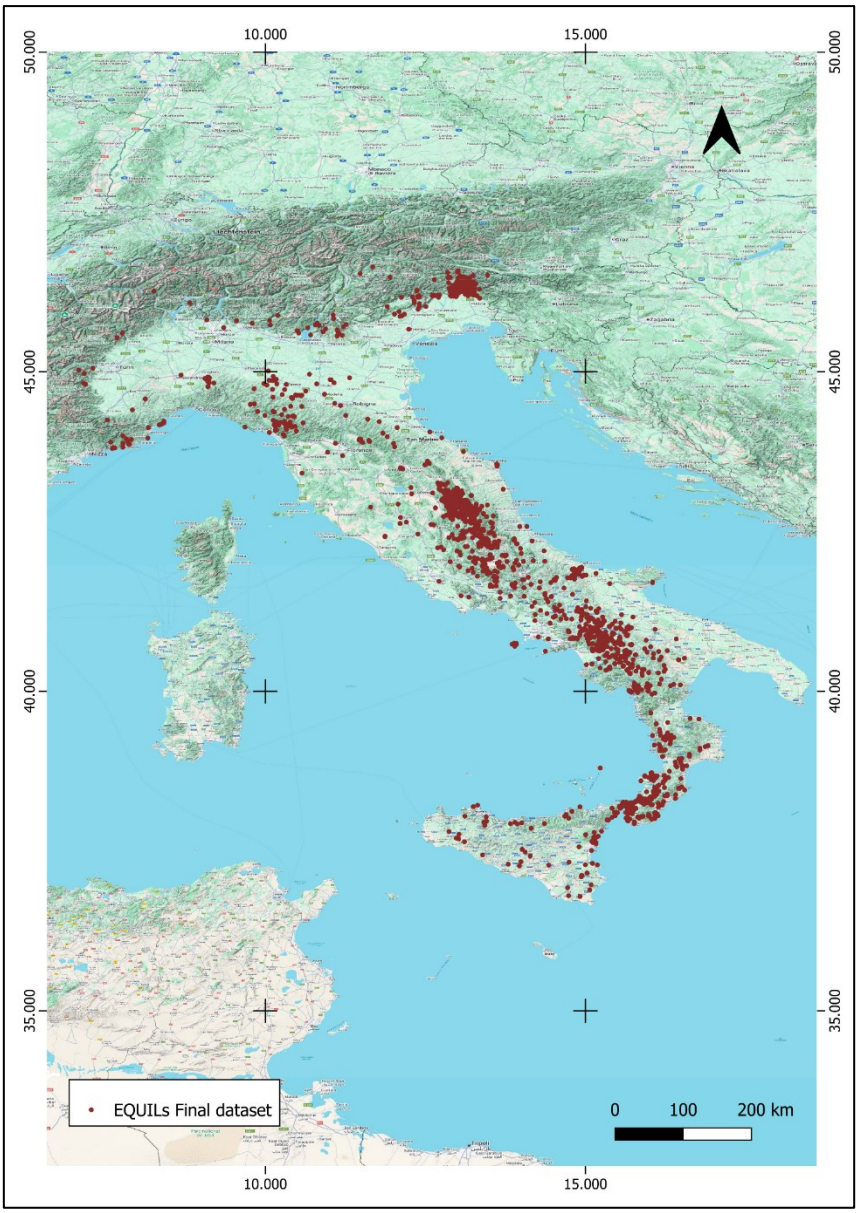

Figure 3.5– Spatial overview of the final EQUILs dataset*. All EQUILs obtained from different sources (e.g., EEE, CEDIT, CFTI catalogue, Govi, 1977 Map (Govi and Sorzana, 1977; Govi, 1977) and University of Insubria works) are displayed across the Italian territory with dark red dots.*

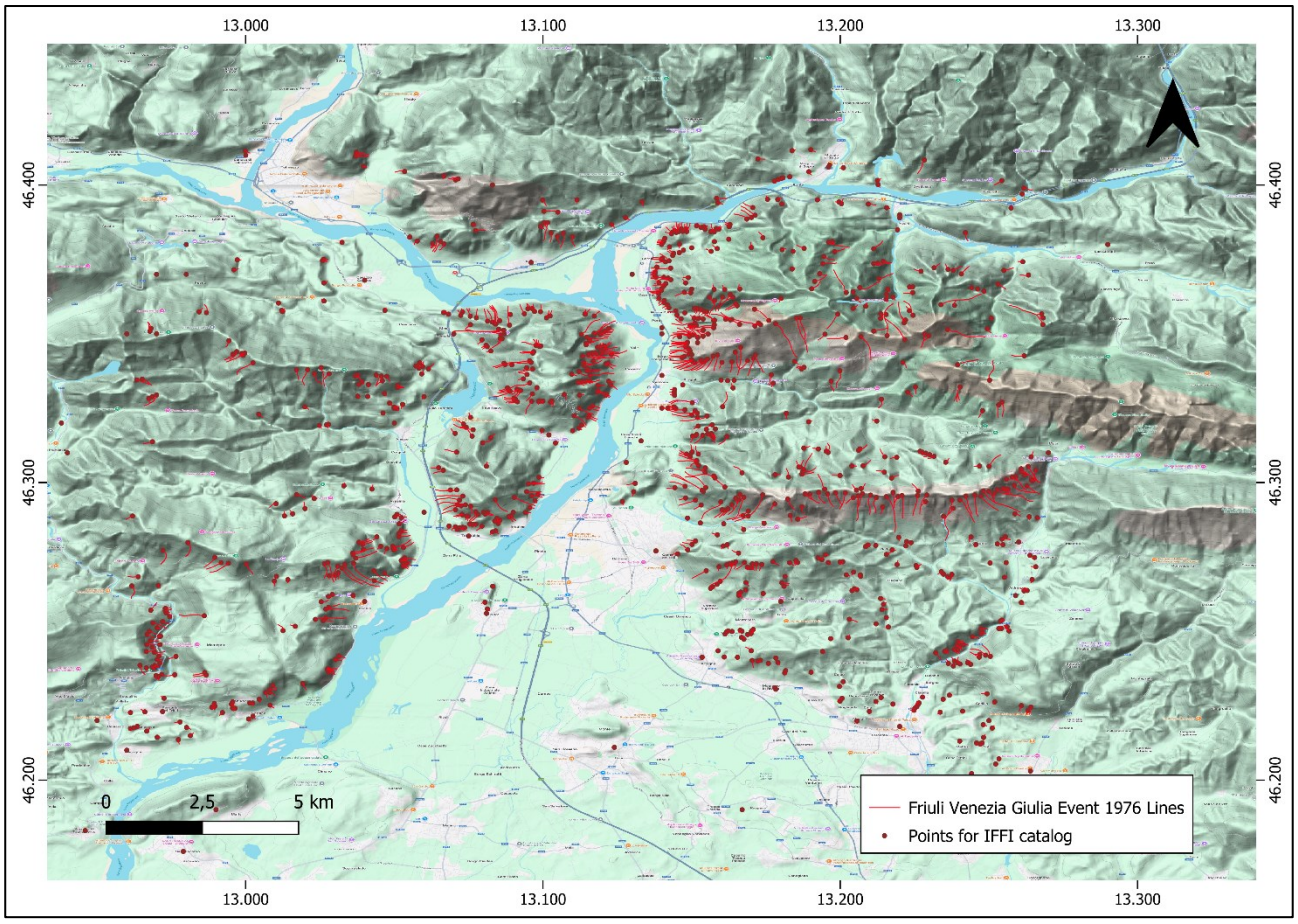

Figure 3.6 – Friuli, 1976 Earthquake dataset from Govi (1977) map. *After the digitalization of mapped line features, a complete dataset of the Friuli 1976 event is constructed, comprising both line and point features, in the map represented as red lines and dark red points.*

The most affected region is Friuli Venezia Giulia, with 1147 landslides (32.9% of the total). This predominance is largely due to the 1976 Friuli earthquake, which triggered widespread slope instability, registered in all sources consulted. Following Friuli Venezia Giulia, the regions with the highest data presence are Marche, with 424 EQUILs, and Umbria, with 344 EQUILs. Valle d'Aosta region is the least affected, with only one recorded event (Fig. 3.7).

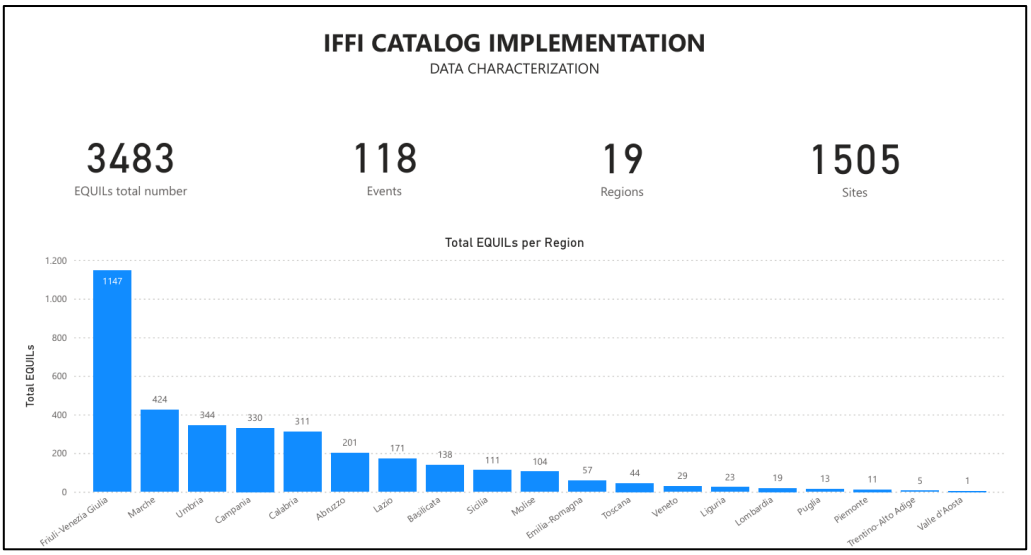

Figure 3.7 – Final dataset data characterization and regional distribution. *The final dataset comprises 3483 points, pertaining to 118 events, and distributed along 19 regions, and 1505 sites. Friuli Venezia Giulia region shows the highest number of EQUILs, followed by Marche and Umbria, while Valle d'Aosta region registers only one record, resulting as the least affected.*

From the total of 3483 point features, 1732 originated from the CEDIT catalogue (49.7%), 1043 from the Govi, 1977 map (29.9%), 293 from the CFTI catalogue (8.4%), 251 from University of Insubria works (7.2%), and 164 from the EEE catalogue (4.7%) (Fig. 3.8).

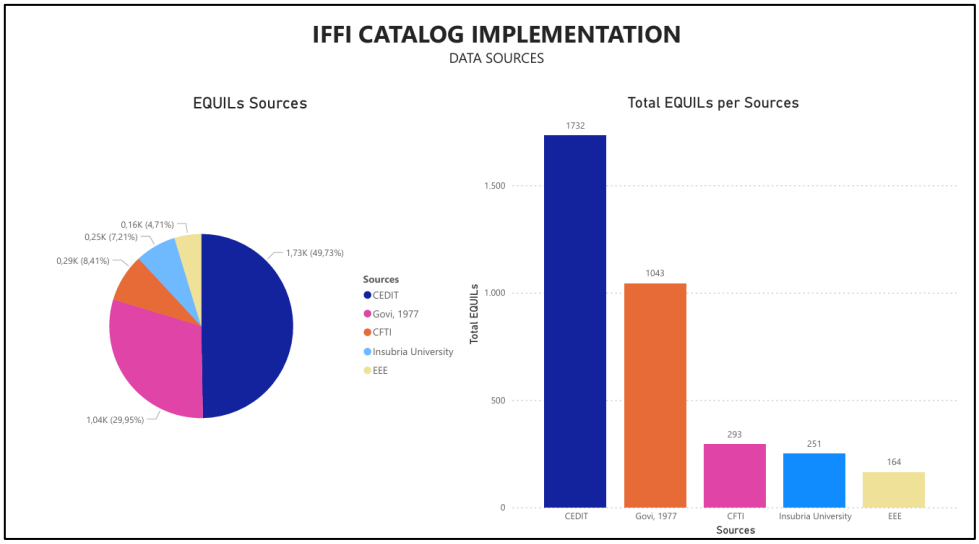

Figure 3.8 – Data sources characterization. *The final dataset integrates three catalogues (i.e., CEDIT, EEE, CFTI catalogue) alongside with Govi, 1977 map (Govi and Sorzana, 1977; Govi, 1977) and University of Insubria works (Pizza et al., 2023; Camarda, 2021; Paganini, 2023, and Lazzati, 2020). CEDIT accounts for the majority of data (1,732 points, 49.7%), while the EEE catalogue has the smallest contribution (164 points, 4.7%).*

The dataset covers a temporal range from 117 BC to 2019 (Fig. 19). Early records are sparse, while from 1000 AD onwards, the number of documented events gradually increases, with a marked acceleration from the

XIX century. The period between 1900 and the present contains most of the records, showing a constant growth on available data (Fig.3.9).

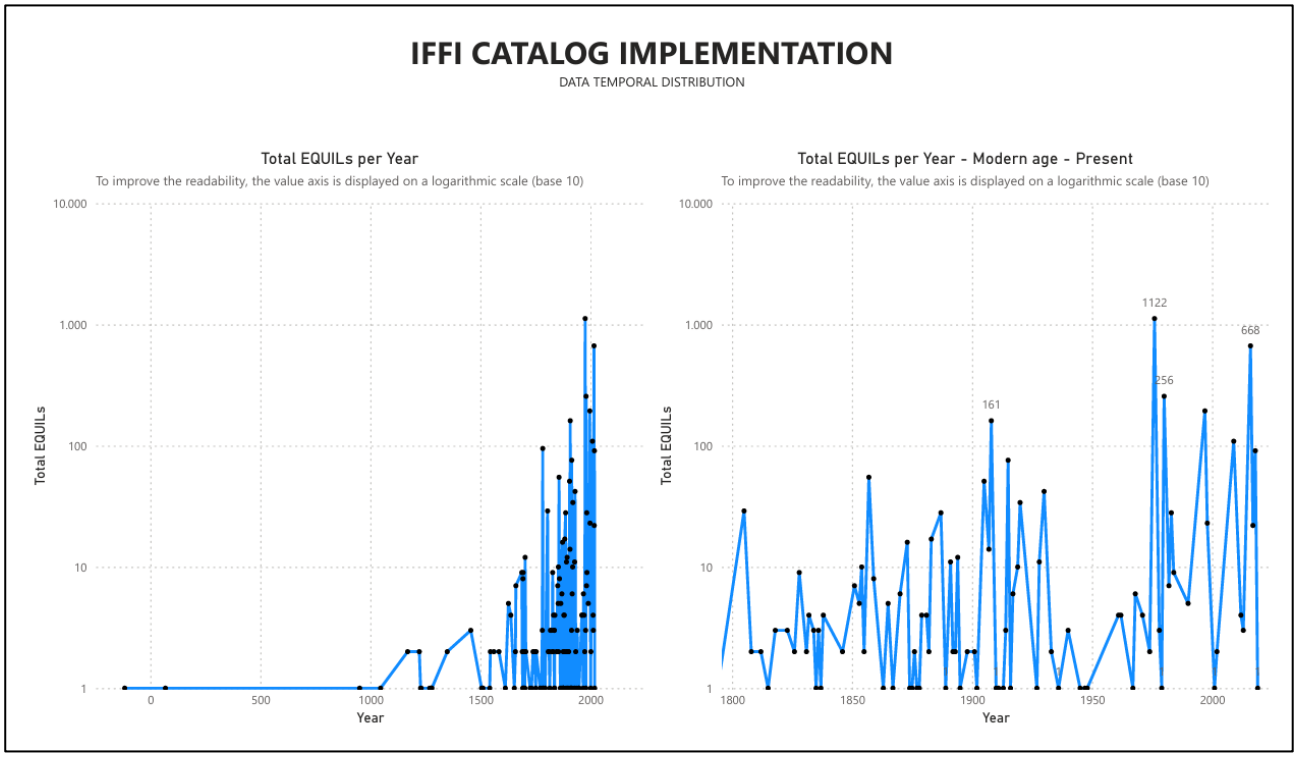

Figure 3.9 - Temporal distribution of data. *EQUILs data are present from 117 BC to 2019. A significant increase in documented events occurs after 1000 AD, with sustained growth in modern times, corresponding to XIX century. The largest concentration of records occurs from 1900 onwards.*

Regarding landslide types, seven categories are identified in the dataset (Fig. 3.10). The most frequent category is "nd" (not determined), which accounts for 2179 records (62.56% of the total). The second most frequent type is "fall/topple", with 952 records (27.33%), followed by "rotational/translational slide" with 309 records (8.87%). The less represented categories are "slow earth flow" (26 records; 0.75%), "complex landslides" (9 records; 0.26%), "rapid debris flow" (5 records; 0.14%), and "lateral spread" (3 records; 0.09%).

The lithological classification of the dataset includes 14 categories (Fig. 3.11). The most represented category is "n.d" (i.e., not determined), with 1859 records (53.37% of the total). This outcome reflects the objectives of the present phase of the study conducted, which was primarily devoted to the compilation and harmonization of the EQUILs database. A systematic lithological characterization, similar to the classification of movement types discussed in the previous paragraph, would represent an added value for the dataset, but it would require a dedicated study, beyond the scope of this stage. Among the classified records, "limestone" is the most common lithology, with 893 records (25.64%), followed by "sandstone/sandstone flysch" with 230 records (6.60%), and debris with 114 records (3.27%). Other relevant categories include "conglomerate or breccia" (112 records; 3.22%) and "marl" (87 records; 2.50%). The least represented lithologies are "clay" (5 records; 0.14%), "evaporite" (11 records; 0.32%), and "foliated metamorphic rock" (11 records; 0.32%).

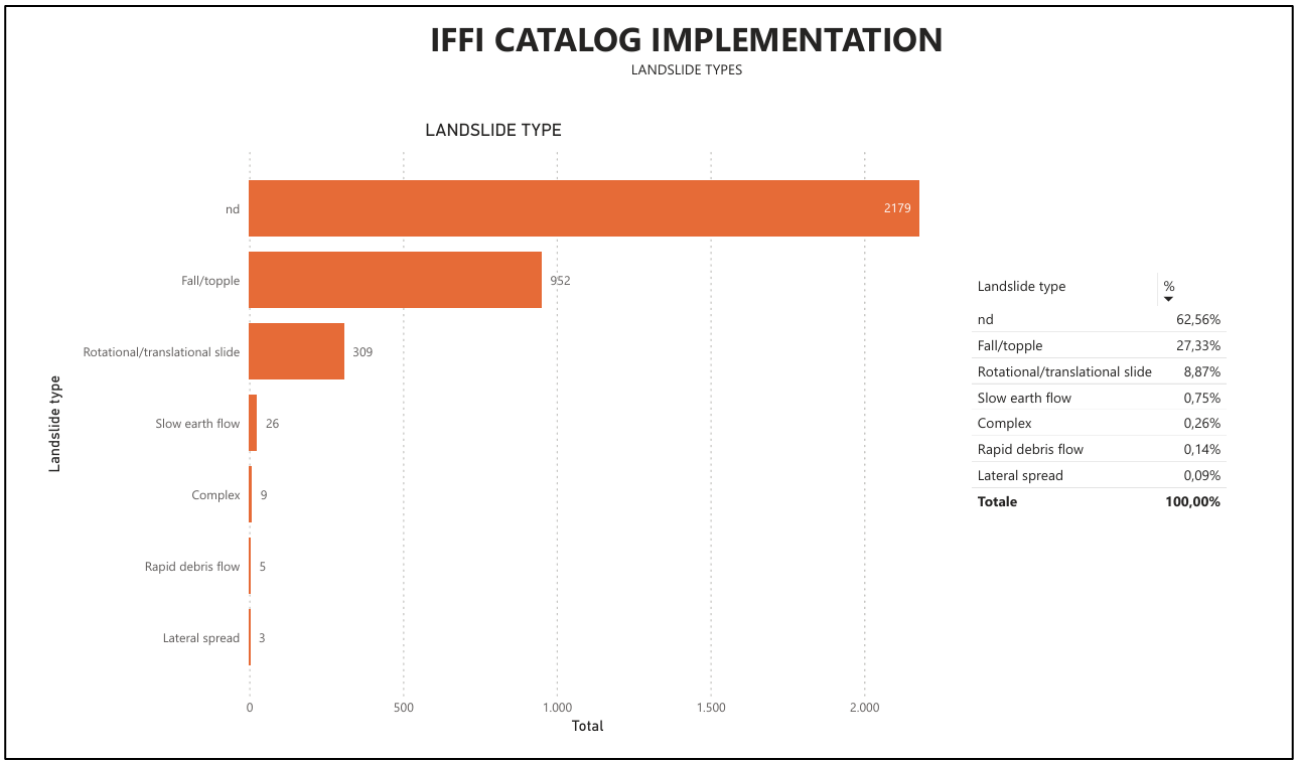

Figure 5 - Landslide types in the final dataset. *The "nd" (not determined) category is the most represented (2,179 records; 62.56%), followed by fall/topple (952; 27.33%) and rotational/translational slide (309; 8.87%). All other categories account for less than 1% of the total.*

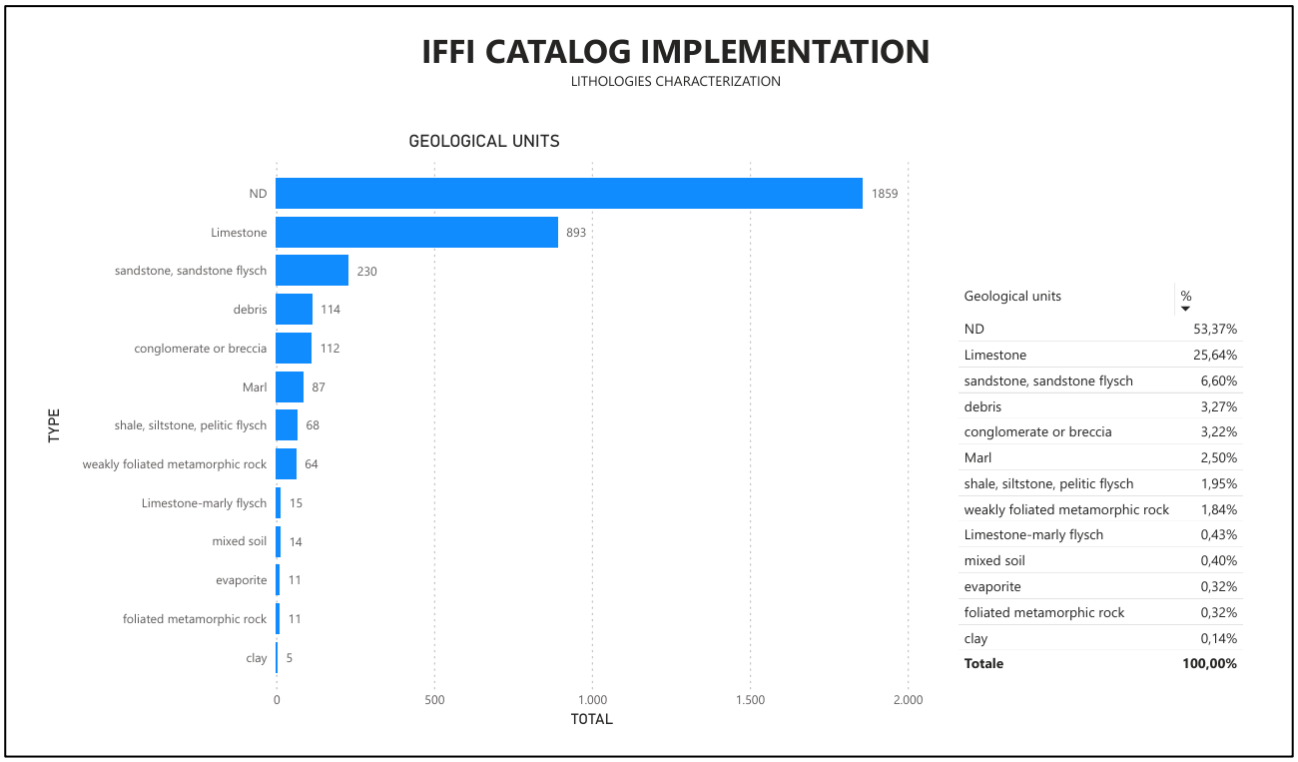

Figure 3.11 – Lithological characterization of the dataset*. The "n.d." category is the most represented (1,859 records; 53.37%), followed by limestone (893; 25.64%) and sandstone/sandstone flysch (230; 6.60%). Clay is the least represented lithology, with only 5 records (0.14%).*

DISCUSSION

3.1 IFFI FINAL DATASET CHARACTERIZATION

The characterization of the final EQUILs dataset highlights important aspects regarding spatial accuracy, temporal coverage, and completeness of the thematic classification applied, each reflecting the heterogeneity of the original data sources and their intrinsic characteristics.

From a spatial distribution perspective, the accuracy of mapped EQUILs resulted to be highly variable. Older events, and particularly those derived from historical sources such as written testimonies, narratives description, and early observational accounts, often bear location uncertainties in order of several kilometers. Such uncertainties are intrinsic to the original references, which are typically produced without applying geodetic control or precise geographic referencing (Tab.4). Conversely, more recent events, associated with higher-quality sources, such as field surveys, aerial photography, high-detailed description or remote sensing, are generally georeferenced with high precision, often within a few meters. This spatial variability directly impacts the applications of the dataset. While it can be used for regional- and\or national scale analyses of seismic-induced slope instability, fine-scale spatial assessments, such as seismic microzonation or site-specific hazard mapping, could be more challenging, and should only be attempted after a systematic positional revision is undertaken.

In terms of temporal coverage, the final dataset contains records that span from 117 BC to 2019, providing an exceptionally long observational window for EQUILs in Italian territory. The temporal distribution of data, reveals sparse documentation for Antiquity and Middle Ages periods, reflecting the limited availability of historical records and the often-anecdotal nature of early seismic events (Tab.3.4).

Table 3.6 – Examples of description for historic earthquakes. *It is worth noting that for older events, anecdotal and descriptive sources are typical.*

ID	YEAR	DESCRIPTION
INS0046	1688	Il monte detto Gisini si spaccò, e quasi metà monte staccandosi con furore sprofondò nel letto della valle detta Carnevale, restando sotto la massa portentosa tre mulini con dentro molta gente.
INS0070	1693	Fu vista da un frate cappuccino, in un luogo tra Fano e Montereale, scuotere violentemente quattro di quei colli, e rotolare giù pietre molto grosse.
INS0066	1693	La cima del monte posto sopra Posta crollò con gran fragore e caddero i sassi in tale quantità da ostruire per lo spazio di due miglia la strada che portava ad Antrodoco...
INS0069	1693	Nella pianura di Ville di Fano tre impetuose valanghe di roccia formarono un lago che a fine giornata scomparve
INS0067	1693	Un monte chiamato del Grillo... è scomparso e una grande fontana che si trovava sulla cima di un altro monte si è notevolmente ridotta di quota. E altri due monti più bassi... sono diventati uno solo

The number of documented seismic events gradually increases from the XIX century. This observed rise reflects the expansion of systematic geological investigations, enabled by the rising knowledge of Earth Sciences, the foundation of national scientific institutions and consequent application of methodological post-seismic surveys (e.g., field surveys, georeferencing, usage of topographic maps). The XX century marks a further step in data availability and accuracy, driven by the advent of instrumental seismology, which

facilitated standardized post-earthquake reconnaissance protocols, and the increasing use of aerial photography and remote sensing techniques. Consequently, the apparent growth in EQUILs occurrence through time is strongly influenced by historical biases versus technological advances.

3.2 LANDSLIDE TYPE AND GEOLOGICAL UNITS' PRESENCE

The final dataset analysis of Landslide Type and Geological Units fields shows how the latter are characterized by strong heterogeneity and by a substantial presence of records for which the type of landslide and geological unit cannot be determined (i.e., "n.d." entries). To understand their distribution and the factors influencing the presence or absence of landslide and geological unit characterization, fields are analyzed across the complete dataset and compared between the different source catalogues (i.e., CEDIT, EEE, CFTI catalogue, Insubria University works, Govi 1997 map) (Fig. 3.12).

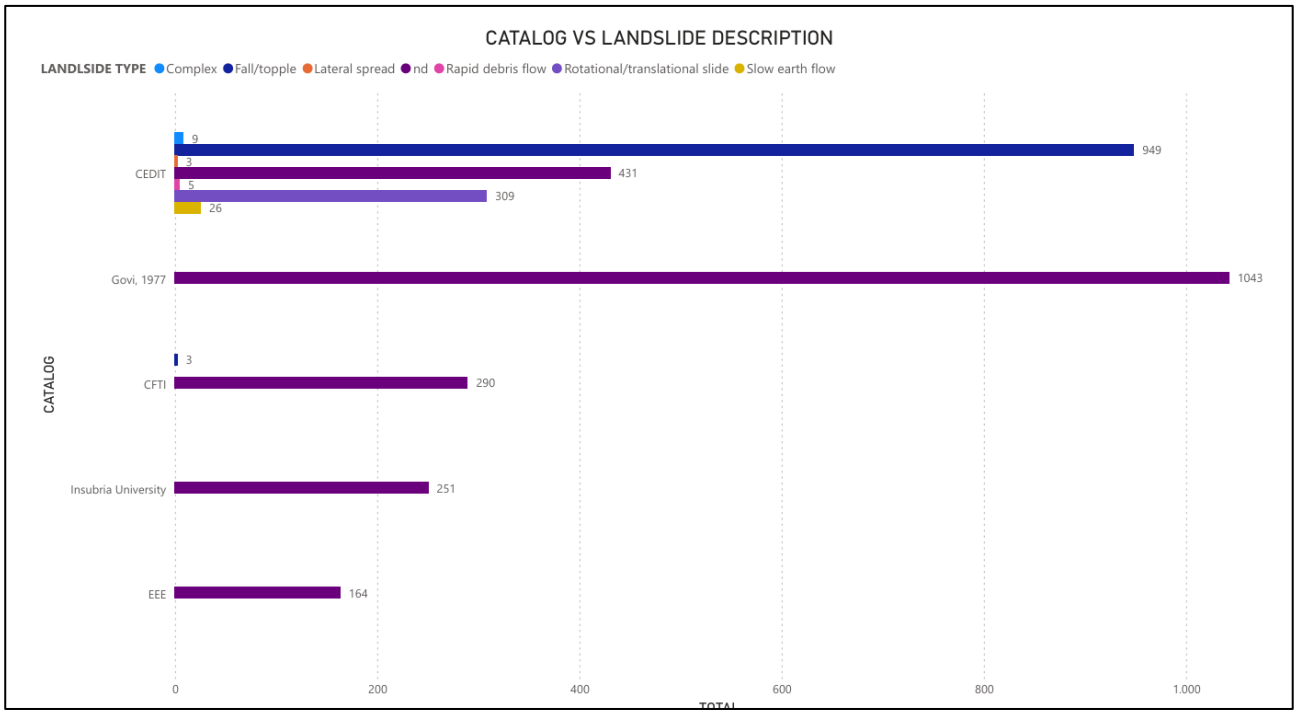

Figure 3.12 – Landslide description versus catalogue *. The comparison shows how CEDIT catalogue is the most detailed and thematically characterized, respect to type records registered across other sources.*

Among all the inventories examined, the CEDIT catalogue stands out as the source with the most consisted and diversified regarding classification of landslide types, showing a substantial reduction in the proportion of "n.d." entries compared to other inventories. By contrast, other sources are entirely devoid (i.e., EEE, CFTI catalogue, University of Insubria works and Govi map, 1977) or marginally (i.e., CFT catalogue) characterized by classified entries (Fig. 3.12). This reflects how these inventories, although valuable for documenting spatial and temporal occurrence, could limit their standalone usability, and increase the need for post-processing and data enrichment.

The same approach is applied to investigate the distribution of Geological units across the dataset. The distribution is compared across catalogues, revealing the same pattern observed for landslide types: the CEDIT catalogue provides a complete and diversified classification, whereas other inventories are characterized by a near-total predominance of "n.d." entries (fig.3.13).

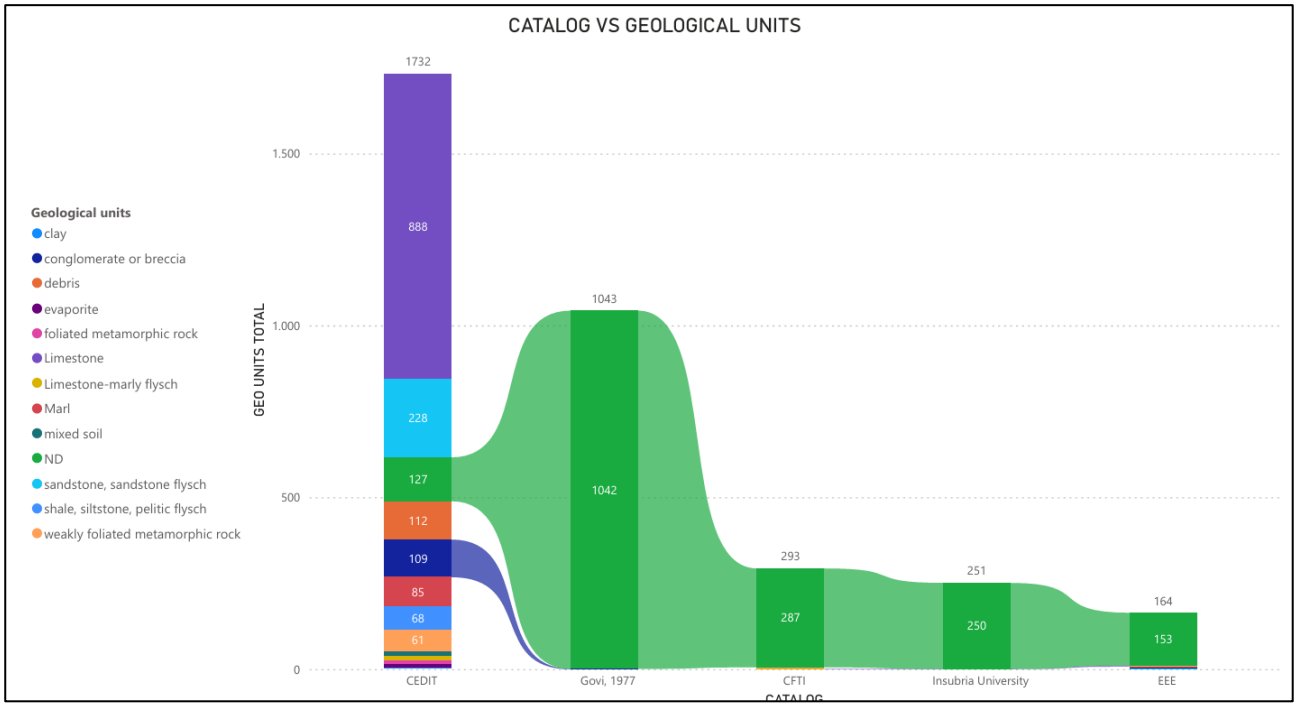

Figure 3.13 – Geological units versus catalogue. *The comparison shows how CEDIT catalogue contains a complete characterization, in sharp contrast to all the other inventories.*

The analysis confirms that source quality is the primary determinant of thematic completeness. The morphological and lithological gaps observed in most catalogues largely reflect the characteristics of the original inventories, which were often compiled with heterogeneous standards, limited field documentation, or without or limited systematic geological mapping. In this respect, it is important to stress that the present work had a compilative scope: the effort was devoted to collecting, harmonizing, and making existing datasets interoperable, rather than to improving their thematic completeness through new field checks or retrospective classifications. Consequently, the database preserves both the strengths and the limitations of its source materials.

These limitations may introduce biases in statistical and susceptibility analyses, particularly when aggregating data from sources with different levels of detail, which can lead to an overrepresentation of non-defined records. Addressing such issues would require a dedicated effort for retrospective harmonization or field validation, which is an objective that falls outside the scope and resources of this project. Nevertheless, the chosen approach ensured the construction of a comprehensive and interoperable database of EQUILs, which represents a solid baseline for future work. The outcome should therefore be regarded as a first step,

preliminary in some respects but essential for highlighting gaps, guiding further investigations, and supporting the continuous update and refinement of national inventories such as IFFI.

CONCLUSION

In this study, a final dataset of EQUILs to be integrated within the Italian Landslide Inventory (IFFI) is constructed. The dataset is built through a systematic review and harmonization of multiple independent sources, including CEDIT, CFTI, the EEE Database, and original contributions from the University of Insubria. A total of 3483 EQUILs record are compiled, covering a time span from 117 BC to 2019, all distributed across the Italian territory. Friuli Venezia Giulia is the region with the highest number of EQUILs recorded, and CEDIT catalogue is the source from which most of the data are collected. The spatial distribution of the dataset highlights clustering in seismically active regions, particularly along the Apennines and in areas affected by large earthquakes. The utility of the study lays in the systematic integration and standardization of heterogeneous data and sources, ensuring compatibility with IFFI catalogue. At the same time, the compilation reveals gaps in the spatial and temporal coverage of available records, underlining the importance of continued efforts in historical source revision, field documentation, and the use of innovative tools such as remote sensing and citizen science.

Overall, the final dataset provides a useful step towards exploring potential linkages between EEEs and national landslide inventories. Its integration within IFFI enhances the documentation of EQUILs and improves the reliability of macroseismic characterization. Future applications of this dataset include the validation of ESI-07 intensities, the constant update and reconstruction of seismic events through EQUILs evidence, and the extension of this methodology to other national and international inventories.

CHAPTER 4

ESI-07 GRID METHOD: A FIRST APPLICATION TO EQUILs INVENTORIES

INTRODUCTION

EQUILs are among the most destructive geological hazards triggered by seismic events, posing a significant threat to human lives, settlements, and infrastructures (Keefer, 1984; Rodriguez et al., 1999). Based on the catalogue compiled by Marano et al. (2010), which includes events from 1900 to 2008, landslides accounted for approximately 70% of all earthquake-related deaths not directly caused by ground shaking. This underlines the critical role of reliable EQUILs inventories for hazard characterization, susceptibility modeling, and macroseismic assessment (Harp et al., 2011; Xu, 2015a; Bornaetxea et al., 2023).

In recent years, the availability of well-constrained EQUILs inventories has rapidly increased, providing fundamental data for research and land planning at both global and regional scales (e.g., Schmitt et al., 2017; Iadanza et al., 2021; Zhao et al., 2023). The access to a high number of EQUILs inventories is granted by dedicated platforms, among which the one managed by the United States Geological Survey (USGS; Schmitt et al., 2017; Tanyas et al., 2017) plays a pivotal role. Typically, EQUILs inventories are analyzed in terms of landslide number density (LND) and landslide area percentage (LAP), which depict the spatial distribution and intensity of slope failures across affected territories.

Despite their widespread availability, EQUILs inventories have not yet been fully exploited for intensity assessment using the Environmental Seismic Intensity (ESI-07) scale (Michetti et al., 2007). A first attempt to link LND and LAP metrics to ESI-07 intensities was proposed by Ferrario (2022), who introduced a grid-based methodology where the affected area is divided into 1 km^2 cells, and LND, LAP, and ESI-07 values are assigned to each grid element.

Building on this approach, the present study applies the grid-based methodology to 40 EQUILs inventories related to 33 earthquakes worldwide, primarily derived from the USGS catalogue. The analysis provides: a) the first empirical equations relating ESI-07 intensity to LND and LAP, demonstrating that LAP is the more robust metric; b) an evaluation of the influence of earthquake magnitude and faulting style on the metrics; and c) an assessment of epistemic uncertainties associated with input data (i.e., landslide inventory) and volume calculations. Results show that the characteristics of the inventory (i.e., how landslide polygons are delineated) introduces much higher uncertainty into the process compared to the selection of a specific area-volume conversion equation. Furthermore, to validate the method, results are compared with independent ESI-07 data, i.e., published epicentral intensities and isoseismals. The findings confirm the robustness and reliability of the proposed procedure across diverse tectonic settings and climatic conditions. The linkage between ESI-07 intensities and traditional landslide metrics offers a novel way to exploit EQILs inventories for intensity assessment. The grid-based approach tested here demonstrates this potential and could be extended to other EEEs, enhancing its versatility and its value for macroseismic studies.

The content of this chapter is largely based on the publication of Muccignato E. and Ferrario M.F., (2025), Exploiting EQUILs inventories for macroseismic assessment using the environmental seismic intensity (ESI-07) scale, published in Frontiers in Earth Science.

MATERIALS AND METHODS

2.1 MATERIALS: LANDSLIDE INVENTORIES

As input data, the global EQUILs catalogue managed by the US Geological Survey (USGS) is used, which serves as a centralized repository that adopts a standardized format (Schmitt et al., 2017; Tanyas et al., 2017). Point inventories and datasets with fewer than 50 mapped landslides are not considered, as these often show limited spatial coverage and variability, thus compromising the robustness of method. By applying this threshold, a total of 36 polygonal inventories from the USGS catalogue is retrieved. Additionally, 4 inventories mapped by Ferrario, 2022a; Ferrario et al., 2024 are included, bringing the total to 40 inventories, which refers to 33 earthquakes. For 6 of these earthquakes, multiple inventories are available, consequently, these case histories are used to evaluate the different sources of uncertainties in the workflow.

The dataset contains 430 996 EQUILs in total. The selected inventories vary significantly in size, spanning several orders of magnitude in terms of landslide number: the two largest inventories are the Wenchuan inventory, compiled by Xu et al., (2014a) which includes 197 481 EQUILs, and the inventory of Li et al., (2014), of 69 606 EQUILs. Together, they account for 62% of the total. The smallest inventory includes 52 landslides from the Cappellades, Costa Rica earthquake (Ruiz et al., 2020).

Most of the inventories are from tropical regions, either in Asia or Latin America, although the dataset also contains a few inventories outside the tropics (Tab. 4.1; Fig. 4.1). The number of earthquakes and associated landslides, categorized according to magnitude class or earthquake rupture kinematics, is presented in Figure 26. Moment magnitude range between Mw 5.3 and 9.1, with most of the events falling within the Mw 6.0 – 8.0 range. Regarding earthquake rupture kinematics, 50% of the selected inventories correspond to thrust earthquakes, while 42% are associated with strike-slip earthquakes (Fig.4.1).

Table 4.1 - Summary information of the inventories used in the current research, presented in chronological order of occurrence. *Information includes location, country (ISO2 code list), moment magnitude, depth and kinematics, together with the number of landslides and dimension of the investigated area. Data were sourced from the USGS EQUILs catalogue or, for the Davao and Sabah inventories, from the corresponding studies cited in the text. The dimension of the investigated area is provided by the authors or extracted as minimum bounding geometry (see text for details). ID marked as "a, b" refers to events for which multiple inventories are available.*

ID	Locality	Country	Date	Mw	Depth (km)	Kin	Lat	Long	Nr. LS	Inv. area (km2)	References
1	Guatemala	GT	1976/02/04	7.5	5	S	15.324	-89.101	6224	4687	Harp et al. (1981)
2	Mammoth Lakes	US	1980/05/25	5.9	6.0	NDC	37.696	-118.750	4027	2030	Harp et al. (1984)
3	Coalinga	US	1983/05/02	6.5	9.6	T	36.232	-120.312	2980	1537	Harp and Keefer (1990)
4	Valle de la Estrella	CR	1991/04/22	7.6	10	T	9.685	-83.073	1643	1678	Marc et al. (2016)
5a	Northridge	US	1994/01/17	6.7	18.2	T	34.213	-118.537	11111	4044	Harp and Jibson (1995)
5b	Northridge	US	1994/01/17	6.7	18.2	T	34.213	-118.537	5064	293	Townsend et al. (2020)
6	Kobe	JP	1995/01/16	6.9	21.9	S	34.583	135.018	2353	175	Uchida et al. (2017)
7	Jueili	TW	1998/07/17	5.7	12.6	T	23.407	120.736	847	763	Huang (1999)
8	Denali	US	2002/11/03	7.9	4.9	S	63.517	-147.444	1579	14611	Gorum et al. (2014)
9	Lefkada	GR	2003/08/14	6.3	10	S	39.160	20.605	274	168	Papathanassiou et al. (2013)
10	Nigata-Chuetsu	JP	2004/10/23	6.6	16	T	37.226	138.779	4862	410	Sekiguchi and Sato (2006)
11a	Kashmir	PK	2005/10/08	7.6	26	T	34.539	73.588	2930	3845	Basharat et al. (2016)
11b	Kashmir	PK	2005/10/08	7.6	26	T	34.539	73.588	2424	2236	Sato et al. (2007)
11c	Kashmir	PK	2005/10/08	7.6	26	T	34.539	73.588	1453	1453	Basharat et al. (2014)
12	Kiholo Bay	US	2006/10/15	6.7	38.9	N	19.878	-155.935	383	146	Harp et al. (2014)
13a	Aisen	CL	2007/04/21	6.2	36.7	S	-45.243	-72.648	538	1460	Sepulveda et al. (2010)
13b	Aisen	CL	2007/04/21	6.2	36.7	S	-45.243	-72.648	517	1148	Gorum et al. (2017)
14a	Wenchuan	CN	2008/05/12	7.9	19	T	31.002	103.322	197481	75459	Xu et al. (2014a)
14b	Wenchuan	CN	2008/05/12	7.9	19	T	31.002	103.322	69606	37521	Li et al. (2014)
15	Eastern Honshu	JP	2008/06/13	6.9	7.8	T	39.030	140.881	4164	567	Yagi et al. (2009)
16	Cinchona	CR	2009/01/08	6.1	14	S	10.165	-84.197	4826	470	Ruiz et al. (2019)
17a	Haiti	HT	2010/01/12	7.0	13	S	18.443	-72.571	23567	3748	Harp et al. (2016)
17b	Haiti	HT	2010/01/12	7.0	13	S	18.443	-72.571	4490	2756	Gorum et al. (2013)
18	Tohoku-Oki	JP	2011/03/11	9.1	29	T	38.297	142.373	3475	39014	Wartman et al. (2013)
19	Gansu	CN	2013/07/21	5.9	8	T	34.512	104.262	2330	195,92	Xu et al. (2014b)
20	Sichuan	CN	2014/08/03	6.2	12	S	27.189	103.409	1024	233	Xu et al. (2015b)
21a	Nepal	NP	2015/04/25	7.8	8.2	T	28.231	84.731	17638	17568	Gnyawali and Adhikari (2017)
21b	Nepal	NP	2015/04/25	7.8	8.2	T	28.231	84.731	2645	18374	Zhang et al. (2016)
22	Sabah	MY	2015/06/04	6.0	10	N	5.987	116.541	5198	811	Ferrario (2022a)
23	Capellades	CR	2016/11/30	5.3	1.3	S	9.949	-83.807	52	13	Ruiz et al. (2020)
24	Milin	CN	2017/11/17	6.4	8	T	29.833	94.984	766	1428	Hu et al. (2019)
25	Papua New Guinea	PG	2018/02/25	7.5	25.2	T	-6.070	142.754	11607	24297	Tanyas et al. (2022)
26	Lombok	ID	2018/08/05	6.9	34	T	-8.258	116.438	4823	1798	Ferrario (2019)
27	Lombok	ID	2018/08/19	6.9	21	T	-8.319	116.627	9319	1798	Ferrario (2019)
28	Palu	ID	2018/09/28	7.5	20	S	-0.256	119.846	7063	3880	Zhao (2021)
29	Davao1	PH	2019/10/16	6.4	16	S	6.715	125.007	190	653	Ferrario et al. (2024)
30	Davao2	PH	2019/10/29	6.6	15	S	6.757	125.008	4737	1710	Ferrario et al. (2024)
31	Davao3	PH	2019/12/15	6.8	22	S	6.697	125.174	5666	1710	Ferrario et al. (2024)
32	Mesetas	CO	2019/12/24	5.7	10	S	3.450	-74.103	838	3102	Garcia-Delgado et al. (2021)
33	Puerto Rico	PR	2020/01/07	6.4	9	S	17.869	-66.827	309	741	Knoper et al. (2020)

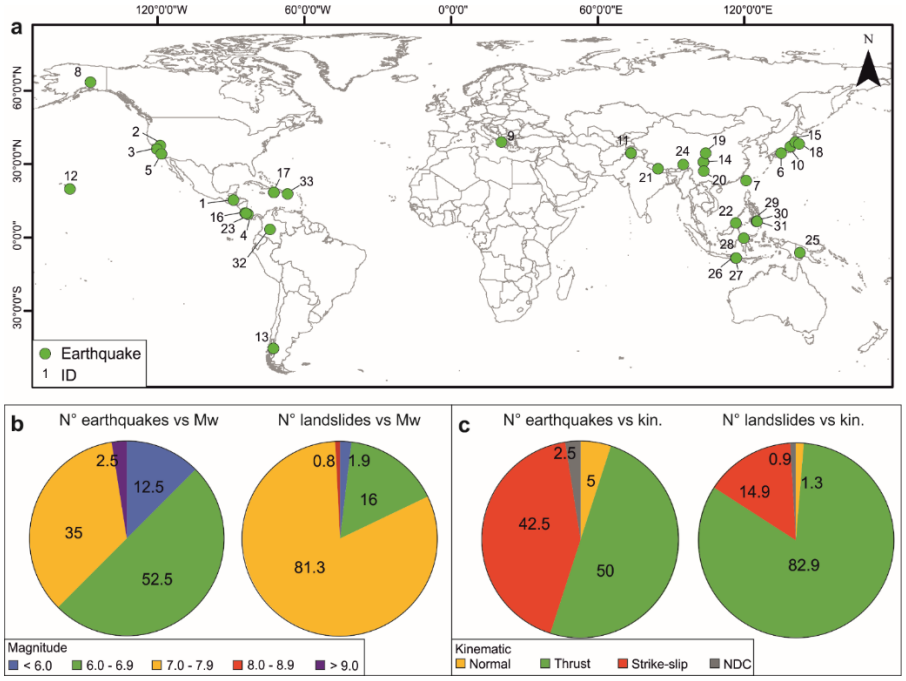

Figure 4.1 *– **Map with distribution of the investigated events and statistics.** a) map showing the locations of the investigated case studies; b) distribution of the number of earthquakes and number of landslides according to moment magnitude; numbers represent the percentage; c) distribution of the number of earthquakes and number of landslides according to earthquake kinematic; NDC: non-double couple.*

2.2 METHODOLOGICAL WORKFLOW

The workflow adopted in this study comprises five sequential steps (A-E), starting with data collection (step A), described in the previous section. Steps B-E are described in the following subsections: each step produces an output that can serve as input for further analyses (Fig. 4.2).

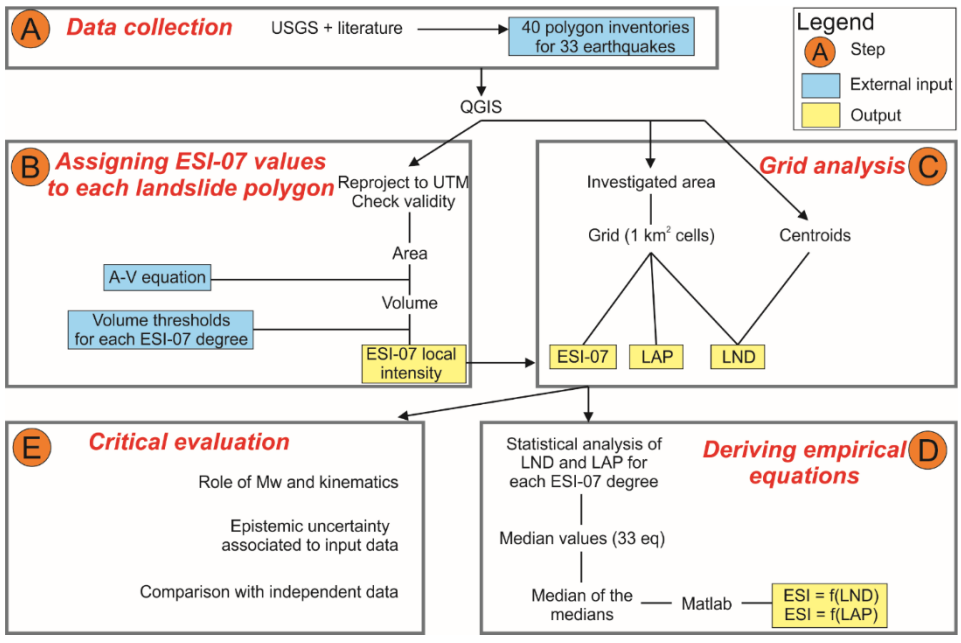

Figure 4.2 - Methodological workflow adopted in this study*. The flow chart consists of five subsequent steps (A-E); input data (blue windows) and outputs (yellow windows) are highlighted.*

2.2.1 STEP B: ASSIGNING AN ESI-07 VALUE TO EACH LANDSLIDE POLYGON

The EQUILs inventories in shapefile format are analyzed individually using QGIS software version 3.26.3. First, the data are reprojected into Universal Transverse Mercator (UTM) coordinates, adopting the correct UTM zone for each earthquake. Invalid geometries are checked using the "Check Validity" tool, and any invalid polygons is manually corrected. Invalid geometries account for a negligible amount of input data (0.8% of the polygons) and were consistently related to self-intersection errors. Consequently, the area of each polygon (in m^2) is computed, using the QGIS Field Calculator.

At this stage, two key external inputs are required to assign an ESI-07 value: A) an area-volume relationship and b) volume thresholds for each ESI-07 degree. Several area-volume (A-V) relationships are available in literature (e.g., Guzzetti et al., 2009; Larsen et al., 2010; Xu et al., 2016; Jaboyedoff et al., 2020; Yunus et al., 2023), which generally adopt the functional form of Equation 1:

$$V_i = \alpha \times A_i^{\gamma} \quad (1)$$

Where V_i is volume in m^3, A_i is the area of individual landslides in m^2, and α and γ are fitting coefficients.

These equations are derived from datasets linked to different triggering processes and encompass a wide range of environmental and climatic conditions (Tab. 4.2). For this study, the coefficients proposed by Larsen et al. (2010) are adopted as a baseline (i.e., α = 0.146 and γ = 1.332), but the epistemic uncertainty arising from different coefficient choices is also explored (see Step 5 in the following).

Table 4.2 - Area-volume conversion equations tested in this study. *The relationship proposed by Larsen et al. (2010, all types) is taken as a reference, while the other equations are investigated to evaluate the epistemic uncertainty.*

Eq.	α	γ	Notes	Reference
1	0.146	1.332	Global, all types	Larsen et al., 2010 (all)
2	0.186	1.350	Global, bedrock	Larsen et al., 2010 (bedrock)
3	0.257	1.145	Global, soil	Larsen et al., 2010 (soil)
4	0.074	1.450	Global, slide type, several triggering processes	Guzzetti et al., 2009
5	1.315	1.208	Subset of landslides triggered by 2008 Wenchuan earthquake	Xu et al., 2016

To manage ESI-07 volumetric values (Michetti et al., see App. 1.1) in QGIS, an unequivocal numerical thresholds is set (last column of Table 8). The thresholds set cover one order of magnitude for intensities VII to IX, while it must be noted that for intensity degrees X to XII the volume threshold is fixed (> 10^6 m^3), reflecting the critical saturation point of landslides in the ESI-07 framework (see App. 1.4). As a result, it is not possible to assign intensities higher than X based solely on individual landslides (Tab. 4.3).

Table 4.3 – Landslides volume thresholds. *Volume thresholds for ESI-07 intensity degrees VI to XII, as defined in Michetti et al. (2007, central column) and adopted in this study (right column).*

ESI-07 degree	Landslide volume (m3)	Volume thresholds adopted in this study
VI	Up to 10^3	< 1000
VII	10^3 – 10^5	>1000 - <100000
VIII	Typically 10^3 – 10^5, up to 10^6	>10000 - < 100000
IX	Up to 10^6	> 100000 - < 1000000
X	>10^6	> 1000000
XI	>10^6	> 1000000
XII	>10^6	> 1000000

2.2.2 STEP C: GRID ANALYSIS

The mutual relationships between ESI-07, LND and LAP values are investigated using a grid-based approach, similar to the method proposed by Ferrario (2022) and adopted by Sridharan et al. (2023). The grid is built as a shapefile composed of 1 km^2 square cells using the "Create Grid" tool in QGIS. The grid shapefile is generated with the same UTM coordinates as the landslide inventory. The grid extent is determined from the area originally investigated by the authors who realized the inventory, whenever this information is available. In contrast, if data is lacking on the mapped area, the minimum bounding geometry encompassing the mapped landslides is defined and used as the grid extent. This approach aligns with a similar methodology recently adopted by Marc et al. (2018) and Emberson et al. (2022). LND, LAP and ESI-07 values are then calculated for each 1 km^2 of the grid cell. Centroids of the polygons are extracted and counted in each grid cell, obtaining LND. For LAP evaluation, the proportion of each grid cell covered by landslide polygons is calculated, expressed as a percentage.

Intensity values are calculated by selecting the largest landslide for each 1 km^2 grid cell and keeping the corresponding ESI-07 value, following a procedure similar to those described by Ota et al. (2009), Silva et al. (2013) and Ferrario (2022a); thus, the ESI-07 value is determined by the single largest landslide within each grid cell. The output of Step C is a shapefile of 1 km^2 grid cells, each with three associated numerical fields: LND, LAP and ESI-07.

2.2.3 STEP D: DERIVING EMPIRICAL EQUATIONS

The output of Step C is exported into a spreadsheet and statistical analysis of the data are performed. For each ESI-07 degree, the mean and median LND and LAP values across all 40 landslide inventories are calculated. The next step involves deriving scaling relationships between ESI-07 intensity and either LND or LAP values. Notably, multiple inventories are available for 6 earthquakes (Northridge 1994, Kashmir 2005, Aisen 2007, Wenchuan 2008, Haiti 2010, Nepal 2015); to avoid double counting, only the most complete inventory in terms of number of mapped landslides and extent of the investigated area is retained. In this

way, from the 40 landslide inventories, 33 case studies are selected. The "median of the medians" is computed, by first investigating one single earthquake and determining the median LND and LAP for each ESI-07 intensity degree. Then, the median across all the earthquakes is calculated, ultimately obtaining one single LND and LAP value for each ESI-07 intensity degree. Data are imported in MATLAB and empirical regressions are derived using the Curve Fitter App. The functional form of the relationships is chosen based on the best-fit parameters, including R^2, adjusted-R^2, and root mean squared error (RMSE).

2.2.4 STEP E: CRITICAL EVALUATION OF THE RESULTS

As a final step, the results obtained are critically explored, focusing on three key aspects:

- Role of magnitude and kinematics. The eventual dependence of the proposed relations by creating subsets of case studies is investigated, categorized according to magnitude or type of earthquake (normal, reverse, strike-slip).
- Epistemic uncertainty associated with input data. Earthquakes with multiple available inventories are analyzed. This allows to assess how variations in original data (i.e., landslide polygons) and methodological choices (i.e., adopted A-V relation) influenced the results.
- Comparison with independent data. Case histories that are analyzed in terms of ESI-07 intensity are examined; results are compared with independent estimates of ESI-07 epicentral intensities (available for 15 earthquakes) and ESI-07 isoseismals (4 selected earthquakes).

RESULTS

3.1 TRENDS OF LAP AND LND WITH RESPECT TO ESI-07 VALUES

As example, the 2009 Cinchona event ESI-07 grid map is presented (Costa Rica, ID 16 in table 4.4) (Fig.4.3). In this case, the investigated area encompasses 502 cells, and the maps display the spatial distribution of ESI-07, LAP and LND values. The highest values are concentrated in the center of the area, and the distribution is fairly regular, with lower values observed toward the periphery of the area investigated. The relative frequency of LAP and LND values, categorized according to ESI-07 classes, shows that for lower intensities (ESI-07 VI and VII) LAP and LND exhibit low to medium values; ESI-07 VIII covers a broader range of LAP and LND values (Fig. 4.3d - 4.3e). Intensities IX and ≥ X show a different pattern: LAP is constrained to high values only (LAP > 4%), whereas LND encompasses nearly all the classes (i.e., about 20% of the cells with LND = 2 are categorized as ESI-07 ≥ X) (Fig. 4.3d - 4.3e). A comparable spatial distribution of LAP, LND and ESI-07 intensities is observed in all the inventories analyzed, confirming the general trend observed in the inventory of Cinchona earthquake. Results are reported in Appendix (App. 4.1).

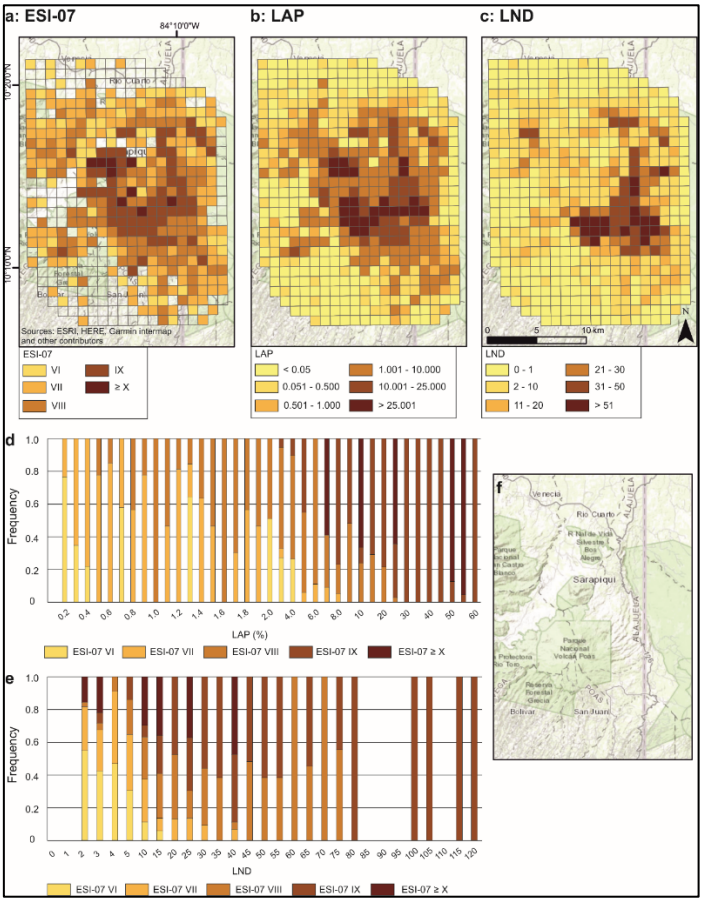

Figure 4.3 – Case example. *Example of the results obtained for the Cinchona (Costa Rica, ID 16) earthquake. Grid maps of ESI-07 (a), LAP (b) and LND (c) values are shown. Column plots represent the relative frequency of LAP (d) and LND (e) values, categorized according to ESI-07 intensity. Panel (f) presents the clean basemap, to visually inspect the local topography.*

To evaluate the consistency and repeatability of the procedure, each inventory is analyzed individually. Hypothetically, ESI-07 values should be positively correlated with either LAP or LND values. To evaluate the latter, the median LAP or LND value for each ESI-07 degree is computed (Tab. 4.4; Fig. 4.4). When multiple inventories are available for a single earthquake, only the most complete dataset is retained (i.e., with the highest landslide count and largest area investigated), to avoid double counting.

All the analyzed inventories provide consistent trends: as LAP or LND increases, so does the ESI-07 intensity. LAP values (Figure 4.4 a) show a steady increase over the entire range of intensities, moving from 0.06% at ESI-07 VI to LAP 24% at ESI-07 ≥ X. Additionally, a low dispersion is observed for ESI-07 VI to VIII, while a higher dispersion is observed for ESI-07 IX and ≥ X.

Regarding LND (Figure 4.4 b), a positive correlation is observed for ESI-07 VI to IX, with the highest density at ESI-07 IX (median LND 8 landslides/km^2), after which it decreases to 4 for ESI-07 ≥ X. The dispersion is greatest at intensity IX, with remarkable differences among individual inventories, especially for the Gansu earthquake (ID 19 in Table 4.1). The lower LND values for intensity ≥ X likely reflect a "physical" limitation: the largest landslides (volume > 10^6 m^3) correspond to an area of approximately 130 000 m^2 according to our baseline A-V relation. This constraint limits the number of large landslides that can fit within each cell of the 1 km^2 grid, thus fundamentally limiting the resulting LND values.

Table 4.4 – LAP and LND Summary. *Summary of the LAP and LND values for each ESI-07 intensity degree.*

ID	LAP VALUES					LND VALUES				
	ESI-07 VI	ESI-07 VII	ESI-07 VIII	ESI-07 IX	ESI-07 ≥ X	ESI-07 VI	ESI-07 VII	ESI-07 VIII	ESI-07 IX	ESI-07 ≥ X
1	0.04	0.34	1.69	7.04	22.25	1	2	3.5	4.5	4
2	0.02	0.50	3.19	10.38	23.93	1	2	6	8	7
3	0.01	0.45	2.03	5.81		1	5	13	20	
4	0.33	0.48	1.71	4.86		1	2	3	4	
5a	0.08	0.38	2.60	8.66	23.94	2	3	12	23	12
5b	0.09	1.03	4.19	12.45		2	11	26	34	
6	0.09	0.60	1.26			5	16.5	18		
7	0.04	0.39	1.46	5.04		1	1	3	3	
8		0.47	1.88	5.81	25.61		1	1	2	1
9			3.50	13.50			1	4	5	
10		1.00	6.00	14.50	24.00	2	5	29.5	32.5	23
11a		0.58	2.18	8.08	22.84		1	2	2	2
11b	0.07	0.29	1.93	8.49	23.49	1	2	6	8	11.5
11c		0.34	1.80	7.71	33.14		1	2	3	3
12	0.08	0.25	1.73	6.20	19.67	2	2	4	4.5	5
13a	0.05	0.38	1.54	6.33	30.66	1	1	2	2	4
13b		0.40	1.39	7.18	34.84		1	1	3	4
14a	0.06	0.33	2.31	19.28	40.64	1	2	6	23	20
14b	0.06	0.35	2.62	14.20	37.02	1	2	5	12	11
15	0.09	0.52	3.17	12.47	20.95	2	5	12	16.5	1
16	0.07	0.38	3.04	17.28	47.66	2	4	12	21.5	9
17a	0.06	0.46	2.48	9.07	18.03	3	8	18	24	11
17b	0.05	0.37	1.70	5.83		2	3	7	11	
18	0.03	0.18	0.88	3.86		1	1	2	1	
19	0.06	0.60	3.75	8.42		3	22	43	44	
20	0.06	0.30	1.90	12.32	27.04	1	2	5	10	12
21a	0.04	0.29	1.64	6.54	24.08	1	2	5	6	6
21b	0.104	0.39	1.31	5.28	18.01	1	2	2	2	1
22			2.00	14.00	33.00	1	3	8	29	26
23		0.40	2.25	11.08			1	4	5	
24	0.11	0.36	1.66	9.32	36.61	2	1	2	5	2
25	0.07	0.31	1.70	9.09	35.52	1	2	3	5	4
26	0.09	0.56	2.45	9.62	13.51	2	6	18	22	18
27	0.11	0.42	2.02	6.42	12.67	2	4	15	22	3
28	0.06	0.38	1.96	8.61	25.40	1	2	6	10	1
29	0.06	0.27	1.01			1	1	2		
30	0.08	0.38	1.77	8.86	12.16	1	3	6	17	3
31	0.08	0.38	1.77	8.62	12.16	1	3	7	19.5	3
32	0.09	0.32	2.14	4.77		1	2	6	8.5	
33	0.03	0.32				2	4			
Median	**0.07**	**0.38**	**1.93**	**8.61**	**24.00**	**1**	**2**	**6**	**8.5**	**4**

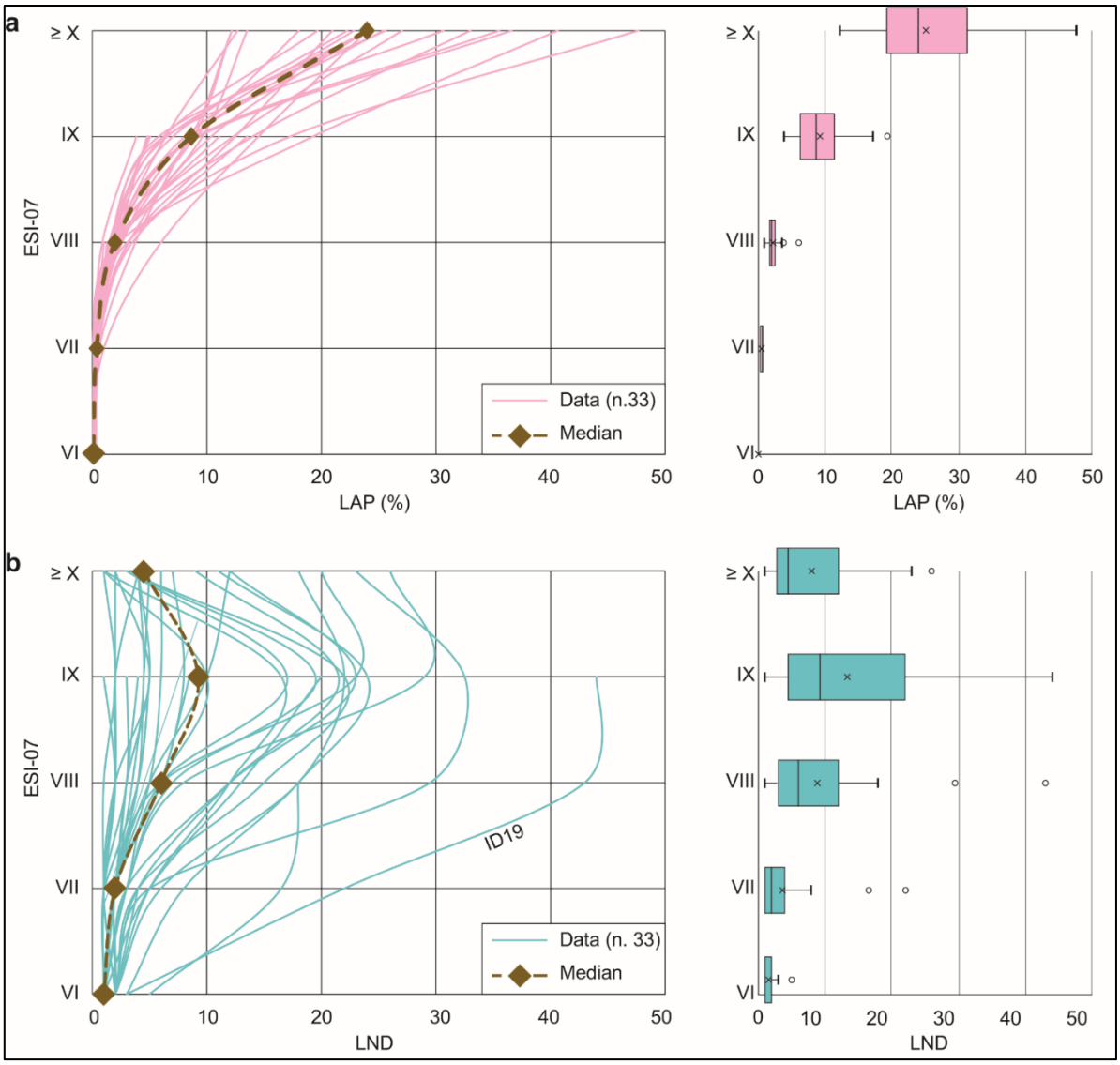

Figure 4.4 - Statistics of LAP (a) and LND (b) values with respect to ESI-07 intensity. *All the individual case studies are represented as thin lines, while the dotted line represents the median value for each ESI-07 degree. To the right, boxplots are presented, reporting average (crosses), median (line), 1 standard deviation (boxes), 2 standard deviations (whiskers) and outliers (small circles).*

3.2 DERIVING THE EMPIRICAL REGRESSIONS

By analyzing the case histories, consistent results over a wide range of magnitudes and territorial settings are obtained. Consequently, empirical regressions linking ESI-07 values to either LAP or LND are derived.

The median of the 33 earthquakes is considered, and various functional forms were tested. Following the observation that LND values increase in the ESI-07 range VI to IX, while ESI-07 ≥ X has a lower LND value, data are fitted over the range of intensities VI to IX. For LAP values, data are fitted over the entire range of intensities, i.e., ESI-07 VI to ≥ X. Both power-law and logarithmic forms consistently give the best fitting results; for LAP values, power-law model perform slightly better than the logarithmic law. Power-law functional form is selected for both LAP and LND, prioritizing LAP dataset , with priority given to the LAP

dataset, as it is more suitable for deriving ESI-07 values (Fig.4.5; Table 4.5). The equations have the general formula:

$$ESI07 = a \cdot x^b \quad (2)$$

Where x stands for LAP or LND, a and b are fitting coefficients.

LAP is considered as a better descriptor: indeed, LND depends more strongly on the quality of input data and is a more local metric, being more influenced by the topography, geo-mechanical characteristics and mapping style of the user who generated the inventory. One common issue in landslide inventories is the amalgamation of multiple landslides into a single polygon (Marc and Hovius, 2015); which can significantly affect the computation of LND but does not affect LAP values. Nevertheless, in the case of point inventories, LND is the only suitable option. Therefore, empirical equation for LND is provided as well.

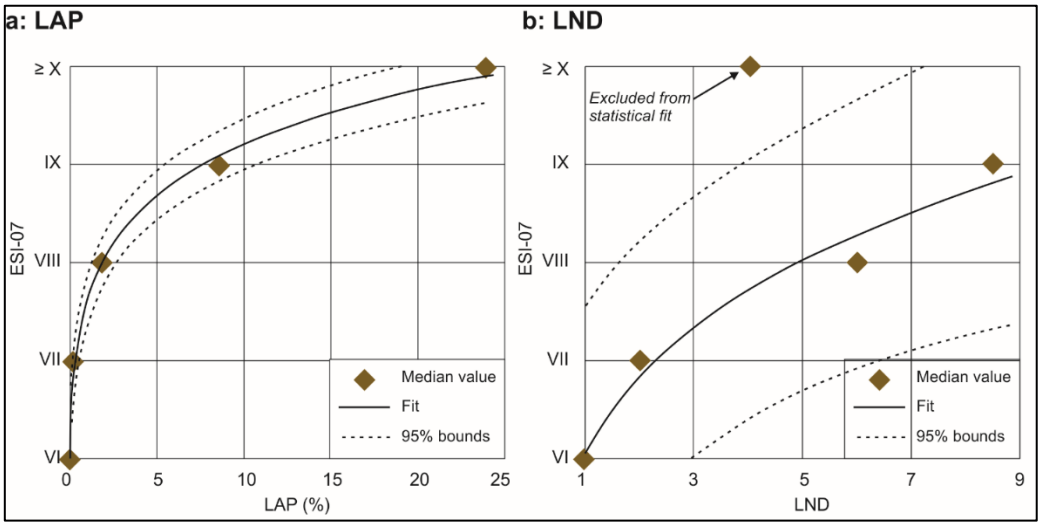

Figure 4.5 – Distribution graph of median LAP and LND. *Median LAP (a) or LND (b) values (brown diamonds) for each ESI-07 intensity class. The black lines are the empirical regressions derived in this study.*

Table 4.5 – Coefficients and parameters for the equation derived. *Fitting coefficients and goodness-of-fit parameters for the equations derived in this study and referring to Equation 2. RMSE: root mean squared error.*

Equation	a	b	R^2	Adj. R^2	RMSE
LAP	7.57 ± 0.1	0.09 ± 0.01	0.99	0.99	0.07
LND	6.06 ± 0.9	0.1751 ± 0.1	0.97	0.96	0.28

DISCUSSION

4.1 INVESTIGATING THE ROLE OF EARTHQUAKE MAGNITUDE AND KINEMATICS

The number and dimension of triggered landslides are influenced by several factors, related to terrain (e.g., elevation, slope), as well as climatic, geological and seismological parameters. A plethora of studies have analyzed susceptibility factors, even focusing on LAP or LND metrics (e.g., Chang et al., 2021; Dai et al., 2023; Shao et al., 2023). In this study, the analysis is limited to seismological and tectonic factors, specifically moment magnitude and earthquake kinematics, to evaluate the possibility of deriving empirical regressions dependent on these two factors. Landslide inventories are grouped according to either magnitude or kinematics, looking for eventual differences in the obtained results. One hypothesis tested is whether a higher magnitude, which corresponds to a greater energy release, leads to higher LAP and LND values. Similarly, different earthquake kinematics may vary in their effectiveness in triggering landslides. Fault geometry, the type of fault movement and the presence or absence of surface faulting indeed all influence the distribution and dimension of the area affected by coseismic landslides (Gorum et al., 2014; Xu, 2014c).

As already observed for results, when comparing LAP and LND to 3 classes of moment magnitude, LAP values exhibit a much narrower distribution than LND (Fig. 4.6). No clear dependence on magnitude is found for LAP values, as the 3 magnitude classes considered here have very similar median LAP values and overall distribution. LND showed lower values for stronger earthquakes (Mw class 7.0 - 7.9) with respect to weaker earthquakes. The result is not unexpected when considering the general scenario: stronger earthquakes tend to mobilize substantial masses of material, resulting in fewer but more extensive landslides, a key factor that reduces the overall LND value.

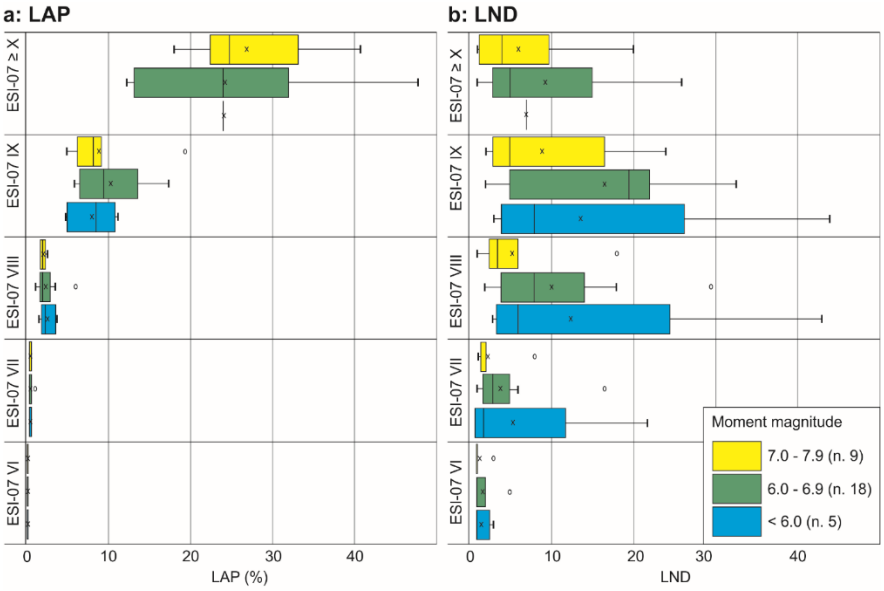

Figure 4.6 - Distribution of LAP (a) and LND (b) values within each ESI-07 intensity degree. *Data have been categorized according to moment magnitude. The boxplot reports average (crosses), median (line), 1 standard deviation (boxes), 2 standard deviations (whiskers) and outliers (small circles).*

LAP and LND distribution is then compared to earthquake kinematics. A robust evaluation can be conducted for thrust and strike-slip earthquakes (15 case histories each), while normal earthquakes are not adequately represented (2 cases only). LAP again provides more informative results than LND. Thrust events tend to have slightly lower LAP values, especially for intensity classes IX and ≥ X (Fig.4.7).

Overall, results show that magnitude and kinematics exert a limited influence on LAP and LND values. A clear step in LAP values is noticed, especially from ESI-07 intensity VII to intensity ≥ X, indicating that intensity classes are characterized by increasing LAP values. This confirms that LAP provides the most robust relationship.

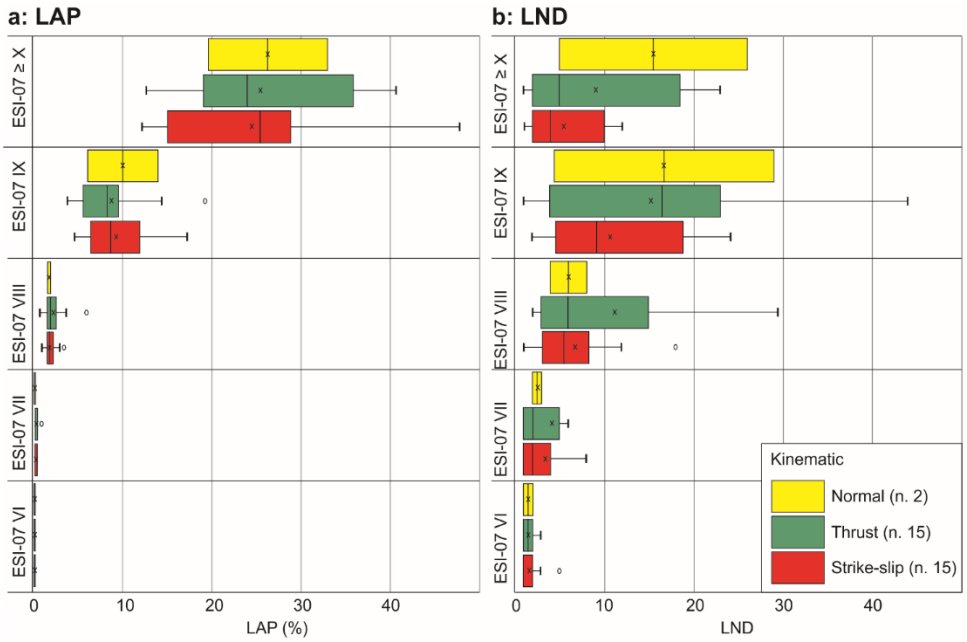

Figure 4.7 - Distribution of LAP (a) and LND (b) values within each ESI-07 intensity degree. *Data have been categorized according to earthquake kinematics; the boxplot reports average (crosses), median (line), 1 standard deviation (boxes), 2 standard deviations (whiskers) and outliers (small circles).*

4.2 SOURCES OF EPISTEMIC UNCERTAINTY

The ESI-07 intensity value assigned to each landslide fundamentally depends on two key factors: the area of the polygon and the choice of an area-volume scaling relation. Both elements represent sources of epistemic uncertainty, as they are dependent on the mapping procedure and the methodological choices made by the users. These aspects are analyzed, taking advantage of the six earthquakes where multiple landslide inventories are available.

The inventories may have been realized by different research groups (e.g., Harp and Jibson (1995) and Townsend et al. (2020) for the 1994 Northridge earthquake) or represent successive refinements of an initial inventory (e.g., Basharat et al., 2014, 2016 for the 2005 Kashmir earthquake). In some cases, the number of mapped landslides and the dimensions of the investigated area are similar (e.g., Sepulveda et al. (2010) and

Gorum et al. (2017) for the 2007 Aisen earthquake), while in other cases they are sensibly different (e.g., Gorum et al. (2013) and Harp et al. (2016) for the 2010 Haiti earthquake). The inventories are produced with different methods (manual vs semi-automatic mapping) and using pre- and post-event images with variable resolution.

Five different A-V relations are applied, selected based on their derivation from global databases (Larsen et al. 2010; Guzzetti et al., 2009), their focus on earthquake-triggered landslides or their relevance to study areas examined in this work (Xu et al., 2016). For each A-V relation, the frequency of landslide polygons belonging to each ESI-07 intensity degree is calculated (Fig. 4.8). Results show how input data (i.e., landslide inventories) are the first-order element in driving the ESI-07 assessment, while the selected A-V relation plays a secondary role. Indeed, in almost all the plots (apart from the Aisen and partly of the Kashmir events) the lines are clustered by color, representing the different inventories (Fig.4.8). The critical role exerted by different inventories on derived products was investigated by Bornaetxea et al. (2023) in a susceptibility study in Spain, where they demonstrated that altering the input landslide inventory leads to significantly different results.

The A-V relation by Xu et al. (2016) and Larsen et al. (2010, soil) deviate from the other equations, especially for ESI-07 intensity VI. For the Northridge, Haiti and Nepal events a sensible difference in the number of small landslides (ESI-07 intensity VI) is observed between the inventories, pointing to a different degree of completeness.

Results support the arguments made by Ferrario (2022) and Sridharan et al. (2023), who claim that the choice of a given A-V relation has limited implications on the final output. Thoroughly delineating coseismic landslides and selecting the most appropriate A-V scaling relation, which is consistent with the local terrain and geologic conditions, represents critical factors. It is worth noting that ESI-07 classes are broad in terms of volume, which helps smooth out overall variability. If the inventories are instead used for purposes other than intensity assessment, for instance to calculate the amount of mobilized sediments or denudation rates, a well-constrained A-V relation is a crucial input.

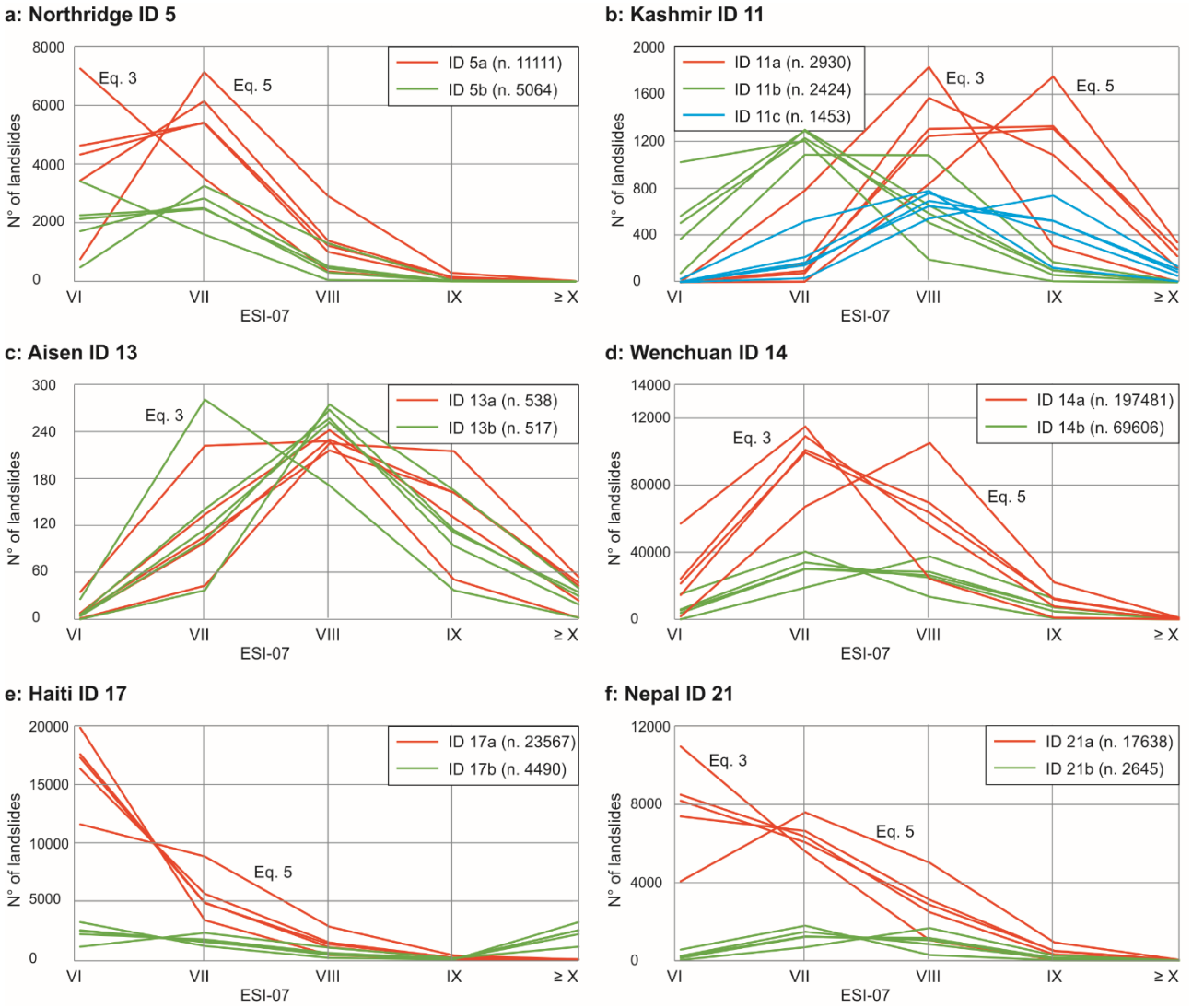

Figure 4.8 - Landslide vs A-V equations. *number of landslides fitting within each ESI-07 intensity class by adopting different A-V equations (Eq. 3: Larsen et al. (2010) soil type; Eq. 5: Xu et al., (2016)).*

4.3 COMPARISON WITH INDEPENDENT ESI-07 DATA

To evaluate the reliability and applicability of the ESI-07 methodology developed in this study, the results are compared with independent data, searching for those events that are already analyzed in terms of ESI-07 scale. A recent review of the earthquakes analyzed with the ESI-07 scale (Ferrario et al., 2022b) included a dataset of more than 150 events with an available ESI-07 epicentral intensity (I0) estimate. A total of 15 earthquakes from this review overlap with the dataset (Tab.4.6). The data are extracted from Ferrario et al. (2022), supplemented with the most recent studies of Sridharan et al. (2023; ID 25 in table 1), Naik et al. (2023; ID 28 in table 4.1, in this case isoseismals are from an unpublished thesis, and Ferrario et al. 2024 (ID 29-31).

In the last column of Table 4.6, the highest ESI-07 value assigned in our study is reported (i.e., deriving from the analysis of slope movements only) together with the percentage of cells with such value. Results show

that the ESI-07 I0 is generally higher than the estimate derived from slope movements; this is given by: a) intensities XI and XII cannot be assigned from slope movements and b) widespread EEEs other than slope movements that may have been triggered. Additionally, slope movements on emerged lands are analyzed, while some of the earthquakes had their epicenter offshore (e.g., ID 18 Tohoku-Oki, which triggered a devastating tsunami). In a few cases (ID 10, 30 and 31) landslides returned to an ESI-07 value slightly greater than I0; nevertheless, the percentage of cells with such anomalous outcome is less than 0.5%. It is worth nothing that ESI-07 I0 is estimated based on the amount of permanent ground deformation (surface faulting and tectonic uplift/subsidence) or on the dimensions of the area affected by secondary effects (Michetti et al., 2007); thus, the analysis of slope movements alone provides no clue for ESI-07 I0 estimation.

Table 4.6 - Earthquakes analyzed in the study. List of events independently analyzed using the ESI-07 intensity scale, with an available estimate of ESI-07 epicentral intensity (I0).

ID	Locality	Date	ESI-07 I0	Highest ESI-07 from landslides and relative percentage
1	Guatemala	1976/02/04	XI	≥ X (3.7%)
6	Kobe	1995/01/16	X	VIII (2.0%)
8	Denali	2002/11/03	XII	≥ X (11.2%)
9	Lefkada	2003/08/14	VIII-IX	IX (32.1%)
10	Nigata-Chuetsu	2004/10/23	IX	≥ X (0.4%)
11	Kashmir	2005/10/08	XI	≥ X (0.4-9.5%)
14	Wenchuan	2008/05/12	XII	≥ X (1.3-2.0%)
18	Tohoku-Oki	2011/03/11	XII	IX (1.0%)
25	Papua New Guinea	2018/02/25	XI	≥ X (5.1%)
26	Lombok	2018/08/05	X	≥ X (0.1%)
27	Lombok	2018/08/19	X	≥ X (0.2%)
28	Palu	2018/09/28	XI	≥ X (0.9%)
29	Davao1	2019/10/16	VIII	VIII (22.6%)
30	Davao2	2019/10/29	IX	≥ X (0.4%)
31	Davao3	2019/12/15	IX	≥ X (0.4%)

Four earthquakes where reliable ESI-07 isoseismals are available are selected, and a careful comparison of the macroseismic field proposed in the literature with the grid results obtained in our study is performed. The selected events include Guatemala (ID 1), Denali (ID 8), Wenchuan (ID 14) and Palu (ID 28); therefore, events with only one or two ESI-07 isoseismals (e.g., Davao, ID 29-31) or an incomplete macroseismic field due to large offshore areas (e.g., Tohoku, ID 18) are excluded.

The ESI-07 isoseismals are superimposed to the ESI-07 grids obtained in the study and the difference between the two for each grid element is calculated. It is worth mentioning that all the 4 investigated earthquakes generated extensive surface faulting, which resulted in ESI-07 isoseismals elongated in the direction of the seismogenic source (Figure 4.9). The histograms show the difference between ESI-07 from isoseismals and ESI-07 derived in the study from slope movements; positive values indicate that the estimate

from isoseismals is higher. The histogram patterns for the four investigated earthquakes appear to be similar, with a frequency peak at 1 degree of difference, except for the Denali event, where the distribution is slightly shifted toward higher values. This analysis must be intended as a first approximation, since the territory covered by the isoseismals and the area investigated with landslides may differ: for instance, the Guatemala inventory covers only a small portion of the isoseismals (Figure 4.9). Moreover, the grid analysis results in a "salt and pepper" pattern, with high variations between cells close to each other, while isoseismals by definition tend to smooth out such high-frequency variations and provide a more homogeneous description of earthquake effects. It is worth nothing that the maximum ESI-07 value obtainable from landslides is ≥ X; thus, all the cells with ESI-07 isoseismal XI and XII have a minimum "difference" value of 1 and 2, respectively. A total of 1815 cells lie within isoseismal XI, and 924 cells within isoseismal XII, constituting 21% of the analyzed grid elements. These results show that the overall distribution of the values is not heavily affected by the inability to fully compare the ESI-07 values from isoseismal lines and the analysis of slope movements.

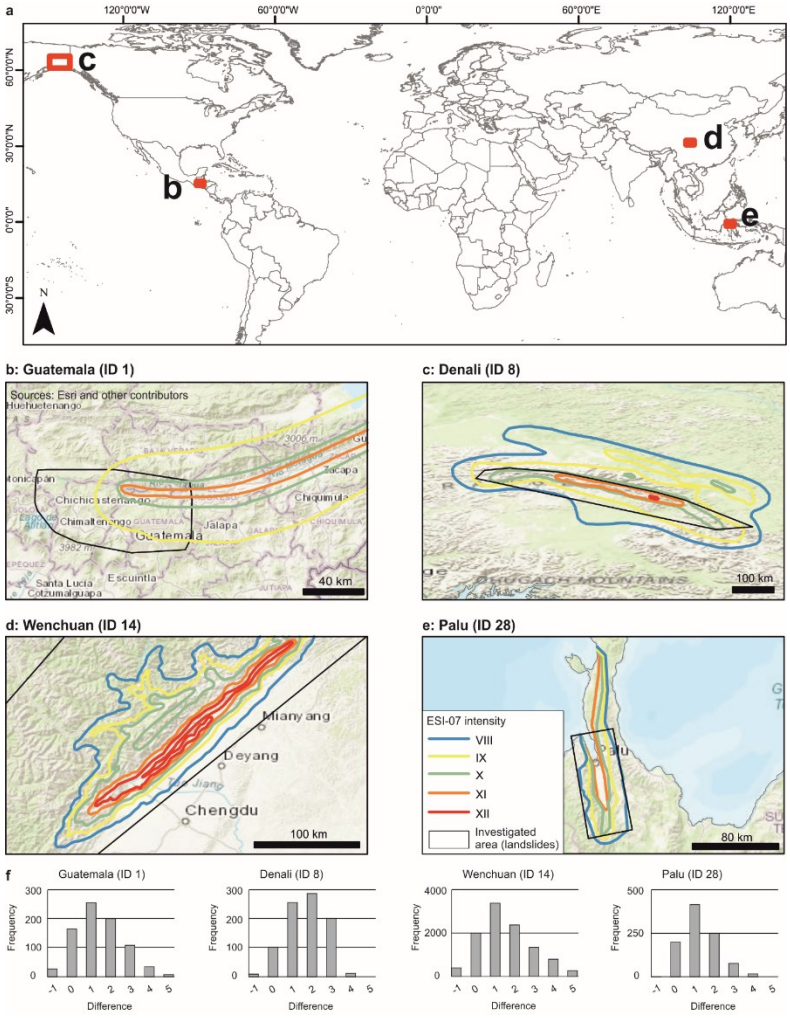

Figure 4.9 – Comparation between case studies with ESI-07 isoseismals. *Distribution of the case histories where ESI-07 isoseismals have been compared to the grid analysis realized here (a). ESI-07 isoseismal maps for the Guatemala (b; isoseismals after Caccavale et al., 2019), Denali (c; Comerci et al., 2015), Wenchuan (d; Lekkas, 2010) and Palu (e; Sioli E., unpublished thesis). Frequency plots of the difference between ESI-07 from isoseismals and from the grid analysis on landslides (f).*

Despite the above-mentioned limitations, results show the suitability of this comparison. Additional insight could be gained from the analysis of a wider number of case histories, including earthquakes that did not generate surface faulting. Indeed, some studies have already pointed out a correlation between landslide concentration and distance from the seismic rupture (Chen et al., 2021; Zhao et al., 2023). The results support the notion proposed by Ota et al. (2009) and Silva et al. (2013), who first attempted to an ESI-07 evaluation via a box-counting approach.

CONCLUSION

In this study an ESI-07 grid methodological approach first proposed by Ferrario (2022) is applied, which aims to retrieve useful information from EQUILs inventories from the perspective of intensity assessment using the ESI-07 scale. The ESI-07 grid approach is tested on a dataset of 33 earthquakes in various settings and results demonstrate that the procedure produced consistent results. The first empirical equations to relate the ESI-07 intensity to LAP and LND is developed; the equation based on LAP is valid for the intensity range ESI-07 VI to ≥ X, while the equation based on LND is valid up to ESI-07 intensity IX. Generally, magnitude and kinematics exert a limited influence on LAP and LND values. Results show how quality of input data (i.e., landslide inventory) has a much greater impact on the results than the selection of a given area-volume conversion. Furthermore, LAP resulted to be a better metric than LND, so it is recommended to derive ESI-07 data from LAP values whenever possible; the use of the scaling relation based on LND should be considered more cautiously. Landslides represent only one category of EEES included in the ESI-07 Intensity scale.

While landslide inventories generally provide a detailed representation of earthquake damage with higher resolution than is typically achieved in ESI-07 studies, the ESI-07 scale offers the complementary advantage of enabling comparison of different types of effects across both space and time. Future steps should focus on extending the proposed workflow beyond EQUILs inventories to encompass other categories of EEEs included in the ESI-07 scale.

CHAPTER 5

ESI-07 CHARACTERIZATION OF THE 1 JANUARY 2024 MW 7.5 NOTO EARTHQUAKE

INTRODUCTION

Japan is one of the most seismically active regions worldwide, due to the complex interaction of multiple tectonic plates and associated volcanic and crustal processes. Numerous historical and instrumental earthquakes have affected the country, resulting in significant EEEs, including surface ruptures, slope movements, and anomalous waves and tsunamis (Mori and Takahashi, 2012; Mikumo and Ando, 1976; Wald and Somerville, 1995; Fukuyama et al., 2003; Wald, 1996; Mimura et al., 2011). Documenting these effects is essential for macroseismic characterization, for assessing secondary hazards and for supporting emergency management (Ferrario et al., 2022b; Comerci et al., 2015b; Naik et al., 2020; Velázquez-Bucio et al., 2021; Boulton et al., 2025). On 1 January 2024, a Mw 7.5 earthquake struck the Noto Peninsula in central Japan, generating a wide range of EEEs across a vast area. The event triggered widespread surface deformation, particularly along the northeastern coast, and produced effects including ground cracks, tectonic uplift/subsidence, slope movements, and tsunamis. To capture and characterize these effects, a comprehensive dataset is compiled, integrating heterogeneous data from multiple sources. The specific objectives of the study are: a) to test the applicability of a semi-automatic, GIS-based methodology for assigning ESI-07 intensity across multiple categories of EEEs, based on previous studies (Ferrario, 2022; Sridharan et al., 2023; Muccignato and Ferrario, 2025); b) to generate ESI-07 grid maps that improve spatial interpretation and detection of localized intensity peaks; and c) to expand the existing EEE catalogue by providing a new case study from a recent subduction earthquake. This study characterizes the 44 535 EEEs and produces two ESI-07 intensity grid maps at resolutions of 1×1 km and 5×5 km. Ground cracks and tectonic uplift/subsidence emerge as the most frequent categories, with intensity values ranging from V to XI. The ESI-07 grid maps reveal clear spatial patterns, with high-intensity values concentrated along the northeastern coast of Noto peninsula, consistent with the fault geometry and rupture propagation. The grid-based approach enables spatial smoothing and value aggregation, enhancing the readability of spatial patterns, the identification of amplification phenomena, and the detection of clusters of local maxima. Non-traditional sources, including social media and press reports, are also integrated. Although they represent a limited fraction of the dataset, they contribute to its completeness and usability by providing visual documentation that supported both the identification and validation of EEEs. Beyond their scientific value, these data hold a complementary role in participatory and citizen science, as their accessibility and interpretability facilitate public engagement and citizen-oriented outputs. Overall, this study represents the first application of a semi-automatic method for assigning ESI-07 intensities to an extensive and heterogeneous EEE dataset and for constructing high-resolution gridded intensity maps for a high-magnitude subduction earthquake. The results demonstrate the effectiveness of the semi-automatic method and the ESI-07 grid-based approach in managing large and heterogeneous datasets, particularly by facilitating the processing of data and supporting the spatial interpretation of ESI-07 intensity values. Furthermore, the results provide new insights into the spatial distribution of EEEs and demonstrate the effectiveness of the method in managing large and heterogeneous datasets, highlight its potential for future applications in different seismotectonic contexts, contributing to advancing methodologies for seismic-impact assessment.

STUDY AREA

1.1 GEOGRAPHY

Japan is an archipelagic country in East Asia, identified by four major island (Honshu, Hokkaido, Kyushu and Shikoku), and 14 125 smaller islands (GSI, 2023). It extends roughly 3000 km from NE to SW and covers an area of 377,975.68 km^2 (GSI, 2025). Japan is bounded by the Sea of Okhotosk to the North, the Pacific Ocean and East China Sea to the East, South and South West, and Japan Sea to thes West and North West.

The Noto Peninsula is located in north-central sector of the main island of Honshu, projecting northwestward, into the Sea of Japan. It is part of Ishikawa Prefecture and it is almost entirely sourronded by the Sea of Japan, which form the Toyama Bay in South-East direction. The local climate is humid continental (Köppen Cfa), defined by mild summers and cold winters with heavy snowfall. Annual precipitation is 2282 mm, with September as wettest month. The temperatures are highest on average in August (25.2°C) and lowest in January (2.1°C) (Climate-Data.org:, 2025).

1.2 TECTONIC AND GEOLOGY

Japan lies in a complex tectonic settting, at the convergence of four major tectonic plates: a) two continental plates: the Okhotsk Plate and Amurian Plate; respectively part of North American and Eurasian plate and b) two oceanic plates: the Philippine Sea and Pacific Plate (Hasegawa et al., 2009). Their interaction is along three subduction zones and one collisional zone with two triple junctions (Maruyama et al., 1997) (Fig.5.1).

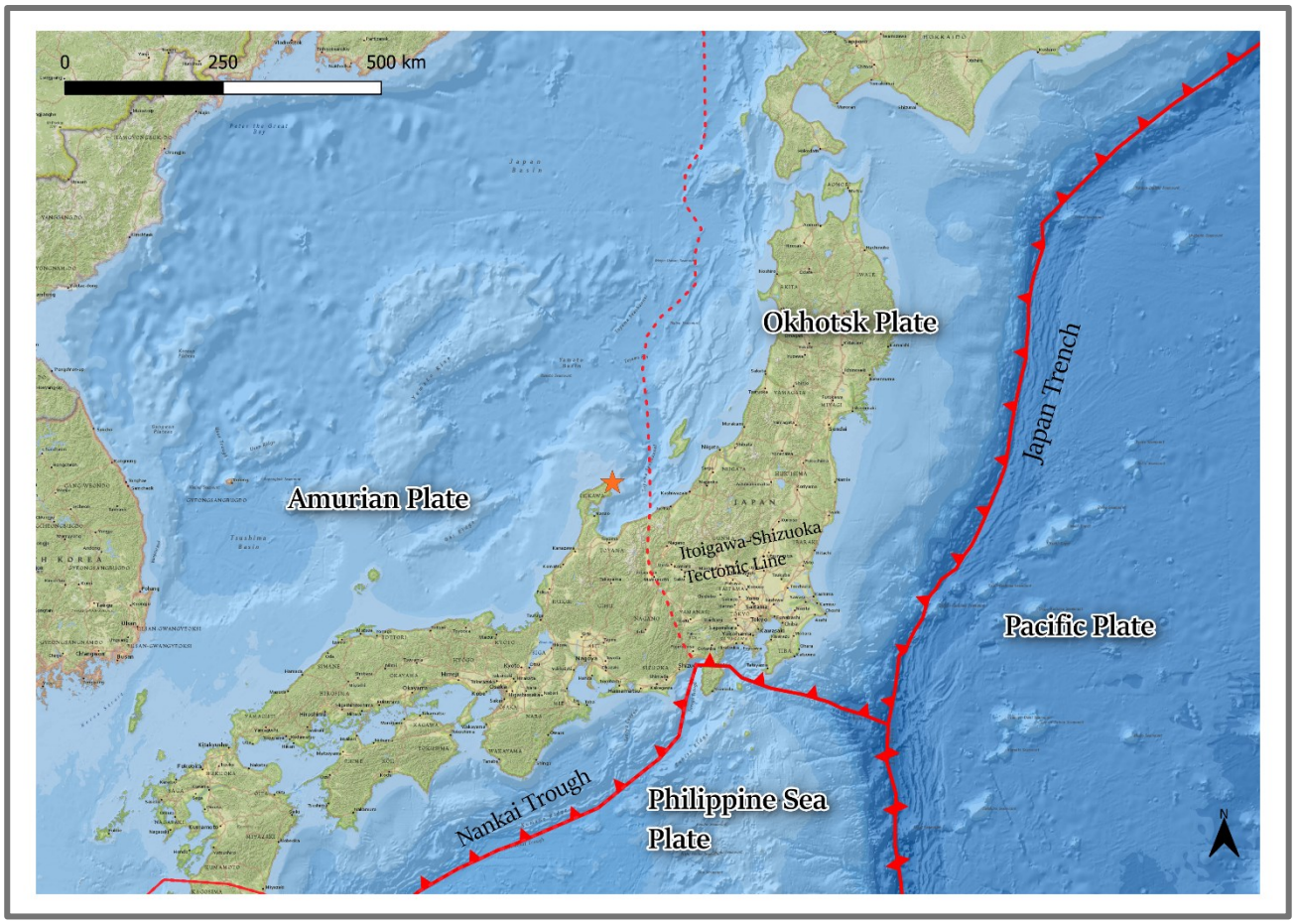

Figure 5.1 *– **Tectonic setting of the study area**. The orange star shows the epicenter of the 1 January 2024 Mw 7.5 Noto earthquake; red lines show tectonic plate subduction margins. The dotted lines represent the continental margin of the Amurian and Okhotsk plate.*

The Noto Peninsula is characterized Paleozoic-Mesozoic gneiss and granite intrusions covered by cenozoic volcanic and sedimentary rocks as Oligo-Miocene mafic and intermediate lavas, breccias and acidic pyroclastic rocks, deposited in non-marine environments, and Miocene-Pliocene sedimentary and volcanic rocks formed in marine environment (Lopez and Ishiwatari, 2002).

In accordance with the general tectonic context, Noto peninsula is characterized by crustal shortening and compressional stress, related to ongoing tectonic inversion processes affecting western Honshu, which began in late Miocene – Plicoene and which caused the reactivation of buried, steeply dipping faults originally formed during earlier extensional phases (Liu et al., 2024a, 2025b; Kato et al., 2008; Ishiyama et al., 2017).

The subduction of the Philippine Sea plate and Pacific plate caused, from the Miocene (25 Ma) the opening of the Japan Sea, a back-arc type basin (Maruyama et al., 1997), which resulted in crustal stretching along the costline and the consequent formation of a horst-graben structure and normal faults from 15-20 Ma (Ishikawa and Bai, 2024; Jolivet et al., 1994; Xu et al., 2024; Lopez and Ishiwatari, 2002). In the late Miocene to Pliocene, the area was charactetrized by tectonic inversion and the extensional regime was replaced by a

compressional stress regime. This caused the the pre-existing normal faults to be re-activated as reverse faults due to NW-SE crustal shortening (AIST, 2012, Okuwaki et al., 2024; Okamura et al., 1995; Sato, 1994; Nakajima, 2022) (Fig. 5.2).

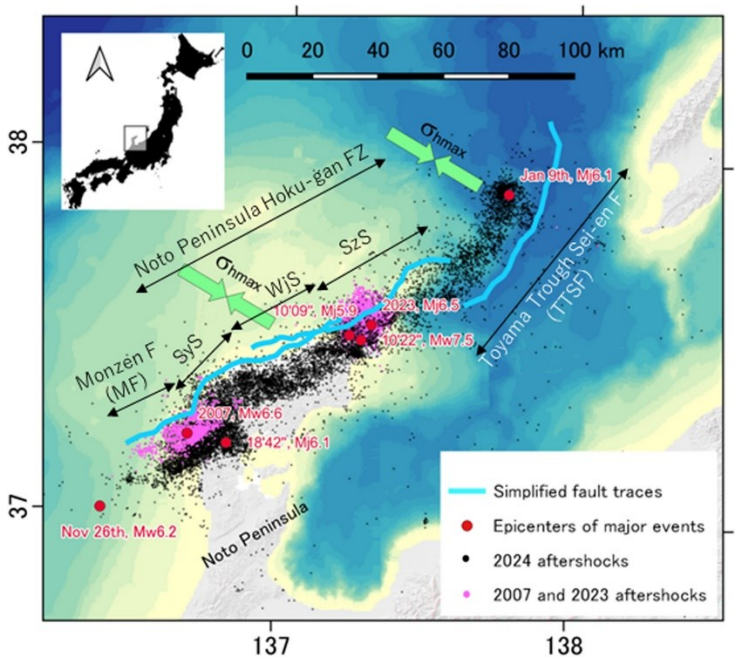

***Figure 5.2** - **2024 Mw7.5 Noto Peninsula earthquake and tectonic background**. Light blue lines indicate fault traces (simplified from Okamura, 2019). Red dots mark the epicenters of major seismic events. 2024 events are labeled by date or time (UTC, Jan 1 baseline). Black and pink dots show aftershocks of the 2024 event (5 days) and the 2007 and 2023 events (1 day). Green arrows represent the maximum principal stress direction (Uchide et al., 2022). The acronyms represent the major tectonic segment: SyS: Saruyama–oki Segment; WjS: Wajima–oki Segment; SzS: Suzu–oki Segment. Modified from Ando et al., 2025.*

1.3 1 JANUARY 2024 NOTO EARTHQUAKE (Mw 7.5)

On 1 January 2024, at 07:10:09 UTC (16:10:09 local time) the largest shallow earthquake of the area since the aftershock of the Mw 9 Tohoku (11-03-2011) struck the Noto Peninsula (Fujii and Satake, 2024; Mori et al., 2012; Tsuji et al., 2011, 2014). The Mw 7.5 event occurred near the locality of Suzu (37°29'13.2"N 137°16'15.6"E), with a reverse fault mechanism and a shallow focal depth of 10 km. The focal mechanism was characterized by a strike of 49°, a dip of 41° and a slip of 102° (USGS, 2024; Heidarzadeh et al., 2024). The fault trend was SW-NE, consistent with regional compressional stress regime characteristic of the area (Xiang et al., 2024, Okuwaki et al., 2024; Ishikawa and Bai, 2024). Intense ground shaking was recorded, with a maximum peak ground acceleration (PGA) of 2.6g (Ma et al., 2024) (Fig.5.3).

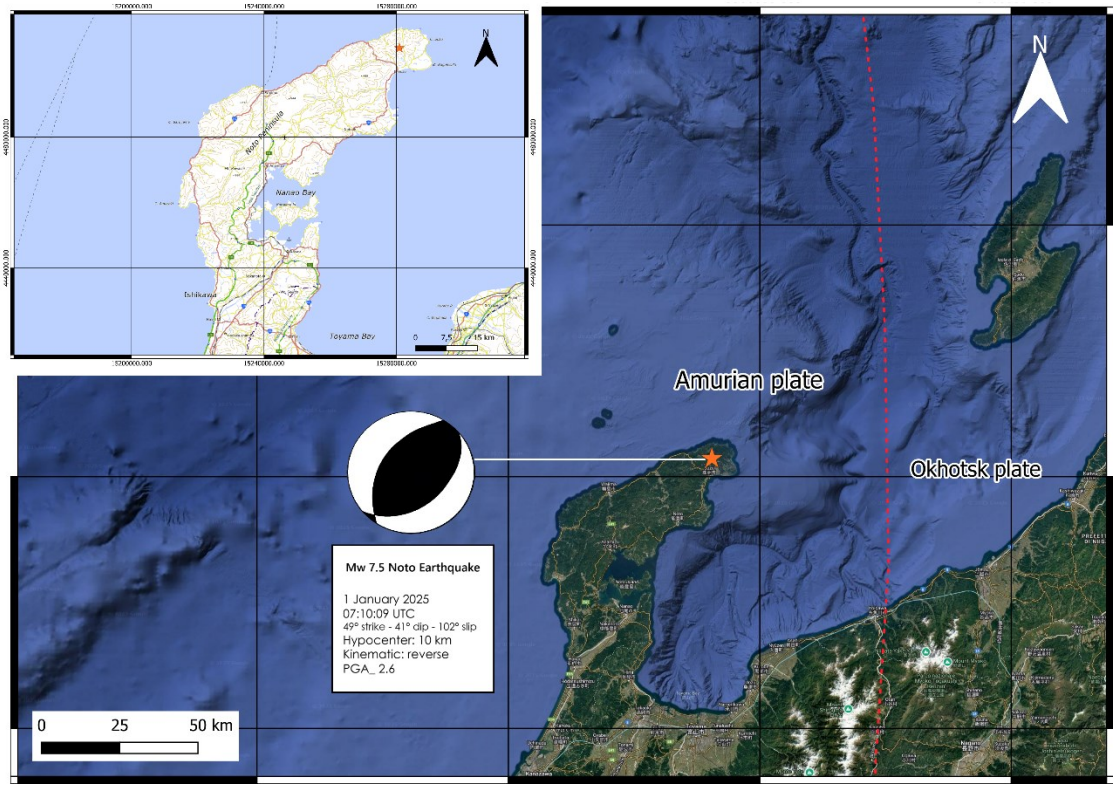

Figure 5.3 – Seismotectonic context of the 2024 Noto earthquake. *The orange star represents the hypocenter of the Mw 7.5 Noto earthquake. The focal mechanism solution illustrates the reverse faulting nature of the rupture. The dashed line delineates the approximate boundary between the Amurian and Okhotsk tectonic plates.*

The event nucleated with an unusually low average rupture velocity propagation, lasting 15 to 20 seconds near the hypocenter (Ma et al., 2024). Geodetic and dense seismic analysis and tsunami observation revealed a large shallow slip in the crust below the peninsula, extending offshore to the northeast. The rupture occurred within a fluid-rich fault zone and displayed a heterogeneous slip distribution with a bilateral, two-stage rupture pattern. Slip reached up to 8 m in several patches along an about 150 km long fault, exceeding 10 meters on an offshore fault. The event was associated with a peak stress drop greater than 10 MPa (Liu et al., 2024c; Ma et al., 2024; Okuwaki et al., 2024; Yoshida et al., 2024). The aftershock region extended for approximately 150 km (Yoshida et al., 2024)

Fault weakening driven by fluid intrusion is a widely recognized phenomenon in intraplate earthquake swarms (Yukutake et al., 2011; Shelly and Hill, 2011; Shelly et al., 2013; Fischer et al., 2014; Yoshida et al., 2016; Ross et al., 2017). Recent studies have shown evidence that aseismic slip triggered by migrating fluids can initiate seismic events (Cornet et al., 1997; Guglielmi et al., 2015; Wei et al., 2015; Ruhl et al., 2016; Yoshida and Hasegawa, 2018; De Barros et al., 2019; Hatch et al., 2020).

The 2024 Mw 7.5 Noto event was preceded by a long-lasting swarm activity, which began in 2020, in the northeastern part of Noto Peninsula (Fig. 5.3). Over 20 000 low to moderate magnitude events are recorded across four distinct clusters in a 15 km^2 area, at dephts of 10-18 km and with thrust mechanism (Amezawa et al., 2023; Ishikawa, 2023; Ishikawa and Bai, 2024; Liu et al., 2024c; Nakajima, 2022; Toda and Stein, 2024;

Yoshida et al., 2023a). The events migrated progressively towards shallower depths, following a complex network of faults, likely driven by upward fluid movements and producing crustal deformation (Yoshida et al., 2023a).

The event caused surface deformation, with peak uplift reaching 5 meters along the western coast of the Noto Peninsula (Ma et al., 2024), and a wide range of cascading hazards, including: a) liquefaction; b) ground cracking c) landslides; d) fires and; e) tsunamis (Suppasri et al., 2024; Fukushima et al., 2024, Heidarzadeh et al., 2024, Tajima et al., 2024, Yuhi et al., 2024; Ma et al., 2024).

MATERIAL AND METHODS

2.1 OVERVIEW

This study applies a comprehensive and multi-stage methodology for the ESI-07 characterization of the 2024 Noto Peninsula Earthquake. The workflow is structured in seven main stages (Fig. 5.4), beginning with the general characterization of the Mw7.5 Noto earthquake and the collection and description of Earthquake induced EEEs, and ending with a GIS-based procedure, aimed at generating an ESI-07 intensity grid map.

EEEs data are gathered from Institutional repositories, public datasets, peer-reviewed scientific literature, and Social Media platforms. The EEEs data are then characterized according to the ESI-07 Intensity scale (Michetti et al., 2004; Michetti et al., 2007; Serva et al., 2016). The analysis is conducted using the following software and tools:

- Draw.io: for the creation of schematic workflow diagrams
- Microsoft Excel and Microsoft Word: for dataset compilation and documentation
- QGIS (version 3.38.1): for spatial data processing and visualization
- Python scripts: for automated classification and computational procedures

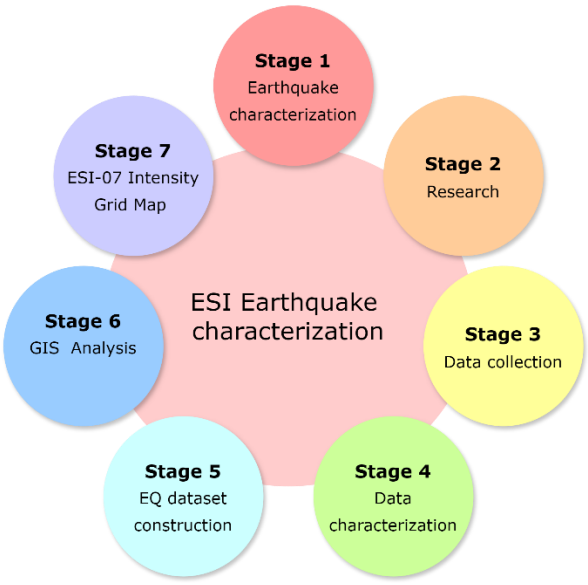

Figure 5.4 - Complete workflow and stages for the Mw 7.5 Noto Earthquake ESI-07 characterization*. The workflow is characterized by 7 different stages, starting from earthquake characterization and ending with ESI-07 Grid map.*

2.2 EARTHQUAKE CHARACTERIZATION AND PRELIMINARY RESEARCH (STAGES 1–2)

The initial phase consists in the identification of the target earthquake and the compilation of key seismological parameters, including location, magnitude, origin time (UTC and local), focal depth, and

kinematic parameters, obtained through an extensive literature review (Fig. 5.5). Primary and secondary EEEs are preliminarily identified and listed, according to the ESI-07 guidelines (See App.1.1) (Fig. 5.5).

Subsequently, an extensive review is conducted to collect all available EEEs data from online resources. Specific keywords are defined and applied (e.g., *country, date, earthquake, and primary and secondary effect related terms*) to retrieve relevant information. Data sources included peer-reviewed scientific publications (e.g., Acharya et., 2024; Fukushima et al., 2024, Heidarzadeh et al., 2024; Inagaki et al., 2024, Mizuno et al., 2024; Mulia et al., 2024; Ohno et al., 2024; Tajima et al., 2024; Yoshida et al., 2024; Yuhi et al., 2024) reports from public and governmental institutions and agencies (GSI, 2024), press articles, and content from social media platforms (Facebook, Instagram, TikTok, YouTube, X). This phase allows to generate a preliminary raw dataset (Fig.5.5).

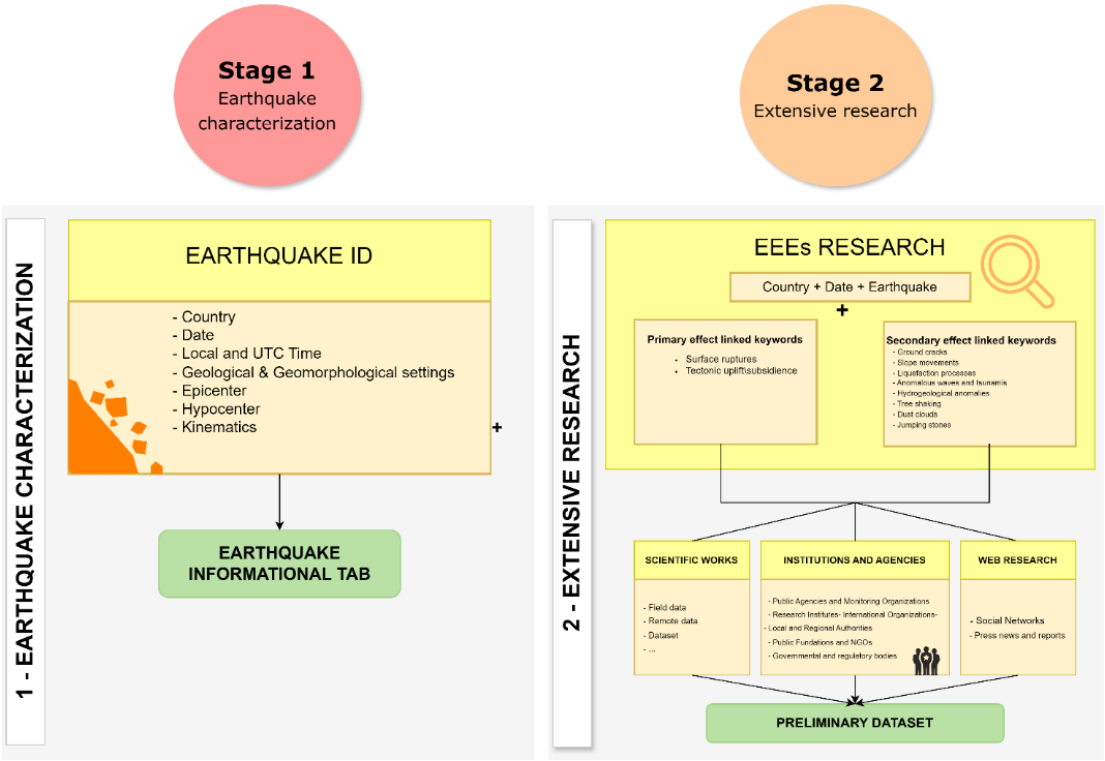

Figure 5.5 - Stage 1 and 2. *Stage 1 comprises the identification and seismological characterization of the target event. Stage 2 involves the definition of research keyword, and the execution of extensive research aimed at compiling a preliminary dataset.*

2.3 DATA COLLECTION AND CHARACTERIZATION (STAGES 3–4-5)

Stage 3 involves the management and refinement of the preliminary dataset. This phase focuses on the amalgamation and standardization of the collected data. Duplicates, low-quality entries, entries with uncertain provenance and non-quantifiable parameters are removed to ensure data reliability (Fig. 5.6).

Stage 4 is characterized by the creation of a descriptive table in textual format, in which a detailed characterization of each entry is performed. Data are divided into two main categories, based on the source of acquisition (e.g., reconnaissance field survey data and remote sensing data) and nature of the data: a) *single data* (manually acquired, isolated records) and; b) *author datasets* (aggregated data from external authors or sources)

For each category, EEEs are described through two levels of characterization:

a) General characterization: defined by a) Site ID assignment, b) Upload/reference date definition, c) Coordinates definition in decimal format; d) City and locality identification; e) citation of sources and references (Fig.38).
b) ESI characterization, based on ESI-07 Guidelines (App. 1.1): defined by a) EEE type definition, b) EEE Description, c) attachment of photographic documentation (when available) and d) ESI-07 Intensity assignment (Fig.5.6) .

For the *single data* category, all the parameters are completed, while for the *author dataset* category, only EEE type definition is assigned, while the complete ESI-07 characterization is postponed to Stage 6 (Fig. 5.6).

In particular, for ESI-07 characterization, guidelines from Michetti et al., 2007 are used for Ground cracks (note: after ESI-07 X grade, saturation phenomenon is present), Hydrogeological anomalies, Tree shaking, dust clouds categories (App. 1.4). For Surface ruptures and Tectonic uplift and subsidence a quantitative classification is developed to ensure progressive value increase and consistency with other ESI-07 categories. Qualitative terms, originally present in the ESI-07 scale definitions, are converted into quantitative ranges using proportional scaling based on orders of magnitude (App 1.4). For Anomalous waves and tsunamis category the classification follows the threshold proposed by Lario et al., 2016, based on Tsunami Height (m) and Run-Up (m) (App 1.4). For Slope Movements category the classification by Ferrario M.F. (2022a) is adopted (note: after ESI-07 X grade, saturation phenomenon is present) (App. 1.4).

Stage 5 involves the construction of two preliminary dataset: a) *single data datasets* and; b) *authors dataset*. Each dataset includes the following standardized fields:

- Latitude and longitude (decimal format)
- Type of EEE
- Assigned ESI-07 intensity
- Data source/type (i.e., Remote sensing data, reconnaissance field survey data, social data).

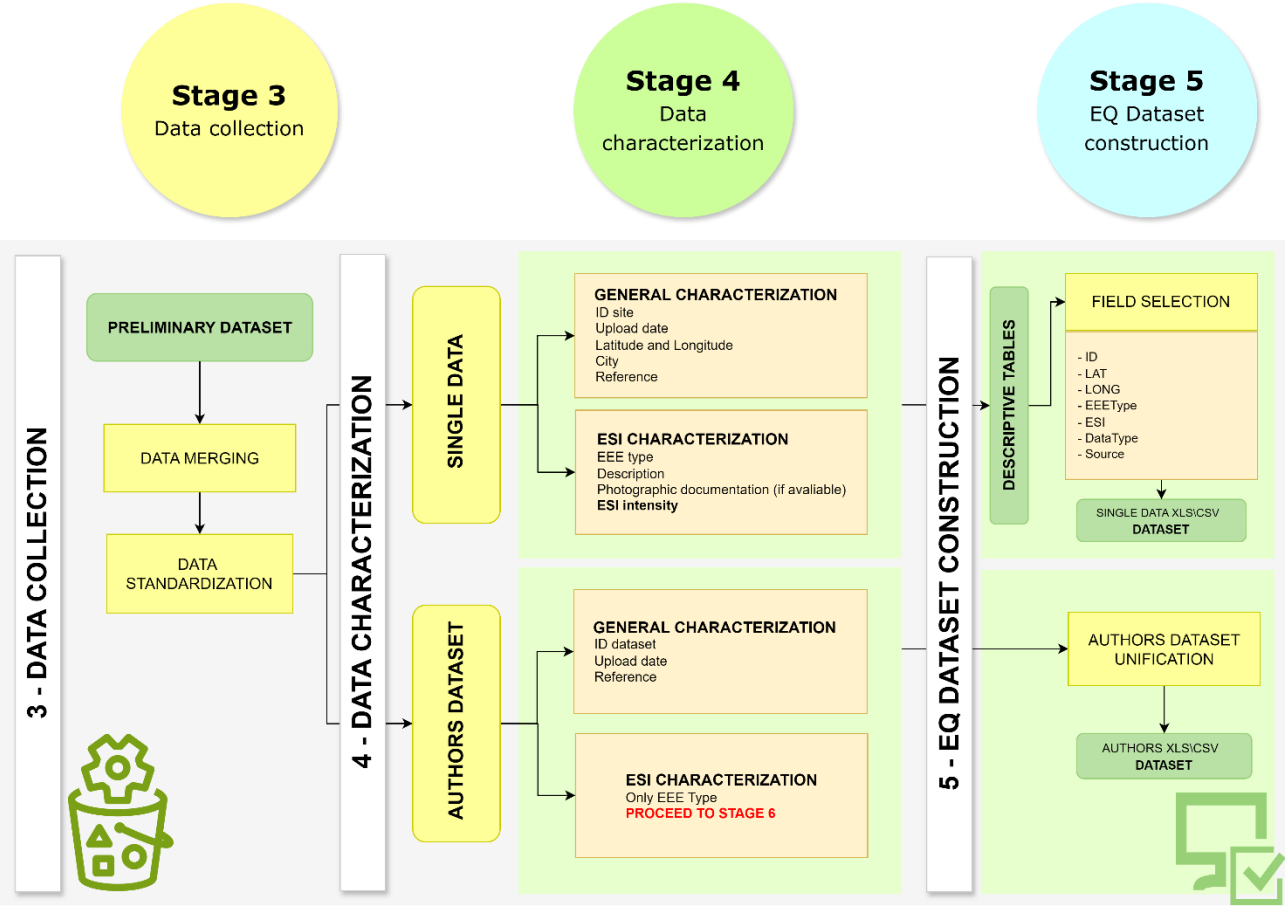

Figure 5.6 - Stage 3, 4 and 5. *Stage 3 focuses on data merging and standardization. Stage 4 is defined by the classification of data into two categories and their detailed characterization. Stage 5 consists in the construction of two structured preliminary datasets.*

2.3.1 DESCRIPTIVE TABLES

Stage 4 involves the compilation of a descriptive table in textual format, providing a detailed characterization of each entry. Each EEE descriptive table is compiled via specific fields: site ID, upload date, coordinates, reference locality, EEE type and description, estimated ESI-07 intensity, photographic documentation and references. Two types of EEEs descriptive tables are compiled, depending on the type of data sources: single data and authors dataset. In the case of single data entries, each EEEs descriptive table provides a general characterization of the site and a corresponding ESI-07 characterization and intensity estimation, derived from the direct assessment of the observed effect. In contrast, for author datasets, EEEs descriptive table report general information and EEEs type definition of the dataset as whole. ESI-07 estimation is not compiled; instead, an indication of the script used in QGis for the automated assignment of ESI-07 intensities across the dataset features is given.

2.4 GIS-BASED ANALYSIS AND ESI VALUE ASSIGNMENT (STAGE 6)

In stage 6 Authors dataset is imported into a Geographic Information System (GIS) environment, in order to perform spatial analysis and assign ESI-07 intensity (Fig. 5.7). The dataset is imported into QGis (version 3.38.1), where dimensional thresholds are defined (App. 1.4) for each category of EEE. These thresholds are implemented using conditional expressions (e.g., CASE WHEN logic) that allows for the automated assignment of ESI-07 intensities. For each record, a new field called "ESI" is created, and specific formulas are applied for each EEE category, to estimate the corresponding ESI-07 value (Fig. 5.7). Once the calculations are completed, the attribute table is exported as an Excel (xls) and a final manual verification is conducted to ensure the accuracy and consistency of the conditional expressions used. This resulted in a finalized and validated *Authors dataset* in .xls format. After validating this dataset, it is merged with the .xls *single data dataset*, previously compiled in stage 5. From the merged table, final fields of interest are selected: a) Id; b) Latitude; c) Longitude; d) EEEType; e) DataType; f) Source

The resulting table is then exported as a UTF-8 encoded CSV file, suitable for GIS import. This operation enables the creation of the final shapefile dataset (.shp), which included both *single data* and *authors data*, now homogenized and fully characterized in terms of ESI-07 intensity (Fig. 5.7).

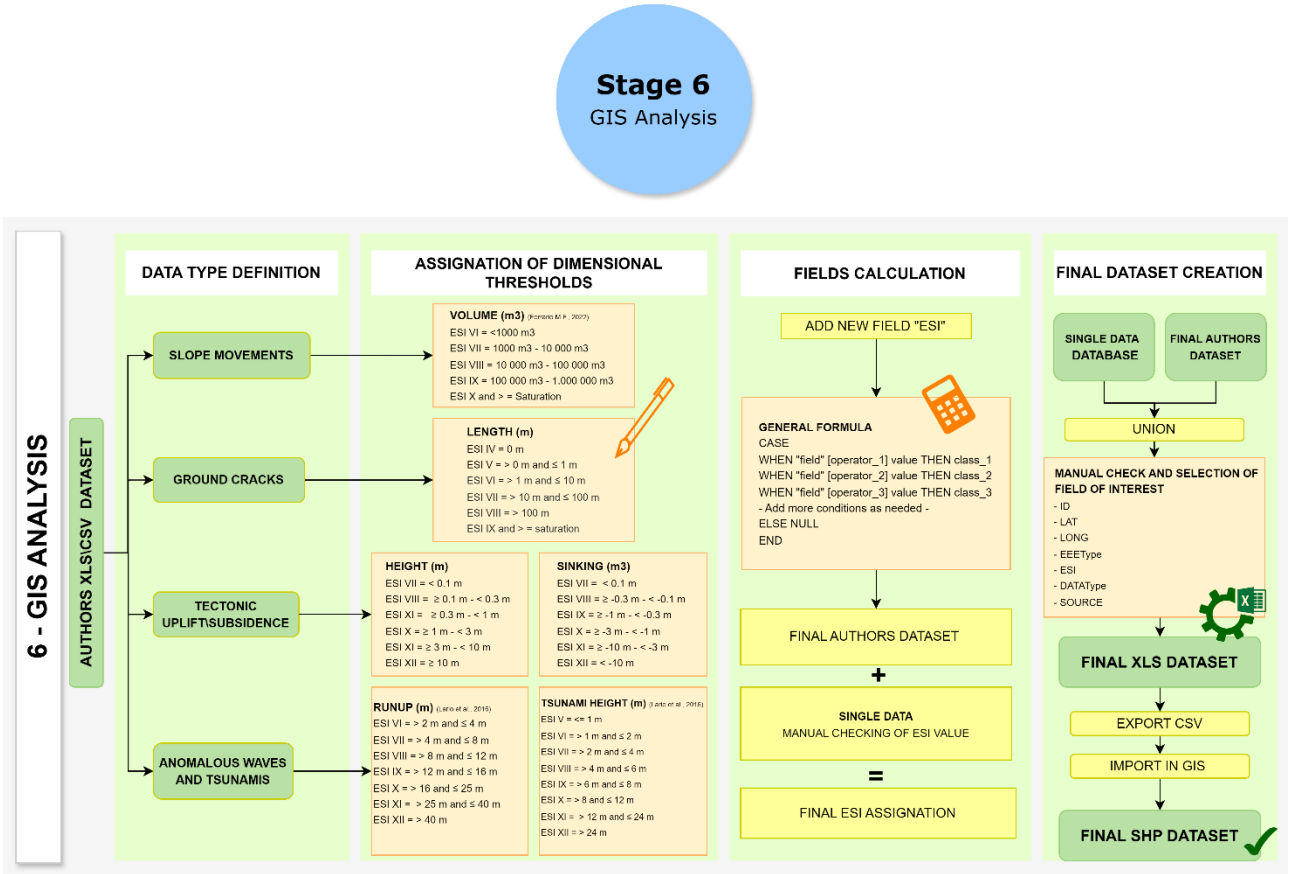

Figure 5.7 - Stage 6. *Stage 6 is defined by a preliminary identification of dimensional thresholds for each EEE category, allowing for the automated assignment of ESI-07 intensity values in a GIS environment. The processed authors dataset is subsequently merged with the single data dataset, leading to the generation of the final shapefile dataset.*

2.5 ESI-07 INTENSITY GRID MAP CONSTRUCTION (STAGE 7)

Stage 7 follows the grid-based methodology outlined in Chapter 4. A regular grid is generated over the study area and intersected with the compiled EEEs dataset, so that each cell is associated with the EEE occurring within its extent. For each cell, the maximum ESI-07 value is extracted and used to construct the intensity field, applying a spatial smoothing criterion to reduce local anomalies and highlight coherent macroseismic patterns. Cells without data are removed, and the resulting grid is classified according to ESI-07 intensity values, producing the final Intensity Grid Map (Fig. 5.8).

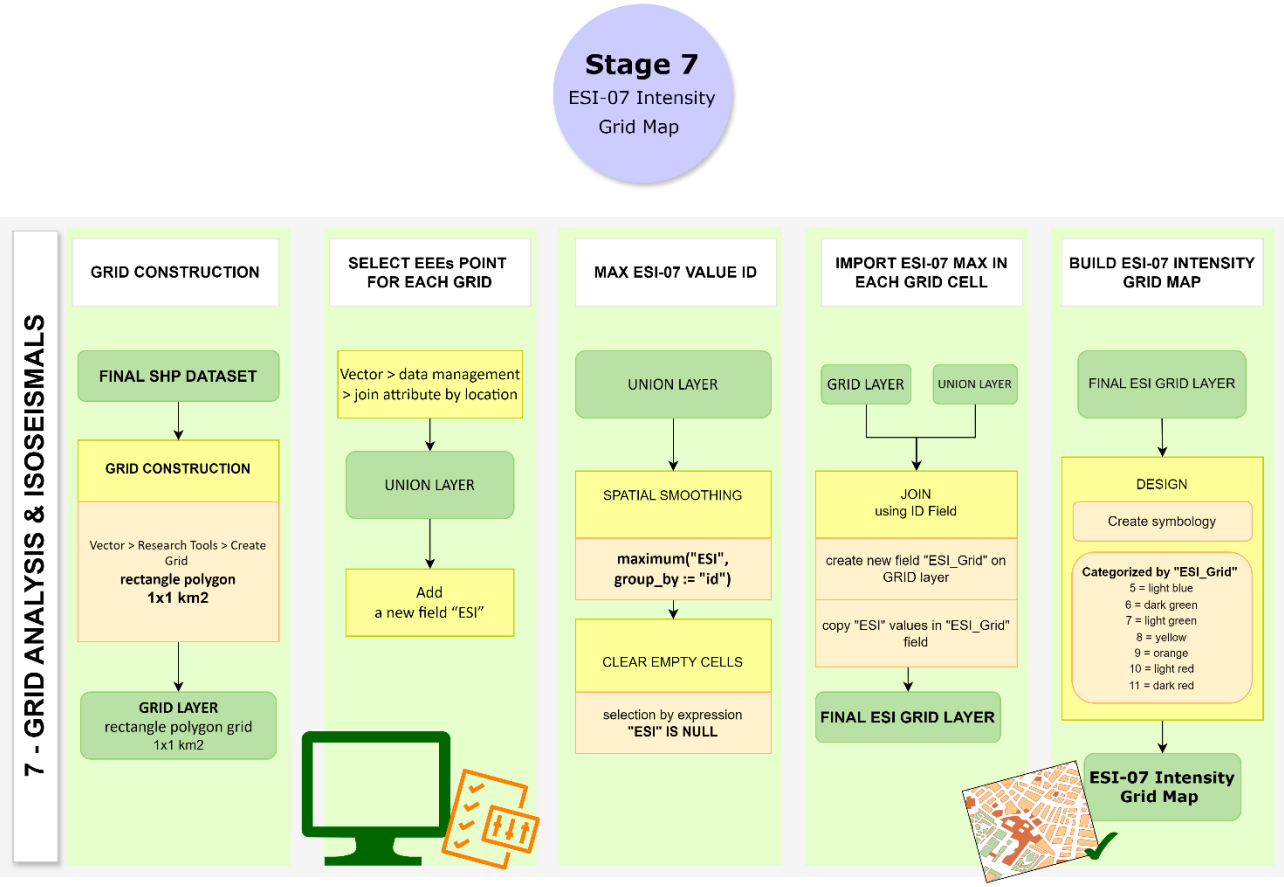

Figure 5.8 – Stage 7. *Stage 7 is defined by a grid approach used to extract and visualize the maximum ESI-07 intensity value for each cell. The process is conducted through five steps: grid creation, EEE point selection per cell, maximum ESI-07 value extraction, cleanup of null values, and construction of the final ESI-07 Intensity grid map.*

RESULTS

3.1 GENERAL DATASET OVERVIEW AND EEES ANALYSIS

The preliminary data collection led to the compilation of 266 descriptive tables, each providing essential information for the consequent identification and characterization of the EEEs data. An example of descriptive table is here reported (Fig. 5.9). The complete set of EEEs Descriptive tables is available in the supplementary material (App. 5.1).

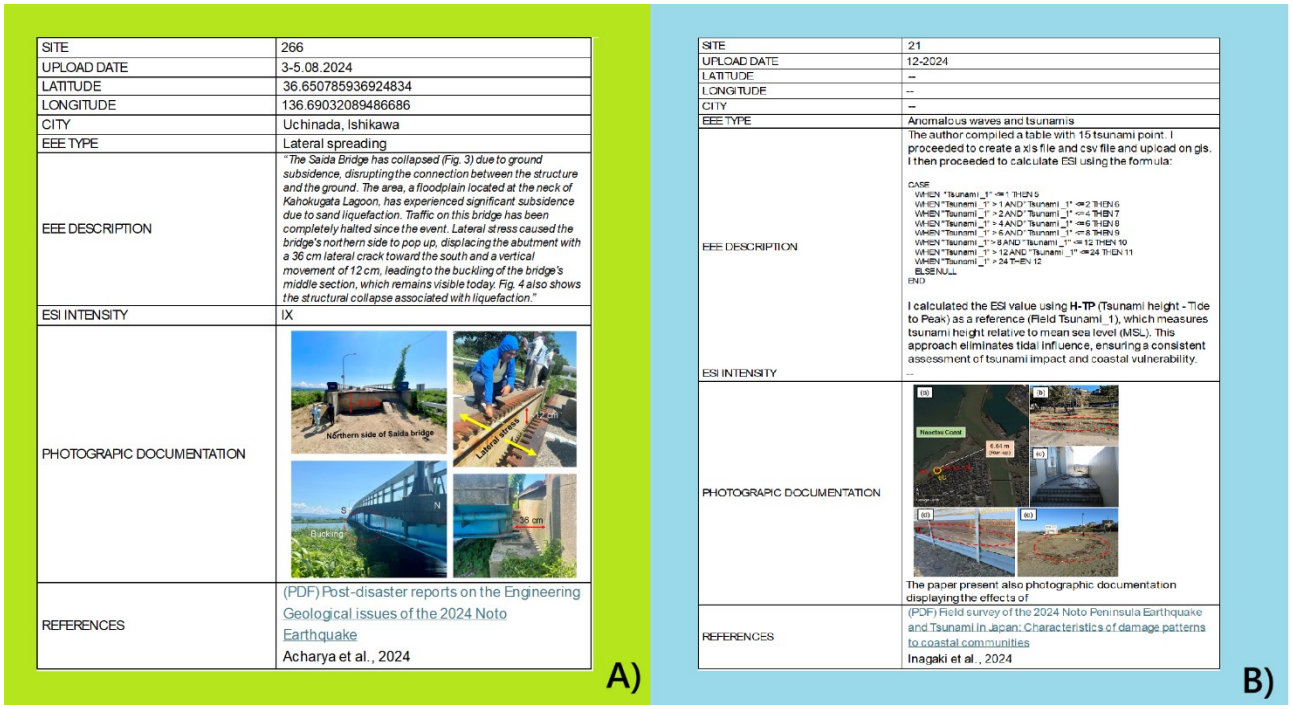

Figure 5.9 - EEEs Descriptive Table. *Each descriptive table compiled reports key data to characterize individual EEEs. A) For single data, an ESI-07 intensity value is assigned, based on EEE type definition and a EEE description. B) For author dataset general EEE type is identified along with the QGis script used for ESI-07 Intensity assignation.*

After the preliminary compilation of EEEs descriptive table a final comprehensive dataset is compiled, both in xls. And .shp format. The dataset compiled comprises a total of 44 535 EEEs, divided into 9 distinct ESI-07 EEEs categories (Fig. 5.10).

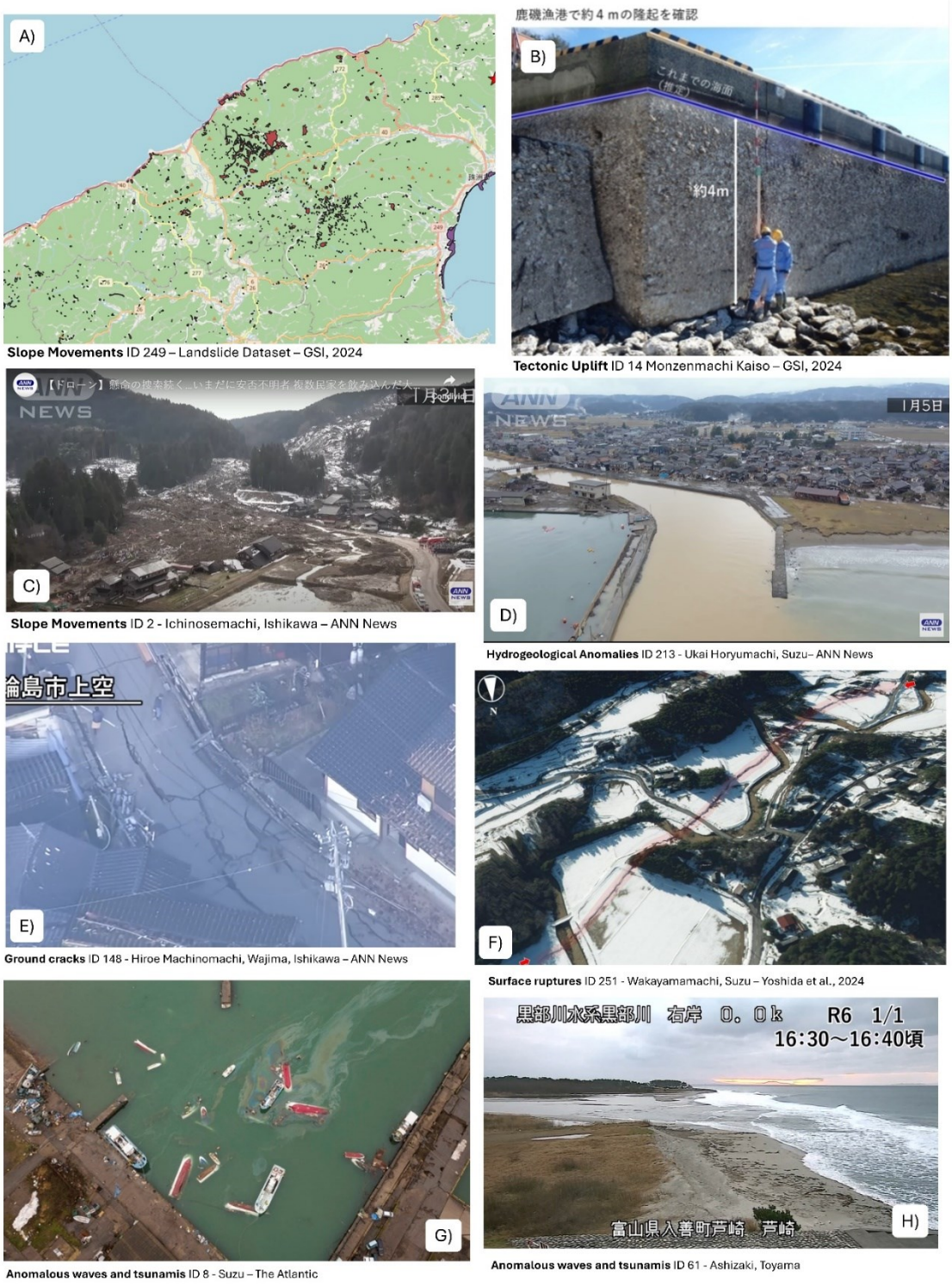

Slope Movements ID 249 – Landslide Dataset – GSI, 2024

Tectonic Uplift ID 14 Monzenmachi Kaiso – GSI, 2024

Slope Movements ID 2 - Ichinosemachi, Ishikawa – ANN News

Hydrogeological Anomalies ID 213 - Ukai Horyumachi, Suzu– ANN News

Ground cracks ID 148 - Hiroe Machinomachi, Wajima, Ishikawa – ANN News

Surface ruptures ID 251 - Wakayamamachi, Suzu – Yoshida et al., 2024

Anomalous waves and tsunamis ID 8 - Suzu – The Atlantic

Anomalous waves and tsunamis ID 61 - Ashizaki, Toyama

Figure 5.10 – EEEs data documentation. *The heterogeneity of source and data enabled the collection of multiple documentation types, including: dataset, technical reports, visual graphics, videos and images collected by aerial recognition, automatic detection, CCTV cameras and citizen science contribution.*

The distribution of EEE types highlights the predominance of ground cracks (50.2%) and Tectonic uplift\subsidence (43.8%) categories, which together account for most of the dataset. Slope movements (5.4%) represent a smaller but relevant part of the dataset, while other categories represent less than 1% of

the total. The total area affected, firstly calculated with "concave Hull" tool in QGis, and then redefined manually, is about 20674,020 km^2, representing a broad and spatially extensive set of effects (Fig. 5.11).

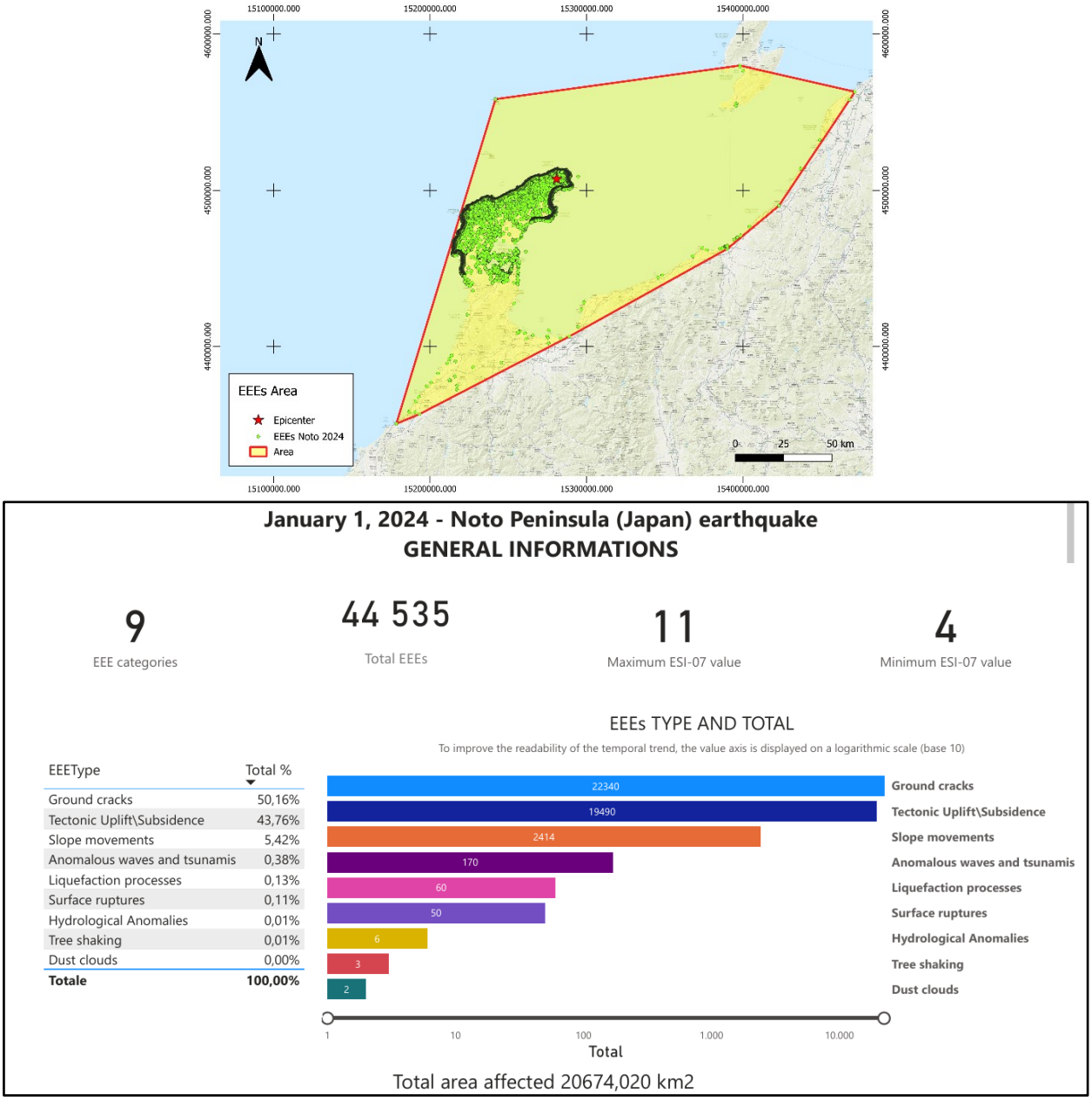

Figure 5.11 – Visual explanation of EEEs categories and their total. The total area affected is about 20674,020 km² The dataset comprises 44 535 data points classified into 9 ESI-07 EEEs categories. Ground cracks, tectonic uplift\subsidence and slope movements represent the main categories collected, each with thousands of entries. Other categories are represented by hundreds and tens of occurrence.

3.1.1 DATA SOURCE AND ACQUISITION METHODS

The dataset is edited with diversified set of sources, including a) institutional repositories; b) peer-reviewed scientific literature, and; c) crowd-sourced content from social media and press articles. Each EEE entry is attributed to a specific acquisition method and source (Tab.5.1).

The EEEs data are derived from multiple data sources, as follows: a) Remote sensing data: 44 162 (99,2%); b) Social data: 239 (0.5%); c) Field data: 126 (0.3%); d) not available: 8 (0,0%). These values highlight the dominant role of remote sensing and instrumental techniques over direct field observation, which remain comparatively marginal (Fig. 5.12).

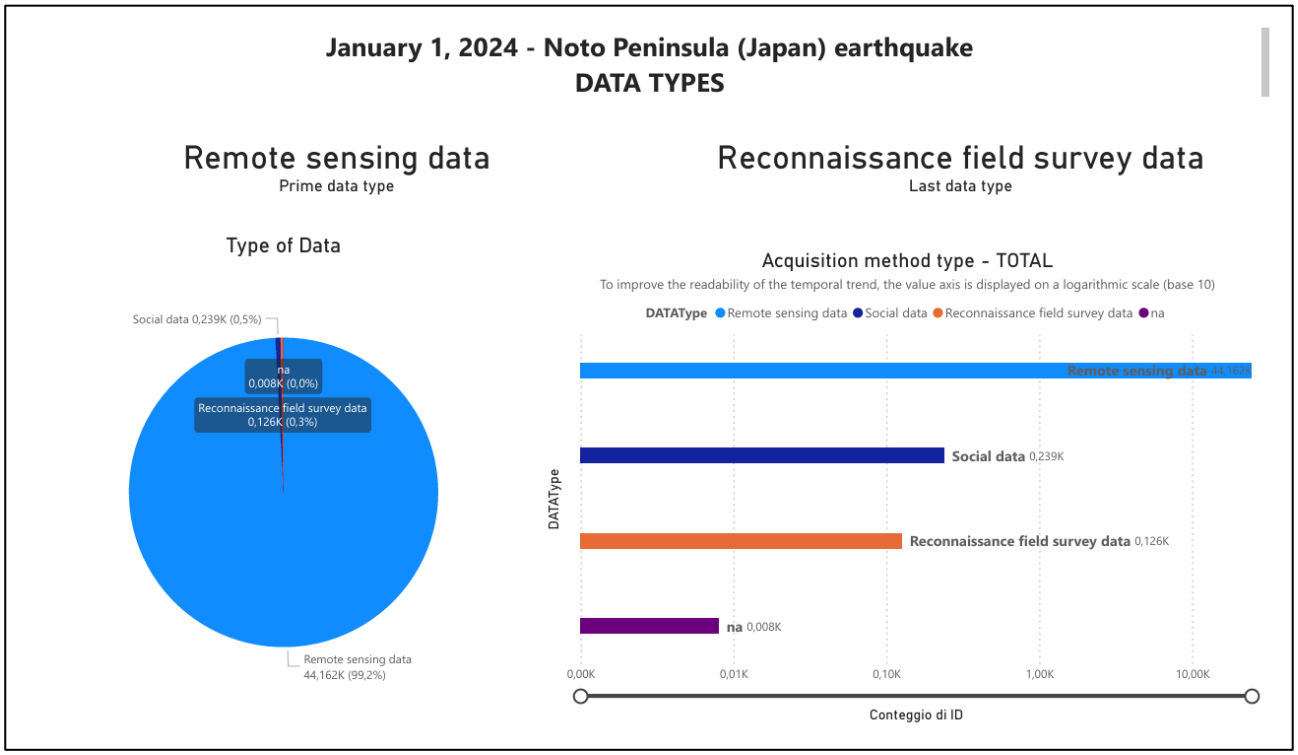

Figure 5.12 - Visual explanation of EEEs data source and acquisition methods. *Remote sensing data constitute the vast majority (99,2% of the data), while the other categories represent the 0,8% of the data. This confirms the primacy of remote sensing techniques.*

Ground cracks EEE category

Ground cracks represent the largest EEE category, accounting for 50,16% of the total dataset (22 340 records). The vast majority are derived from remote sensing data (22 299 out of 22340 records), with minor contributions from social data (40 records) and reconnaissance field surveys (1 record). The structured interpretation and characterization of most features is largely based on high-resolution remote sensing techniques, promoted by the Geospatial Information Authority of Japan (GSI, 2024) (Tab. 5.1).

Tectonic uplift/subsidence EEE category

Tectonic uplift and subsidence account for 43.77% of the total (19 490 records) and are almost entirely derived from remote sensing data (19 470 records), with additional contributions from social data (14) and field surveys (6). Data are sourced primarily from the Geospatial Information Authority of Japan (GSI, 2024) and from scientific publications (Tajima et al., 2024; Ohno et al., 2024; Mizuno et al., 2024) (Tab. 5.1).

Slope movements EEE category

Slope movements total 2414 records (5,42%) are predominantly identified through remote sensing data (2345 records), with additional contributions from social data (67) and field surveys (2). These data are derived from the Geospatial Information Authority of Japan (GSI, 2024), academic references (Yuhi et al., 2024; Fukushima et al., 2024), and social media documentation. Some records are also linked to field-based analyses, especially for large-scale landslides and disrupted slopes in mountainous regions (Tab. 5.1).

Anomalous waves and tsunamis EEE category

Anomalous waves and tsunamis data, which account for 170 records (0,38%) are distributed across field surveys (108 records), social data (50), and limited remote sensing data (4). These observations are reported in recent studies by Heidarzadeh et al. (2024), Inagaki et al. (2024), and Mulia et al. (2024), which include tsunami field surveys and modeling analyses, allowing for cross-validation of models, reports, and official survey datasets (Tab. 5.1).

Liquefaction and hydrological anomalies EEE category

Liquefaction and hydrological anomalies account for 66 records (0,14%), including 60 related to liquefaction processes and 6 to hydrological anomalies. Most data are derived from social sources (57 records for liquefaction, and 6 for hydrological anomalies), complemented by reconnaissance field surveys (3 records). The effects are reported and interpreted in the studies of Acharya et al. (2024) and Yoshida et al. (2024) (Tab. 5.1).

Surface ruptures EEE category

Surface ruptures are represented by 50 records (0,11%), the majority of which are derived from remote sensing data (44 records), while 6 are from reconnaissance field survey data. Their compilation is reported in the work of Yoshida et al. (2024) (Tab. 5.1).

Tree shaking and Dust clouds EEE categories

These are the least represented EEE categories in the dataset. Tree shaking includes 3 records (0.01%), and dust clouds account for 2 records (0.00%), both exclusively derived from social data (Tab. 5.1).

Table 5.1 - EEEs data source and acquisition methods. *EEEs categories and acquisition methods are listed, showing both total and percentage values.*

EEE Type	Social data	Reconnaissance field survey data	Remote sensing data	na	Total	Total %
TOTAL	239	126	44162	8	44535	100%
Ground cracks	40 (0.2%)	1 (0.0%)	22299 (99.8%)	0 (0.0%)	22340	50.16%
Tectonic Uplift\Subsidence	14 (0.1%)	6 (0.0%)	19470 (99.9%)	0 (0.0%)	19490	43.76%
Slope movements	67 (2.8%)	2 (0.1%)	2345 (97.1%)	0 (0.0%)	2414	5.42%
Anomalous waves and tsunamis	50 (29.4%)	108 (63.5%)	4 (2.3%)	8 (4,71%)	170	0.38%
Liquefaction processes	57 (95.0%)	3 (5.0%)	0 (0.0%)	0 (0.0%)	60	0.13%
Surface ruptures	0 (0.0%)	6 (12.0%)	44 (88.0%)	0 (0.0%)	50	0.11%
Hydrological Anomalies	6 (100.0%)	0 (0.0%)	0 (0.0%)	0 (0.0%)	6	0.01%
Tree shaking	3 (100.0%)	0 (0.0%)	0 (0.0%)	0 (0.0%)	3	0.01%
Dust clouds	2 (100.0%)	0 (0.0%)	0 (0.0%)	0 (0.0%)	2	0.0%

3.2 EEES SPATIAL ANALYSIS

The QGIS-based spatial analysis enables a detailed spatial representation of the EEEs and their associated ESI-07 intensities. The high volume and density of data collected allowed the edition of different high-resolution maps, showing fine scale spatial distribution patterns and localized amplification phenomena (Fig. 5.13). Although the majority of EEEs are concentrated in the Noto Peninsula, EEEs are also documented at greater distances, including the Niigata Peninsula.

The general EEEs distribution map shows the presence of all nine EEEs categories in the Noto Peninsula. These include, in descending order of frequency: *ground cracks, tectonic uplift/subsidence, slope movements, anomalous waves and tsunamis, liquefaction processes, surface ruptures, hydrological anomalies, dust clouds, and tree shaking.*

In contrast, outside the epicentral area of Noto peninsula, and especially along the coasts of Toyama and Niigata, only the categories of *Anomalous waves and Tsunamis* and *hydrogeological anomalies* are dominant. The spatial pattern of the general EEEs distribution map confirms a sharp attenuation of EEEs with distance

from the epicenter. Evidence of amplification effects is observed in Kanazawa, Imizu, Itoigawa, and Joetsu cities and their vicinity.

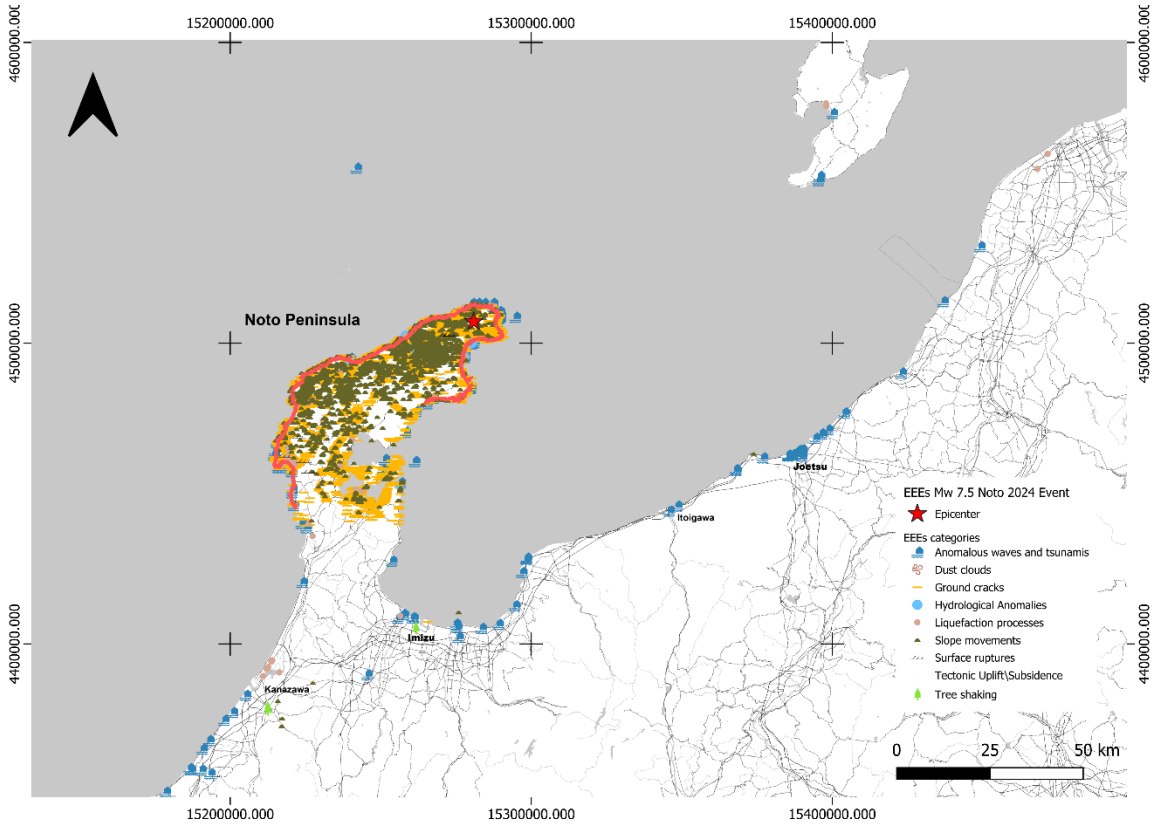

***Figure 5.13 - General EEEs distribution map**. The EEEs distribution map displays all the EEEs recorded for the Mw 7.5 Noto Earthquake. All nine EEEs categories identified in the study are present across the Noto Peninsula, whereas in distal areas, anomalous waves and hydrogeological anomalies are the most frequently observed effects.*

The highest intensity values (ESI-07 XI) associated with tectonic uplift and subsidence, are concentrated along the northwestern coast, particularly in the Saruyama coastal area (Fig.45). The inland area and the Toyama Bay region exhibit a broader intensity range, spanning from ESI-07 XI to V, associated primarily with slope movements and ground cracks (Fig. 5.14). Major ground fractures are predominantly located along critical infrastructure corridors (e.g., highways and main roads), while slope movements are primarily found in mountainous regions with moderate to steep slopes, both inland and along sections of the northwestern coastline (Fig. 5.15). A hotspot of surface ruptures is identified near Wakayama town along a 5 km uplift zone, where scarps up to 2.2 m high are observed (Yoshida et al., 2024). Their distribution suggests coseismic growth of pre-existing folds. The maximum ESI-07 value assigned is X.

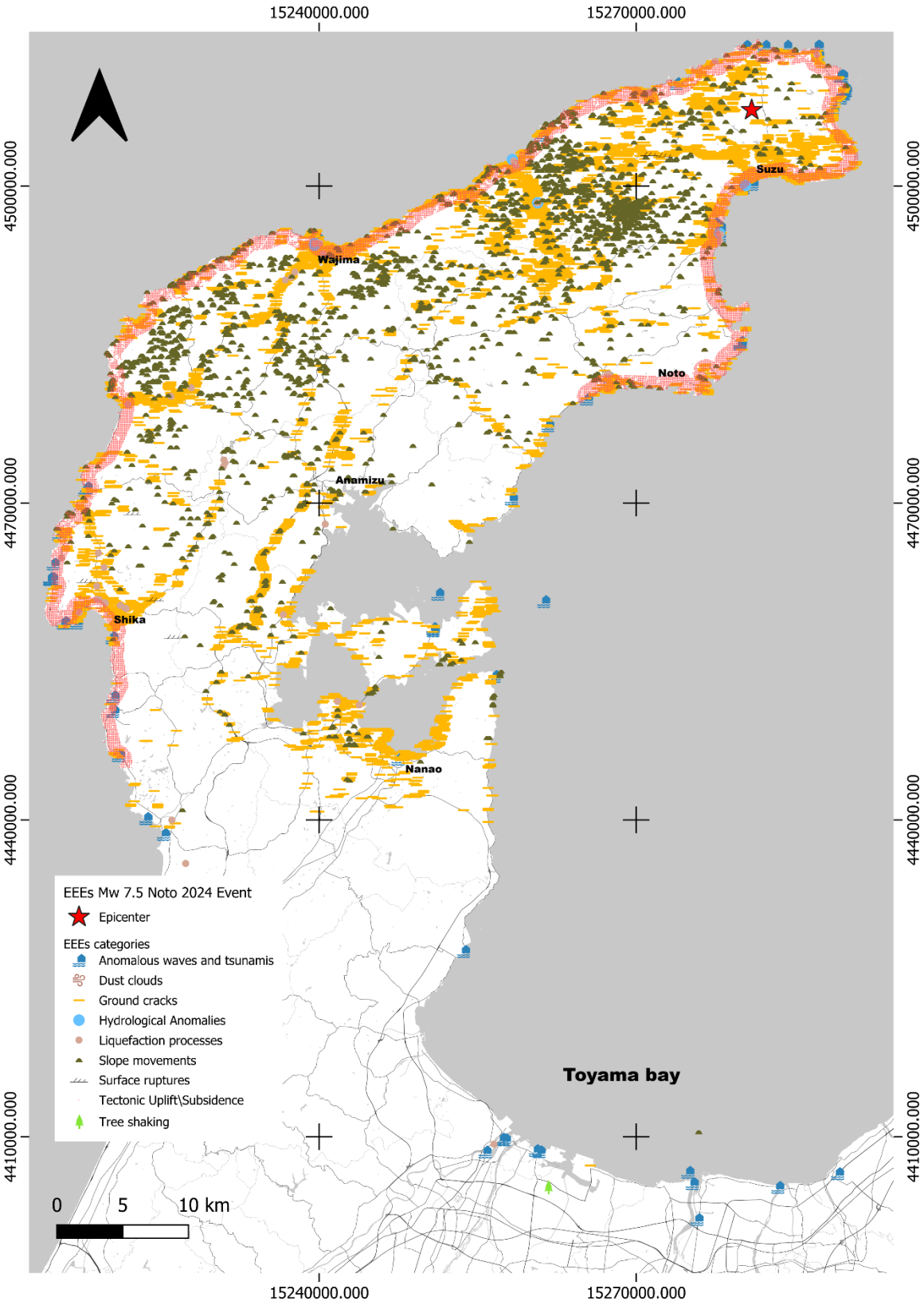

Figure 5.14 -EEEs distribution map of the Noto Peninsula. *EEEs distribution map shows all the EEEs registered for the Mw 7.5 Noto Earthquake on Noto Peninsula. Uplift and subsidence are recorded along all coasts, while slope movements and ground cracks are dominant in the inland area.*

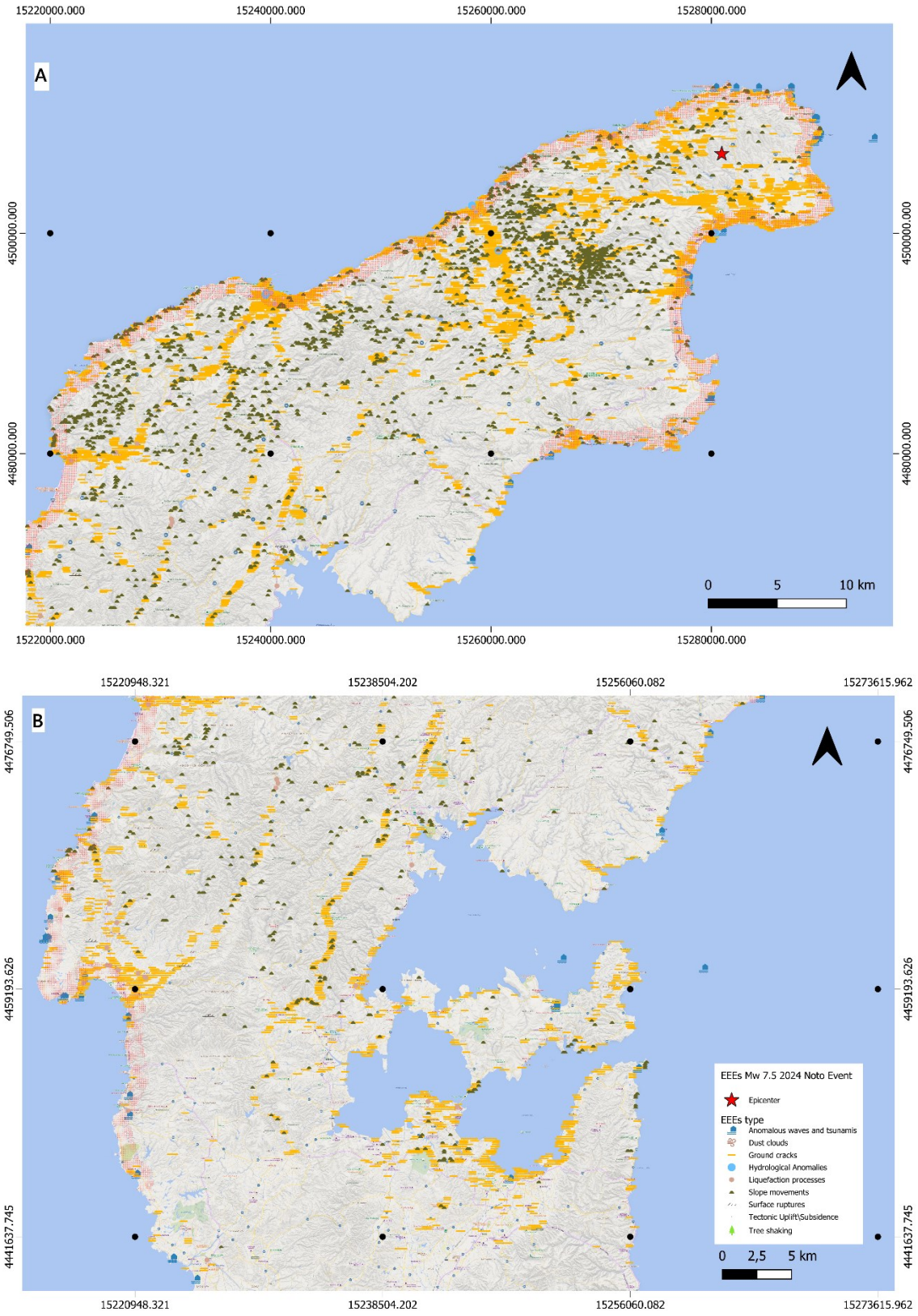

Figure 5.15 6 – Spatial distribution of environmental effects (EEEs) recorded after the Mw 7.5 2024 Noto Peninsula earthquake. *Symbols represent different EEEs categories. The epicenter is marked by a red star.*
(A) Northern Noto Peninsula, with high concentrations of tectonic uplift/subsidence along the northwestern coast (e.g., Saruyama and Anamizu), slope movements clustered near Suzu, and ground cracks aligned with major roads.
(B) Southern sector and surrounding areas, including Toyama Bay and the Niigata coast. Here ground cracks dominate along infrastructure corridors, and slope movements and hydrological anomalies are scattered across both coastal and inland zones.

3.3 ESI-07 INTENSITY GRID ANALYSIS

To quantitatively observe the spatial distribution of ESI-07 intensities among the EEEs recorded, two ESI-07 intensity grids with different cell resolution (1x1 km^2 and a 5x5 km^2) are produced. Each grid is populated by assigning the maximum ESI value observed within each cell.

The 1x1 km^2 ESI-07 intensity grid is composed by 1753 active cell. The maximum ESI-07 value recorded is XI, while the minimum is V. The mean ESI is 7.87 (rounded), the median is 7, and the standard deviation is 1.37 (rounded) (Tab.5.2).

The 5x5 km^2 ESI-07 intensity grid is composed by197 active cells. The maximum and the minimum ESI-07 values do not change. The mean ESI increases to 8.48 and the median increases to 8. The standard deviation is of 1.58 (Tab. 5.3).

Table 5.2 - 1x1 km² ESI-07 Intensity Grid. *The table displays mean, median, standard deviation, minimum and maximum value and active cells number values.*

1x1 km^2 ESI-07 Intensity Grid

Indicator	Value
Mean	7.87
Median	7
Standard deviation (population)	1.37
Min value	5
Max Value	11
Active cells number	1753

Table 5.3 - 5x5 km² ESI-07 Intensity Grid. *The table displays mean, median, standard deviation, minimum and maximum value and active cells number values.*

5X5 km^2 ESI-07 Intensity Grid

Indicator	Value
Mean	8.48
Median	8
Standard deviation (population)	1.58
Min value	5
Max Value	11
Active cells number	197

The 1x1 km^2 ESI-07 intensity grid exhibits a high grade of spatial detail (Fig. 50). The general distribution ESI-07 intensities decrease from north to south. The areas with the highest intensities (ESI-07 XI and X) are concentrated around the epicentral region and along the northwestern coast. The southwestern and northeastern coast are characterized by ESI-07 IX and VIII intensities. The inland area is characterized by ESI-07 from IX grade to V grade. The intensity field is heterogeneous, with notable local variations and isolated cells of high intensity values, reflecting amplification phenomena and local geological and geomorphological local diversities (Fig. 5.16).

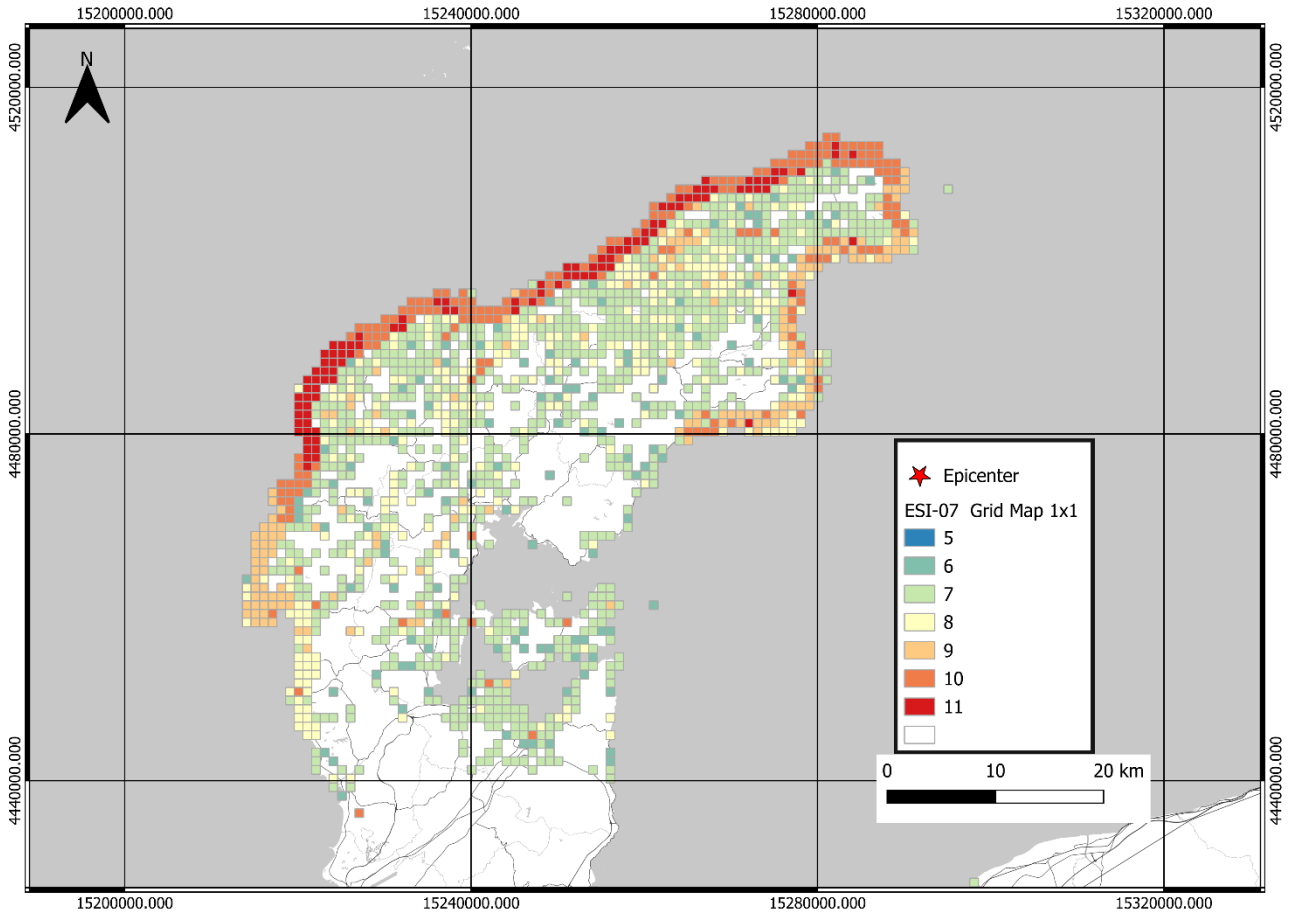

Figure 5.16 – 1x1 km² ESI-07 intensity grid. *The map shows the spatial distribution of ESI-07 values. Each cell represents the maximum ESI-07 intensity observed within a 1 km² area. Higher intensities are concentrated along the northeastern coast, while the rest of the region shows a heterogeneous distribution of intensities. The high resolution of the grid captures local variations and site-specific phenomena, highlighting the fine scale complexity of the intensity field.*

The 5x5 km² ESI-07 intensity grid (Fig. 5.17) shows a smoother spatial variation, resulting in a flatter frequency distribution across ESI-07 grades. The general distribution ESI-07 intensities decrease from north-west to south-west. The highest intensities are still located in proximity to the epicenter and along the northwestern coast of the peninsula, covering a broader area compared to the 1x1 grid, while the inland area is characterized by decreasing ESI-07 intensities from north-west to south-west. The coarser resolution of the 5x5 km² ESI-07 intensity grid allows the smoothing of local geological and geomorphological variability, enabling the display of a more homogeneous regional pattern.

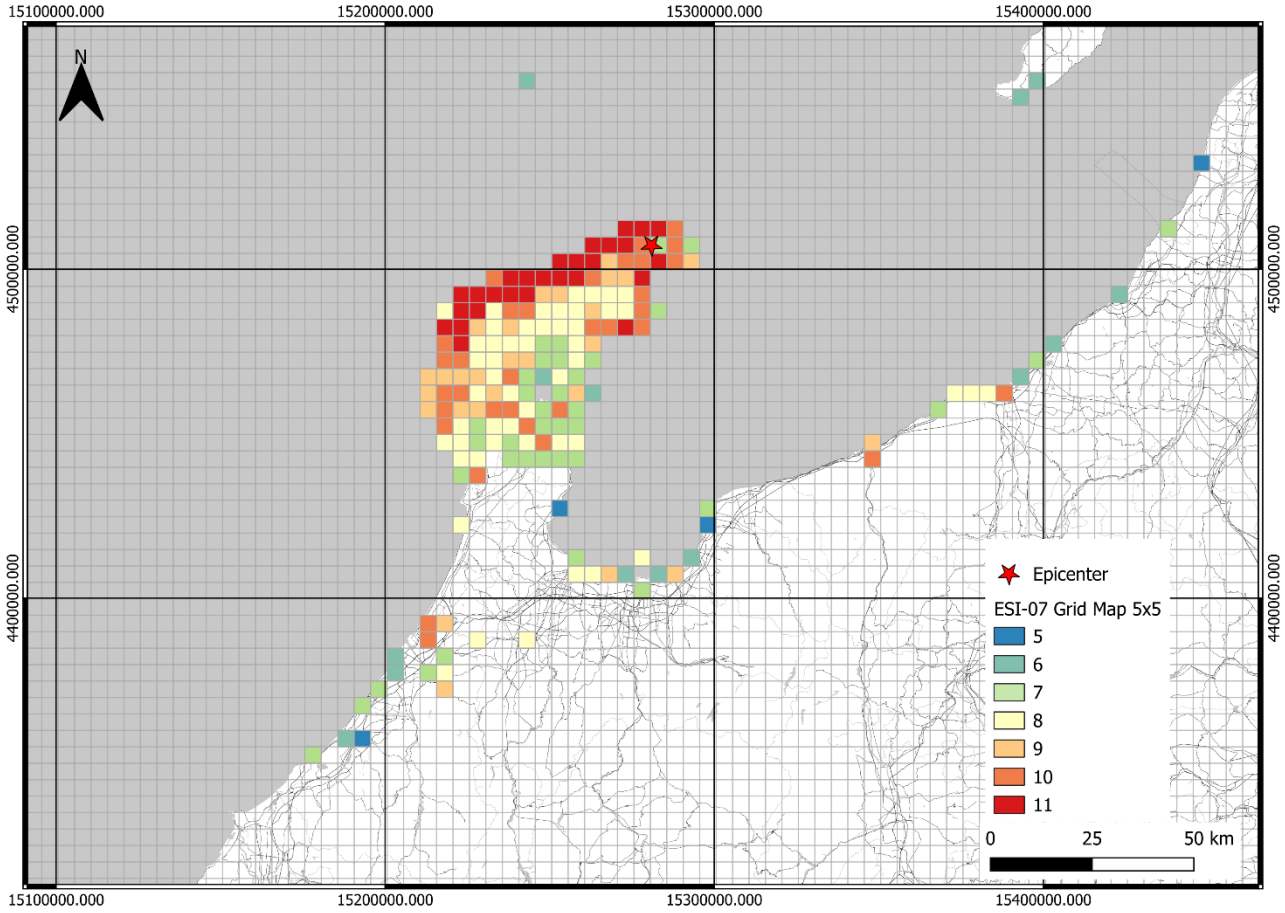

Figure 5.17 – 5x5 km² ESI-07 intensity grid. *The map shows the spatial distribution of ESI-07 values. Each cell represents the maximum ESI-07 intensity observed within a 5x5 km² area. Higher intensities are concentrated along the northeastern coast, while the rest of the region displays a more generalized distribution, which enables to see a decreasing patterns of intensities from north-west to south-west. Local phenomena such as amplification are still visible in different areas, even far from the epicenter. The coarser resolution smooths out local variability, emphasizing broader spatial trends and regional-scale patterns.*

For the 1x1 km^2 ESI-07 intensity grid (Fig. 5.18), the most frequent ESI-07 intensity class is VII, accounting for 45.98% of the total cells, while ESI-07 intensity class V is the less frequent, accounting for 0.285% of the total. ESI-07 VIII and ESI-07 VI represent respectively 18.43% and 8.16% of the total. Higher intensities (ESI-07 X and XI) together represent 17.06% of the total, while lower intensities (ESI-07 V and VI) constitute 8.44%. The distribution is strongly centered around intermediate intensities, with a peak on ESI-07 and with a gradual decrease toward both lower and higher classes. As seen for the 1x1 km^2 ESI-07 intensity grid map, the bar chart captures more localized variability, resulting in the visualization of a sharper concentration around intermediate values and a steeper decline toward the extremes.

For the 5x5 km^2 ESI-07 intensity grid (Fig. 5.18) the highest frequency is observed for ESI-07 VIII (26.90%), followed by ESI-07 VII (19.29%) and ESI-07 X (16.75%). Low intensities (ESI-07 V and VI) represent 9.64% of the total while high intensities (ESI-07 X and XI) represent 30.46%. All ESI-07 intensity grades are more evenly represented compared to the 1x1 km^2 grid, although a general decline toward the extremes is still evident. The pattern displayed in the bar chart reflects how the coarser resolution leads to a smoothing of local

variations and an aggregation of higher intensities across broader areas, resulting in a flatter frequency distribution of ESI-07 grades (Fig. 5.18).

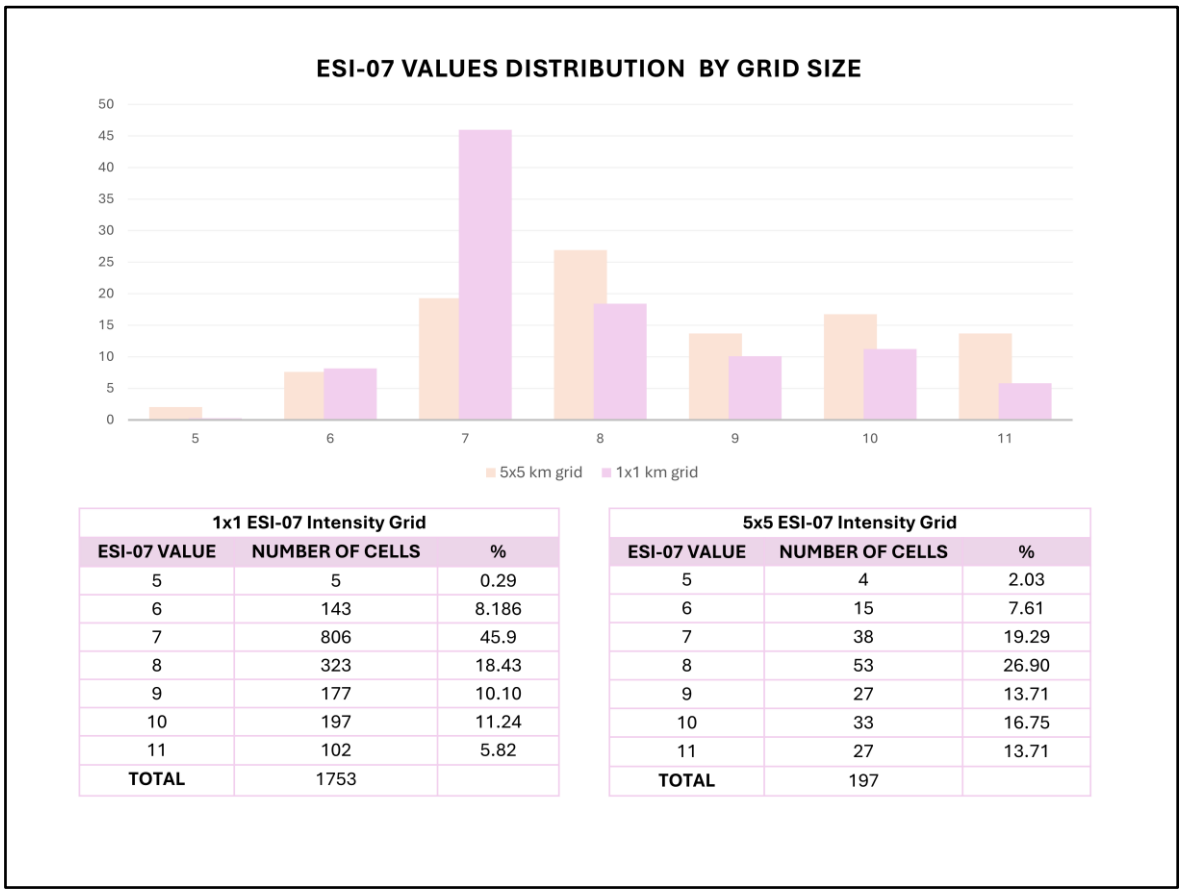

1x1 ESI-07 Intensity Grid		
ESI-07 VALUE	NUMBER OF CELLS	%
5	5	0.29
6	143	8.186
7	806	45.9
8	323	18.43
9	177	10.10
10	197	11.24
11	102	5.82
TOTAL	1753	

5x5 ESI-07 Intensity Grid		
ESI-07 VALUE	NUMBER OF CELLS	%
5	4	2.03
6	15	7.61
7	38	19.29
8	53	26.90
9	27	13.71
10	33	16.75
11	27	13.71
TOTAL	197	

Figure 5.18 - Bar chart and tables for ESI-07 value distribution by grid size. *A Bar chart which compares the frequency distribution of ESI-07 intensity classes between the 1x1 km² and 5x5 km² grids is reported. Each bar represents the percentage of cells assigned to a given ESI-07 value. The 1x1 km² grid shows a peak at ESI-07 VII grade, while the 5x5 km² grid presents a more balanced distribution, with ESI 8 being the most represented class. The difference reflects the influence of spatial resolution on local variabilities.*

DISCUSSION

4.1 DATA MANAGEMENT

The construction of the ESI-07 dataset for the 2024 Mw 7.5 Noto Peninsula earthquake relies on data acquired from multiple sources, including: scientific publications, datasets provided by national agencies (e.g., GSI), field surveys and content derived from social media and press agencies. Among these, automated or semi-automated datasets from national agencies and studies from authors constitute the majority of the data in terms of both volume and spatial coverage. Field survey data and visual data derived from authors, social media and press agencies, although more limited in terms of number, provide valuable visual documentation and qualitative validation of the EEEs, particularly through to the inclusion of photographic and video documentation.

Overall, the study confirms how quality and reliability of the collected data constitute the foundation for the development of building a representative and robust ESI-07 dataset. This was previously emphasized by Ferrario (2022a) and more recently by Muccignato and Ferrario (2025).

However, several obstacles are noted during the dataset construction process. One of the most significant key limitations is the language barrier. A substantial proportion of the data acquired (e.g., GSI datasets, social media content, and press materials) are available exclusively in Japanese. The lack of English metadata or accompanying descriptions often hinders the ability to identify data authorship, origin, location and acquisition methodology.

A second major obstacle is the lack of data completeness such as: absence of visual references, dimensional information, georeferencing details, and clear description of acquisition methods. This is particularly true for social media and press data, and for GSI datasets, in case of acquisition method description. These issues interfere with the critical assessment of data, interpretation and description of EEEs, ESI-07 estimation, and ultimately the overall reliability of the dataset.

4.2 ESI-07 GRID ANALYSIS

The work present6ed is the first application of the ESI-07 grid methodology to a major earthquake, characterized by a large dataset, integrating multiple levels of complexity in terms of data geometry (point, line, polygon features), data types and authors (technical reports, authors, national agencies, social media and press), EEEs categories (nine out of ten ESI-07 EEEs categories), and ESI-07 attribution methods (manual and semi-automatic ESI-07 intensity assignment).

The adoption of quantitative, threshold-based and semi-automatic classification significantly improves both the efficiency and the reproducibility of the ESI-07 intensity assignment process. Thresholds are adopted from established standards (e.g., Michetti et al., 2007; Lario et al., 2016; Ferrario, 2022) or are newly

developed for categories lacking pre-existing standards (e.g., ground cracks, uplift/subsidence) using proportional scaling and magnitude-based logic (see Appendix – Tab. 1.4).

While effective, limitations of the approach must be acknowledged. Input errors (e.g., syntax errors, missing or imprecise dimensions), introduce uncertainties in the semi-automatic process of ESI-07 intensity attribution. Furthermore, the robustness of the ESI-07 grid-based method is dependent on the availability and quality of input datasets. In this regard, the January 1, 2024, Noto earthquake represents an exceptional case: at one year from the event, numerous high-resolution datasets and scientific publications were already available (e.g., InSAR datasets, GNSS-based deformation fields, extensive EEE-specific inventories from GSI). This abundance of data ensured the success of the method, but it also underlines that its transferability to earthquakes with more limited documentation may be constrained.
Compared to traditional features-based inventories, this approach provides three main advantages: a) aggregation of data and spatial smoothing; b) multi-scale comparison of ESI-07 intensity distribution and; c) facilitated visualization of EEEs cluster and amplification hotspots.

The spatial aggregation process proves particularly effective in managing the extensive and heterogeneous dataset. Some sectors of the Noto Peninsula are densely covered by high resolution EEEs-specific datasets (e.g., GNSS data and landslide\ground crack inventories of GSI) but lacks coverage of other EEE types. In some cases, the high density of low to moderate ESI-07 intensity data hinder the visual identification of spatial cluster or local maxima. Conversely, other areas present low data density but still included significant isolated EEEs (Fig.53A). The ESI-07-grid-based approach ensures a balanced representation across all these contrasts, by smoothing local variability and avoiding the dominance of overrepresented categories, without compromising analytical robustness (Fig. 5.19).

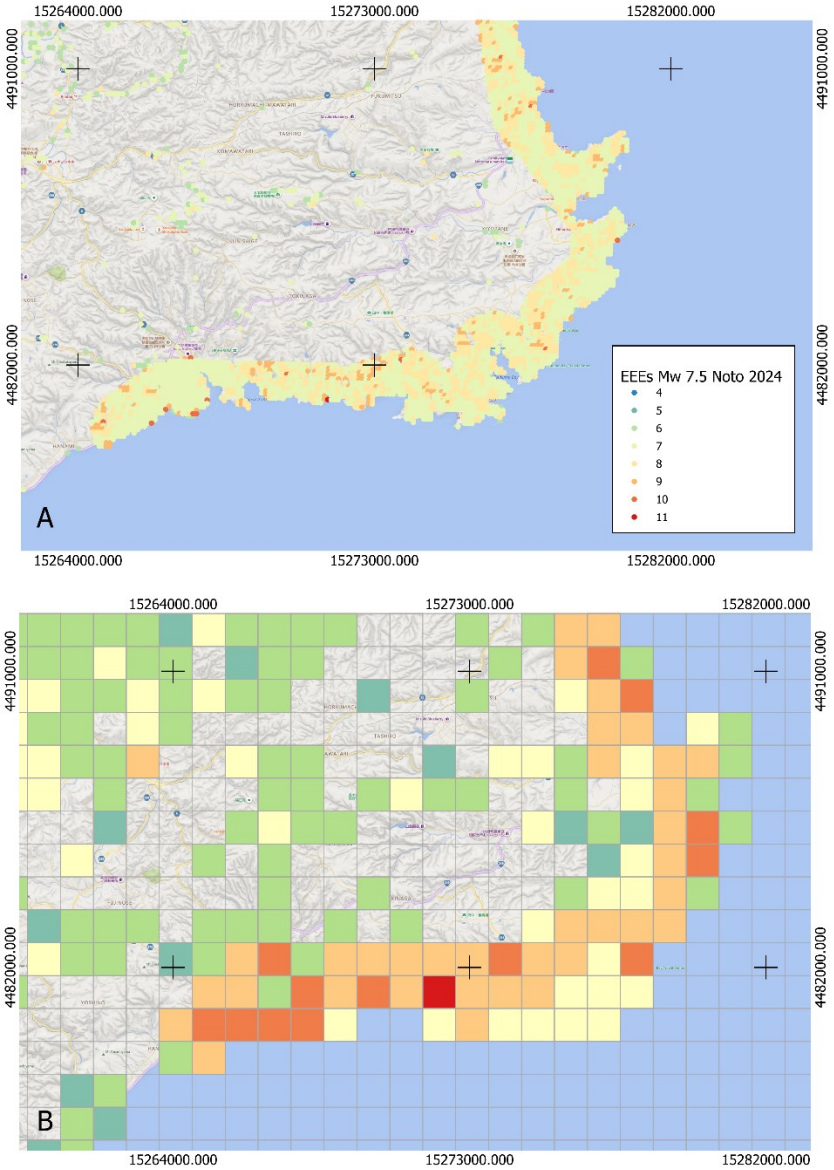

Figure 5.19 – Comparison between ESI-07 feature dataset and ESI-07 grid dataset. *Figure A displays the point dataset. The high density of data hinders the visual detection of areas characterized by high ESI-07 values. Figure B shows the same area represented by a 1x1 km grid approach. Aggregation and spatial smoothing enable the visualization of distribution patterns, local maxima, and enhancing interpretability of results.*

Finally, the adoption of two resolution grids (1x1 km and 5x5 km) proves optimal for the display and detection of spatial heterogeneities and amplification phenomena, as well as the recognition of distribution patterns of different EEEs and ESI-07 intensity values.

4.3 SOCIAL MEDIA DATA: A CRITICAL ASSESSMENT

The rationale that lead to the detailed classification and critical assessment presented in the previous paragraphs lies in the potential utility of high-quality EEEs social data across multiple scientific and operational framework as: macroseismic assessment (Flanagan et al., 2021), hazard and risk assessment and communication (Hicks et al., 2019; Cho et al., 2013; Velev and Zlateva, 2012; White et al., 2009), and more broadly, data enrichment within participatory macroseismology frameworks (Tosi et al., 2024). Through greater public engagement and accessibility, such data can also contribute to the process of democratization of environmental and geoscientific knowledge (Aberasturi Rodríguez et al., 2024; Vayena et al., 2015; Mustac et al., 2022)

In macroseismic assessment, several citizen-based platforms have already demonstrated the relevance of non-expert contributions. Initiatives such as MyShake network (Kong et al., 2015), Did You Feel It?" from USGS (Quitoriano and Wald, 2020), "Hai Sentito il Terremoto? - Mappe degli effetti" from INGV (Tosi et al., 2007), and "LastQuake" from EMSC, are valuable examples of how citizen observations (e.g., EEEs and shaking report) and personal devices used as seismic sensor, can be successfully integrated in macroseismic analyses and mapping, both in local and global scale.

Furthermore, visual and text social media data have already been employed for earthquake damage assessment (Comunello et al., 2016; Poblete et al., 2018, Earle et al., 2011; Chuo Y-J, 2020; Earle et al., 2011), to estimate Mercalli intensity (Mendoza et al., 2019) and computation of perception indexes (D'Auria and Convertito, 2016; Kong et al., 2016).

4.3.1 EEES SOCIAL DATA CHARACTERIZATION AND METHODOLOGY

For Mw 7.5 Noto earthquake a total of 239 EEEs social data are obtained and included in the study, covering eight EEEs categories and ESI-07 grades from VI to X. These data are associated with an extensive archive of visual content obtained from photographs and videos from citizens, press and experts. These data are derived from eight different acquisition methods, distributed unevenly across different user types (Fig. 5.20)

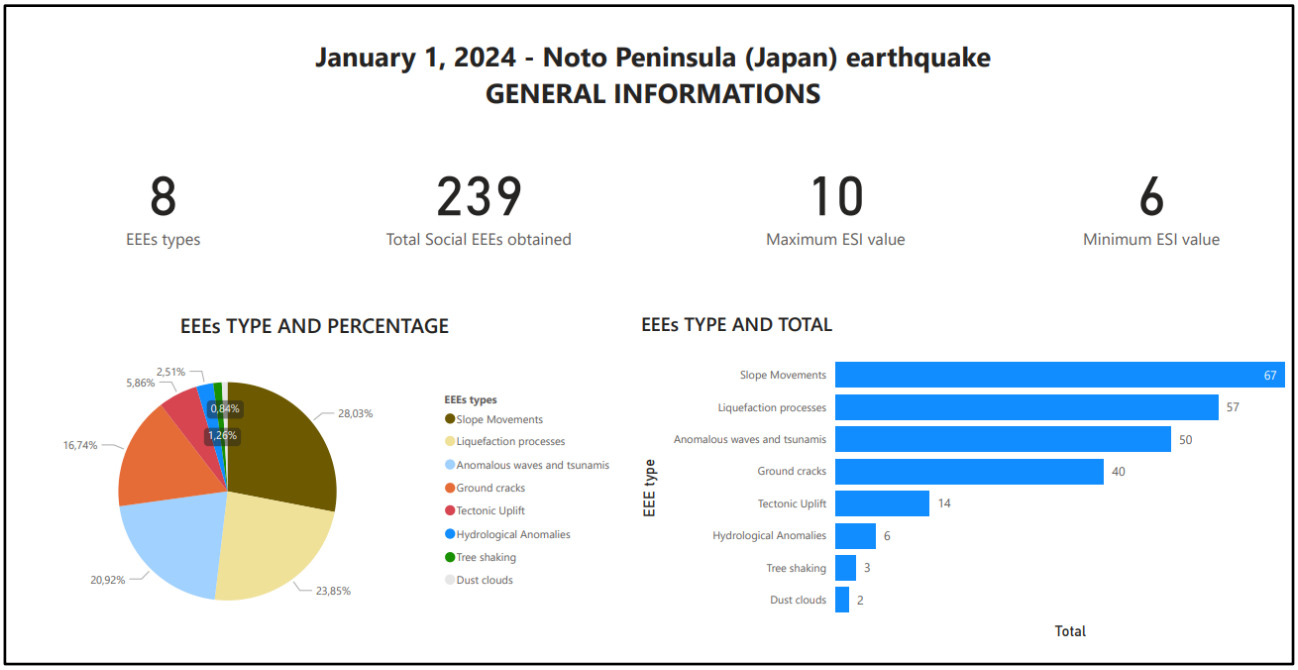

***Figure 5.20 – Characterization of EEEs social data**. The report displays the complete characterization of EEEs social data obtained from the study: type and percentage, total, maximum and minimum ESI-07 values.*

One of the major critical factors encountered during the management of EEEs social data are concerning the reposting\reuploading across platforms, leading to the loss of original authorship. This is particularly true for TikTok and Facebook, where video content is frequently reuploaded and\or reposted to obtain visuals via emotional or visual impact. Out of 239 total EEEs social data, 80,3% (192 data) are classified as original, while 19,7% (47 data) are reuploads (Fig. 5.21).

In addition, significant heterogeneity in terms of spatial and resolution accuracy is observed. EEEs social data obtained range from high-definition drone footage and coordinate sharing to low-resolution, smartphone recordings lacking contextual information. For this reason, a rigorous selection process is applied, which leads to the retrieve of data characterized by sufficient spatial and resolution accuracy, in line with the principled already described in paragraph 4.2 (Ferrario M.F., 2022; Muccignato and Ferrario, 2025).

To critically assess spatial and resolution accuracy of the data obtained, and ensure consistency, two different classification systems are created. For spatial accuracy, a 3-level quantitative scale for spatial resolution are defined where: A) 10^1 m accuracy; B) 10^2 m accuracy; C) only location is known. For resolution accuracy a qualitative scale of 3-level is created where: A) high quality resolution; B) good quality resolution; C) scarce quality resolution.

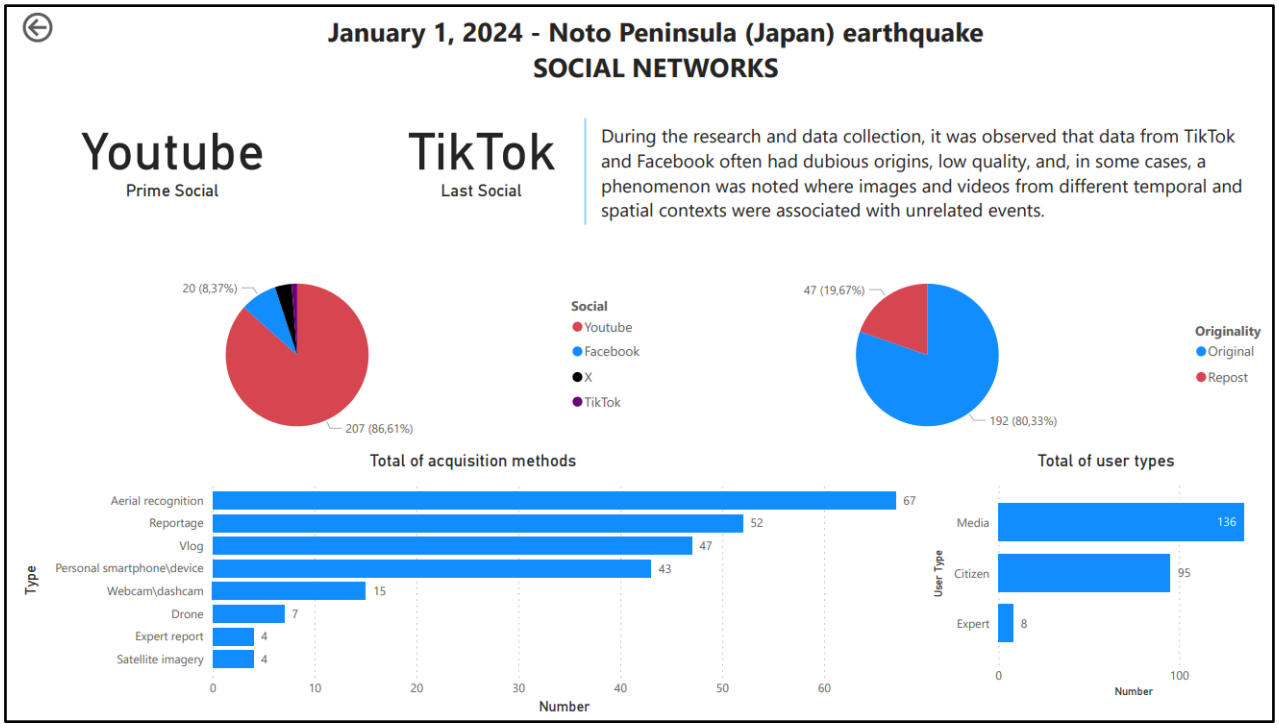

Figure 5.21 -Social Network, Acquisition methods and user types analysis for EEEs social data. *The report shows how the data are distributed along social, data type and user type.*

4.3.2 EEES SOCIAL DATA QUALITY ASSESSMENT AND INFLUENCING FACTORS

For resolution accuracy 138 out of 239 (57,74%) EEEs social data are classified as high resolution (class A), meaning they feature clear and well-defined visual content suitable to identify possible EEEs. 89 EEEs social data (37,42%) fall into good resolution (class B), while only 12 entries (5,02%) are assigned to scarce resolution accuracy (Class C).

In terms of spatial accuracy, the dataset shows a markedly higher overall quality: 213 out of 239 EEEs social data (89,12%) are characterized by high spatial accuracy (class A), indicating precise georeferencing. Only 15 entries (6,28%) are characterized by good spatial accuracy (class B), while 11 (4,6%) have scarce spatial accuracy (Fig. 5.22).

These results highlight a difference in quality tolerance between the two accuracy classes. Resolution accuracy appears to be more flexible, because even moderately defined images may allow identification and classification of EEEs. In contrast, spatial accuracy emerged as a critical parameter: the precise geolocation of potential observed EEEs is essential to validate occurrence, integrate potential EEEs into GIS-based inventories and include them in quantitative analyses, as gridded ESI-07 mapping proposed in this study.

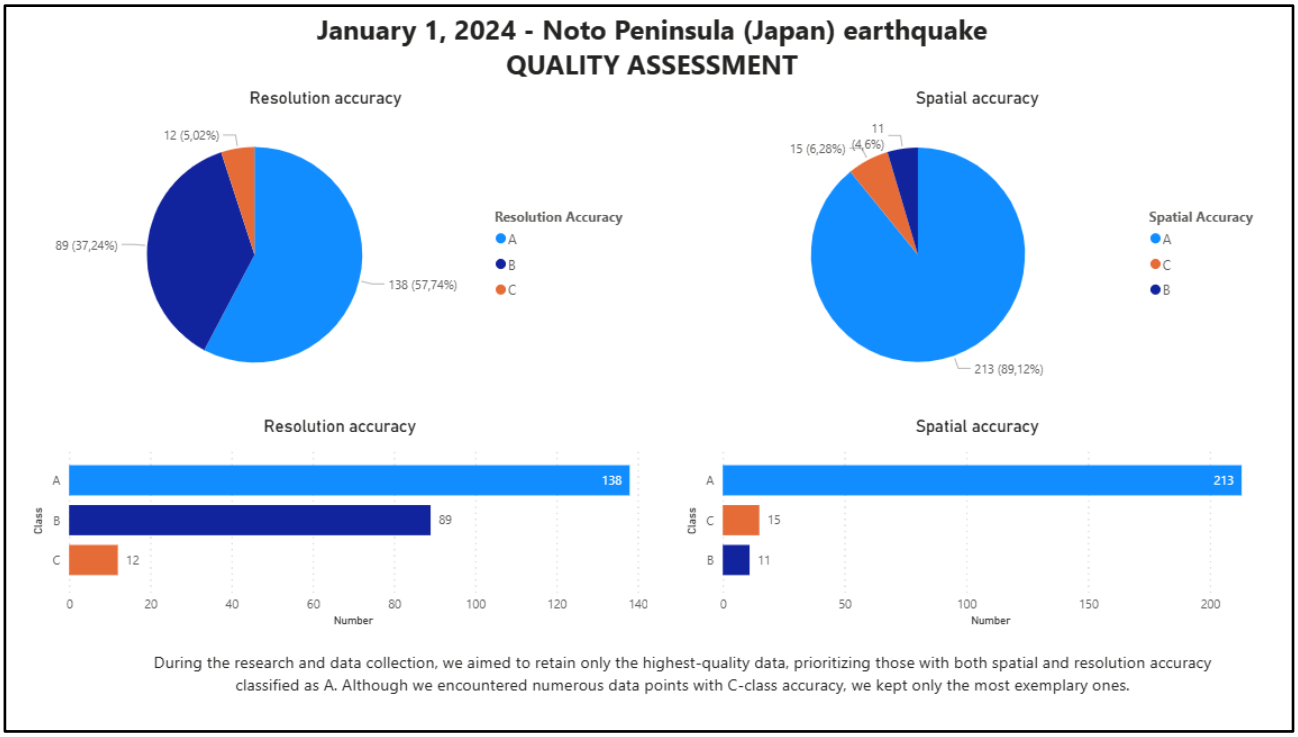

***Figure 5.22 – Resolution and Spatial accuracy of Social Data**. In the image, pie chart and bar chart display the proportion of data falling in each quality class, both for resolution and spatial accuracy.*

An exploratory correlation analysis is then conducted to examine whether EEEs social data quality is influenced by social network, EEEs type, acquisition methods or user type.

Results indicate that user types and acquisition methods can partially influence both spatial and resolution accuracy (Fig. 5.23). In the case of acquisition methods, data acquired through aerial recognition and field survey reports are more frequently present in high quality (A class) for both accuracy classes. For resolution accuracy case, the results show that Expert user category is exclusively present within the higher accuracy class (class A – high resolution). Media users also show a strong presence in class A, representing its majority. The results show that all contribution from these groups are characterized by high-definition content, typically obtained through professional or semi-professional devices and structured documentation standards. In contrast, citizen user category is predominantly distributed across class B (good resolution) and C (scarce resolution), suggesting a greater heterogeneity in equipment type and intents.

A comparable trend is observed for spatial accuracy category. Expert user type is again exclusively represented in class A. Media user type forms the majority of entries in class A, and B, while citizen user type represents the majority of entries in class C (Fig. 5.24).

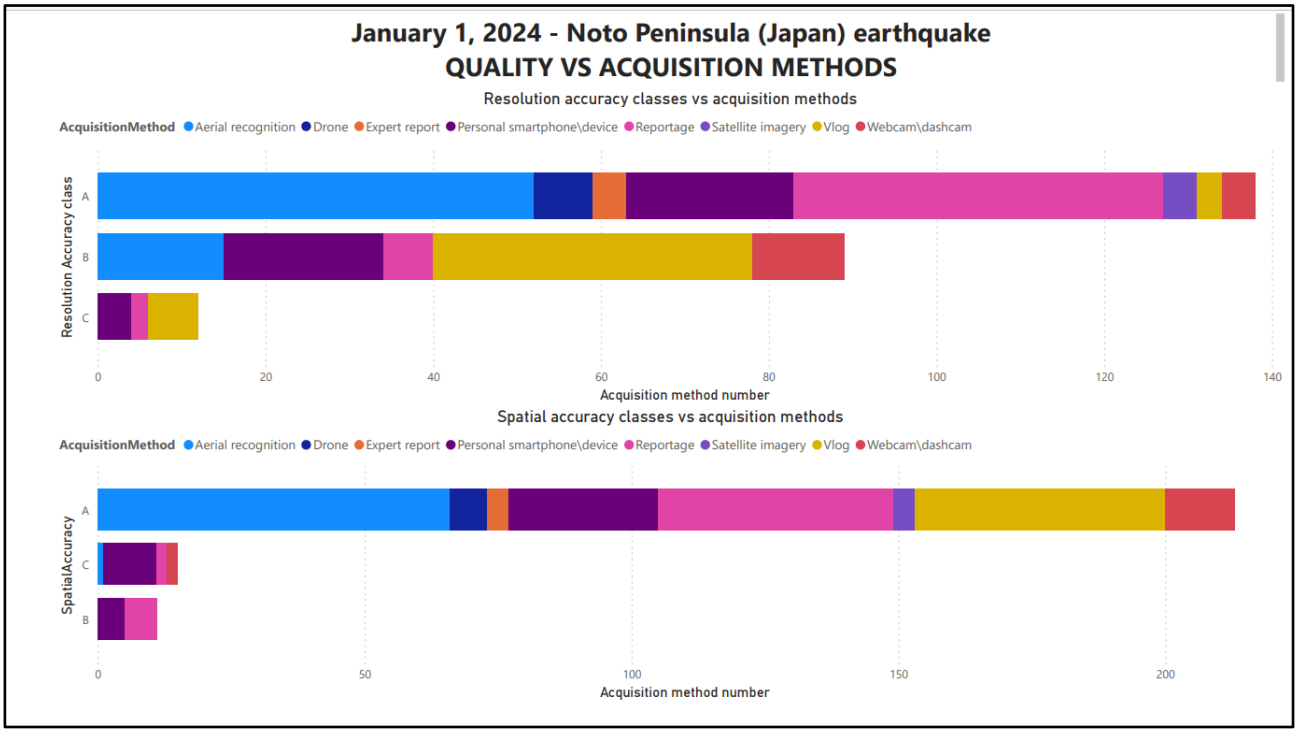

Figure 5.23 - Quality and acquisition methods. *The bar chart shows how the different acquisition methods are distributed along the three different quality classes. It is worth noting that aerial recognition and drone data are only present in high quality data (type A) for resolution accuracy and spatial accuracy.*

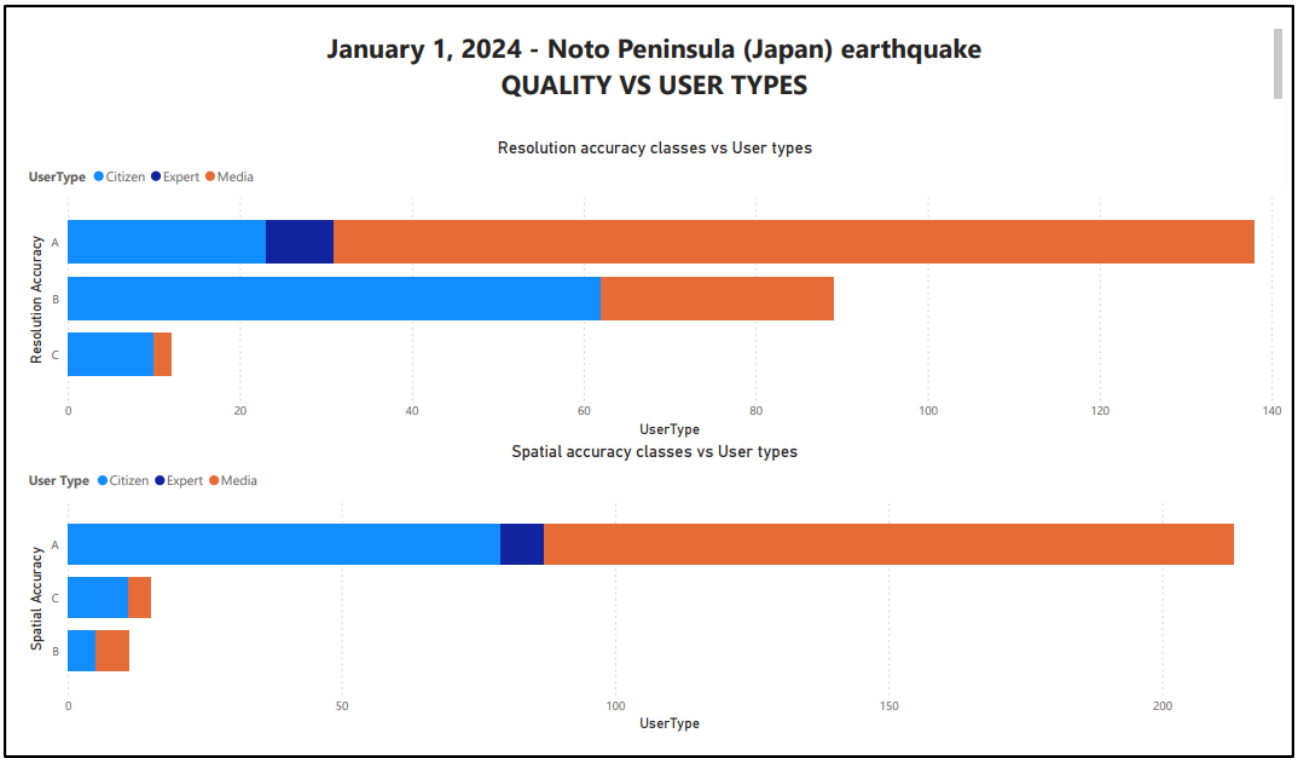

Figure 5.24 - Quality and user types. *Bar chart shows user type distribution along the three classes for resolution accuracy. We ese how media is predominantly present in A and B classes, while expert type is only present in A class.*

The heterogeneous results underline the intrinsic variability of EEEs social data, which depends not only by technical means and user type, which are useful proxies for predicting quality, but also by user's awareness, intentions and familiarity with geospatial practices. As already noted, (Ferrario M.F., 2022; Muccignato and Ferrario, 2025), individual data screening and validation represent a discriminator to select useful and high-quality data.

4.3.3 FROM EVALUATION TO APPLICATION: THE SCIENTIFIC POTENTIAL OF EEES SOCIAL DATA

Despite the broad potential of social data in the context of EEEs, their integration and use into operational or scientific frameworks still face distinct challenges, especially in terms of standardization, source reliability and spatial resolution. This study proposes a methodological framework to enhance the scientific usability of EEEs social data, through the validation, source attribution, classification of spatial and resolution accuracy, and exploratory correlation with standard macroseismic variables. In this context, social data can be effectively used in order to generate integrated product such as ESI-07 intensity assignment, damage mapping, Citizen Science and citizen engagement outputs.

A representative outcome of this approach is shown (Fig. 5.25), which displays the Social ESI-07 Intensity Map, constructed by applying a 5x5 grid-based methodology, similar to the one used for the entire Noto Dataset. The ESI-07 grid map is constructed only with EEEs data retrieved from social media, with each cell reporting the maximum ESI-07 intensity and a specific symbol indicating the type and location of observed social EEEEs. The layout is designed not only to act a synthesis product, but also as an engagement tool, aiming to raise awareness among general public about type and distribution of EEEs. To support the communicative and Citizen Science function, the map includes a call-to-action, with a QR code linking to a Google Form questionnaire. Citizens are invited to contribute by reporting additional EEEs they observed during or after the event, specifying location, type of EEE, time and uploading multimedia files as photo and videos. This participatory mechanism contributes to expanding the dataset, supporting the scientific validation of social data and promoting public involvement in seismic risk awareness and data collection.

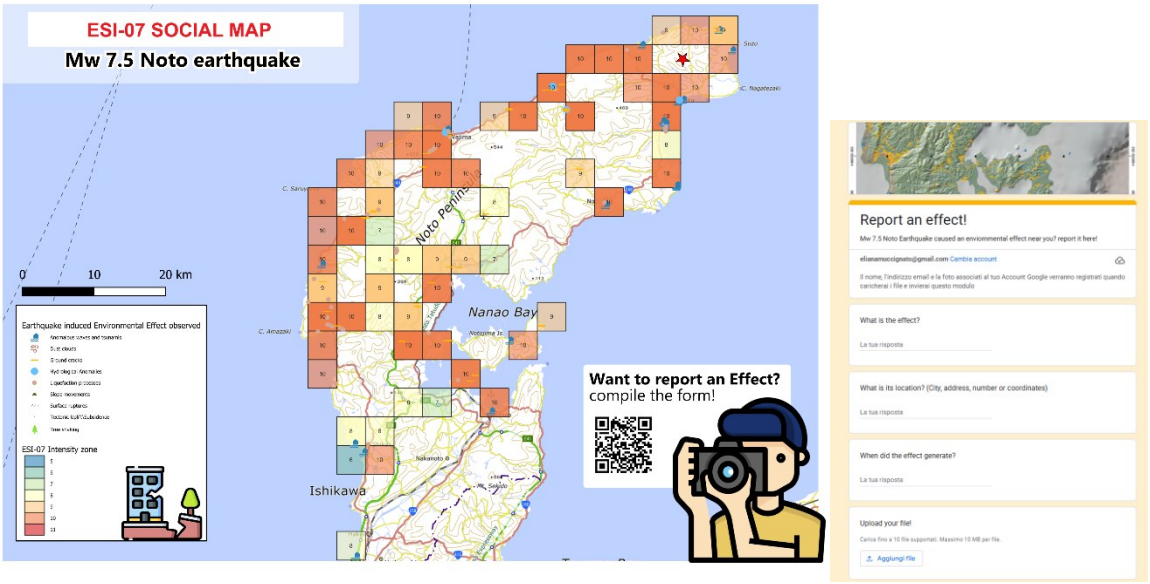

Figure 5.25 – ESI-07 Social intensity Map. *The map displays spatial distribution of maximum ESI-07 in a 5x5 km grid format, together with location and typology of observed EEEs, marked with a specific symbology. The visual layout is designed also for citizen engagement: a call-to- action is included, inviting citizen to contribute via an embedded QR corde, which links to a questionnaire in Google Form, for reporting observed EEEs and uploading related media files.*

CONCLUSION

In this study, an ESI-07 grid-based methodology is implemented to estimate ESI-07 intensity for the Mw 7.5 1 January 2024 Noto event. A total of 44 535 multisource EEEs are collected across an area of 101,197.63 km^2. EEEs ESI-07 intensity is then computed using a GIS-based, semi-automatic method, based on quantitative thresholds. Two different resolution ESI-07 grid maps (1x1 km and 5x5 km) are constructed, and maximum ESI-07 intensity value is extracted for each cell of the grids. 9 Different ESI-07 EEE categories are identified, among which *ground crack* and *tectonic uplift* emerge as the predominant. The ESI-07 intensity values span from V to XI. The highest ESI-07 values are clustered along the northeastern coast of Noto Peninsula, consistent with the proximity of the seismogenic fault trace. The 1x1 km resolution ESI-07 grid provides finer details, capturing localized peaks of intensity. In contrast, the 5x5 km ESI-07 grid provides a smoother output, with a broader spatial gradient, useful for the visualization of broader amplification areas and regional-scale patterns. The results of the study demonstrate that the proposed semi-automatic method is particularly effective for the processing and standardization of large and heterogeneous datasets. The use of ESI-07 grid maps allows optimal spatial analysis and enables spatial smoothing and aggregation, which facilitates the identification of spatial clusters, amplification zones and local maxima. Furthermore, non-traditional data sources integrated, such as social media and press data, proved to be of high quality and reliability. These data contributed to the final ESI-07 grid output and demonstrated to have the potential for enhancing participatory science and citizen science applications.

Overall, the ESI-07 grid estimation method introduced in this study appears to be a robust and replicable approach, effective in the managing and standardization of large dataset of heterogeneous EEEs. Its application can be extended to other cases studies, offering opportunities for further validation and methodological refinement in different geodynamic and geomorphological contexts, expanding the relevance of macroseismic characterization with the ESI-07 Intensity scale.

CHAPTER 6

THESIS DISCUSSION

1. DATA EVALUATION

1.1 IMPORTANCE OF DATA QUALITY FOR ESI-07 CHARACTERIZATION

The analysis conducted in this thesis confirms that data quality, particularly in terms of dimensional and spatial information, is a fundamental prerequisite for the application of the ESI-07 Intensity Scale, which requires information on the amount and dimension of EEEs, expressed through thresholds such as volumes, areas, or lengths (Michetti et al., 2007; Serva et al., 2016; Ferrario et al., 2022). Where such parameters are absent, the possibility of transforming descriptive accounts into quantitative macroseismic information is reduced or inapplicable (Comerci et al., 2015).

This issue emerges clearly from the compilation of the EQUILs dataset for IFFI catalogue (Chap.3). A critical evaluation is performed to the entire dataset compiled, in order to assess how the nature of the original records affects the applicability of the ESI-07 framework and the consequent intensity estimation. In historical earthquakes, a key step is the revision of EEEs reported in documentary and cartographic sources (Michetti et al., 2007; King et al., 2019; Camelbeeck et al., 2021; Ahmad et al., 2014). In accordance with this, the IFFI dataset is analyzed to evaluate its potential utility for ESI-07 characterization. For this purpose, each record is classified into one of two distinct categories:

- Qualitative: narrative or descriptive records without explicit dimensional parameters.
- Quantitative: descriptions including numerical values, spatial dimensions, or other measurable parameters as visual references.

This classification reveals a predominance of qualitative records: out of the entire EQUILs dataset, 60.9% (2118 records) consist of descriptive accounts, while 32.5% (1130 records) include quantitative information. In 235 cases (6.6%), the available information is insufficient to determine whether the record is qualitative or quantitative. The comparison among dataset sources reveals heterogeneity, with the CEDIT catalogue (827 records) and the University of Insubria works (247 records) containing the highest proportion of quantitative entries. The Govi 1977 map, exceptionally detailed for its time, report geometries for detachment zones and rocks (i.e., polygons and lines) but does not report volume references, while the CFTI and the EEE catalogue account for most of the uncharacterized records (i.e., n.a. entries) with 197 and 38 records, respectively (Fig. 6.1).

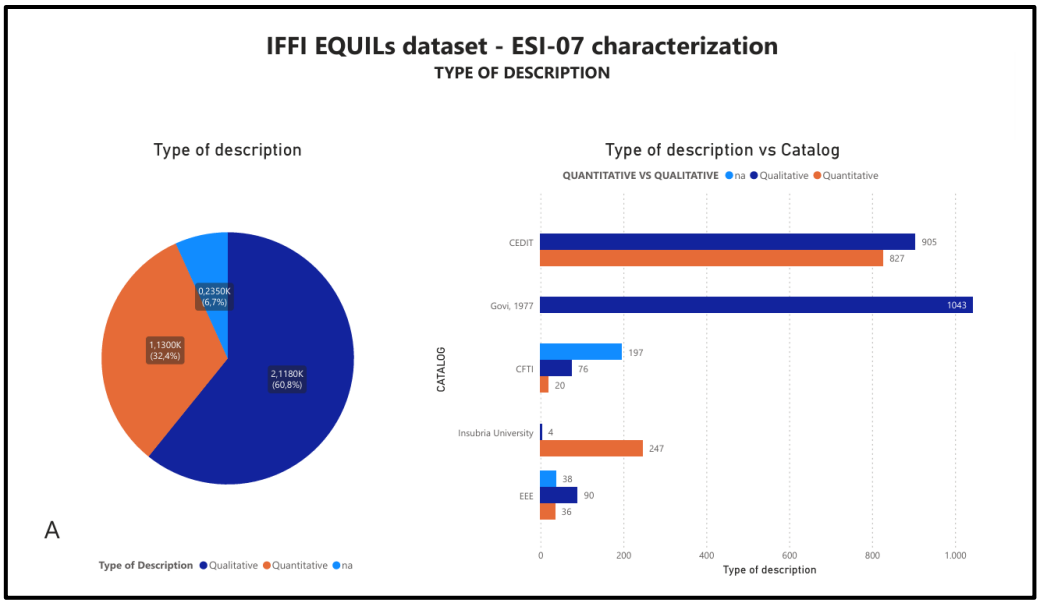

Figure 6.1 – Distribution of records by dataset and type of description. The analysis distinguishes qualitative and quantitative records, with additional "n.a." entries where the classification is not possible. The highest concentration of quantitative records is found in the CEDIT catalog and Insubria works, while the Govi 1977 map exclusively contains qualitative data.

Among the 1130 quantitative records, further discrimination is made to identify those already containing ESI-07 intensities already assigned. Out of this subset, 410 records are found to include ESI-07 values, and particularly 165 from CEDIT catalogue, 1 from EEE catalogue, and 247 from the University of Insubria works, particularly from Pizza et al. (2023).

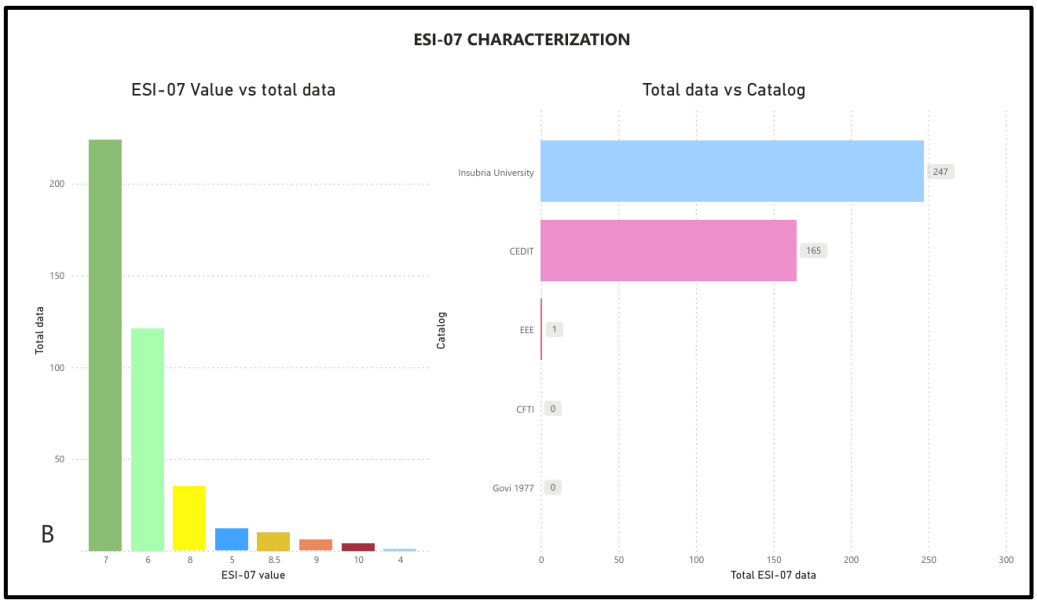

Figure 6.2 – Subset of quantitative records containing explicit ESI-07 intensities. A total of 410 records already include ESI-07 values, with the highest contributions from Insubria University works and CEDIT catalogue. ESI-07 grade is the most present, with more than 200 records, while ESI-07 grade is the least present, with only 4 records.

For the remaining 662 quantitative records, the possibility of deriving ESI-07 intensities is evaluated. The estimate is made through individual analysis of the descriptions of each quantitative record. For the entire subset originating from the CEDIT catalogue, intensities could not be assigned, as the reported values (e.g., landslides < 5 m^3 or < 1 m^3) fall below the volumetric thresholds required by the ESI-07 scale (see App. 1.4). 56 historical records contain dimensional references (e.g., relative heights, approximate lengths), but these reveal to be too imprecise to yield reliable volumetric estimates. Attempting to translate such information into quantitative values would risk overinterpretation and the introduction of bias.

Table 6.1 – Examples of historical quantitative descriptions of EQUILs. Although the records contain dimensional references, the level of precision is insufficient to derive reliable volumetric estimates. The table provides examples for each source catalogue.

EQUIL ID	CATALOGUE	DESCRIPTION
INS2521	CEDIT	*< 1m^3*
INS3358	CFTI	*Collasso di terreno e pietre con una scarpata verticale intorno ai 10 centimetri e lunghezza intorno ai 6 metri*
INS3356	CFTI	*Frane di piccole dimensioni, intorno ai 10 m^3*
INS3446	CFTI	*Dal monte soprastante la contrada Acqua Fredda si staccarono grossi massi di roccia che rotolarono a valle poco lontano dal romitaggio di Polvi andando a ostruire il torrente.*
INS0047	EEE	*Nella zona tra Ferla e Cassaro, un'imponente frana ha sbarrato un ruscello creando un lago con una circonferenza di circa 4,5 km e un'altezza di 250 passi (450 m).*
INS3678	CFTI	*In località San Pietro una frana andò a ostruire un corso d'acqua e si forma un lago lungo circa 185 m (100 passi) e largo circa 110 m (60 passi).*
INS0468	EEE	*Sulla strada rotabile al confine occidentale di S. Procopio, proprio vicino alla Chiesa dell'Addolorata, si è aperta una spaccatura, larga 10 centimetri, con piccole interruzioni la spaccatura continua per 4 o 5 km, verso NE fino alla contrada Cancelli*

The analysis confirms that catalogues compiled with data devoid of numerical and spatial parameters, ESI-07 characterization cannot be performed reliably. Qualitative records included in the EQUILS dataset for IFFI catalog implementation remain useful for documenting the occurrence of EEEs, but they lack the dimensional basis required for systematic macroseismic assessment. While datasets related to historical events may lack of explicit measurements, their critical re-examination, possibly complemented by additional historical sources, may allow the recovery of spatial or dimensional information. This operation proves to be effective also in the re-evaluation and reconsideration of source ruptures and faults characteristics, taking into account updated data, modern analysis and updated earth-science concept, as noted in the work of King et al., (2019) and Boulton et al., (2025). Establishing shared guidelines and harmonized cataloguing practices, aimed at systematically including such parameters whenever available, proved to be serviceable for macroseismic assessment, as already noted in previous works (Silva P., 2019; Zei et al., 2024; Seal et al., 2022; Sørensen et al., 2023; M.F. Ferrario, 2019), and can be expanded to further enhance the application of the ESI-07 scale.

1.2 IMPORTANCE OF DATA DISTRIBUTION FOR ESI-07 CHARACTERIZATION

The robustness of macroseismic analyses based on EEEs depends not only on the intrinsic quality of the data, but also on their spatial distribution and representativeness, in order to construct an adequate macroseismic field (Camelbeeck et al., 2021; . This may reflect or be conditioned by the local geological conditions, survey strategy, and accessibility of locations rather than the actual physical extent of the seismic aftermaths (Papathanassiou et al., 2022). The distribution of effects is also influenced by the attention of the focus of data collection, which can be concentrated in area where human emergencies are present. As a result, earthquake datasets may overrepresent areas along critical transport infrastructures, near-settlements areas, and coastlines, while remote environments may remain under-sampled (Comerci et al., 2015; Ferrario et al., 2020; Mavroulis et al., 2013) Finally, the reliability of GIS-based analyses, including grid methodologies, is directly proportional to the representativeness of the base data: poor or uneven spatial or temporal coverage and temporal obliteration of past EEEs, inevitably propagates into biased outputs (Comerci et al., 2015).

In the case of the 2024 Noto earthquake, this bias is expressed by ground cracks, which are clustered along the main road network of the peninsula (Fig. 6.3), leaving wide areas underrepresented, especially concentrated in the south-eastern part of Noto, leading to an underestimation of the EEEs distribution.

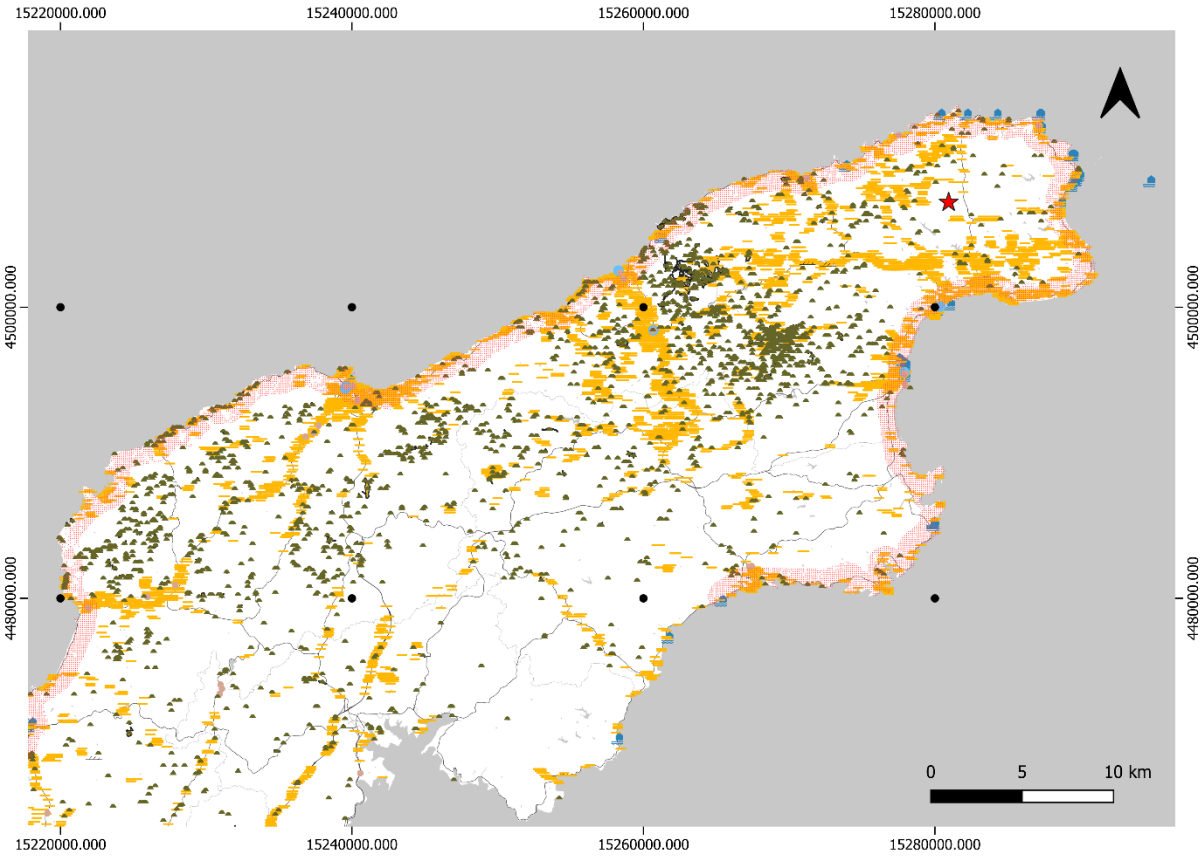

Figure 6.3 – General map of the spatial distribution of EEEs recorded after the 2024 Noto earthquake. The concentration of ground cracks along the main roads highlights the sampling bias introduced by accessibility.

The problem of distribution is not limited to ground cracks category. Similar issues are recurrent for slope movements, which are usually documented near road cuts or inhabited valleys, tsunamis and anomalous waves, which are preferentially described along populated shorelines, and liquefaction phenomena, which are often reported where infrastructures are affected (Mavroulis and Lekkas, 2021; Mavroulis et al., 2021). In each case, the underlying physical process is broader, but the perceived spatial pattern is narrowed by accessibility and observation priorities (Comerci et al., 2015).

To mitigate these limitations, the integration of multiple and complementary sources is critical. Reconnaissance field surveys allow targeted data acquisition, which can be performed in remote or marginal areas. At the same time, citizen-generated information and social media data provide an additional layer of coverage: residents can potentially report effects in places not systematically surveyed, (e.g., small settlements, secondary valleys, or remote coastal sectors). These contributions, although heterogeneous, enhance spatial completeness and improve the identification of localized but significant EEEs.

In the study, the added value of source integration is illustrated by three main examples (Fig. 6.4A–C). In area A (Fig. 6.4A), corresponding to Nakajimamachi Sodohara (central-southern Noto), remote sensing and social media data are concentrated along the Ishikawa Prefectural Road 1 and within the main settlement of Nakajimamachi. A reconnaissance field survey, however, extended coverage to the peripheral hamlet of Hiyo, a location that would otherwise remain undocumented. In area B (Fig. 6.4B), corresponding to Inashiki (southwestern Noto coast), remote sensing data are aligned with the National Highway 249 and the flat coastal plain. Here again, field surveys provide the only data from upland villages on the slopes, which otherwise would not have been included. The area C (Fig. 6.4C), corresponding to Nishiwakimachi (north-central Noto), shows a relatively balanced dataset, with reconnaissance field, remote sensing, and social data all contributing. Nevertheless, the majority of remote sensing data remain concentrated along Ishikawa Prefectural Road 1 and in the inhabited slopes near Ishiyasumibamachi.

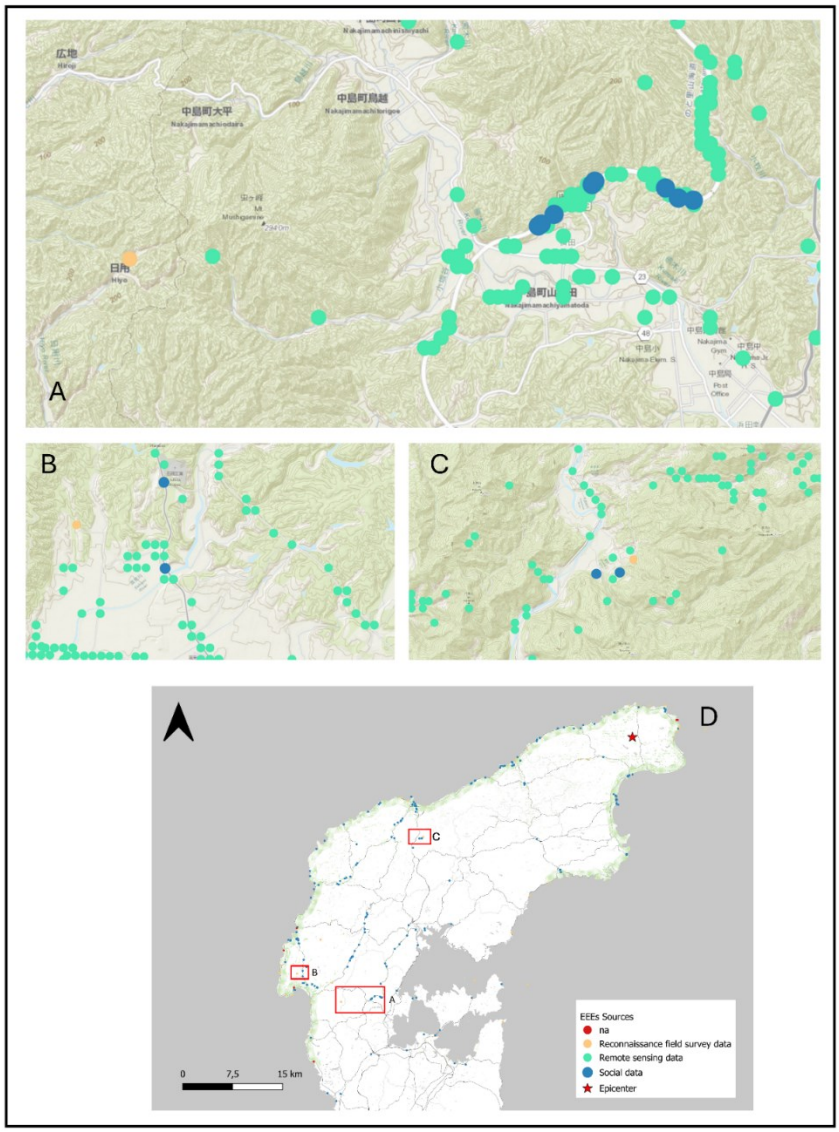

Figure 6.4 – Detailed views of selected areas in the Noto Peninsula, illustrating the integration of different data sources. A) Nakajimamachi Sodohara: field surveys extend coverage to peripheral hamlets. B) Inashiki: integration of field and remote sensing data improves slope coverage. C) Nishiwakimachi: multiple sources contribute to a more balanced dataset. D) General overview map with red rectangles indicating the analyzed areas.

From the analysis conducted on Noto areas, two key considerations emerge and are confirmed: a) data diversity, in terms of both sources and EEE categories and; b) spatial representativeness: without coverage across the full distribution of areas affected, any subsequent analysis will remain partial. In particular, the identification of the latter is in line with what is noted in previous work. In Radziminovich et al., (2010), the lack of EEEs spatial representativeness hindered the evaluation of epicentral intensity of the 27 August 2008 Mw 6.3 Kultuk event, in eastern Siberia; while in the work of Comerci et al., (2015), the fragmented spatial distribution of 365 EEEs for the 28 December 1908 event in Southern Italy, was strongly uneven due to the conduction of an undefined pattern of investigation.

Naturally, certain limitations are intrinsic and unavoidable. Temporal constraints, availability of resources (e.g., personnel, instruments), and logistic difficulties restrict the completeness of data collection. While the 1

January 2024 Noto earthquake represents a favorable case, with a high number of EEEs, diverse data sources, and extended spatial coverage, other cases may rely on more fragmentary information. For such events, analytical strategies must be adapted to the scenario, taking into account the potential unevenness of the EEEs dataset.

In this perspective, the grid-based methodology adopted in this thesis offers a compromise. It provides a flexible and agile framework to manage heterogeneous data, highlight areas of high and low coverage, and generates reproducible and illustrative outputs. At the same time, the case of Noto demonstrates that the interpretative power of grid analyses is ultimately constrained by the spatial quality of the input data, underlying the importance of balancing methodological choices and observational biases.

2. ESI-07 GRID METHOD EVALUATION

2.1 EVALUATION OF THE METHOD THROUGH EQUILS, LAP AND LND

In order to assess the reliability and consistency of the ESI-07 grid-based methodology proposed in the thesis, a comparative and quantitative evaluation is performed, focusing on EQUILs collected for the Noto event. The analysis consists in the computation of LND and LAP parameters, their comparison with ESI-07 values and the subsequent evaluation of how the Noto results fit within the framework of previously analyzed EQUILs inventories presented by *Muccignato and Ferrario (2025)* (see Chapter 4). The same methodology implied to calculate LND and LAP and the equation are retained.

LND and LAP median values for the 2024 Noto Peninsula earthquake are reported in Table 6.2. The two metrics display a coherent trend. LAP values exhibit a progressive increase with intensity, ranging from 0.09% at ESI-07 VI to 28.27% at ESI-07 X, thus reflecting the progressive enlargement of the area affected by EQUILs associated with stronger shaking levels. Conversely, LND values show a maximum at ESI-07 IX, with 4 landslides for km^2, followed by a decrease at intensity X, with 2 landslides for km^2. This decrease expresses the physical limitation, already observed (see chap. 4) as the dimensions of individual EQUILs increase with intensity, the number of distinct landslides that can occur within a 1 km^2 cell necessarily declines.

Table 6.2 – Median LAP and LND values for the 2024 Noto Peninsula earthquake. Median values of LAP and LND calculated for each ESI-07 intensity class are reported. LAP shows a steady increase with intensity, from 0.09% at ESI-07 VI to 28.27% at ESI-07 X, while LND peaks at ESI-07 IX and decreases at X, reflecting physical limits on landslide density within 1 km^2 cells.

ESI-07 VALUE	MEDIAN LAP	MEDIAN LND
10	28.27	2
9	9.10	4
8	1.95	3
7	0.40	2
6	0.09	1

The trends observed for the Noto event are compared with the reference USGS and authors inventories analyzed by Muccignato and Ferrario (2025) (chap. 4). When plotted together, the curves derived for Noto align with those of previous inventories (Fig. 6.5). The LAP vs ESI-07 curve follows the global median trend with coherence, displaying a steady increase across the ESI-07 intensity range and a limited dispersion at intermediate degrees. The LND vs ESI-07 curve reproduces the characteristic pattern already identified previously, corresponding to a gradual increase up to ESI-07 IX and a subsequent decline at the highest degree, related to the spatial constraint of large EQUILs within fixed-size cells.

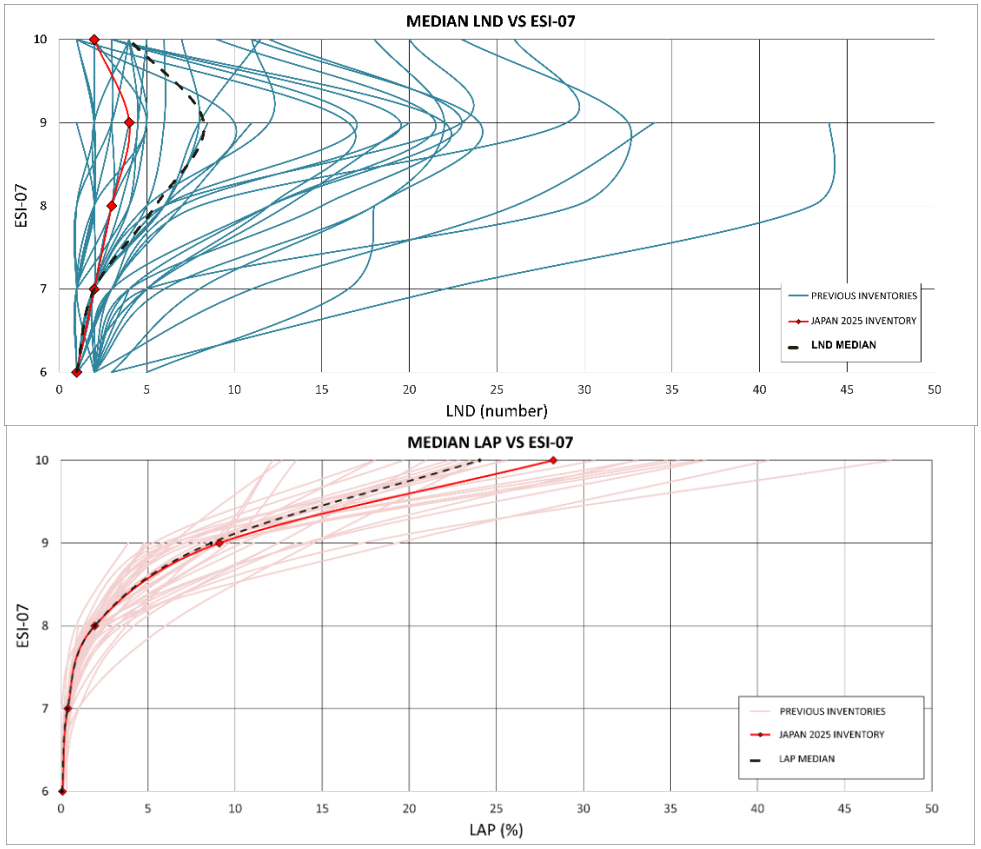

Figure 6.5 - Median LND and LAP vs ESI-07 for the 2024 Noto earthquake compared with previous inventories. Comparison between the Noto 2024 curves (red) and global inventories (thin lines) with median trends (black dashed). The Noto event aligns with the overall global trend, showing the expected progressive increase of LAP and the LND peak at intensity ESI-07 IX grade, and thus confirming the consistency of the ESI-07 grid-based method applied for the Noto case.

The results demonstrate that the Noto inventory fits consistently with previously analyzed EQUILs inventories, supporting the reliability and reproducibility of the ESI-07 grid-based methodology. The consistency between the observed LND and LAP values for Noto case and the global medians indicates that the method successfully captures the expected relationship between ESI-07 intensity and the and the spatial distribution of EQUILs. The dispersion for LND observed already in previous inventories persists with the Noto case. This is due to geometric and methodological factors, including: a) the influence of cell resolution and; b(the different levels of completeness among EQUILs inventories. These differences highlight the importance of

considering the quality and completeness of the inventory, as already noted by Ferrario M.F., (2022) and Muccignato and Ferrario (2025). Despite these limitations, the comparison between the Noto case and the global inventories previously analyzed supports the notion that the equations derived in Muccignato & Ferrario (2025) can be used for predictive purposes. The observed consistency confirms that LAP and LND represent robust quantitative indicators of ESI-07 intensity and can be used to assess the coherence of ESI-07 grids derived from heterogeneous sources, using EQUILs as a robust base for validation.

2.2 ESI-07 GRID METHODOLOGY EVALUATION

To evaluate the accuracy of the ESI-07 grid-based approach in relation to traditional ESI-07 representations, a comparative analysis is conducted between the ESI-07 grid maps resulted and isoseismal lines manually drawn from the point dataset of EEEs collected for the 2024 Noto event. Point data are used to observe the spatial distribution of EEEs and isoseismals from ESI-07 VI to XI are delineated (Fig. 6.6). The resulting pattern describes an elongated area, oriented northeast–southwest, consistent with the strike of the main fault rupture that generated the earthquake.

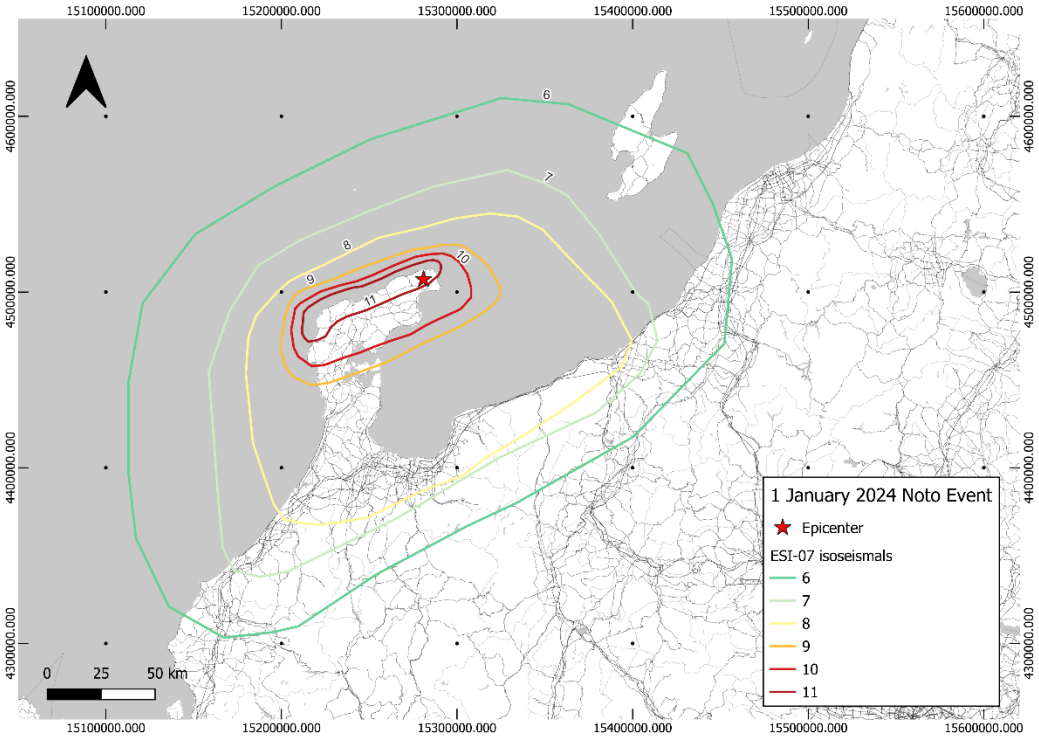

Figure 6.6 - ESI-07 isoseismals for the 2024 Noto Peninsula earthquake. ESI-07 isoseismals derived from the complete point dataset of EEEs. Isoseismals range from ESI-07 degree VI to XI and display a northeast–southwest orientation, in accordance with the rupture direction of the main fault and the distribution of major surface deformation.

To validate the reliability of the grid-based approach, the ESI-07 grids at 5×5 km^2 and 1×1 km^2 resolution are compared with the ESI-07 isoseismal map. The comparison highlights a partial consistency between the two

representations, particularly for the higher intensity classes (X–XI), where both approaches reproduce similar spatial patterns (Fig. 6.7). However, notable differences emerge in general intensities distribution. The 5×5 km grid reproduces the general geometry of the ESI-07 isoseismals, but shows localized variations in adjacent cells. This indicates that, even at relatively coarse resolution, the ESI-07 grid approach retains a higher degree of spatial detail than the manually smoothed ESI-07 isoseismal.

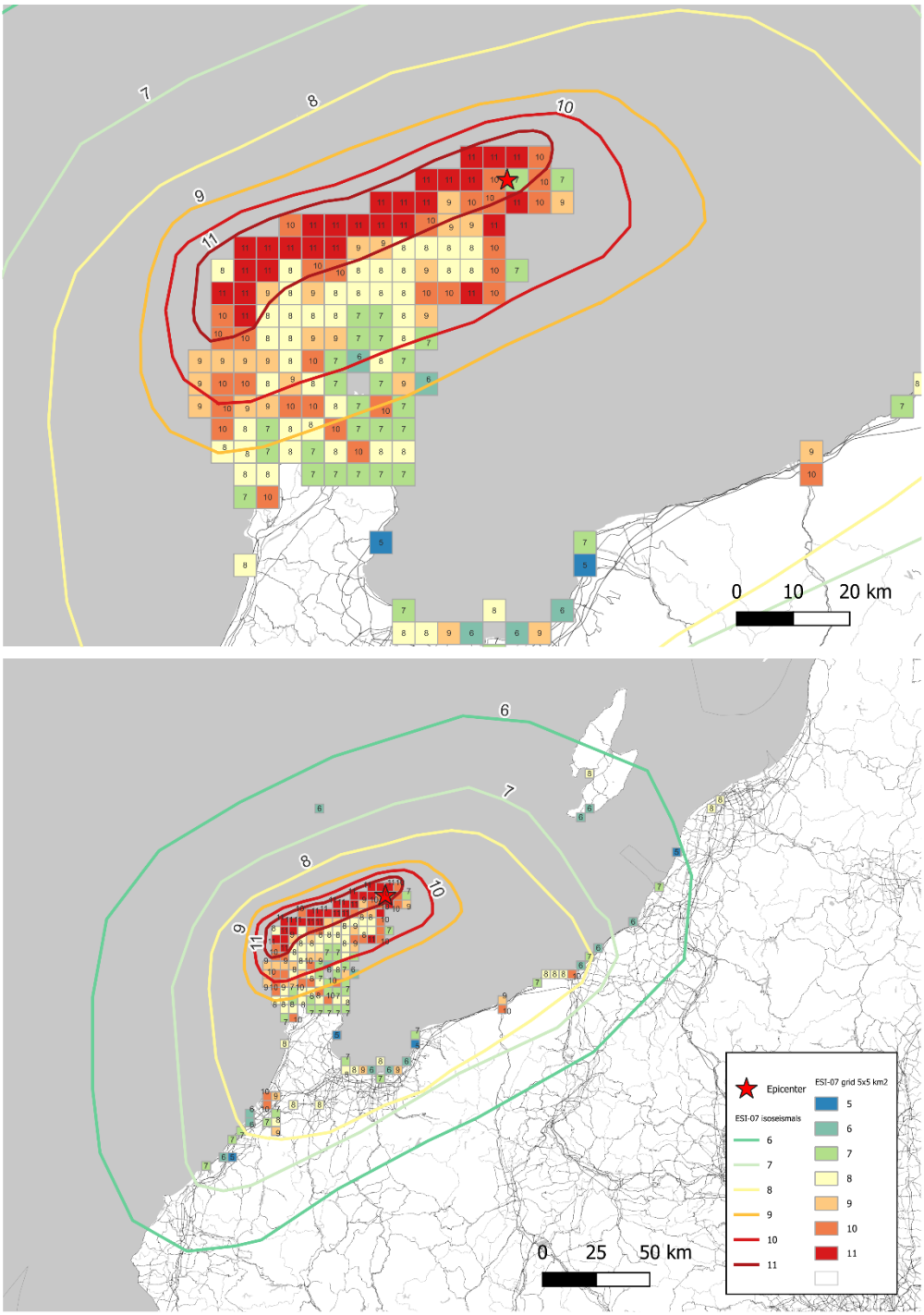

Figure 6.7 – Comparison between ESI-07 isoseismals and 5×5 km² ESI-07 grid for the 2024 Noto earthquake. The 5×5 km² grid shows good agreement with the manually drawn isoseismals, particularly for the highest ESI-07 intensities (X–XI). Despite the moderate smoothing effect introduced by the grid resolution, local variations are still visible among adjacent cells, highlighting the greater spatial sensitivity of the ESI-07 grid approach.

At finer resolution, the differences become more pronounced. When the 1×1 km^2 grid is compared with the same set of isoseismals the results reveal a marked "salt and pepper" pattern, characterized by sharp variations between adjacent cells (Fig. 6.8). This pattern reflects the strong local control exerted by geological, topographical, and climate factors, as well as the intrinsic heterogeneity of EEEs observations, as already observed (par. 1.1-1.2). In contrast, isoseismal lines, by definition, smooth out local fluctuations, producing a more continuous and generalized description of intensity. The grid method, therefore, preserves high-frequency spatial variability, while the isoseismal approach emphasizes regional coherence and overall trends.

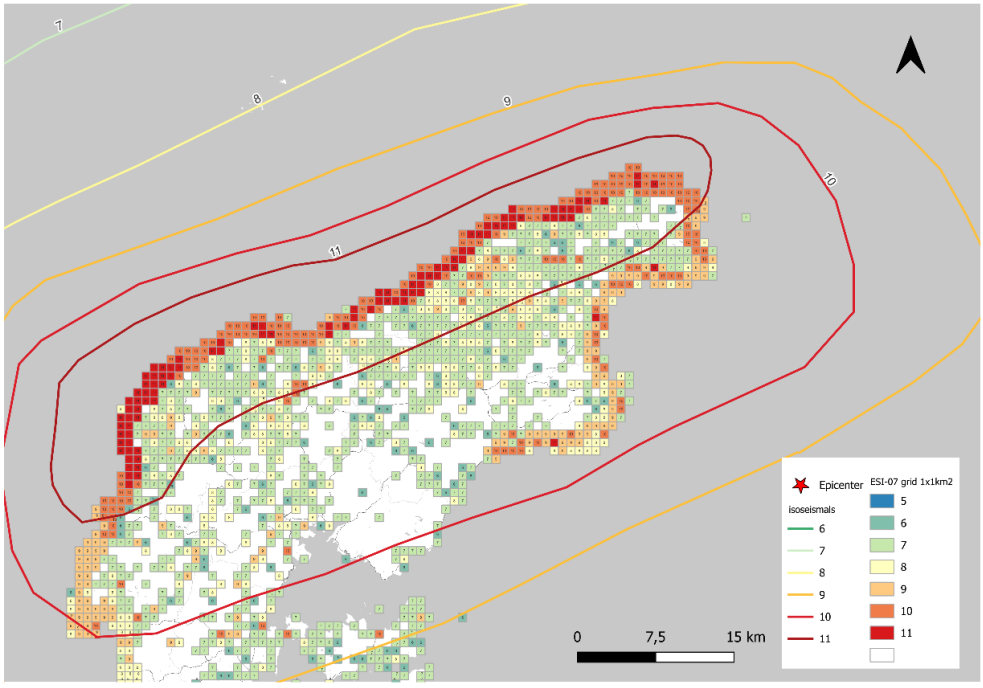

Figure 6.8 – Comparison between ESI-07 isoseismals and 1×1 km² ESI-07 grid for the 2024 Noto earthquake. At higher resolution, the grid analysis produces a "salt and pepper" pattern, with strong variations between adjacent cells. Isoseismal lines, in contrast, smooth out local variability, providing a generalized representation of seismic intensity. The 1×1 km² grid highlights local contrasts and areas of concentrated EEE occurrence, revealing sub-kilometric variability that is not captured by isoseismals.

The comparison between the two approaches confirms that each method serves different analytical purposes. Isoseismals are particularly effective to represent regional patterns of intensity, while the grid-based approach allows a finer visualization of EEEs distribution and variance, capturing local variation. The two methods are therefore complementary: isoseismals provide a macroscopic visualization of the event impact, while the grid framework offers a finer, data-driven representation of spatial variability. Nevertheless, the grid approach introduces certain challenges, particularly when comparing results with classical macroseismic scales. As already noted by Michetti et al. (2007), the direct integration between grid-derived ESI-07 intensities and "standard" macroseismic values may be complex, due to differences in the conceptual basis and spatial resolution of the two representations.

The performance of the ESI-07 grid methodology presented in this work is compared with the work by Ota et al. (2009), which adopted a similar grid methodology. Firstly, it is worth nothing that the authors primarily used data on surface faulting, landslides, and liquefaction to derive ESI-07 intensities, whereas in the present case all EEE categories are considered. This broader dataset allows a more comprehensive assessment of spatial clustering phenomena influenced by different factors displayed above (see paragraphs 1.1–1.2). Ota et al. (2009) also highlighted that for the 1999 Chi-Chi earthquake, strong local geological effects prevented the drawing of concentric isoseismal contours. Similarly, the 2024 Noto case confirms that local factors can strongly influence the ESI-07 intensity distribution, especially in high-resolution grids (1×1 km^2), where the detailed structure of local variability becomes apparent. As in the previous work of Ota et al., (2009), the comparison between point-based isoseismals and the grid-based maps reveals differences in intensity distribution, arising from the different ways in which data are represented and generalized.

Ultimately, the two methods are complementary rather than mutually exclusive. Isoseismals effectively summarize regional seismic impact, while the grid-based approach captures fine-scale variations essential for understanding the physical mechanisms and local amplification effects. When applied consistently, the grid methodology provides a transparent and adaptable tool capable of transforming heterogeneous datasets into a standardized quantitative framework, thereby extending the operational potential of the ESI-07 scale.

CONCLUSIONS

This dissertation contributes to advancing the use of EEEs and, more broadly, the ESI-07 Intensity scale, as robust indicators for macroseismic characterization, reinforcing their role as direct, measurable expressions of seismic aftermath on environment. Through the compilation of harmonized datasets, the refinement of analytical grid-based workflows, and the application of the ESI-07 scale, the research confirms how environmental evidence can be effectively transformed into reproducible and scalable parameters for intensity assessment.

At the global scale, the updated catalogue of 218 ESI-07 events provides a comprehensive overview to date of the methodologies, outputs, and applications of the ESI-07scale, while at the national level, the harmonized database of 3483 data represent an integration of EQUILs into the *Inventario dei Fenomeni Franosi in Italia* (IFFI), improving the capacity to identify and interpret spatial and temporal patterns of EQUILs within a standardized framework and their potential usefulness in macroseismic assessment. The development of a grid-based workflow, firstly validated on 40 global EQUILs inventories and consequently applied to the 2024 Mw 7.5 Noto Peninsula earthquake, marks a methodological advancement that enhances the reproducibility, comparability, and operational value of ESI-07 assessments in managing large and heterogeneous dataset.

Collectively, the results obtained in the present PhD dissertation confirm that EEEs can serve as a robust basis for quantitative macroseismic analysis. The integration of multiple datasets at diverse temporal and geographical scale, within FAIR-compliant and interoperable frameworks promotes cross-validation between historical, geological and seismological data, improving the utility of such data and the reliability of intensity estimation. The Noto case study, in particular, demonstrates the scalability and practical feasibility of semi-automatic grid-based ESI-07 applications.

Nevertheless, several challenges remain open. The uneven quality and completeness of historical inventories, the heterogeneity in landslide mapping criteria, and the limited availability of co-seismic data in underrepresented regions all call for further harmonization and standardization efforts. Future work should extend the grid-based methodology to additional spatial context and events, foster participatory approaches for near-real-time data collection, and compare ESI-07 grid outputs with established seismic-related output such as shake maps, ground-motion models, and attenuation relationships.

Ultimately, this research highlights and confirms the value of integrating environmental effects within the broader framework of macroseismic analysis. By viewing the landscape as both a witness and a measure of earthquake processes and aftermaths, the ESI-07 scale, the dataset compiled, and the ESI-07 grid-based methodology here implemented provide a consistent and physically grounded approach to characterizing seismic intensity. This integrated perspective strengthens the link between environmental and geological observation, quantitative modeling, and practical application, contributing to a more comprehensive and interdisciplinary understanding of earthquakes and their environmental impact.

REFERENCES

Aberasturi Rodríguez A., Fierro Bandera I., Navarro-Pedreño J., (2024). Can Citizens Do Science? Science in Common and Social Responsibility. Sci. Vol. 6(2), p. 26. https://doi.org/10.3390/sci6020026

Acharya A., Malla A. B., Guragain S., Dahal R. K., Hasegawa S., (2024). Post-disaster engineering geological assessment of the 2024 Noto Earthquake, Noto Peninsula, Japan. Shimane University. 10.13140/RG.2.2.10071.48807.

Ahmad B., Sana H., Alam A., (2014). Macroseismic intensity assessment of 1885 Baramulla Earthquake of northwestern Kashmir Himalaya, using the Environmental Seismic Intensity scale (ESI 2007). Quaternary International. Vol. 321, p. 59–64. https://doi.org/10.1016/j.quaint.2013.12.043

AIST (2012). Active Fault database of Japan. Retrieved from https://gbank.gsj.jp/activefault/index_e_gmap.html

Amezawa Y., Hiramatsu Y., Miyakawa A., Imanishi K., Otsubo M., (2023). Long-Living Earthquake Swarm and Intermittent Seismicity in the Northeastern Tip of the Noto Peninsula, Japan. Geophysical Research Letters. Vol. 50(8), e2022GL102670. https://doi.org/10.1029/2022GL102670

Ando R., Fukushima Y., Yoshida K., Imanishi K., (2025). Nonplanar 3D fault geometry controls the spatiotemporal distributions of slip and uplift: evidence from the Mw 7.5 2024 Noto Peninsula, Japan, Earthquake. Earth Planets Space. Vol. 77, p. 53. https://doi.org/10.1186/s40623-025-02187-9

Audemard F. A., Azuma T., Baiocco F., et al., (2015). Earthquake Environmental Effect for seismic hazard assessment: the ESI intensity scale and the EEE Catalogue. Memorie Descrittive della Carta Geologica d'Italia. Vol. 97. 10.13140/RG.2.1.3629.3202

Basharat M., Ali A., Jadoon I.A.K, Rohn J., (2016). Using PCA in evaluating event-controlling attributes of landsliding in the 2005 Kashmir earthquake region, NW Himalayas, Pakistan. Natural Hazards. Vol. 81, p. 1999-2017. https://doi.org/10.1007/s11069-016-2172-9

Basharat M., Rohn J., Baig M.S., Khan M.R., (2014). Spatial distribution analysis of mass movements triggered by the 2005 Kashmir earthquake in the Northeast Himalayas of Pakistan. Journal of Geomorphology. Vol. 206, p. 203-214. https://doi.org/10.1016/j.geomorph.2013.09.025

Basharat, M., Ali, A., Jadoon, I. A. K., and Rohn, J. (2016). Using PCA in evaluating event-controlling attributes of landsliding in the 2005 Kashmir earthquake region, NW Himalayas, Pakistan. Nat. Hazards 81, 1999–2017. doi:10.1007/s11069-016 2172-9

Basharat, M., Rohn, J., Baig, M. S., and Khan, M. R. (2014). Spatial distribution analysis of mass movements triggered by the 2005 Kashmir earthquake in the Northeast Himalayas of Pakistan. J. Geomorphol. 206, 203–214. doi:10.1016/j.geomorph.2013.09.025

Berzhinskii Y. A., Ordynskaya A. P., Gladkov A. S., Lunina O. V., Berzhinskaya L. P., Radziminovich N. A., Radziminovich Y. B., Imayev V. S., Chipizubov A. V., Smekalin O. P., (2010). Application of the ESI-2007 Scale for Estimating the Intensity of the Kultuk Earthquake, August 27, 2008 (South Baikal). Seismic Instruments. Vol. 46(4), p. 307–324. https://doi.org/10.3103/S0747923910040018308

Bornaetxea T., Remondo J., Bonachea J., Valenzuela P., (2023). Exploring available landslide inventories for susceptibility analysis in Gipuzkoa province (Spain). Natural Hazards. Vol. 118, p. 2513–2542. https://doi.org/10.1007/s11069-023-06103-w

Bornaetxea, T., Remondo, J., Bonachea, J., and Valenzuela, P. (2023). Exploring available landslide inventories for susceptibility analysis in Gipuzkoa province (Spain). Nat. Hazards 118, 2513–2542. doi:10.1007/s11069-023 06103-w

Boschi, E., Guidoboni, E., Ferrari, G., Valensise, G., Gasperini, P., (1997). Catalogo dei Forti Terremoti in Italia dal 461 aC al 1990. ING/SGA, Bologna, 644p.

Boulton S. J., Jones J. N., Malcioglu F. S., O'Kane A., Cleave M. D., Adamidis O., Efeoglu T., Aktas Y. D., (2025). Earthquake environmental effects and ESI 2007 of the 6th February 2023 Kahramanmaras earthquakes along the East Anatolian Fault Zone (Türkiye). Quaternary International. Vol. 732, p. 109804. https://doi.org/10.1016/j.quaint.2025.109804

Caccavale M., Sacchi M, Spiga E., Porfido S., (2019). The 1976 Guatemala Earthquake: ESI Scale and Probabilistic/Deterministic Seismic Hazard Analysis Approaches. Geosciences. Vol. 9, p.403. https://doi.org/10.3390/geosciences9090403

Caccavale, M., Sacchi, M., Spiga, E., and Porfido, S. (2019). The 1976 Guatemala earthquake: ESI scale and probabilistic/deterministic seismic hazard analysis approaches. Geosciences 9, 403. doi:10.3390/geosciences9090403

Camarda A. (2021). Classificazione degli effetti di terremoti storici in corrispondenza della Faglia di Moscarello e di S. Tecla, in relazione all'attività del vulcano Etna. Tesi di laurea, Università degli Studi dell'Insubria.

Caprari P., Della Seta M., Martino S., Fantini A., Fiorucci M., Priore T., (2018). Upgrade of the CEDIT database of earthquake-induced ground effects in Italy. Italian Journal of Engineering Geology and Environment. Vol. 2.

Chang M., Zhou Y., Zhou C., Hales T.C., (2021). Coseismic landslides induced by the 2018 M w 6.6 Iburi, Japan, Earthquake: spatial distribution, key factors weight, and susceptibility regionalization. Landslides. Vol. 18, p. 755-772. https://doi.org/10.1007/s10346-020-01522-3

Chang, M.,Zhou,Y., Zhou,C., andHales, T. C. (2021). Coseismic landslides induced by the 2018 M w 6.6 Iburi, Japan, Earthquake: spatial distribution, key factors weight, and susceptibility regionalization. Landslides 18, 755–772. doi:10.1007/s10346-020 01522-3

Chen C.W., Sato M., Yamada R., Iida T., Matsuda M, Chen H., (2021). Modeling of earthquake-induced landslide distributions based on the active fault parameters. Engineering Geology. Vol. 303, p. 106640. https://doi.org/10.1016/j.enggeo.2022.106640

Chen, C. W., Sato, M., Yamada, R., Iida, T., Matsuda, M., and Chen, H. (2022). Modeling of earthquake-induced landslide distributions based on the active fault parameters. Eng. Geol. 303, 106640. doi:10.1016/j.enggeo.2022.106640

Cho S., Jung K., and Park H., (2013). Social Media Use during the 2011 Japan Earthquake: How Twitter Transforms the Locus of Crisis Communication. Media International Australia incorporating Culture and Policy. Vol. 149, p. 28-40.

Chuo, Y.-J. (2020). Earthquake shake detecting by data mining from social network platforms. Applied Sciences. Vol. 10(3), p. 812. https://doi.org/10.3390/app10030812

Climate-Data.org, (2025). Noto climate: Weather Noto and temperature by month. Retrieved May 29, 2025, from https://en.climate-data.org/asia/japan/ishikawa-prefecture/noto-1068223/.

Colón S., Leal A., Audemard F., Vásquez R., Rodríguez J. A., (2019). Análisis macrosísmico del sismo Mw~7,6 de San Narciso del 29 de octubre de 1900, aplicando la Escala Medio-Ambiental de Intensidad Sísmica ESI 2007. Fundación Venezolana de Investigaciones Sismológicas (FUNVISIS).

Comerci V., Michetti A.M., Serva L., Vittori E., (2015a). The November 2, 2002, Denali (Alaska) earthquake. Memorie Descrittive della Carta Geologica d'Italia. Vol. XCVII, p.125 – 132.

Comerci V., Vittori E., Blumetti A. M., Brustia E., Di Manna P., Guerrieri L., Lucarini M., Serva L., (2015b). Environmental effects of the December 28, 1908, Southern Calabria–Messina (Southern Italy) earthquake. Natural Hazards. Vol. 76(2), p. 1849–1891. https://doi.org/10.1007/s11069-014-1573-x

Comerci, V., Michetti, A. M., Serva, L., and Vittori, E. (2015). The November 2, 2002, Denali (Alaska) earthquake, mem. Descr, Carta Geol. D'It., XCVII, 125–132. Dai, L., Fan, X., Wang, X., Fang, C., Zou, C., Tang, X., et al. (2023). Coseismic landslides triggered by the 2022 Luding Ms6.8 earthquake, China. Landslides 20 (6), 1277–1292. doi:10.1007/s10346-023-02061-3

Comunello F., Parisi L., Lauciani V., Magnoni F., Casarotti E., (2016). Tweeting after an earthquake: User localization and communication patterns during the 2012 Emilia seismic sequence. Annals of Geophysics. Vol. 59(2), p. S0537. https://doi.org/10.4401/ag-6945

Cornet F. H., Helm J., Poitrenaud H., Etchecopar A., (1997). Seismic and aseismic slips induced by large-scale fluid injections. Pure and Applied Geophysics. Vol. 150(3–4), p. 563–583. https://doi.org/10.1007/s000240050093

D'Auria L., and Convertito V., (2016) Real-time mapping of earthquake perception areas in the Italian region from Twitter streams analysis. In: D'Amico S (ed) Earthquakes and their impact on society. Springer Natural Hazards, Springer, Cham. https://doi.org/10.1007/978-3-319-21753-6_26

Dai L., Fan X., Wang X., Fang C., Zou C., Tang X., Wei Z., Xia M., Wang D., Xu, Q., (2023). Coseismic landslides triggered by the 2022 Luding Ms6.8 earthquake, China. Landslides. Vol. 20, p. 1277–1292. https://doi.org/10.1007/s10346-023-02061-3

De Barros L., Baques M., Godano M., Helmstetter A., Deschamps A., Larroque C., Courboulex F., (2019). Fluid-induced swarms and coseismic stress transfer: A dual process highlighted in the aftershock sequence of the 7 April 2014 earthquake (Ml 4.8, Ubaye, France). Journal of Geophysical Research: Solid Earth. Vol. 124(4), p. 3918–3932. https://doi.org/10.1029/2018JB017226

Delfino L., and Romeo R.W., (1997). C.E.D.I.T., Catalogo nazionale degli Effetti Deformativi del suolo Indotti da forti Terremoti. Rapporto Tecnico SSN/RT/97/04.

Dengler, L., and McPherson, R. (1993). The 17 August 1991 Honeydew earthquake, North Coast California: a case for revising the Modified Mercalli scale in sparsely populated areas. *Bulletin of the Seismological Society of America*, *83*(4), 1081-1094.

Di Manna P., Guerrieri L., Piccardi L., Vittori E., Castaldini D., Berlusconi A., Bonadeo L., Comerci V., Ferrario F., Gambillara R., Livio F., Lucarini M., Michetti, A. M., (2012). Ground effects induced by the 2012 seismic sequence in Emilia: Implications for seismic hazard assessment in the Po Plain. Annals of Geophysics. Vol. 55(4). https://doi.org/10.4401/ag-6143

Di Paola G., Iadanza C., Trigila, A., (2024). Italian Landslide Inventory (IFFI). ISPRA – Indicatori Ambientali. https://indicatoriambientali.isprambiente.it/en/landslide-hazard/italian-landslide-inventory-iffi

Dretaki A., Chatzipetros A., Psomadakis S., (2022). Site effects and surface deformation associated with the M 6.3 Sitia (eastern Crete) earthquake of October 12, 2021. Poster presentato al 16th International Congress of the Geological Society of Greece, Patras, Grecia. Bulletin of the Geological Society of Greece, Sp. Publ. 10, Ext. Abs. GSG2022-229. https://doi.org/10.13140/RG.2.2.27729.40807

Earle P. S., Bowden D., Guy M., (2011). Twitter earthquake detection: Earthquake monitoring in a social world. Annals of Geophysics. Vol. 54(6), p. 708–715. https://doi.org/10.3929/ethz-b-000364555

Emberson R., Kirschbaum D.B., Amatya P., Tanyas H., Marc O., (2022). Insights from the topographic characteristics of a large global catalog of rainfall-induced landslide event inventories. Natural Hazards and Earth System Sciences. Vol. 22(3), p.1129-1149. https://doi.org/10.5194/nhess-22-1129-2022

Esposito E., Porfido S., Mastrolorenzo G., Nikonov A.A., Serva, L., (1996). Brief review and preliminary proposal for the use of ground effects in the macroseismic intensity assessment. In Proceedings of the 30th IUGS Congress, Beijing, China, 4–14 August 1996. Contemporary Lithospheric Motion Seismic Geology International Science Publishers: Zeist, The Netherlands, 1997. P. 233–243. https://hdl.handle.net/20.500.14243/124480

Fan X., Scaringi G., Korup O., West A.J., van Westen C.J., Tanyas H. et al., (2019). Earthquake-induced chains of geologic hazards: Patterns, mechanisms, and impacts. Reviews of geophysics. Vol. 57(2), p. 421-503. https://doi.org/10.1029/2018RG000626

Ferrario M.F., (2019): Landslides triggered by multiple earthquakes: insights from the 2018 Lombok (Indonesia) events. Natural Hazards. Vol. 100(1), p. 223–253. https://doi.org/10.1007/s11069-019-03718-w

Ferrario, M. F., F. Liv10, S. S. Capizzano, and A. M. Michetti (2020). Developing the First Intensity Prediction Equation Based on the Environmental Scale Intensity: A Case Study from Strong Normal-Faulting Earthquakes in the Italian Apennines, Seismol. Res. Lett. XX, 1-13, doi: 10.1785/ 0220200044.

Ferrario M.F., (2022a). Landslides triggered by the 2015 M w 6.0 Sabah (Malaysia) earthquake: inventory and ESI-07 intensity assignment. Natural Hazards and Earth System Sciences. Vol. 22(10), p. 3527-3542. https://doi.org/10.5194/nhess-22-3527-2022

Ferrario M.F., Livio F., Michetti A.M., (2022b). Fifteen years of Environmental Seismic Intensity (ESI-07) scale: Dataset compilation and insights from empirical regressions. Quaternary International. Vol. 625, p.107-119. https://doi.org/10.1016/j.quaint.2022.04.011

Ferrario M.F., Perez J.S., Dizon M., Livio F., Rimando J., Michetti A.M., (2024). Environmental effects following a seismic sequence: the 2019 Cotabato - Davao del Sur (Philippines). Natural Hazards. Vol. 120, p. 6125-6147. https://doi.org/10.1007/s11069-024-06467-7

Fischer T., Horálek J., Hrubcová P., Vavryčuk V., Bräuer K., Kämpf H., (2014). Intra-continental earthquake swarms in west-Bohemia and Vogtland: A review. Tectonophysics. Vol. 611, p. 1–27. https://doi.org/10.1016/j.tecto.2013.11.001

Flanagan M., Tang V., Ranadive O., Thomas A., Van der Lee, S., (2021, December). Earthquake Detective: Citizen Scientists Use Eyes and Ears to Classify Small Seismic Events. Paper presented at the AGU Fall Meeting 2021, New Orleans, LA. Abstract retrieved from https://ui.adsabs.harvard.edu/abs/2021AGUFMED55

Fountoulis I. G., and Mavroulis S. D. (2013). Application of the Environmental Seismic Intensity scale (ESI 2007) and the European Macroseismic Scale (EMS-98) to the Kalamata (SW Peloponnese, Greece) earthquake (Ms=6.2, September 13, 1986) and correlation with neotectonic structures and active faults. Annals of Geophysics. Vol. 56(6), p. S0675. https://doi.org/10.4401/ag-6237

Fujii Y., and Satake K., (2024). Slip distribution of the 2024 Noto Peninsula earthquake (M_{JMA} 7.6) estimated from tsunami waveforms and GNSS data. Earth, Planets and Space. Vol. 76, p. 44. https://doi.org/10.1186/s40623-024-01991-z

Fukushima Y., Ishimura D., Takahashi N., Iwasa Y., Malatesta L. C., Takahashi T., Tang C.-H., Yoshida K., and Toda S. (2024). Landscape changes caused by the 2024 Noto Peninsula earthquake in Japan. Science Advances. Vol. 10(eadp9193). Retrieved from https://www.science.org

Fukuyama E., Ellsworth W. L., Waldhauser F., and Kubo A. (2003). Detailed fault structure of the 2000 Western Tottori, Japan, earthquake sequence. Bulletin of the Seismological Society of America. Vol. 93(4), p.1468–1478. https://doi.org/10.1785/0120020123

García-Delgado H., Chaparro J., Gamboa C., Ruiz G., (2021). Landslides triggered by the December 24, 2019 Mesetas (Meta, Colombia) Earthquake. In: Cabrera MA, Prada-Sarmiento LF (eds.) Proceedings of the 13th International Symposium on Landslides. ISSMGE, Cartagena.

Gnyawali K.R., Adhikari B.R., (2016). Spatial relations of earthquake induced landslides triggered by 2015 Gorkha earthquake Mw 7.8. European Geosciences Union General Assembly Conference Abstracts. Vol.18, p.18429.

Gorum T., Korup O., van Westen C.J., van der Meijde M., Xu C., van der Meer F.D., (2014). Why so few? Landslides triggered by the 2002 Denali earthquake, Alaska. Quaternary Science Reviews. Vol. 95, p. 80-94. https://doi.org/10.1016/j.quascirev.2014.04.032

Gorum T., van Westen C.J., Korup O., van der Meijde M., Fan X., van der Meer F.D., (2013). Complex rupture mechanism and topography control symmetry of mass-wasting pattern, 2010 Haiti earthquake. Journal of Geomorphology. Vol. 184, p.127-138. https://doi.org/10.1016/j.geomorph.2012.11.027

Govi M. and Sorzana P. F., (1977). Effetti geologici del terremoto: frane. Studio geologico dell'area maggiormente colpita dal terremoto friulano del 1976. P. 329-368.

Govi M., (1977). Carta delle frane prodotte dal terremoto. Scala 1:50.000. CNR.

GSI, Geospatial Information Authority of Japan. (2023). 我が国の島を数えました. Retrieved from https://www.gsi.go.jp/kihonjohochousa/pressrelease2

GSI, Geospatial Information Authority of Japan. (2024). Information on the Noto Peninsula Earthquake in Reiwa 6. https://www.gsi.go.jp/BOUSAI/20240101_noto_earthq

GSI, Geospatial Information Authority of Japan. (2025). Area by prefecture, municipality, and nationwide. Retrieved from https://www.gsi.go.jp/KOKUJYOHO/MENCHO-title.htm

Guerrieri L., Baiocco F., Blumetti A.M., Brustia E., Lucarini M., Scaramella A., Vittori E., (2015b). EEE Catalogue: guidelines for public consultation and remote compilation. In F. Audemard, T. Azuma, and F. Baiocco (Eds.), Earthquake Environmental Effect for seismic hazard assessment: the ESI intensity scale and the EEE Catalogue. P. 33–42. Rome: ISPRA – Geological Survey of Italy. Memorie Descrittive della Carta Geologica d'Italia. Vol. XCVII. https://doi.org/10.1016/S1464-1895(99)00003-4

Guerrieri L., Blumetti A.M., Brustia E., Esposito E., Lucarini M., Michetti A.M, Porfido S., Serva L., Vittori E., INQUA TERPRO Project #0811 Working Group, (2011). Earthquake environmental effects, intensity and seismic hazard assessment: the EEE Catalogue (INQUA Project #0418). 2nd INQUA-IGCP-567 International Workshop on Active Tectonics, Earthquake Geology, Archaeology and Engineering, Corinth, Greece.

Guerrieri L., Blumetti A.M., Esposito, E., Michetti, A.M., Porfido, S., Serva, L., Tondi, E., Vittori, E., (2009a). Capable faulting, environmental effects and seismic landscape in the area affected by the1997Umbria–Marche (Central Italy) seismic sequence. Tectonophysic. Vol. 476, p. 269–281.

Guerrieri L., Michetti A.M., Silva P.G., (2015a). EEE Catalogue: A Global Database of Earthquake Environmental Effects. In: Beer, M., Kougioumtzoglou, I.A., Patelli, E., Au, SK. (eds) Encyclopedia of Earthquake Engineering. Springer, Berlin, Heidelberg. https://doi.org/10.1007/978-3-642-35344-4_32

Guerrieri L., Porfido S., Esposito E., Blumetti A.M., Michetti A. M., and Vittori E., (2009b). Cataloguing Earthquake Environmental Effects: a tool for the comparison of recent, historical and paleoearthquakes. 1st INQUA-IGCP-567 International Workshop on Earthquake Archaeology and Palaeoseismology, Baelo Claudia, Spain.

Guerrieri L., Tatevossian R., Vittori E., Comerci V., Esposito E., Michetti A.M., Serva L., (2007). Earthquake environmental effects (EEE) and intensity assessment: the INQUA scale project. Bollettino-Società Geologica Italiana. Vol. 126 (2), p. 375–386, 0037-8763.

Guglielmi Y., Cappa F., Avouac J. P., Henry P., and Elsworth D., (2015). Seismicity triggered by fluid injection-induced aseismic slip. Science. Vol. 348(6240), p. 1224–1226. https://doi.org/10.1126/science.aab0476

Guidoboni E., (1994). Catalogue of Ancient Earthquakes in the Mediterranean Area up to the 10th Century. ING/SGA, Bologna. P. 504.

Guidoboni E., Ferrari G., Tarabusi G., Sgattoni G., Comastri A., Mariotti D., Ciuccarelli C., Bianchi M. G., Valensise G., (2019). CFTI5Med, the new release of the catalogue of strong earthquakes in Italy and in the Mediterranean area. Scientific Data. Vol. 6, Article 98. https://doi.org/10.1038/s41597-019-0091-9

Guzzetti F., Ardizzone F., Cardinali M., Rossi M., and Valigi D., (2009). Landslide volumes and landslide mobilization rates in Umbria, central Italy. Earth and Planetary Science Letters. Vol. 279, p. 222–229. https://doi.org/10.1016/j.epsl.2009.01.005.

Hancox G.T., Perrin N.D., Dellow G.D., (2002). Recent studies of historical earthquake-induced landsliding, ground damage, and MM intensity in New Zealand. Bulletin of the New Zealand Society for Earthquake Engineering. Vol. 35, 2, p. 59-95. https://doi.org/10.5459/bnzsee.35.2.59-95

Harp E.L, Jibson R.W., (1995). Inventory of landslides triggered by the 1994 Northridge, California earthquake. U.S. Geological Survey Open-File Report. 95-213 17:2, pl. scale 1:50,000 and 1:100,000. https://doi.org/10.3133/ofr95213

Harp E.L., Hartzell S.H., Jibson R.W., Ramirez-Guzman L., Schmitt R.G., (2014). Relation of landslides triggered by the Kiholo Bay earthquake to modeled ground motion. Seismological Society of America Bulletin. 104-52529-2540. https://doi.org/10.1785/0120140047

Harp E.L., Jibson, R.W., Schmitt R.G., (2016). Map of landslides triggered by the January 12, 2010, Haiti earthquake. U.S. Geological Survey Scientific Investigations. Map 3353: 15 p., 1 sheet, scale 1:150,000. https://doi.org/10.3133/sim3353

Harp E.L., Keefer D.K., (1990). Landslides triggered by the earthquake. In: Rymer MJ, Ellsworth WL, eds., The Coalinga, California, Earthquake of May 2, 1983. U.S. Geological Survey Professional Paper. 1487, 335–347, 1 pl., scale 1:48,000.

Harp E.L., Keefer D.K., Sato H.P., Yagi H., (2011). Landslide inventories: the essential part of seismic landslide hazard analyses. Engineering Geology. Vol. 122(1-2), p. 9-21. https://doi.org/10.1016/j.enggeo.2010.06.013

Harp E.L., Tanaka K., Sarmiento J., Keefer D.K., (1984). Landslides from the May 25– 27, 1980, Mammoth Lakes, California, earthquake sequence. U.S. Geological Survey Miscellaneous Investigations. Map. I-1612, scale 1:62,500. https://doi.org/10.3133/i1612

Harp E.L., Wilson R.C., Wieczorek G.F., (1981). Landslides from the February 4, 1976, Guatemala earthquake. U.S. Geological Survey Professional Paper. 1204-A 35:2 pl., scale 1:50,000. https://doi.org/10.3133/pp1204A

Hasegawa A., Nakajima J., Uchida N., Okada T., Zhao D., Matsuzawa T., Umino N. (2009). Plate subduction, and generation of earthquakes and magmas in Japan as inferred from seismic observations: An overview. Gondwana Research. Vol. 16(3–4), p. 370-400. DOI: 10.1016/j.gr.2009.03.007

Hatch R. L., Abercrombie R. E., Ruhl C. J., Smith K. D., (2020). Evidence of aseismic and fluid-driven processes in a small complex seismic swarm near Virginia city, Nevada. Geophysical Research Letters. Vol. 47(4). https://doi.org/10.1029/2019gl085477

Heidarzadeh M., Ishibe T., Gusman A.R., Miyazaki H., (2024). Field surveys of tsunami runup and damage following the January 2024 Mw 7.5 Noto (Japan sea) tsunamigenic earthquake. Ocean Engineering. Vol. 307, p. 118149. https://doi.org/10.1016/j.oceaneng.2024.118140

Hicks A., Barclay J., Chilvers J., Armijos M. T., Oven K., Simmons P., Haklay M. (2019). Global Mapping of Citizen Science Projects for Disaster Risk Reduction. Frontiers in Earth Science. Vol. 7, p. 226. https://doi.org/10.3389/feart.2019.00226

Hu K., Zhang X., You Y., Hu X., Liu W., Li Y., (2019). Landslides and dammed lakes triggered by the 2017 Ms6.9 Milin earthquake in the Tsangpo gorge. Landslides. Vol. 16, p. 993–1001. https://doi.org/10.1007/s10346-019-01168-w

Huang T.F., (1999) Landslides Triggered by Jueili Earthquake. In Schmitt R, Tanyas H, Jessee MA, Zhu J, Biegel K, Allstadt KE et al. An Open Repository of Earthquake-triggered Ground Failure Inventories, U.S. Geological Survey data release collection. (2017). https://doi.org/10.5066/F7H70DB4.

Huayong N., Hua G., Yanchao G., Blumetti A. M., Comerci V., Di Manna P., Guerrieri L., Vittori E., (2019). Comparison of Earthquake Environmental Effects and ESI intensities for recent seismic events in different tectonic settings: Sichuan (SW China) and Central Apennines (Italy). Engineering Geology. Vol. 258, p. 105149. https://doi.org/10.1016/j.enggeo.2019.105149

Iadanza C., Trigila A., Starace P., Dragoni A., Biondo T., Roccisano M., (2021). IdroGEO: A collaborative web mapping application based on REST API services and open data on landslides and floods in Italy. ISPRS International Journal of Geo-Information. Vol. 10(2), p. 89. https://doi.org/10.3390/ijgi10020089

Inagaki N., Nishida Y., Mikami T., Nakamura R., Nistor I., Soltanpour M., Goseberg N., Shibayama T., (2025). Field survey of the 2024 Noto Peninsula Earthquake and Tsunami in Japan: Characteristics of damage patterns to coastal communities. Ocean Engineering. DOI: 10.1016/j.oceaneng.2024.119765.

Ishikawa Y., (2023). Earthquake Swarm in Noto Peninsula. Japan Society of Geoinformatics. Vol. 34, p. 45–46. http://www.jsgi.org/geoinforum2023.html.

Ishikawa Y., Bai L., (2024). The 2024 M_j 7.6 Noto Peninsula, Japan earthquake caused by the fluid flow in the crust. Earthquake Research Advances. Vol.4, issue 3, p. 100292. https://doi.org/10.1016/j.eqrea.2024.100292

Ishiyama T., Sato H., Kato N., Koshiya S., Abe S., Shiraishi K., Matsubara M., (2017). Structures and active tectonics of compressionally reactivated back-arc failed rift across the Toyama trough in the Sea of Japan, revealed by multiscale seismic profiling. Tectonophysics. Vol. 710–711, p. 21-36. https://doi.org/10.1016/j.tecto.2016.09.029

ISPRA (2025a). Inventario dei Fenomeni Franosi in Italia – IFFI. IdroGEO. https://beta.idrogeo.isprambiente.it/app/page/inventario-dei-fenomeni-franosi-in-italia-iffi

ISPRA,(2025b). Inventario dei fenomeni franosi in Italia (IFFI). ProgettoIFFI. https://www.progettoiffi.isprambiente.it

Jaboyedoff M., Carrea D., Derron M.H., Oppikofer T., Penna I.M., Rudaz B., (2020). A review of methods used to estimate initial landslide failure surface depths and volumes. Engineering Geology. 267:105478. https://doi.org/10.1016/j.enggeo.2020.105478

Jolivet L., Tamaki K., Fournier M., (1994). Japan Sea, opening history and mechanism: A synthesis. Journal of Geophysical Research: Solid Earth. Vol. 99(B11), 22237-22259. https://doi.org/10.1029/93JB03463

Kato A., Sakai S., Iidaka T., Iwasaki T., Kurashimo E., Igarashi T., Hirata N., Kanazawa T., (2008). Three-dimensional velocity structure in the source region of the Noto Hanto Earthquake in 2007 imaged by a dense seismic observation. Earth, Planets and Space. Vol. 60(2), p. 105-110. https://doi.org/10.1186/BF03352769

Keefer D.K., (1984). Landslides caused by earthquakes. Geological Society of America Bulletin. Vol. 95(4), p. 406-421.
https://doi.org/10.1130/00167606(1984)95andamp;amp;lt;406:LCBEandamp;amp;gt;2.0.C;2

King, T. R., Quigley, M., and Clark, D. (2019). Surface-rupturing historical earthquakes in Australia and their environmental effects: New insights from re-analyses of observational data. *Geosciences, 9*(10), 408. https://doi.org/10.3390/geosciences9100408

Knoper L., Allstadt K.E., Clark M.K., Thompson E.M., Schmitt R.G., (2020). Inventory of landslides triggered by the 2020 Puerto Rico earthquake sequence. U.S. Geological Survey data release. https://doi.org/10.5066/P9U0IXLP.

Kolyva M., (1997). Catalogue of the Historical Archive of Zakynthos– B. Mnimon 19 (in Greek).

Kong Q., Allen R. M., Schreier L., Kwon Y.-W., (2016). MyShake: A smartphone seismic network for earthquake early warning and beyond. Science Advances. Vol. 2(2), e1501055. https://doi.org/10.1126/sciadv.1501055

Koto T., (2000). Relationship between the Japan Meteorological Agency's Seismic Intensity Based on K-NET Strong Motion Meter Records and the Revised Mercalli Seismic Intensity. Zisin (Journal of the Seismological Society of Japan. 2nd Series), 53(1), 89–93.
https://doi.org/10.4294/zisin1948.53.1_89

Lario J., Bardají T., Silva P. G., Zazo C., Goy J. L., (2016). Improving the coastal record of tsunamis in the ESI-07 scale: Tsunami Environmental Effects Scale (TEE-16 scale). Geologica Acta. Vol. 14(2), p. 179-193. https://doi.org/10.1344/GeologicaActa2016.14.2.6

Larsen I.J., Montgomery D.R., Korup O., (2010). Landslide erosion controlled by hillslope material, Nature Geoscience. Vol. 3, p. 247–251. https://doi.org/10.1038/ngeo776.

Lazzati M., (2020). Effetti ambientali del terremoto del 26 dicembre 2018 lungo la Faglia di Fiandaca e pericolosità sismica dell'area etnea. Tesi di laurea, Università degli Studi dell'Insubria.

Lekkas E. L., (2010). The 12 May 2008 M w 7.9 Wenchuan, China, Earthquake: Macroseismic Intensity Assessment Using the EMS-98 and ESI 2007 Scales and their correlation with the geological structure. Bulletin of the Seismological Society of America. Vol. 100(5B), p. 2791- 2804. https://doi.org/10.1785/0120090244

Li G., West A. J., Densmore A. L., Jin Z., Parker R. N., Hilton R. G., (2014). Seismic mountain building: landslides associated with the 2008 Wenchuan earthquake in the context of a generalized model for earthquake volume balance. Geochemistry, Geophysics, Geosystems. Vol. 15, p. 833–844. doi:10.1002/2013GC005067

Liu C., Bai Y., Lay T., He P., Wen Y., Wei X., Xiong N., Xiong X. (2024c). Shallow crustal rupture in a major MW 7.5 earthquake above a deep crustal seismic swarm along the Noto Peninsula in western Japan. Earth and Planetary Science Letters. Vol. 648, p. 119107. https://doi.org/10.1016/j.epsl.2024.119107

Liu Y., Wu Z., Zhang Y., Yin X. (2024a). Tracing the pace of an approaching 'seismic dragon king': Additional evidence for the Noto earthquake swarm and the 2024 MW 7.5 Noto earthquake. Earthquake Research Advances. Vol. 4(2), p. 100290. https://doi.org/10.1016/j.eqrea.2024.100290

Liu Y., Wu Z.L., Zhang Y.X., (2024b). The January 1, 2024, Noto peninsula, Japan, Mw7.5 earthquake as a plausible 'dragon king' event. Reviews of Geophysics and Planetary Physics. Vol. 55. https://doi.org/10.19975/j.dqyxx.2024-003 (in Chinese with English abstract).

Lopez J.C. and Ishiwatari A., (2002): Petrogenesis of the tholeiitic basalt, calc-alkaline basaltic andesite and high magnesian andesite lava succession of the Oligo-Miocene Anamizu Formation in northeastern Noto Peninsula, Central Japan. J. Mineralogical and Petrological Sciences. Vol. 97, p. 85-113.

Ma Z., Zeng H., Luo H., Liu Z., Jiang Y., Aoki Y., Wang W., Itoh Y., Lyu M., Cui Y., Yun S.-H., Hill E. M., Wei S., (2024). Slow rupture in a fluid-rich fault zone initiated the 2024 Mw 7.5 Noto earthquake. Science. Vol. 385, p. 866–871. https://doi.org/10.1126/science.ado5143

Mäntyniemi P., Sørensen M. B., Tatevossian R. E., (2021). Testing the Environmental Seismic Intensity scale on data derived from the earthquakes of 1626, 1759, 1819, and 1904 in Fennoscandia, northern Europe. Geosciences. Vol. 11(1), p. 14. https://doi.org/10.3390/geosciences11010014

Marano K.D., Wald D.J., Allen T.I., (2010). Global earthquake casualties due to secondary effects: a quantitative analysis for improving rapid loss analyses. Natural hazards. Vol. 52, p. 319-328. https://doi.org/10.1007/s11069-009-9372-5

Marc O., Hovius N., (2015). Amalgamation in landslide maps: effects and automatic detection. Natural Hazards and Earth Systems Sciences (NHESS). Vol. 15, p. 723–733. https://doi.org/10.5194/nhess-15-723-2015

Marc O., Hovius N., Meunier P., Gorum T., Uchida T., (2016). A seismologically consistent expression for the total area and volume of earthquake-triggered landsliding. Journal of Geophysical Research-Earth Surface. Vol. 121-4, p. 640-663. https://doi.org/10.1002/2015JF003732

Marc O., Stumpf A., Malet J.P., Gosset M., Uchida T., Chiang S.H., (2018). Initial insights from a global database of rainfall induced landslide inventories: the weak influence of slope and strong influence of total storm rainfall. Earth Surface Dynamics. Vol. 6, p. 903–922. https://doi.org/10.5194/esurf-6-903-2018.

Martino S., Caprari P.., Fiorucci M., Marmoni G. M., (2020). Il Catalogo CEDIT. Dall'inventario degli effetti sismoindotti all'analisi di scenario. In Giornate di Geologia and Storia. Memorie Descrittive della Carta Geologica d'Italia (pp. 441–450). ISBN: 9788893110839. Sapienza Università di Roma – IRIS

Martino S., Prestininzi A. and Romeo R. W., (2014). Earthquake-induced ground failures in Italy from a reviewed Database. Natural Hazards and Earth Systems Sciences (NHESS). Vol.14, p. 799–814.

Maruyama S., Isozaki Y., Kimura G., Terabayashi M., (1997). Paleogeographic maps of the Japanese Islands: Plate tectonic synthesis from 750 Ma to the present. The Island Arc. Vol. 6(1), p. 121-142. DOI: 10.1111/j.1440-1738.1997.tb00043.x

Mavroulis, S., Fountoulis, I. G., Skourtsos, E., & Papanikolaou, I. D. (2013). *Seismic intensity assignments for the 2008 Andravida (NW Peloponnese, Greece) strike-slip event (June 8, Mw=6.4) based on the application of the Environmental Seismic Intensity scale (ESI 2007) and the European Macroseismic scale (EMS-98). Geological structure, active tectonics, earthquake environmental effects and damage pattern*. *Annals of Geophysics*, 56(6). https://doi.org/10.4401/ag-6239

Mavroulis S., Stanota E.-S., Lekkas E. (2019). Evaluation of environmental seismic intensities of all known historical and recent earthquakes felt in Zakynthos Island, Greece using the Environmental Seismic Intensity (ESI 2007) scale. Quaternary International. Vol. 532, p. 1-22. https://doi.org/10.1016/j.quaint.2019.09.006.

Mccalpin J.P., (ed.) (2009), Paleoseismology, 2nd Edition, International Geophysics Series 95, Elsevier Publishing, p. 647.

Medvedev S., Sponheuer W., Karník V., (1964). Neue seismische Skala Intensity scale of earthquakes, 7. Tagung der Europ aischen Seismologischen Kommission vom 24.9. bis 30.9.1962. In: Jena, Veroff. Institut für Bodendynamik und Erdbebenforschung in Jena, 77. Deutsche Akademie der Wissenschaften zu Berlin, p. 69–76.

Mercalli, G. (1902). *Sulle modificazioni proposte alla scala sismica De Rossi-Forel*. Società tipografica modenese.

Michetti A.M., Esposito E., Guerrieri L., Porfido S., Serva L., Tatevossian R., Vittori E., E., Audemard, F., Azuma, T., Clague, J., Comerci, V., (2007). Environmental seismic intensity scale-ESI 2007. Memorie descrittive della carta geologica d'Italia. Vol. 74, p. 41.

Michetti A.M., Esposito E., Guerrieri L., Porfido S., Serva L., Tatevossian R., Vittori E., Audemard F., Azuma T., Clague J., Comerci V., Gürpinar A., McCalpin J., Mohammadioun B., Mörner N.A., Ota Y., Roghozin E., (2015). Environmental Seismic Intensity scale – ESI 2007. In F. Audemard, T. Azuma, F. Baiocco (Eds.), Earthquake Environmental Effect for seismic hazard assessment: the ESI intensity scale and the EEE Catalogue p. 11–20. Rome: ISPRA – Geological Survey of Italy. Memorie Descrittive della Carta Geologica d'Italia. Vol. XCVII. https://doi.org/10.1016/S1464-1895(99)00003-4

Michetti A.M., Esposito E., Gürpinar A., Mohammadioun B., Porfido S., Rogozhin E., Serva L., Tatevossian R., Vittori, E., Audemard F., Comerci V., (2004). The INQUA scale. An innovative approach for assessing earthquake intensities based on seismically induced ground effects in natural environment. Special paper of the Italian Environment Protection and Technical Services Agency (APAT), Italy, Memorie Descrittive della Carta Geologica d'Italia. Vol. LXVII.

Mikumo T., Ando M., (1976). A search into the faulting mechanism of the 1891 great Nobi earthquake. Journal of Physics of the Earth. Vol. 24, p. 63–87.

Mimura N., Yasuhara K., Kawagoe S., Nakagawa H., Kazama S. (2011). Damage from the Great East Japan Earthquake and Tsunami: A quick report. Mitigation and Adaptation Strategies for Global Change. Vol. 16(6), p. 803–818. https://doi.org/10.1007/s11027-011-9297-7

Miyazaki K., Nakajima J., Suenaga N., Yoshioka S., (2023). Deep subduction of the Philippine Sea slab and formation of slab window beneath central Japan. Earth, Planets and Space. Vol. 75(1), Article 93. https://doi.org/10.1186/s40623-023-01846-z

Mizuno C., Wang X., Dang J. A., (2024). Fast Survey Report About Bridge Damages by the 2024 Noto Peninsula Earthquake. Earthquake Research Advances. 100312, accepted.

Montgomery D.R., Manga M., (2003) Streamflow and Water Well Responses to Earthquakes. Science. Vol. 300, p. 2047-2049. https://doi.org/10.1126/science.1082980

Mori N., Takahashi T., the 2011 Tohoku Earthquake Tsunami Joint Survey Group, (2012). Nationwide post event survey and analysis of the 2011 Tohoku earthquake tsunami. Coastal Engineering. Journal. Vol. 54 (1), 1250001. https://doi.org/10.1142/ S0578563412500015.

Mori N., Takahashi T., Yasuda T., Yanagisawa H. (2011). Survey of 2011 Tohoku earthquake tsunami inundation and run-up. Geophysical Research Letters. Vol. 38(L00G14). https://doi.org/10.1029/2011GL049210

Muccignato E. (2025). Mw 7.5 Noto Earthquake (Japan) ESI-07 Dataset and ESI-07 Intensity Grid Map [Data set]. Zenodo. https://doi.org/10.5281/zenodo.15594097

Muccignato E., and Ferrario M. F., (2025). Exploiting earthquake-induced landslide inventories for macroseismic assessment using the environmental seismic intensity (ESI-07) scale. Frontiers in Earth Science. Vol. 13. https://doi.org/10.3389/feart.2025.1468787

Mulia I. E., Heidarzadeh M., Gusman A. R., Satake K., Fujii Y., Sujatmiko K. A., Meilano I., Windupranata W., (2024). Compounding impacts of the earthquake and submarine landslide on the Toyama Bay tsunami during the January 2024 Noto Peninsula event. Ocean Engineering. Vol. 310, p. 118698. https://doi.org/10.1016/j.oceaneng.2024.118698

Musson, R. M., Cecić, I. (2012). Intensity and Intensity Scales. In: Bormann, P. (Ed.), New Manual of Seismological Observatory Practice 2 (NMSOP-2), Potsdam : Deutsches GeoForschungsZentrum

GFZ, p. 1-41. https://doi.org/10.2312/GFZ.NMSOP-2_ch12

Mustac M., Dasović I., Latečki H., Cecić I., (2022). The public response and educational outreach through social media after the Zagreb earthquake of 22 March 2020Odziv javnosti i edukacija javnosti pomoću društvenih mreža nakon potresa u Zagrebu 22. ožujka 2020. Geofizika. Vol. 38, p. 215-234. 10.15233/gfz.2021.38.7

Naik S. P., Gwon O., Porfido S., Park K., Jin K., Kim Y.-S., Kyung J.-B., (2020). Intensity Reassessment of the 2017 Pohang Earthquake Mw = 5.4 (South Korea) Using ESI-07 Scale. Geosciences. Vol. 10(11), p. 471. https://doi.org/10.3390/geosciences10110471

Naik S. P., Mohanty A., Valkaniotis S., Mittal H., Porfido S., Michetti A. M., Gwon O., Park K., Jaya A., Paulik R., Li C., Mikami T., Kim Y.-S., (2023). 28th September 2018 Mw 7.5 Sulawesi Supershear Earthquake, Indonesia: Ground effects and macroseismic intensity estimation using ESI-2007 scale. Engineering Geology. Vol. 317, p. 107054. https://doi.org/10.1016/j.enggeo.2023.107054

Nakajima J. (2022). Crustal structure beneath earthquake swarm in the Noto peninsula, Japan. Earth, Planets and Space. Vol. 74(1), p. 160. https://doi.org/10.1186/s40623-022-01719-x

Nappi R., Porfido S., Paganini E., Vezzoli L., Ferrario M. F., Gaudiosi G., Alessio G., Michetti, A. M., (2021). The 2017, MD= 4.0, Casamicciola earthquake: ESI-07 scale evaluation and implications for the source model. Geosciences. Vol. 11(2), p. 44. https://doi.org/10.3390/geosciences11020044

Nishimura T., Hiramatsu Y., Ohta Y., (2023). Episodic transient deformation revealed by the analysis of multiple GNSS networks in the Noto Peninsula, central Japan. Scientific Reports Nature. Vol. 13 p. 8381. https://doi.org/10.1038/s41598-023-35459-z

Ohno H., Tsutsumi D., Furuya G., Takiguchi S., Ikeda M., Miyagi A., Miike T., Sawa Y., (2024). Sediment-related disasters induced by the Noto Peninsula Earthquake in January 2024. International Journal of Erosion Control Engineering. Vol. 17-4, p. 42-50.

Okamura Y., (2019) Distribution of Active Faults in Japan Sea and Future Issues. Zisin, Journal of the Seismological Society of Japan. Vol. 71, p.185–199. https://doi.org/10.4294/zisin.2017-21

Okamura Y., Watanabe M., Morijiri R., Satoh M., (1995). Rifting and basin inversion in the eastern margin of the Japan Sea. Island Arc. Vol. 4(3), p. 166–181. https://doi.org/10.1111/j.1440-1738.1995.tb00141.x

Okuwaki R., Yagi Y., Murakami A., Fukahata Y., (2024). A multiplex rupture sequence under complex fault network due to preceding earthquake swarms during the 2024 Mw 7.5 Noto Peninsula, Japan, earthquake. Geophysical Research Letters, 51, e2024GL109224. https://doi.org/10.1029/2024GL109224

Ota Y., Azuma T., Lin Y.N., (2009). Application of INQUA Environmental Seismic Intensity Scale to recent earthquakes in Japan and Taiwan. Geological Society of London Special Publications. Vol. 316, p. 55–71. https://doi.org/10.1144/SP316.4

Paganini E., (2023). Valutazione degli effetti ambientali generati dal terremoto di Casamicciola Terme (Na), 21 agosto 2017 (Md 4.0), e implicazioni per il rischio sismico a Ischia. Tesi di laurea, Università degli Studi dell'Insubria.

Papanikolaou I. D., and Lekkas E. L., (2009). Advances and limitations of the Environmental Seismic Intensity scale (ESI 2007) regarding near-field and far-field effects from recent earthquakes in Greece: implications for the seismic hazard assessment. Geological Society, London, Special Publications. Vol. 316(1), p. 11-30.

Papanikolaou I., Melaki M., (2017) The Environmental Seismic Intensity Scale (ESI 2007) in Greece, addition of newevents and its relationship with magnitude in Greece and the Mediterranean; preliminary attenuation relationships. Quaternary International. Vol. 451, p. 37–55.

Papathanassiou G., Valkaniotis S., Ganas A., Pavlides S., (2013). GIS-based statistical analysis of the spatial distribution of earthquake-induced landslides in the island of Lefkada, Ionian Islands, Greece. Landslides. Vol. 10-6, p. 771-783. https://doi.org/10.1007/s10346-012-0357-1

Papathanassiou G., Valkaniotis S., Pavlides S., (2019). The July 20, 2017 Bodrum-Kos, Aegean Sea Mw = 6.6 earthquake; preliminary field observations and image-based survey on a lateral spreading site. *Soil Dynamics and Earthquake Engineering*. Vol. 116, p. 668–680. https://doi.org/10.1016/j.soildyn.2018.10.038

Papathanassiou, G., Valkaniotis, S., Ganas, A., Stampolidis, A., Rapti, D., & Caputo, R. (2022). Floodplain evolution and its influence on liquefaction clustering: The case study of March 2021 Thessaly, Greece, seismic sequence. *Engineering Geology, 298*, 106542. https://doi.org/10.1016/j.enggeo.2022.106542

Papazachos B.C., Comninakis P.E., Karakaisis G.F., Karakostas B.G., Papaioannou C.H.A., Papazachos C.B., Scordilis E.M., (2000). A catalogue of earthquakes in Greece and surrounding area for the period 550BC 1999, Publ Geoph Lab, University of Thessaloniki

Papazachos B.C., Comninakis P.E., Scordilis E.M., Karakaisis G.F., Papazachos C.B., (2010) A catalogue of earthquakes in the Mediterranean and surrounding area for the period 1901–2010, Publ Geoph Lab, University of Thessaloniki

Pizza, M., Ferrario, M. F., Michetti, A. M., Nappi, R., Velázquez-Bucio, M. M., Lacan, P., and Porfido, S. (2023). Environmental effects caused by the Mw 6.9 23 November 1980 Irpinia-Basilicata Earthquake, Italy [Data set]. Zenodo. https://doi.org/10.5281/zenodo.10277164

Poblete B., Guzmán J., Maldonado J., Tobar F. (2018). Robust Detection of Extreme Events Using Twitter: Worldwide Earthquake Monitoring. IEEE Transactions on Multimedia. Vol. 20(10), p. 2551–2564. https://doi.org/10.1109/TMM.2018.2818020

Quitoriano V., Wald, D. J., (2020). USGS "Did You Feel It?"—Science and Lessons From 20 Years of Citizen Science-Based Macroseismology. Frontiers in Earth Science. Vol. 8, p. 120. https://doi.org/10.3389/feart.2020.00120

Richter C.F., (1958). Elementary Seismology. P. 768. W.H. Freeman and Co, San Francisco.

Rodríguez C.E., Bommer J.J., Chandler R.J., (1999). Earthquake-induced Landslides: 1980-1997, Soil Dynamics and Earthquake Engineering. Vol. 18, p. 325-346. https://doi.org/10.1016/S0267-7261(99)00012-3

Rodriguez L.M., Audemard F.A. And Rodriguez J.A., (2002), Casos històricos y contemporaneos de licuefacion de sedimentos inducidos por sismos en Venezuela desde 1530III Jornadas Venezolanas de Sismologìa Historica, Serie Tecnica n. 1, p 4-10.

Ross Z. E., Rollins C., Cochran E. S., Hauksson E., Avouac J.-P., Ben-Zion Y. , (2017). Aftershocks driven by afterslip and fluid pressure sweeping through a fault-fracture mesh. Geophysical Research Letters. Vol. 44(16), p. 8260–8267. https://doi.org/10.1002/2017GL074634

Ruhl C. J., Abercrombie R. E., Smith K. D., Zaliapin I., (2016). Complex spatiotemporal evolution of the 2008 Mw 4.9 Mogul earthquake swarm (Reno, Nevada): Interplay of fluid and faulting. Journal of Geophysical Research: Solid Earth. Vol. 121(11), p. 8196–8216. https://doi.org/10.1002/2016JB013399

Ruiz P., Rodríguez N., Valverde J., Marden A., Vecchiarelli L., Seal D.M., Nowicki Jessee M.A., Hamburger M.W., (2020). Landslide Inventory from the M 5.3 Capellades, Costa Rica Earthquake: U.S. Geological Survey data release. https://doi.org/10.5066/P92R269I

Ruiz, P., Carr J.C., Alvarad E., Soto G.J., Mana S., Feigenson M.D., Sáenz S.L.F., (2019). Coseismic Landslide Susceptibility Analysis Using LiDAR Data PGA Attenuation and GIS: The Case of Poás Volcano, Costa Rica, Central America. In: Tassi F, Vaselli O, Mora Amador R (eds) Poás Volcano. Active Volcanoes of the World. 79-118. https://doi.org/10.1007/978-3-319-02156-0_4

Sato H.P., Hasegawa H., Fujiwara S., Tobita M., Koarai M., Une H., Iwahashi J., (2007). Interpretation of landslide distribution triggered by the 2005 nothern Pakistan earthquake using SPOT 5 imagery: Landslides. 4:113-122. https://doi.org/10.1007/s10346-006-0069-5

Sato, H. (1994). The relationship between Late Cenozoic tectonic events and stress field and basin development in northeast Japan. Journal of Geophysical Research, 99(B11), 22261–22274. https://doi.org/10.1029/94JB00854

Schmitt R.G., Tanyas H., Nowicki Jessee M.A., Zhu J., Biegel K.M., Allstadt K.E. et al., (2017). An Open Repository of Earthquake-Triggered Ground-Failure Inventories. U.S. Geological Survey data release collection. https://doi.org/10.5066/F7H70DB4

Seal, D. M., Nowicki Jessee, A., Hamburger, M., Dills, C., and Allstadt, K. E. (2022). *Comprehensive global database of earthquake-induced landslide events and their impacts (ver. 2.0, February 2022)* [Data release]. U.S. Geological Survey. https://doi.org/10.5066/P9RG3MBE

Sekiguchi T., Sato H.P., (2006). Feature and distribution of landslides induced by the Mid Niigata Prefecture Earthquake in 2004, Japan. Journal of Japan Landslide Society. 43:142-154. https://doi.org/10.3313/jls.43.142

Sepulveda S., Serey A., Lara M., Pavez A., Rebolledo S., (2010). Landslides induced by the April 2007 Aisen Fjord earthquake, Chilean Patagonia. Landslides. 7(4):483-492. https://doi.org/10.1007/s10346-010-0203-2

Serva L., Vittori E., Comerci V., Esposito E., Guerrieri L., Michetti A.M. et al., (2016). Earthquake hazard and the Environmental Seismic Intensity (ESI) scale. Pure and Applied Geophysics. 173, 1479-1515. https://doi.org/10.1007/s00024-015-1177-8

Serva, L. (1994). Ground effects in intensity scales. Terra Nova 1994, 6, 414–416

Serva, L. (2019). History of the Environmental Seismic Intensity Scale ESI-07. Geosciences, 9(5), 210. https://doi.org/10.3390/geosciences9050210

Serva, L., Blumetti, A.M., Esposito, E., Guerrieri, L., Michetti, A.M., Okumura, K., Porfido, S., Reicherter, K., Silva, P.G., and Vittori, E. (2015a). Earthquake Environmental Effects, intensity and seismic hazard assessment: the lesson of some recent large earthquakes. In F. Audemard, T. Azuma and F. Baiocco (Eds.), Earthquake Environmental Effect for seismic hazard assessment: the ESI intensity scale and the EEE Catalogue (pp. 5–8). Rome: ISPRA – Geological Survey of Italy. Memorie Descrittive della Carta Geologica d'Italia, Vol. XCVII. https://doi.org/10.1016/S1464-1895(99)00003-4

Serva, L., Esposito, E., Guerrieri, L., Porfido, S., Vittori, E., Comerci, V., (2007). Environmental Effects from some historical earthquakes in Southern Apennines (Italy) and macroseismic intensity asseessment. Contribution to INQUA EEE scale project. Quat. Int. 173–174, 30–44

Serva, L., Vittori, E., Comerci, V., Esposito, E., Guerrieri, L., Michetti, A. M., Mohammadioun, B., Mohammadioun, G. C., Porfido, S., and Tatevossian, R. E. (2015b). Earthquake hazard and the Environmental Seismic Intensity (ESI) scale. Pure and Applied Geophysics. https://doi.org/10.1007/s00024-015-1177-8

Shao X., Ma S., Xu C., (2023). Distribution and characteristics of shallow landslides triggered by the 2018 Mw 7.5 Palu earthquake, Indonesia. Landslides. 20(1):157-175. https://doi.org/10.1007/s10346-022-01972-x

Shelly, D. R., and Hill, D. P. (2011). Migrating swarms of brittle-failure earthquakes in the lower crust beneath Mammoth Mountain, California. Geophysical Research Letters, 38(20), 1–6. https://doi.org/10.1029/2011GL049336

Shelly, D. R., Moran, S. C., and Thelen, W. A. (2013). Evidence for fluid-triggered slip in the 2009 Mount Rainier, Washington earthquake swarm. Geophysical Research Letters, 40(8), 1506–1512. https://doi.org/10.1002/grl.50354

Sieberg, A., (1930). Geologie der Erdbeden. Handbuch der Geophys 2 (4), 550–555.

Silva, P. G. (2019). Catálogo de los efectos geológicos de los terremotos en España. Cuaternario y Geomorfología: Revista de la Sociedad Española de Geomorfología y Asociación Española para el Estudio del Cuaternario, 33(1–2), 3–6.

Silva, P.G., Pérez-López R., Rodríguez-Pascua M.A., Giner J.L., Huerta P., Bardají T., Martín-González F., (2013). Earthquake environmental effects (EEEs) triggered by the 2011 Lorca earthquake (Mw 5.2, Betic Cordillera, SE Spain): Application of the ESI-07 macroseismic scale. 4th INQUA PATA meeting, Aachen, Germany, 9–14 October 2013, Aachen, ISBN 978-3-00-042796-1

Silva, P.G.; Rodríguez-Pascua, M.A.; Giner-Robles, J.L.; Pérez-López, R.; Lario, J.; Perucha, M.A.; Bardají, T.; Huerta, P.; Roquero, E.; Bautista Davila, M.B. (2014). Catálogo de los Efectos Geológicos de los Terremotos de España, 1ª Ed; Riesgos Geológicos y Geotecnia 4. IGME: Madrid, Spain, 2014; p. 352. (In Spanish)

Sørensen, M. B., Haga, T., & Nesje, A. (2023). Earthquake-induced landslides in Norway. *Natural Hazards and Earth System Sciences, 23*(4), 1577–1592. https://doi.org/10.5194/nhess-23-1577-2023.

Sridharan A., Ferrario M.F., Gopalan S., (2023). Earthquake-triggered landslides and Environmental Seismic Intensity: insights from the 2018 Papua New Guinea earthquake (Mw 7.5). All Earth. 35(1):195-209. https://doi.org/10.1080/27669645.2023.2233140

Suppasri, A., Kitamura, M., Alexander, D., Seto, S., and Imamura, F. (2024). The 2024 Noto Peninsula earthquake: Preliminary observations and lessons to be learned. International Journal of Disaster Risk Reduction, 110, 104611. https://doi.org/10.1016/j.ijdrr.2024.104611

Tajima, Y., Matsuba, Y., Yamanaka, Y., Shimozono, T., and Kato, F. (2024). Estimation of tsunami characteristics under rough wind waves in the 2024 Noto Peninsula Earthquake. Coastal Engineering Journal, 66(3), 419-433. https://doi.org/10.1080/21664250.2024.2385784

Tanyaş H., Hill K., Mahoney L., Fadel I., Lombardo L. , (2022). The world's second-largest, recorded landslide event: Lessons learnt from the landslides triggered during and after the 2018 Mw 7.5 Papua New Guinea earthquake. Engineering Geology. 297: 106504. https://doi.org/https://doi.org/10.1016/j.enggeo.2021.106504

Tanyaş H., van Westen C.J., Allstadt K.E., Anna Nowicki Jessee M., Görüm T., Jibson R et al., (2017). Presentation and analysis of a worldwide database of earthquake-induced landslide inventories. Journal of Geophysical Research: Earth Surface. 122(10):1991-2015. https://doi.org/10.1002/2017JF004236

Tatevossian, R. E. (2007). The Verny, 1887, earthquake in Central Asia: Application of the INQUA scale, based on coseismic environmental effects. *Quaternary International, 173–174*, 23–29. https://doi.org/10.1016/j.quaint.2007.02.006

Toda, S., Stein, R.S., 2024. Intense seismic swarm punctuated by a magnitude 7.5 Japan shock[EB/OL]. Temblor. https://doi.org/10.32858/temblor.333. https://www.dropbox.com/scl/fi/t721by6wunu1jnb9nl5v1/GSJ_MAP_ASIA-E_HZD02_2016_D-2.pdf?rlkey¼ambvu1ydf3wv2d70gbefdtwuzanddl¼0

Torabi, M., Fattahi, M., Amini, H., Ghassemi, M. R., and Karimi, N. (2020). OSL dating of landslide-dammed-lake deposits in the North of Tehran, Iran: 958 Ray-Taleghan/Ruyan earthquake. Quaternary International, 562, 46–57. https://doi.org/10.1016/j.quaint.2020.07.006

Tosi, P., De Rubeis, V., and Sbarra, P. (2024). HSIT system: Citizen Participation in Seismology for Data Collection and Enhanced Understanding of Earthquake Effects. Journal of Geoethics and Social Geosciences, 2(Special Issue), 1–20. https://doi.org/10.13127/jgsg-51

Tosi, P., De Rubeis, V., Sbarra, P., and Sorrentino, D. (2007). Hai Sentito Il Terremoto (HSIT), Istituto Nazionale di Geofisica e Vulcanologia (INGV), https://doi.org/10.13127/HSIT

Tovar, F., and Sánchez, J. J. (2020). Reassessment of macroseismic intensities for two earthquakes in Colombia: Tumaco (1979, Mw= 8.1) and Armenia (1999, Mw= 6.1), using the ESI-2007 scale. Journal of South American Earth Sciences, 103, 102703.

Townsend K.F., Gallen S.F., Clark M.K., (2020). Quantifying near-surface rock strength on a regional scale from hillslope stability models. Journal of Geophysical Research: Earth Surface. 125: e2020JF005665. https://doi.org/10.1029/2020JF005665

Triantafyllou, I., Papadopoulos, G. A., and Lekkas, E. (2020). Impact on built and natural environment of the strong earthquakes of April 23, 1933, and July 20, 2017, in the southeast Aegean Sea, eastern Mediterranean. Natural Hazards, 100(2), 671-695.

Trigila A., Iadanza C., Esposito C., Scarascia Mugnozza G. (2015) Comparison of Logistic Regression and Random Forests techniques for shallow landslide susceptibility assessment in Giampilieri (NE Sicily, Italy). Geomorphology, 249, 119-136, ISSN: 0169-555X.

Trigila A., Iadanza C., Spizzichino D. (2010) Quality assessment of the Italian Landslide Inventory using GIS processing. Landslides, 7, Number 4, 455-470, ISSN: 1612-510X.

Tsuji, Y., Satake, K., Ishibe, T., Harada, T., Nishiyama, A., Kusumoto, S., 2014. Tsunami heights along the pacific coast of northern honshu recorded from the 2011 Tohoku and previous Great earthquakes. Pure Appl. Geophys. 171, 3183–3215. https://doi. org/10.1007/s00024-014-0779-x.

Tsuji, Y., Satake, K., Ishibe, T., Kusumoto, S., Heidarzadeh, M., et al., 2011. Field surveys of tsunami heights from the 2011 off the pacific coast of Tohoku, Japan earthquake. Bull. Earthq. Res. Inst. Univ. Tokyo 86, 29–279 (in Japanese with English abstract).

U.S. Geological Survey. (2024). M 7.5 - 2024 Noto Peninsula, Japan Earthquake. Retrieved from https://earthquake.usgs.gov/earthquakes/eventpage

Uchida T., Kataoka S., Iwao T., Matsuo O., Terada H., Nakano Y., Sugiura N., Osanai N. (2017) Landslides triggered by the January 16, 1995, M 6.9 Kobe, Japan Earthquake. https://doi.org/10.5066/F7TH8K60

Uchida T., Kataoka S., Iwao T., Matsuo O., Terada H., Nakano Y., Sugiura N., Osanai N., (2004). A study on methodology for assessing the potential of slope failures during earthquakes. Technical note of National Institute for Land and Infrastructure Management. 91.

Uchide T, Shiina T, Imanishi K (2022) Stress map of Japan: detailed nationwide crustal stress field inferred from focal mechanism solutions of numerous microearthquakes. J Geophys Res.

Valente, E., Ascione, A., Ciotoli, G., Cozzolino, M., Porfido, S., and Sciarra, A. (2018). Do moderate magnitude earthquakes generate seismically induced ground effects? The case study of the M w= 5.16, 29th December 2013 Matese earthquake (southern Apennines, Italy). International Journal of Earth Sciences, 107(2), 517-537.

Vayena, E., and Tasioulas, J. (2015). "We the Scientists": A Human Right to Citizen Science. Philosophy and Technology, 28(3), 479–485. https://doi.org/10.1007/s13347-015-0204-0

Velázquez-Bucio MM, Ferrario MF, Lacan P, Muccignato E, Pizza M, Sridharan A, Porfido S, GopalanS, Nuñez-Meneses A, Michetti AM (2024) Environmental effects and ESI-07 intensity of the Mw 7.7, September 19th, 2022, Michoacán, Mexico, earthquake. Engineering Geology, Volume 343, 2024, 107776, ISSN 0013-7952.https://doi.org/10.1016/j.enggeo.2024.107776.

Velázquez-Bucio, M. M., Ferrario, M. F., Muccignato, E., Porfido, S., Sridharan, A., Chunga, K., Livio, F., Gopalan, S., and Michetti, A. M. (2021). Environmental effects caused by the Mw 8.2, September 8, 2017, and Mw 7.4, June 23, 2020, Chiapas-Oaxaca (Mexico) subduction events: Comparison of large intraslab and interface earthquakes. Quaternary International. https://doi.org/10.1016/j.quaint.2021.11.028

Velev D., and Zlateva P., (2012). Use of Social Media in Natural Disaster Management

Vezio, P., Mingozzi, E., and Poli, N. (2024). Characterizing smartphone capabilities for seismic and structural monitoring. Scientific Reports, 14, Article 23017. https://doi.org/10.1038/s41598-024-72929-4

Vittori, E., Blumetti, A. M., Comerci, V., Di Manna, P., Piccardi, L., Gega, D., and Hoxha, I. (2021). Geological effects and tectonic environment of the 26 November 2019, Mw 6.4 Durres earthquake (Albania). Geophysical Journal International, 225(2), 1174–1191. https://doi.org/10.1093/gji/ggaa582

Wald, D. J. (1996). Slip history of the 1995 Kobe, Japan, earthquake determined from strong motion, teleseismic, and geodetic data. Journal of Physics of the Earth, 44(5), 489–503. https://doi.org/10.4294/jpe1952.44.489

Wald, D. J., and Somerville, P. G. (1995). Variable-slip rupture model of the great 1923 Kanto, Japan, earthquake: Geodetic and body-waveform analysis. Bulletin of the Seismological Society of America, 85(1), 159–177. https://doi.org/10.1785/BSSA0850010159

Wartman J., Dunham L., Tiwari B., and Pradel D., (2013). Landslides in eastern Honshu induced by the 2011 Tohoku earthquake. Seismological Society of America Bulletin. 103-2B:1503-1521. https://doi.org/10.1785/0120120128

Wei, S., Avouac, J. P., Hudnut, K. W., Donnellan, A., Parker, J. W., Graves, R. W., et al. (2015). The 2012 Brawley swarm triggered by injection- induced aseismic slip. Earth and Planetary Science Letters, 422, 115–125. https://doi.org/10.1016/j.epsl.2015.03.054

White, Connie and Plotnick, Linda and Kushma, Jane and Hiltz, Starr and Turoff, Murray. (2009). An Online Social Network for Emergency Management. International Journal of Emergency Management. 6. 10.1504/IJEM.2009.031572

Wood H.O. And Neumann F., (1931). Modified Mercalli intensity scale of 1931. Bull. Seis. Soc. Am., 21, pp. 277-283.

Xiang, Y.; Qin, M.; Chen, Y.; Xing, Y.; Bian, Y. (2024). Co-Seismic and Post-Seismic Slip Properties Associated with the 2024 M 7.5 Noto Peninsula, Japan Earthquake Determined by GNSS Observations. Remote Sens., 16, 4057. https://doi.org/10.3390/rs16214057

Xu C., (2014c). Do buried-rupture earthquakes trigger less landslides than surface-rupture earthquakes for reverse faults? Geomorphology 216:53-57. 216:53-57. https://doi.org/10.1016/j.geomorph.2014.03.029

Xu C., (2015a). Preparation of earthquake-triggered landslide inventory maps using remote sensing and GIS technologies: Principles and case studies. Geoscience Frontiers. 6(6):825-836. https://doi.org/10.1016/j.gsf.2014.03.004

Xu C., Xu X., Shen L., Yao Q., Tan X., Kang W. et al., (2016) Optimized volume models of earthquake-triggered landslides. Scientific Reports. 6(1). https://doi.org/10.1038/srep29797

Xu C., Xu X., Shyu J.B.H., (2015b). Database and spatial distribution of landslides triggered by the Lushan, China Mw 6.6 earthquake of 20 April 2013. Geomorphology. 248:77-92. https://doi.org/10.1016/j.geomorph.2015.07.002

Xu C., Xu X., Shyu J.B.H., Zheng W., Min W., (2014b). Landslides triggered by the 22 July 2013 Minxian Zhangxian, China, Mw 5.9 earthquake: Inventory compiling and spatial distribution analysis. Journal of Asian Earth Sciences. 92: 125-142. https://doi.org/10.1016/j.jseaes.2014.06.014

Xu C., Xu X., Yao X., Dai F., (2014a) Three (nearly) complete inventories of landslides triggered by the May 12, 2008 Wenchuan Mw 7.9 earthquake of China and their spatial distribution statistical analysis. Landslides. 11-3: 441-461. https://doi.org/10.1007/s10346-013-0404-6

Xu C., Xu X., Zhou B., and Yu G., (2013). Revisions of the M 8.0 Wenchuan earthquake seismic intensity map based on coseismic landslide abundance. Nat. Hazards. 69: 1459–1476. https://doi.org/10.1007/s11069-013-0757-0

Xu, L., Ji, C., Meng, L., Ampuero, J.-P., Yunjun, Z., Mohanna, S., and Aoki, Y. (2024). Dual-initiation ruptures in the 2024 Noto earthquake encircling a fault asperity at a swarm edge. Science, 385(871-876). DOI: adp0493.

Yagi H., Sato G., Higaki D., Yamamoto M,. Yamasaki T., (2009). Distribution and characteristics of landslides induced by the Iwate–Miyagi Nairiku Earthquake in 2008 in Tohoku District, Northeast Japan. Landslides. 6:335. https://doi.org/10.1007/s10346-009-0182-3

Yang Z., Pang B., Dong W., Li D., (2023). Spatial Pattern and Intensity Mapping of Coseismic Landslides Triggered by the 2022 Luding Earthquake in China. Remote Sensing. 15(5): 1323. https://doi.org/10.3390/rs15051323

Yoshida, K., and Hasegawa, A. (2018). Sendai-Okura earthquake swarm induced by the 2011 Tohoku-Oki earthquake in the stress shadow of NE Japan: Detailed fault structure and hypocenter migration. Tectonophysics, 733, 132-147. https://doi.org/10.1016/j.tecto.2017.12.031

Yoshida, K., Hasegawa, A., and Yoshida, T. (2016). Temporal variation of frictional strength in an earthquake swarm in NE Japan caused by fluid migration. Journal of Geophysical Research: Solid Earth, 121(8), 5953–5965. https://doi.org/10.1002/2016JB013022

Yoshida, K., Takagi, R., Fukushima, Y., Ando, R., Ohta, Y., and Hiramatsu, Y. (2024). Role of a hidden fault in the early process of the 2024 Mw7.5 Noto Peninsula earthquake. Geophysical Research Letters, 51, e2024GL110993. https://doi.org/10. 1029/2024GL110993

Yoshida, K., Uchida, N., Matsumoto, Y., Orimo, M., Okada, T., Hirahara, S., Kimura, S., Hino, R. (2023b) Updip fluid flow in the crust of the northeastern Noto Peninsula, Japan, triggered the 2023 Mw 6.2 Suzu earthquake during swarm activity. Geophys. Res. Lett. 50:e2023GL106023. doi: 10.1029/2023GL106023

Yoshida, K., Uno, M., Matsuzawa, T., Yukutake, Y., Mukuhira, Y., Sato, H., and Yoshida, T. (2023a). Upward earthquake swarm migration in the northeastern Noto Peninsula, Japan, initiated from a deep ring-

shaped cluster: Possibility of fluid leakage from a hidden magma system. Journal of Geophysical Research: Solid Earth, 128(6), e2022JB026047. https://doi.org/10.1029/2022JB026047

Yuhi, M., Umeda, S., Arita, M., Ninomiya, J., Gokon, H., Arikawa, T., Baba, T., Imamura, F., Kumagai, K., Kure, S., Miyashita, T., Suppasri, A., Kawai, A., Nobuoka, H., Shibayama, T., Koshimura, S., and Mori, N. (2024). Dataset of Post-Event Survey of the 2024 Noto Peninsula Earthquake Tsunami in Japan. Scientific Data, 11, 786. https://doi.org/10.1038/s41597-024-03619-z

Yukutake, Y., Ito, H., Honda, R., Harada, M., Tanada, T., and Yoshida, A. (2011). Fluid-induced swarm earthquake sequence revealed by precisely determined hypocenters and focal mechanisms in the 2009 activity at Hakone Volcano, Japan. Journal of Geophysical Research, 116(4), 13. https://doi.org/10.1029/2010JB008036

Yunus A.P., Xinyu C., Catani F., Subramaniam S.S., Fan X., Jie D. et al., (2023). Earthquake-induced soil landslides: volume estimates and uncertainties with the existing scaling exponents. Scientific Reports. 13(1)8151. https://doi.org/10.1038/s41598-023-35088-6

Zei C., Tarabusi G., Ciuccarelli C., Burrato P., Sgattoni G., Taccone R.C., Mariotti D. (2024). CFTIlandslides, Italian database of historical earthquake-induced landslides. Istituto Nazionale di Geofisica e Vulcanologia (INGV). https://doi.org/10.13127/cfti/landslides

Zhang J., Liu R., Deng W., Khanal N.R., Gurung D.R., Murthy M.S.R., and Wahid S., (2016). Characteristics of Landslide in Koshi River Basin, Central Himalaya. Journal of Mountain Science. 13 (10):1711–1722. https://doi.org/10.1007/s11629-016-4017-0

Zhang, Y., Kong, Q., Ruan, T., Lv, Q., and Allen, R. (2024). A comprehensive analysis of real-world accelerometer data quality in a global smartphone-based seismic network (arXiv:2407.03570). arXiv. https://doi.org/10.48550/arXiv.2407.03570

Zhao B., (2021) Landslides triggered by the 2018 Mw 7.5 Palu supershear earthquake in Indonesia. Engineering Geology. 294, 106406.
https://doi.org/https://doi.org/10.1016/j.enggeo.2021.10640

Zhao B., Su L., Xu Q., Li W., Xu C., Wang Y., (2023) A review of recent earthquake-induced landslides on the Tibetan Plateau. Earth-Science Reviews. 104534.
https://doi.org/10.1016/j.earscirev.2023.104534

APPENDIX

CHAPTER 1

1.1 ESI-07 INTENSITY SCALE GUIDELINES

ESI-07 Intensity scale guidelines are reported below. Intensity grades and associated EEEs, both primary and secondary, are listed and described, according to Michetti et al., (2007).

From grade I to III: There are no environmental effects that can be used as diagnostic.

Grade IV: First unequivocal effects in the environment

Primary effects: absent

Secondary effects:

a) *Rare small variations of the water level in wells and/or of the flow-rate of springs are locally recorded, as well as extremely rare small variations of chemical-physical properties of water and turbidity in springs and wells, especially within large karstic spring systems, which appear to be most prone to this phenomenon.*

b) *In closed basins (lakes, even seas) seiches with height not exceeding a few centimeters may develop, commonly observed only by tidal gauges, exceptionally even by naked eye, typically in the far field of strong earthquakes. Anomalous waves are perceived by all people on small boats, few people on larger boats, most people on the coast. Water in swimming pools swings and may sometimes overflows.*

c) *Hair-thin cracks (millimeter-wide) might be occasionally seen where lithology (e.g., loose alluvial depo sits, saturated soils) and/or morphology (slopes or ridge crests) are most prone to this phenomenon.*

d) *Exceptionally, rocks may fall, and small landslide may be (re)activated, along slopes where the equilibrium is already near the limit state, e.g., steep slopes and cuts, with loose and generally saturated soil.*

e) *Tree limbs shake feebly.*

Grade V: Marginal effects in the environment

Primary effects: absent

Secondary effects:

a) *Rare variations of the water level in wells and/or of the flow-rate of springs are locally recorded, as well as small variations of chemical-physical properties of water and turbidity in lakes, springs and wells.*
b) *In closed basins (lakes, evenseas) seiches with height of decimeters may develop, sometimes noted also by naked eye, typically in the far field of strong earthquakes. Anomalous waves up to several tens of cm high are perceived by all people on boats and on the coast. Water in swimming pools overflows.*
c) *Thin cracks (millimeter-wide and several cms up to one meter long) are locally seen where lithology (e.g., loose alluvial deposits, saturated soils) and/or morphology (slopes or ridge crests) are most prone to this phenomenon.*
d) *Rare small rockfalls, rotational landslides and slump earth flows may take place, along often but not necessarily steep slopes where equilibrium is near the limit state, mainly loose deposits and saturated soil. Underwater landslides may be triggered, which can induce small anomalous waves in coastal areas of sea and lakes.*
e) *Tree limbs and bushes shake slightly, very rare cases of fallen dead limbs and ripe fruit.*
f) *Extremely rare cases are reported of liquefaction (sand boil), small in size and in areas most prone to this phenomenon (highly susceptible, recent, alluvial and coastal deposits, near-surface water table)*

Grade VI: Modest effects in the environment

Primary effects: absent

Secondary effects:

a) *Significant variations of the water level in wells and/or of the flow-rate of springs are locally recor ded, as well as small variations of chemical-physical properties of water and turbidity in lakes, springs and wells.*
b) *Anomalous waves up to many tens of cm high flood very limited areas nearshore. Water in swimming pools and small ponds and basins overflows.*
c) *Occasionally, millimeter-centimeter wide and up to several meters long fractures are observed in loose alluvial deposits and/or saturated soils; along steep slopes or riverbanks they can be 1-2 cm wide. A few minor cracks develop in paved (either asphalt or stone) roads.*
d) *Rockfalls and landslides with volume reaching ca. 103 m3 can take place, especially where equilibrium is near the limit state, e.g. steep slopes and cuts, with loose saturated soil, or highly weathered / frac tured rocks. Underwater landslides can be triggered, occasionally provoking small anomalous waves in coastal areas of sea and lakes, commonly seen by intrumental records.*
e) *Trees and bushes shake moderately to strongly; a very few tree tops and unstable-dead limbs may break and fall, also depending on species, fruit load and state of health.*
f) *Rare cases are reported of liquefaction (sand boil), small in size and in areas most prone to this phenomenon (highly susceptible, recent, alluvial and coastal deposits, near surface water table).*

Grade VII: Appreciable effects in the environment

Primary effects: *observed very rarely, and almost exclusively in volcanic areas. Limited surface fault ruptures, tens to hundreds of meters long and with centimetric offset, may occur, essentially associated to very shallow earthquakes.*

Secondary effects: The total affected area is in the order of 10 km2.

a) *Significant temporary variations of the water level in wells and/or of the flow-rate of springs are locally recorded. Seldom, small springs may temporarily run dry or appear. Weak variations of chemical-physical properties of water and turbidity in lakes, springs and wells are locally observed.*
b) *Anomalous waves even higher than a meter may flood limited nearshore areas and damage or wash away objects of variable size. Water overflows from small basins and watercourses.*
c) *Fractures up to 5-10 cm wide and up to hundred meters long are observed, commonly in loose alluvial deposits and/or saturated soils; rarely, in dry sand, sand-clay, and clay soil fractures are also seen, up to 1 cm wide. Centimeter-wide cracks are common in paved (asphalt or stone) roads.*
d) *Scattered landslides occur in prone areas, where equilibrium is unstable (steep slopes of loose / saturated soils), while modest rock falls are common on steep gorges, cliffs). Their size is sometimes significant (103- 105 m3); in dry sand, sand-clay, and clay soil, the volumes are usually up to 100 m3. Ruptures, slides and falls may affect riverbanks and artificial embankments and excavations (e.g., road cuts, quarries) in loose sediment or weathered / fractured rock. Significant underwater landslides can be triggered, provoking anomalous waves in coastal areas of sea and lakes, directly felt by people on boats and ports.*
e) *Trees and bushes shake vigorously, especially in densely forested areas, many limbs and tops break and fall.*
f) *Rare cases are reported of liquefaction, with sand boils up to 50 cm in diameter, in areas most prone to this phenome non (highly susceptible, recent, alluvial and coastal deposits, near surface water table)*

Grade VIII: Extensive effects in the environment

Primary effects: *observed rarely. Ground ruptures (surface faulting) may develop, up to several hundred meters long, with offsets not exceeding a few cm, particularly for very shallow focus earthquakes such as those common in volcanic areas. Tectonic subsidence or uplift of the ground surface with maximum values on the order of a few centimeters may occur.*

Secondary effects: The total affected area is in the order of 100 km2.

a) *Springs may change, generally temporarily, their flow-rate and/or elevation of outcrop. Some small springs may even run dry. Variations in water level are observed in wells. Weak variations of chemical-physical properties of water, most commonly temperature, may be observed in springs and/or wells. Water turbidity may appear in closed basins, rivers, wells and springs. Gas emissions, often sulphureous, are locally observed.*
b) *Anomalous waves up to 1-2 meters high flood nearshore areas and may damage or wash away objects of variable size. Erosion and dumping of waste are observed along the beaches, where some bushes and even small weak-rooted trees can be eradicated and drifted away. Water violently overflows from small basins and watercourses.*
c) *Fractures up to 50 cm wide and up to hundreds meters long, are commonly observed in loose alluvial deposits and/or saturated soils; in rare cases fractures up to 1 cm can be observed in competent dry rocks. Decimetric cracks are common in paved (asphalt or stone) roads, as well as small pressure undulations.*
d) *Small to moderate (103- 105 m3) landslides are widespread in prone areas; rarely they can occur also on gentle slopes; where equilibrium is unstable (steep slopes of loose / saturated soils; rock falls on steep gorges, coastal cliffs) their size is sometimes large (105- 106 m3). Landslides can occasionally dam narrow valleys causing temporary or even permanent lakes. Ruptures, slides and falls affect riverbanks and artificial embankments and excavations (e.g., road cuts, quarries) in loose sediment or weathered / fractured rock. Frequent is the occurrence of landslides under the sea level in coastal areas.*
e) *Trees shake vigorously; branches may break and fall, trees may be uprooted , especially along steep slopes.*
f) *Liquefaction may be frequent in the epicentral area, depending on local conditions; the most typical effects are: sand boils up to ca. 1 m in diameter; apparent water fountains in still waters; localized lateral spreading and settlements (subsidence up to ca. 30 cm), with fissuring parallel to waterfront areas (river banks, lakes, canals, seashores). g) In dry areas, dust clouds may rise from the ground in the epicentral area. h)Stones and even small boulders and tree trunks may be thrown in the air, leaving typical imprints in soft soil.*

Grade IX: Effects in the environment are a widespread source of considerable hazard and become important for intensity assessment

Primary effects: *observed commonly. Ground ruptures (surface faulting) develop, up to a few km long, with offsets generally in the order of several cm. Tectonic subsidence or uplift of the ground surface with maximum values in the order of a few decimeters may occur.*

Secondary effects: The total affected area is in the order of 1000 km2.

a) *Springs can change, generally temporarily, their flow-rate and/or location to a considerable extent. Some modest springs may even run dry. Temporary variations of water level are commonly observed in wells. Variations of chemical-physical properties of water, most commonly temperature, are observed in springs and/or wells. Water turbidity is common in closed basins, rivers, wells and springs. Gas emissions, often sulphureous, are observed, and bushes and grass near emission zones may burn.*
b) *Meters high waves develop in still and running waters. In flood plains water streams may even change their course, also because of land subsidence. Small basins may appear or be emptied. Depending on shape of sea bottom and coastline, dangerous tsunamis may reach the shores with runups of up to several meters flooding wide areas. Widespread erosion and dumping of waste are observed along the beaches, where bushes and trees can be eradicated and drifted away.*
c) *Fractures up to 100 cm wide and up to hundreds meters long are commonly observed in loose alluvial deposits and/or saturated soils; in competent rocks they can reach up to 10 cm. Significant cracks are common in paved (asphalt or stone) roads, as well as small pressure undulations.*
d) *Landsliding is widespread in prone areas, also on gentle slopes; where equilibrium is unstable (steep slopes of loose / saturated soils; rock falls on steep gorges, coastal cliffs) their size is frequently large (105 m3), sometimes very large (106 m3). Landslides can dam narrow valleys causing temporary or even permanent lakes. Riverbanks, artificial embankments and excavations (e.g., road cuts, quarries) frequently collapse. Frequent are large landslides under the sea level.*
e) *Trees shake vigorously; branches and thin tree trunks frequently break and fall. Some trees might be uprooted and fall, especially along steep slopes.*
f) *Liquefaction and water upsurge are frequent; the most typical effects are sand boils up to 3 m in diameter; apparent water fountains in still waters; frequent lateral spreading and settlements (subsidence of more than ca. 30 cm), with fissuring parallel to waterfront areas (riverbanks, lakes, canals, seashores).*
g) *In dry areas, dust clouds may rise from the ground. h)Small boulders and tree trunks may be thrown in the air and move away from their site for meters, also depending on slope angle and roundness, leaving typical imprints in soft soil.*

Grade X: Effects on the environment become a leading source of hazard and are critical for intensity assessment

Primary effects: *become leading. Surface faulting can extend for few tens of km, with offsets from tens of cm up to a few meters. Gravity grabens and elongated depressions develop; for very shallow focus earthquakes in volcanic areas rupture lengths might be much lower. Tectonic subsidence or uplift of the ground surface with maximum values in the order of few meters may occur.*

Secondary effects: The total affected area is in the order of 5,000 km2.

a) *Many springs significantly change their flow-rate and/or elevation of outcrop. Some springs may run temporarily or even permanently dry. Temporary variations of water level are commonly observed in wells. Even strong variations of chemical-physical properties of water, most commonly temperature, are observed in springs and/or wells. Often water becomes very muddy in even large basins, rivers, wells and springs. Gas emissions, often sulphureous, are observed, and bushes and grass near emission zones may burn.*
b) *Meters high waves develop in even big lakes and rivers, which overflow from their beds. In flood plains rivers may change their course, temporary or even permanently, also because of widespread land subsidence. Basins may appear or be emptied. Depending on shape of sea bottom and coastline, tsunamis may reach the shores with runups exceeding 5 m flooding flat areas for thousands of meters inland. Small boulders can be dragged for many meters. Widespread deep erosion is observed along the shores, with noteworthy changes of the coastline profile. Trees nearshore are eradicated and drifted away.*
c) *Open ground cracks up to more than 1 m wide and up to hundred meters long are frequent, mainly in loose alluvial depo sits and/or saturated soils; in competent rocks opening reaches several decimeters. Wide cracks develop in paved (asphalt or stone) roads, as well as pressure undulations.*
d) *Large landslides and rock-falls (> 105- 106m3) are frequent, practically regardless of equilibrium state of slopes, causing temporary or permanent barrier lakes. Riverbanks, artificial embankments, and sides of excavations typically collapse. Levees and earth dams may also incur serious damage. Frequent are large landslides under the sea level in coastal areas.*
e) *Trees shake vigorously; many branches and tree trunks break and fall. Some trees might be uprooted and fall.*
f) *Liquefaction, with water upsurge and soil compaction, may change the aspect of wide zones; sand volcanoes even more than 6 m in diameter; vertical subsidence even > 1m; large and long fissures due to lateral spreading are common.*
g) *In dry areas, dust clouds commonly rise from the ground. h)Boulders (diameter in excess of 2-3 meters) can be thrown in the air and move away from their site for hundreds of meters down even gentle slopes, leaving typical imprints in soil.*

Grade XI: Effects on the environment become decisive for intensity assessment, due to saturation of structural damage

Primary effects: are dominant. *Surface faulting extends from several tens of km up to more than one hundred km, accompanied by slips reaching several meters. Gravity graben, elongated depressions and pressure ridges develop. Drainage lines can be seriously offset. Tectonic subsidence or uplift of the ground surface with maximum values in the order of numerous meters may occur.*

Secondary effects. The total affected area is in the order of 10,000 km2.

a) *Many springs significantly change their flow-rate and/or elevation of outcrop. Many springs may run temporarily or even permanently dry. Temporary or permanent variations of water level are generally observed in wells. Even strong variations of chemical-physical properties of water, most commonly temperature, are observed in springs and/or wells. Often water becomes very muddy in even large basins, rivers, wells and springs. Gas emissions, often sulphureous, are observed, and bushes and grass near emission zones may burn.*
b) *Large waves develop in big lakes and rivers, which overflow from their beds. In flood plains rivers can change their course, temporary or even permanently, also because of widespread land subsidence and landsliding. Basins may appear or be emptied. Depending on shape of sea bottom and coastline, tsunamis may reach the shores with runups reaching 15 meters and more devastating flat areas for kilometers inland. Even meter-sized boulders can be dragged for long distances. Widespread deep erosion is observed along the shores, with noteworthy changes of the coastal morphology. Trees nearshore are eradicated and drifted away.*
c) *Open ground cracks up to several meters wide are very frequent, mainly in loose alluvial deposits and/or saturated soils. In competent rocks they can reach 1 m. Very wide cracks develop in paved (asphalt or stone) roads, as well as large pressure undulations.*
d) *Large landslides and rock-falls (> 105- 106 m3) are frequent, practically regardless of equilibrium state of slopes, causing many temporary or permanent barrier lakes. Riverbanks, artificial embankments, and sides of excavations typically collapse. Levees and earth dams incur serious damage. Significant landslides can occur even at 200 - 300 km distance from the epicenter. Frequent are large landslides under the sea level in coastal areas.*
e) *Trees shake vigorously; many branches and tree trunks break and fall. Many trees are uprooted and fall.*
f) *Liquefaction changes the aspect of extensive zones of lowland, determining vertical subsidence possibly exceeding several meters; numerous large sand volcanoes, and severe lateral spreading can be observed.*
g) *In dry areas dust clouds arise from the ground. h) Big boulders (diameter of several meters) can be thrown in the air and move away from their site for long distances down even gentle slopes., leaving typical imprints in soil.*

Grade XII: Effects in the environment are the only tool for intensity assessment

Primary effects: are dominant. *Surface faulting is at least few hundreds of km long, accompanied by offsets reaching several tens of meters. Gravity graben, elongated depressions and pressure ridges develop. Drainage lines can be seriously offset. Landscape and geomorphological changes induced by primary effects can attain extraordinary extent and size (typical examples are the uplift or subsidence of coastlines by several meters, appearance or disappearance from sight of significant landscape elements, rivers changing course, origination of waterfalls, formation or disappearance of lakes).*

Secondary effects. The total affected area is in the order of 50,000 km2 and more.

a) Many springs significantly change their flow-rate and/or elevation of outcrop. Temporary or permanent variations of water level are generally observed in wells. Many springs and wells may run temporarily or even permanently dry. Strong variations of chemical-physical properties of water, most commonly temperature, are observed in springs and/or wells. Water becomes very muddy in even large basins, rivers, wells and springs. Gas emissions, often sulphureous, are observed, and bushes and grass near emission zones may burn.

b) Giant waves develop in lakes and rivers, which overflow from their beds. In flood plains rivers change their course and even their flow direction, temporary or even permanently, also because of widespread land subsidence and landsliding. Large basins may appear or be emptied. Depending on shape of sea bottom and coastline, tsunamis may reach the shores with runups of several tens of meters devastating flat areas for many kilometers inland. Big boulders can be dragged for long distances. Widespread deep erosion is observed along the shores, with outstanding changes of the coastal morphology. Many trees are eradicated and drifted away. All boats are torn from their moorings and swept away or carried onshore even for long distances. All people outdoor are swept away.

c) Ground open cracks are very frequent, up to one meter or more wide in the bedrock, up to more than 10 m wide in loose alluvial deposits and/or saturated soils. These may extend up to several kilometers.

d) Large landslides and rock-falls (> 105- 106 m3) are frequent, practically regardless to equilibrium state of the slopes, causing many temporary or permanent barrier lakes. Riverbanks, artificial embankments, and sides of excavations typically collapse. Levees and earth dams incur serious damage. Significant landslides can occur at more than 200 - 300 km distance from the epicenter. Frequent are very large landslides under the sea level in coastal areas.

e) Trees shake vigorously; many branches and tree trunks break and fall. Many trees are uprooted and fall.

f) Liquefaction occurs over large areas and changes the morphology of extensive flat zones, determining vertical subsidence exceeding several meters, widespread large sand volcanoes, and extensive severe lateral spreading can be observed.

g) In dry areas dust clouds arise from the ground.

h) *Also very big boulders can be thrown in the air and move for long distances even down very gentle slopes, leaving typical imprints in soil.*

1.2 CONVERSION TABLE FOR SURFACE RUPTURE AND TECTONIC UPLIFT\SUBSIDENCE

For Surface ruptures and Tectonic uplift and subsidence a quantitative classification was developed to ensure progressive value increase and consistency with other ESI categories. Qualitative terms were converted into quantitative ranges using proportional scaling based on orders of magnitude.

I_0 Intensity	PRIMARY EFFECTS		
	ESI07 INTENSITY GRADE DESCRIPTION	MAX SURFACE DISPLACEMENT / DEFORMATION (after Michetti et al., 2007)	TECTONIC UPLIFT (after Muccignato E., 2025)
IV	-	-	-
V	-	-	-
VI	-	-	-
VII	-	(*) (*) Limited surface fault ruptures, tens to hundreds meters long with centimetric offset may occur essentially associated to very shallow earthquakes in volcanic areas.	-
VIII	Tectonic subsidence or uplift of the ground surface with maximum values on the order of a **few centimeters** may occur.	Centimetric	10-30 cm
IX	Tectonic subsidence or uplift of the ground surface with maximum values in the order of a **few decimeters** may occur.	5-40 cm	30-100 cm
X	Tectonic subsidence or uplift of the ground surface with maximum values in the order of **few meters** may occur.	40-300 cm	100-300 cm
XI	Tectonic subsidence or uplift of the ground surface with maximum values in the order of **numerous meters** may occur.	300-700 cm	300-1000 cm
XII	[…] the uplift or subsidence of coastlines by **several meters** […]	> 700 cm	>1000 cm

1.3 CONVERSION TABLE FOR ANOMALOUS WAVES AND TSUNAMIS

A quantitative classification was developed comparing three different scales adopted for Anomalous waves and Tsunami category, and in particular ESI-07 Scale, ITIS-2012 Scale and TEE-16 Scale (Michetti et al., 2007, Lekkas et al., 2013 and Lario et al., 2016). The latter is adopted as the reference scale.

0 Intensity	**ANOMALOUS WAVES AND TSUNAMIS**		
	ESI-07 SCALE (Michetti et al, 2007)	ITIS-2012 (Quantities category) (Lekkas et al., 2013)	TEE-16 SCALE (Lario et al., 2016)
IV	-	**Tsunami height** or tsunami flow depth of a **few cm**.	Tsunami height **≤1m.** No permanent effect in environment.
V	No effect on the environment. Anomalous waves **up to several tens of cm** high are perceived by all people on boats and on the coast	**Tsunami height** or tsunami flow depth **of several cm to dm (0.5 m).** Limited onshore areas inundated.	Tsunami height **≤1m.** No permanent effect in environment.
VI	Anomalous waves **up to many tens of cm** high floods very limited areas near shore.	**Tsunami height** or tsunami flow depth **of some dm (< 1 m).** Small onshore areas are flooded.	**Tsunami height** between **1–2m**. The maximum **run-up** can reach **2–4m**. Limited flooded areas. Absent or scarce erosion. No sedimentation. Some debris near shore.
VII	Anomalous waves **even higher than a meter** flood, limited nearshore areas and damage or wash away objects of variable size.	**Tsunami height** or tsunami flow depth usually **higher than 1 m**. Small onshore areas are flooded.	**Tsunami height** between **2–4m.** The maximum **run-up** reached **4—6m**. Flooded areas can extend tens of meters inland. Presence of sand layers in near-shore areas, commonly discontinuous.
VIII	Anomalous waves **up to 1-2 meters** high flood near-shore areas and may damage or wash away objects of variable size. Erosion and dumping of waste are observed along the beaches, where some bushes and even small weak-rooted trees can be eradicated and drifted away.	**Tsunami height** or tsunami flow depth **higher than 2 m.** Limited onshore areas are flooded. Limited inundation along coastline.	**Tsunami height** between **4–6m**. The maximum **run-up** can reach **8—12m**. Flooded areas can extend few hundreds of meters inland. Presence of largely distributed centimeters-thick sand layers, commonly discontinuous. Occurrence of pebbles and cobbles in near-shore areas. Observable features of beach erosion. Bushes uprooted in near-shore areas.
IX	Depending on the shape of the sea bottom and coastline, dangerous tsunamis may reach the shores with **run-ups of up to several meters** flooding wide areas. Widespread erosion and dumping of waste are observed along the beaches, where bushes and trees can be eradicated and drifted away.	**Tsunami height** or tsunami flow depth of a **few m (< 5).** Wide areas are inundated along the shoreline. **Tsunami run-up** or maximum tsunami water level of **some m,** whereas **maximum inundation** distance reaches **some hundred m**, depending on coastal morphology.	**Tsunami height** between **6—8m.** The maximum **run-up** reached **12–16m.** Flooded areas extended to several hundred meters inland. Presence of largely distributed cm-thick sand layers, commonly continuous over large areas. Occurrence of pebbles and cobbles in near-shore areas. Noticeable features of beach erosion with the development of several cm depth scours. Bushes and some trees uprooted in near-shore areas.
X	Depending on the shape of the sea bottom and coastline, tsunamis may reach the shores with **run-ups exceeding 5 m** flooding flat areas for thousands of meters inland. Small boulders can be dragged for many meters. Widespread deep erosion is observed along the shores, with noteworthy changes of the coastline profile. Trees near-shore are eradicated and drifted away	**Tsunami height** or tsunami flow depth of **many m (< 7). Tsunami run-up** or maximum tsunami water level reaches or **exceeds 10 m**, whereas maximum **inundation** distance reaches some **hundreds of m**, depending on coastal morphology.	**Tsunami height** between **8–12m.** The maximum **run-up** reached **16—25m.** Flooded areas may extend even 1km inland. Presence of largely distributed cm-thick sand layers, normally continuous over large areas. Pebbles and cobbles largely extended in near-shore areas. Metric boulders transported near shore. Significant features of beach erosion with the development of cm to dm depth scours. Bushes and trees wash away in near-shore areas. Noticeable forest erosion in the littoral.
XI	Depending on the shape of sea bottom and coastline, large tsunamis may reach the shores with **run-ups reaching 15 meters** and more	**Tsunami height** or tsunami flow depth of **many m (<10 m).** Tsunami **run-up** or maximum tsunami water level exceeds 15 m, whereas **maximum inundation**	**Tsunami height 12—24m.** The maximum **run-up** reached **25–40m.** Flooded areas extended more than 1 km inland. Widespread deposit of sand layers <30 cm thick even several hundred meters inland. Pebbles

	devastating flat areas for kilometers inland. Even meter-sized boulders can be dragged for long distances. Widespread deep erosion is observed along the shores, with noteworthy changes of the coastal morphology. Trees near shore are eradicated and drifted away.	distance exceeds **1 km**, depending on coastal morphology.	and cobbles largely extended in near shore areas. Tn boulders transported nearshore and inland over distances less than one hundred meters. Important features of beach erosion with the development of dm depth scours. Large erosion and significant morphological changes on beaches, dunes and rivermouths. Significant forest erosion in the littoral. The coastline can retreat several meters.
XII	Depending on the shape of the sea bottom and coastline, giant tsunamis may reach the shores with **run-ups of several tens of meters** devastating flat areas for many kilometers inland. Big boulders can be dragged for long distances. Widespread deep erosion is observed along the shores, with outstanding changes in coastal morphology. Many trees are eradicated and drifted away. All boats are torn from their moorings and swept away or carried onshore even for long distances. All people outdoor are swept away.	**Tsunami height** or tsunami flow depth exceeds **10 m. Run-up** or maximum tsunami water level reaches **many tens of** m and **maximum inundation** distance **some km**. Areas of some tens of km^2 are inundated	**Tsunami height >24m**. The maximum **run-up** reached **>40m**. Flooded areas extended to several kilometers inland. Sand layers to 30cm thick extended inland over distances of more than one kilometer. Pebbles and cobbles largely extended in near shore areas. Tn boulders dragged near-shore and inland over distances of even hundred meters. Outstanding features of beach erosion with the development of dm to m depth scours. Strong erosion and outstanding morphological changes on beaches, dunes and river-mouths. Erosional features can extent hundred meters inland. Strong forest erosion in the littoral. Coast-line can retreat several tens of meters.

1.4 GENERAL EEES CONVERSION TABLE

For Surface ruptures and Tectonic uplift and subsidence a quantitative classification was developed from Michetti et al., 2007 (app. 1.1). For Anomalous waves and tsunamis category, after a comparison between ESI-07, ITIS-2012 and TEE-16 Scale the classification followed the threshold proposed by the latter, based on Tsunami Heigh (m) and Run-Up (m) (see appendix 1.2). For Slope Movements category the classification by Ferrario M.F. (2022) was adopted (note: after ESI-07 X grade, saturation phenomenon is present).

	IV	V	VI	VII	VIII	IX	X	XI	XII
PRIMARY EFFECTS	absent	absent	absent	observed very rarely, almost exclusively in volcanic areas	observed rarely	observed commonly	become leading	dominant	dominant
Surface Ruptures	absent	absent	absent	dm – hm long cm offset. essentially associated with very shallow earthquakes	Hm - Up to several hm long few cm offset particularly for very shallow focus earthquakes, such as those common in volcanic areas	several hm - up to a few km in length several cm offset	Few km - Few tens of km length tens of cm - few meters offset. lower for very shallow focus earthquakes in volcanic areas gravity grabens and elongated depressions	Few tens of km - Several tens up to > 100 km several m slips gravity graben, elongated depressions and pressure ridges drainage lines can be seriously offset	At least few hundreds of km in length offsets > 10 m gravity graben, elongated depressions and pressure ridges drainage lines can be seriously offset.
Tectonic Uplift\Subsidence (cm)	absent	absent	absent	< 10 cm	few cm	few dm	few m	few m – numerous m	landscape and geomorphological changes. uplift or subsidence of coastlines > several m. appearance or disappearance from sight of significant landscape elements, rivers changing course, origination of waterfalls, formation or disappearance of lakes.
E.Muccignato 2025 The classification follows a progressive increase in uplift values, ensuring consistency with other ESI categories. Qualitative terms were converted into quantitative ranges based on orders of magnitude and proportional scaling.	Absent	Absent	Absent	<10 cm	10-30 cm	30-100 cm	100-300 cm	300-1000 cm	> 1000 cm

SECONDARY EFFECTS	IV	V	VI	VII	VIII	IX	X	XI	XII
Ground cracks	**hair-thin** cracks, mm wide in prone lithology or morphology	**mm** wide **several cm– 1 m** long in prone lithology or morphology	**Occasionally** **mm – cm** width **1-2 cm** width in steep slopes or riverbank **Several m** long in loose alluvial deposits\saturated soils **1-2 cm** wide along slopes or riverbanks **minor cracks** in paved roads	**Up to 5 – 10 cm** width **0 – 100** length observed commonly in loose alluvial deposits\saturated soil **0-1 cm** width in sandy – clay and clay soils **cm** width in paved roads	**Up to 50 cm in** width **100 - Up to hms** length observed commonly in loose alluvial deposits\saturated soil. **Rare cases of up to 1 cm** in competent dry rocks **dm** cracks in paved roads **small** pressure undulations	**Up to 100 cm** width **Up to hms** length, commonly observed in loose alluvial deposits\saturated soils. **Up to 10 cm** in competent dry rocks **significant** cracks in paved roads **small** pressure undulations	**> 1 m** width **Up to 100 m** long, mainly in loose alluvial deposits\saturated soils **Several dms** in competent rocks **wide** cracks in paved roads, with pressure undulations	**1 – up to several m** width, mainly in loose alluvial deposit\saturated soils **0 – 1 m** in competent rocks **very wide** cracks in paved roads, **large** pressure undulations	very frequent **> 10 m** width in loose alluvial deposits\saturated soils **Up to several km** length **> 1 m** width in bedrock **very wide** cracks develop in paved roads. **large** pressure undulations
E.Muccignato, 2025 Note: after ESI 10 saturation phenomenon	**-**	**0-1 m**	**1-10 m**	**10 -100 m**	**> 100 m**	**> 100 m** **Saturation**	**> 100 m** **Saturation**	**> 100 m** **Saturation**	**> 100 m** **Saturation**
Slope movements (m^3)	**exceptionally** Rocks may fall. **small** landslide (re)activated along slope where the equilibrium is already near the limit state	**rare small** rockfalls, rotational landslides and slump earth flows Along often but not necessary on slopes **underwater landslide**, which can induce small anomalous waves on costal area of seas\lakes	**Rockfall and landslides of v 10 - 10^3 m^3** where equilibrium is near the limit. **Underwater landslides**, which can induce small anomalous waves in coastal areas of seas and lakes, commonly seen by instrumental records	**scattered** landslides in prone area **modest** rock falls **10^3-10^5 m^3** common on steep gorges and cliffs. Sometimes their size is significant: **10^3-10^5 m^3**. **v of 100 m^3** in dry sand, sandy clay, and clay soil affection in riverbanks, excavations **ruptures, slides and falls** may affect riverbanks and artificial embankments and excavation in loose or weathered sediments\fractured rocks. **significant** underwater landslides, provoking anomalous waves in coastal areas of sea and lakes, directly felt by people on boats and ports.	**Small** to moderate landslides of **10^3-10^5 m^3** widespread in prone areas, rarely on gentle slopes Larger landslides of **10^5-10^6 m^3** in unstable areas and soils **occasionally** dam narrow valley, causing temporary or permanent lakes **ruptures, slides and falls** affect riverbanks, artificial embankments and excavations in loose sediment or weathered\fractured rocks. **Frequent** underwater landslides in coastal areas	**Widespread** large and very large landslides of **10^5-10^6 m^3** in prone areas, also on gentle slope landslides can **dam** narrow valleys: temporary or even permanent lakes. riverbanks, artificial embankments and excavations frequently **collapse.** **frequent large** landslides under the sea level.	**frequent** large landslides and rockfalls of **> 10^5 - 10^6 m^3** practically regardless of equilibrium state of slopes temporary or permanent **barrier lakes** **typical collapse** of riverbanks, artificial embankments, and sides of excavations levees and earth dams incur **serious damage.** **frequent large** landslides under the sea level in coastal areas.	**frequent** large landslides and rockfalls of **> 10^5 - 10^6 m^3** practically regardless of equilibrium state of slopes side of excavation typically collapse. temporary or permanent **barrier lakes** **collapse** of riverbanks, artificial embankments, and sides of excavations levees and earth dams incur **serious damage.** **frequent large** landslides under the sea level in coastal areas. **Significant** landslide can occur even at **200-300 km** distance from the epicenter. **Frequent large** landslides under sea level	**Frequent** large landslides and rockfalls of **> 10^5 - 10^6 m^3** practically regardless of equilibrium state of slopes temporary or permanent barrier lakes **collapse** of riverbanks, artificial embankments, and sides of excavations levees and earth dams incur **serious damage.** **frequent are very** large landslides under the sea level in coastal areas. **Significant** landslide can occur even at **200-300 km** distance from the epicenter. **Frequent very large** landslides under sea level
Ferrario M.F., (2022) Note: after ESI 10 saturation phenomenon			**<10^3**	**10^3-10^4**	**10^4-10^5**	**10^5-10^6**	**>10^6** **Saturation**	**>10^6** **Saturation**	**>10^6** **Saturation**
Liquefaction Processes	-	**extremely rare and small** (sand boils) in susceptible areas	**rare** and **small** (sand boils) in susceptible areas (highly susceptible, recent, alluvial and coastal deposits, near surface water table)	**Rare cases** of liquefaction, with sand boils **up to 50 cm** ø in prone areas	**frequent** in epicentral area. Typical effects: sand boils of up to **1 m** ø. apparent water fountains in still waters **0 – 30 cm subsidence** **localized lateral spreading** and settlements with **fissuring** parallel to waterfront areas (riverbanks, lakes, canals, seashores)	**liquefaction** and **water upsurge** are **frequent.** sand boils **up to 3 m** ø. apparent water fountains in still waters **> 30 cm subsidence** **frequent lateral spreading** and settlements. with **fissuring** parallel to waterfront areas	**liquefaction**, with **water upsurge** and **soil compaction**, may **change the aspect** of wide zones. **> 6 m** ø sand volcanoes **> 1m** vertical subsidence **common large and long** fissures due to lateral spreading	liquefaction **changes** the **aspect** of extensive zones of lowland. **> several ms** vertical subsidence **numerous large** sand volcanoes **severe** lateral spreading	liquefaction in **large areas changes** the aspect of extensive zones of lowland. **Liquefaction** over large areas and changing the morphology of extensive flat zones. **> several m** vertical subsidence **widespread** large sand volcanoes **extensive severe** lateral spreading
Anomalous waves and tsunamis	**seiches** of **0 – few cm** in closed basins (lakes, even seas) observed only by tidal gauges, exceptionally even by naked eye, typically in the far field of strong earthquakes. **Anomalous waves** perceived by all the people on small boats, few people on larger boats, most people on the coast.	**Dm** seiches in closed basins (lakes, even seas), sometimes noted also by naked eye, typically in the far field of strong earthquakes. **anomalous waves** of **several tens of cm,** perceived by all people on boats and on the coast.	**Anomalous waves up to many tens of cm high** flood very limited areas nearshore.	**Anomalous waves > 1 m high** may flood limited nearshore areas and damage\wash away object of variable size.	Anomalous waves up to **1-2 m** flood nearshore areas and may damage\wash away object of variable size.	**ms high** waves in still\running waters. **possible change** of course in streams in flood plains, also because of land subsidence Small basins may **appear** or be **emptied.** **dangerous** tsunamis **runups** of **up to several m** , flooding wide areas, depending on shape of sea bottom and coastline.	**meters high** waves in big lakes and rivers overflow from their beds. **change** of course **temporary** or **permanently** in streams in flood plains, for subsidence and landsliding. basins may **appear** or be **emptied.** dangerous tsunamis **2 - >5m**	**large waves** in big lakes and rivers, overflow **change** of course **temporary** or **permanently** in streams in flood plains, for subsidence and landsliding. basins may **appear** or be **emptied.** dangerous tsunamis of **5 – 15 m runups of several km** inland	**giant waves** in big lakes and rivers, overflow **change** of **course** and **flow direction temporary** or **permanently** in streams in flood plains, for subsidence and landsliding. Large basins may **appear** or be **emptied.** dangerous tsunamis **runups > 15 m, several km** inland

	water in swimming pools swings and may sometimes **overflow**.	**overflows** in pools	**overflows** in pools, small ponds and basins overflows	**overflows** from small basins and watercourses	**erosion** and **dumping** of waste observed along the beaches. **eradication and movement** of bushes and weak-rooted trees **violent overflows** from small basins and watercourses	**widespread erosion and dumping** of waste observed along the beaches. bushes and trees can be **eradicated** and **drifted** away	**runups** of up to **several hm** inland **Small boulders** can be dragged for long distance. **widespread deep erosion along shores**, **noteworthy changes** of the coastal profile. trees are **eradicated** and **drifted** away.	**0-1 m** size boulders can be dragged for long distance. **widespread deep erosion**, **changes** of the coastal morphology trees are **eradicated** and **drifted** away.	**Big boulders** can be dragged for long distance. **widespread deep erosion, outstanding** changes of coastal morphology **many** trees are **eradicated** and **drifted** away. boats and people outdoor **swept away or carried onshore** even for long distances, all people outdoor are swept away.
TEE-16 SCALE (Lario et al., 2016) TSUNAMI HEIGHT (m)	**≤1**	**≤1**	**1-2**	**2-4**	**4-6** **Note: for this class the calculation on QGSI is extended to the interval between 4 and 8 m**	**6-8**	**8-12**	**12-24**	**>24**
TEE-16 SCALE (Lario et al., 2016) RUN-UP (m)	**Absent**	**absent**	**2-4**	**4-6**	**8-12**	**12-16**	**16-25**	**25-40**	**>40**
Hydrogeological anomalies	**rare small** variations of the water level in wells\flow-rate of spring **extremely rare small variations** of chemical-physical properties turbidity in springs and wells, especially in karstic spring systems (most prone to this phenomenon	**rare** variations of the water level in wells\flow-rate of spring **small** variations of chemical-physical properties turbidity in lakes, springs and wells	**significant** variations of the water level in wells\ flow-rate of springs locally recorded **small** variations of chemical-physical properties turbidity in lakes, springs and wells	**significant temporary** variations of the water level in wells\flow-rate of springs locally recorded. Seldom, small springs may **temporarily run dry\appear.** **weak** variations of chemical-physical properties **turbidity** in lakes, springs and wells	**Spring** may change temporally, flow rate\elevation change. **some small springs** run dry. **variation in water level** observed in wells. **weak** variations of chemical-physical properties, most commonly temperature, in springs\wells **turbidity** in closed basins, rivers, wells and springs **gas emissions** (sulphureous) locally observed	**springs** can change, generally temporarily, their flow-rate\location to a considerable extent. **modest springs** may even run dry. **Temporary** variations of water level **are commonly observed** in wells. **variations** of chemical-physical: temperature, in springs\wells **Water turbidity** is **common** in closed basins, rivers, wells and springs. **gas emissions** (sulphureous) observed, **bushes and grass** near emission zones may **burn**	**many springs** significantly change their flow-rate and/or elevation of outcrop**, some springs** may run **temporarily** or even **permanently** dry. **Temporary** variations of water level **are commonly observed** in wells. **strong variations** of chemical-physical properties: temperature in springs\wells water becomes **very muddy** even in large basins, rivers, wells and springs. **gas emissions** (often sulphureous), **bushes and grass** near emission zones may **burn**	**many springs** significantly change their flow-rate and/or elevation of outcrop, **many springs** may run **temporarily** or even **permanently** dry. **Temporary** or **permanent** variations of water level are **generally observed** in wells. **Even strong variations** of chemical-physical properties of water: temperature, in springs\wells **Often** water becomes **very muddy** in even large basins, rivers, wells and springs. **gas emissions** (often sulphureous), **bushes and grass** near emission zones may **burn**	**many springs** significantly change their flow-rate and/or elevation of outcrop. **many springs** and wells may run **temporarily** or even **permanently** dry. **strong variations** of chemical-physical properties of water: temperature in springs\wells Water becomes **very muddy** in even large basins, rivers, wells and springs, **gas emissions** (often sulphureous), **bushes and grass** near emission zones may **burn**
Tree shaking	tree limbs shake **feebly**	Tree limbs and bushes shake **slightly.** very rare cases of fallen dead limbs and ripe fruit	Trees and bushes shake **moderately** to **strongly.** **very few** tree tops and unstable dead limbs may break and fall, depending on species, fruit load and state of health	Trees and bushes shake **vigorously,** especially in densely forested areas. **many** limbs and tops break and fall	Trees shake **vigorously.** **Branches may** break and fall. trees **uprooted** especially along **steep slopes**	Trees shake **vigorously.** branches and thin tree trunks **frequently break** and fall. **some** trees **might be uprooted and fall**, especially along **steep slopes**	Trees shake **vigorously.** **many** branches and tree trunks break and fall. **some** trees **may be uprooted and fall**	Trees shake **vigorously.** **many** branches and tree trunks break and fall. **many** trees are **uprooted and fall**	Trees shake **vigorously.** **many** branches and tree trunks break and fall. **many** trees are **uprooted and fall**
Dust clouds	**absent**	**absent**	**absent**	**absent**	In dry and in **epicentral** area	in **dry area may** arise from the ground	in **dry areas commonly** arise from the ground	in **dry areas** arise from the ground	in **dry areas** arise from the ground
Jumping stones	**absent**	**absent**	**absent**	**absent**	**Stones, small boulders** and **tree trunks** thrown in the air, leaving imprints in soft soil	**Small boulders and tree trunks may** throw in the air and **move away** from their site for **meters,** depending on slope angle and roundness. imprints in soft soil	boulders of **2-3 m** thrown in air and move away for **hms** down even gentle slope. imprints in soil	boulders of **3- several m** thrown in air and move away for long distance down even gentle slope. imprints in soil	**very big** boulders thrown in air and move away for long distance. imprints in soil
Total affected area (km2)				**10 km²**	**100 km²**	**1000 km²**	**5000 km²**	**10.000 km²**	**> 50.000 km²**

CHAPTER 2

2.1 ESI-07 EVENTS FINAL DATASET

Table with all ESI-07 events contained in the final dataset is presented.

id	Date	Epicentre	Country	Lat	Long	Mw	Kinematic	Depth	I0 Esi	Source	Total Eees	Output	Other Int	Imax Other Int	Affectedarea	Srl	Setting	References
1	300	Tobarra	Spain	38.35	-1.39	6.8	strike-slip		10	reconnaissance field survey + bibliography	4	earthquake ESI-07 intensity assignation			1.2	1.5	onshore	Silva et al., 2014
2	8810526	Gulf of Cadiz	Spain	36	-8	7.2			11	bibliography		earthquake ESI-07 intensity assignation	EMS	10.5	100000		coastal	Silva et al., 2014
3	13961218	Tavernes	Spain	39.05	0.13	6.5			10	bibliography	12	earthquake ESI-07 intensity assignation + EEEs characterization	MSK	9	1200		onshore	Giner-Robles et al., 2015
4	14310424	Sur Granada	Spain	37.08	-3.38	6.7			8	bibliography	2	earthquake ESI-07 intensity assignation	EMS	8.5	150	0	onshore	Silva et al., 2014
5	15040405	Carmona	Spain	37.23	-5.28	6.8			9	bibliography	3	ESI-07 intensity assignation + EEEs characterization	EMS	8.5	1300	0	onshore	Silva et al., 2009
6	15130416	Zakynthos	Greece	37.6	20.8	6.5			8.5	bibliography	2	earthquake ESI-07 intensity assignation	MM	8			coastal	Mavroulis et al. (2019)
7	15220922	Alhama de Almeria	Spain	36.58	-2.4	6.5			9	bibliography	11	earthquake ESI-07 intensity assignation	EMS	8.5	10000	0	coastal	Silva et al., 2014
8	15860710	Callao	Peru	-12.2	-77.67	8.1			11	bibliography	3	ESI-07 intensity assignation + EEEs characterization	MM	10			coastal	EEE catalogue
9	15910414	Zakynthos	Greece						6.5	bibliography	1	earthquake ESI-07 intensity assignation					coastal	Mavroulis et al. (2019)
10	16041124	Tacna	Peru	-17.97	-71.47	8			11	bibliography	1	ESI-07 intensity assignation + EEEs characterization	MM	10			coastal	EEE catalogue
11	16220505	Zakynthos	Greece	37.7	20.6	6			8	bibliography	2	earthquake ESI-07 intensity assignation	MM	7			coastal	Mavroulis et al. (2019)
12	16331105	Zakynthos	Greece	37.7	20.8	7			9	bibliography	4	earthquake ESI-07 intensity assignation	MM	9			coastal	Mavroulis et al. (2019)
13	16360930	Cephaloni a	Greece	38.1	20.3	7.2	Strike-slip		6.5	bibliography	3	earthquake ESI-07 intensity assignation	MM	9			coastal	Mavroulis et al. (2019)
14	16801009	Malaga	Spain	36.48	-4.36	6.8		50	9	bibliography	11	earthquake ESI-07 intensity assignation	EMS	8.5	1100	0	coastal	Silva et al., 2014
15	16871020	Canete	Peru	-13	-77.42	8.2			10	bibliography	2	ESI-07 intensity assignation + EEEs characterization	MM	10			coastal	EEE catalogue
16	16880605	Sannio	Italy	41.283	14.561	7.1	normal		10	bibliography	14	earthquake ESI-07 intensity assignation + EEEs characterization	MCS	11	1700	32	onshore	Serva et al., 2007
17	16930111	Avola	Italy	37.12	14.93	7.4	normal		10	bibliography	51	ESI-07 intensity assignation + EEEs characterization	EMS	10.5	6000		coastal	Pirrotta & Barbano, 2020
18	16940908	Irpinia-Basilicata	Italy	40.862	15.406	6.7	normal		10	bibliography	12	earthquake ESI-07 intensity assignation + EEEs characterization	MCS	10	6300	38	onshore	Serva et al., 2007
19	17030114	Umbria	Italy	42.708	13.071	6.8	normal		10	bibliography	5	ESI-07 intensity assignation + EEEs characterization	MCS	11	700	10	onshore	EEE catalogue
20	17030202	L'aquila	Italy	42.47	13.21	6.6	normal		10	bibliography	19	ESI-07 intensity assignation + EEEs characterization	MCS	10	1000	10	onshore	EEE catalogue
21	17390103	Yinchuan	China	38.8	106.46	8	normal		11	bibliography	4	earthquake ESI-07 intensity assignation	MCS	11	1500	88	onshore	EEE catalogue

22	17430220	Apulia	Italy	39.847	18.774	7.1	normal	30	11.5	bibliography	8	ESI-07 intensity assignation + EEEs characterization	MCS	10	30000		coastal	Nappi et al., 2016
23	17461029	Lima	Peru	-11.61	-77.56	8.4	reverse		11	bibliography	3	ESI-07 intensity assignation + EEEs characterization	MM	10			coastal	EEE catalogue
24	17480323	Estubeny	Spain	39.02	-0.38	6.2	normal		9	bibliography	21	earthquake ESI-07 intensity assignation + EEEs characterization	EMS	9	1000		onshore	Giner-Robles et al., 2015
25	17551101	Capo S. Vicente	Portugal	36.3	-10	8.5	reverse		11	bibliography	984	earthquake ESI-07 intensity assignation	EMS	11.5	147000		coastal	Silva et al., in press
26	17591221	Kattegat	Sweden	58.2	10.6	5.7			6	bibliography	7	EEEs characterization	EMS				coastal	Mäntyniemi et al., 2020
27	17830205	Calabria	Italy	38.297	15.97	7.1	normal		11	bibliography		EEEs characterization	MCS	11	3500	35	coastal	Blumetti et al., 2015 (In Audemard Ed.)
28	17911102	Zakynthos	Greece	37.9	21	6.8			8	bibliography	5	earthquake ESI-07 intensity assignation	MM	10			coastal	Mavroulis et al. (2019)
29	18040825	Dalias	Spain	35.46	-2.5	6.4	normal		9	bibliography	11	earthquake ESI-07 intensity assignation	EMS	8.5	1000	0.2	coastal	Silva et al., 2014
30	18050726	Bojano	Italy	41.5	14.474	6.7	normal	10	10	bibliography	50	earthquake ESI-07 intensity assignation + EEEs characterization	MCS	10	5300	40	onshore	Porfido et al., 2007; Serva et al., 2007
31	18090602	Zakynthos	Greece						8	bibliography	2	earthquake ESI-07 intensity assignation					coastal	Mavroulis et al. (2019)
32	18190616	Allah Bund	India	24	69.8	7.6	reverse		11	bibliography		ESI-07 intensity assignation + EEEs characterization	MM	9.5		90	onshore	Naik et al., 2020
33	18190831	Lurøy	Norway	66.25	12.51	5.9			7.5	bibliography	5	EEEs characterization	EMS	8			coastal	Mäntyniemi et al., 2020
34	18201229	Zakynthos	Greece	37.8	21.1	6.9			8	bibliography	4	earthquake ESI-07 intensity assignation	MM	9			coastal	Mavroulis et al. (2019)
35	18280223	Brabant Massif	Belgium	50.7	5.12	5.1		10	7	bibliography	185	earthquake ESI-07 intensity assignation	EMS	7	40	0	onshore	Camelbeeck et al., 2021
36	18290321	Torrevieja	Spain	38.05	-0.41	6.6			10	bibliography	47	earthquake ESI-07 intensity assignation	EMS	9.5	474		coastal	Silva et al., 2014
37	18370803	Zakynthos	Greece						6	bibliography	1	earthquake ESI-07 intensity assignation					coastal	Mavroulis et al. (2019)
38	18401030	Zakynthos	Greece	37.8	20.8	6.5			8	bibliography	17	earthquake ESI-07 intensity assignation	MM	9			coastal	Mavroulis et al. (2019)
39	18571216	Basilicata	Italy	40.35	15.84	7.1	normal		10	bibliography	97	ESI-07 intensity assignation + EEEs characterization	MCS	11	13200	45	onshore	EEE catalogue
40	18630610	Huércal-Overa	Spain	37.22	-1.56	4.2	reverse		8	bibliography	23	ESI-07 intensity assignation + EEEs characterization + isoseismals	EMS	6.5	98		onshore	Silva et al., 2020
41	18670204	Cephalonia	Greece	38.39	20.52	7.2	strike-slip		8	bibliography		earthquake ESI-07 intensity assignation	MM	10			coastal	Papathanassiou et al., 2017
42	18680813	Tacna	Peru	-18.43	-70.36	8.9	reverse		11	bibliography	2	ESI-07 intensity assignation + EEEs characterization	MM	10			coastal	EEE catalogue
43	18841225	Arenas del Rey	Spain	37	-3.59	6.5	normal		10	bibliography	137	earthquake ESI-07 intensity assignation	EMS	9.5	14000	16	onshore	Silva et al., 2014
44	18850530	Baramulla	Kashmir	34.12	74.61	6.3	reverse	12	10	bibliography	12	earthquake ESI-07 intensity assignation	MCS	12	5000	54	onshore	Ahmad et al., 2014
45	18870609	Verny	Central Asia	43.163	76.534	7.3	reverse	20	9.5	bibliography		earthquake ESI-07 intensity assignation	MSK	9	2000		onshore	Tatevossian, 2007
46	18930119	Zakynthos	Greece	37.68	20.81				8.5	bibliography	5	earthquake ESI-07 intensity assignation					coastal	Mavroulis et al. (2019)
47	18930405	Zakynthos	Greece	37.68	20.81	6.5			6.5	bibliography	4	earthquake ESI-07 intensity assignation	MM	9			coastal	Mavroulis et al. (2019)
48	18940427	Atalanti	Greece	38.65	23.08	6.8	normal	10	10	bibliography		ESI-07 intensity assignation + EEEs characterization + isoseismals	EMS	10	2500	25	coastal	Papanikolaou and Melaki, 2017
49	18961105	Zakynthos	Greece						6.5	bibliography	1	earthquake ESI-07 intensity assignation					coastal	Mavroulis et al. (2019)
50	18981203	Zakynthos	Greece	37.42	20.48				5.5	bibliography	1	earthquake ESI-07 intensity assignation					coastal	Mavroulis et al. (2019)
51	18990122	Zakynthos	Greece	37.2	21.6	6.5			5.5	bibliography	1	earthquake ESI-07 intensity assignation					coastal	Mavroulis et al. (2019)

52	19001029	San Narciso	Venezuela			7.6			9	bibliography	46	earthquake ESI-07 intensity assignation + map of EEEs + isoseismals	MM	9	30000		coastal	Colón et al. (2019)
53	19041023	Oslofjord	Norway	58.69	10.86	5.7			7	bibliography	14	EEEs characterization	EMS	7			coastal	Mäntyniemi et al., 2020
54	19050908	Calabria	Italy	38.811	16	7	normal	15	10	bibliography		earthquake ESI-07 intensity assignation + EEEs characterization	MCS	10.5	15000		coastal	Porfido et al., 2007
55	19060110	Dobrà Voda	Slovakia	48.58	17.46	5.8	strike-slip	5	9	bibliography	9	earthquake ESI-07 intensity assignation + EEEs characterization	EMS	8.5	250		onshore	Nasir et al., 2020
56	19060116	Dobrà Voda	Slovakia	48.62	17.56	5.5	strike-slip		8	bibliography	9	earthquake ESI-07 intensity assignation + EEEs characterization	EMS	7.5	80		onshore	Nasir et al., 2020
57	19081228	Messina	Italy	38.146	15.687	7.1	normal	9	11	bibliography	365	earthquake ESI-07 intensity assignation + EEEs characterization	MCS	11	24000		coastal	Comerci et al. 2015
58	19110403	Lorqui	Spain	38.06	-1.12	5.7			8	bibliography	3	earthquake ESI-07 intensity assignation	EMS	8	100	0	onshore	Silva et al., 2014
59	19110531	Santa Fe	Spain	37.12	-3.42	5.3		15	8	bibliography	3	earthquake ESI-07 intensity assignation	EMS	7.5	98	0	onshore	Silva et al., 2014
60	19120124	Cephalonia	Greece	38.11	20.67	6.8	Strike-slip		6	bibliography	1	earthquake ESI-07 intensity assignation	MM	10			coastal	Mavroulis et al. (2019)
61	19121119	Acambay	Mexico	19.493	-99.552	6.9	normal	80	10	bibliography	46	ESI-07 intensity assignation + EEEs characterization + isoseismals	MCS	10	750	33	onshore	Rodríguez-Pascua et al., 2017
62	19150113	Fucino	Italy	42.014	13.53	7.1	normal		10	bibliography	18	ESI-07 intensity assignation + EEEs characterization	MCS	11		24	onshore	EEE catalogue
63	19190629	Mugello	Italy	43.96	11.48	6.4			9	bibliography	39	ESI-07 intensity assignation + EEEs characterization	MCS	10	900		onshore	EEE catalogue
64	19190910	Jacarilla	Spain	38.05	-0.5	5.5			8	bibliography	6	earthquake ESI-07 intensity assignation	EMS	7.5	130	0	onshore	Silva et al., 2014
65	19300723	Irpinia	Italy	41.068	15.318	6.7	normal		10	bibliography	61	earthquake ESI-07 intensity assignation + EEEs characterization	MCS	10	3900	38	onshore	Porfido et al., 2007; Serva et al., 2007
66	19330423	Aegean Sea	Greece	36.8	27.3	6.5	normal	15	8.5	bibliography		earthquake ESI-07 intensity assignation	MM	9.5		0	coastal	Triantafyllou et al., 2020
67	19350421	Hsinshu-Taiching	Taiwan	24.18	120.45	7	reverse	3	11	bibliography		ESI-07 Scale map	CWB	6		16	onshore	Ota et al., 2009
68	19400524	Cajatambo	Peru	-10.51	-76.95	8.4	reverse		9	bibliography	2	ESI-07 intensity assignation + EEEs characterization	MM	10			onshore	EEE catalogue
69	19420824	Nazca	Peru	-14.98	-75.95	8.4	reverse		9	bibliography	2	ESI-07 intensity assignation + EEEs characterization	MM	10			coastal	EEE catalogue
70	19461110	Pallasca	Peru	-8.3	-77.81	7.3	normal		10	bibliography	3	ESI-07 intensity assignation + EEEs characterization	MM	11			onshore	EEE catalogue
71	19500521	Cuzco	Peru	-13.98	-71.98	6.1			7	bibliography	2	ESI-07 intensity assignation + EEEs characterization	MM	7			onshore	EEE catalogue
72	19530812	Ionian Sea	Greece	38.1	20.8	7	strike-slip		9	bibliography	120	ESI-07 intensity assignation + EEEs characterization	MM	9.5			coastal	Mavroulis & Lekkas, 2021
73	19540430	Sofades	Greece	39.3	22.2	6.8	normal	10	9.5	bibliography	10	ESI-07 intensity assignation + EEEs characterization + isoseismals	MM	9		25	onshore	Papathanassiou et al., 2007
74	19560419	Albolote	Spain	37.15	-3.39	5.4	normal		8	bibliography	6	earthquake ESI-07 intensity assignation	EMS	8	44	0	onshore	Silva et al., 2014
75	19570627	Muya	Russia	56.18	116.41	7.6	strike-slip	20	10	bibliography	135	earthquake ESI-07 intensity assignation + EEEs characterization + isoseismals	MSK	8		20	onshore	Tatevossian et al., 2010
76	19591115	Zakynthos	Greece	37.78	20.53	6.8			6.5	bibliography	3	earthquake ESI-07 intensity assignation	MM	7			coastal	Mavroulis et al. (2019)
77	19640327	Alaska	United States	61.2	-147.27	9.2	reverse	25	12	bibliography	95	ESI-07 intensity assignation + EEEs characterization	MM	11	1300000		coastal	EEE catalogue
78	19640706	Galera	Spain	37.44	-2.34	5.1		5	7	bibliography	5	earthquake ESI-07 intensity assignation	EMS	7	34	0	onshore	Silva et al., 2014
79	19661017	Yangas	Peru	-10.72	-78.63	7.5	reverse		8	bibliography	3	ESI-07 intensity assignation + EEEs characterization	MM	9			coastal	EEE catalogue
80	19680619	Moyobamba	Peru	-5.55	-77.17	7	reverse		9	bibliography	5	ESI-07 intensity assignation + EEEs characterization	MM	9			onshore	EEE catalogue
81	19681014	Meckering	Australia	-31.62	116.98	6.6	reverse	2	10	bibliography		earthquake ESI-07 intensity assignation			580	40	onshore	King et al., 2019

82	19690724	Pariahuanca	Peru	-11.78	-75.08	5.8	strike-slip		10	bibliography	1	ESI-07 intensity assignation + EEEs characterization	MM	11		5.5	onshore	EEE catalogue
83	19700310	Calingiri	Australia	-31.11	116.47	5	reverse	1	9	bibliography		earthquake ESI-07 intensity assignation			3	3.3	onshore	King et al., 2019
84	19700926	Bahai Solano	Colombia	5.531	-77.214	6.6	reverse	10	8	ne		earthquake ESI-07 intensity assignation					coastal	Là linde and Sanchez, 2007
85	19760204	Los Amatese	Guatemala	15.32	-89.1	7.5	strike-slip	5	11	bibliography	24	earthquake ESI-07 intensity assignation + map of EEEs + isoseismals	MM	9	18000	230	onshore	Caccavale et al., 2019; Porfido et al 2015
86	19780620	Thessaloniki	Greece	40.8	23.28	6.5	normal	8	9	bibliography		ESI-07 intensity assignation + EEEs characterization + isoseismals	MM	8.5		12	coastal	Papanikolaou & Melaki, 2017
87	19790602	Cadoux	Australia	-30.83	117.18	6.1	reverse	5	9	bibliography		earthquake ESI-07 intensity assignation			55	20	onshore	King et al., 2019
88	19791212	Tumaco	Colombia	1.6	-79.36	8.1	reverse	24	11	bibliography	46	earthquake ESI-07 intensity assignation + map of EEEs + isoseismals	MM	10	18000		coastal	Lalinde and Sanchez, 2007; Tovar & Sanchez, 2020
89	19801123	Irpinia	Italy	40.842	15.283	6.8	normal	12	10	bibliography	564	earthquake ESI-07 intensity assignation + EEEs characterization	MCS	10	7400	45	onshore	Porfido et al., 2007; Serva et al., 2007
90	19810224	Alkyonides	Greece	38.222	22.934	6.7	normal	33	10	bibliography		earthquake ESI-07 intensity assignation + isoseismals	MS	9.5		10	coastal	Papanikolaou et al., 2009
91	19830117	Cephalonia	Greece	38.1	20.2	7	Strike-slip		6	bibliography	1	earthquake ESI-07 intensity assignation	MM	6			coastal	Mavroulis et al. (2019)
92	19830331	Popayan	Colombia	2.461	-76.686	5.6	strike-slip	22	8	na		earthquake ESI-07 intensity assignation	MSK	9		1.3	onshore	Lalinde and Sanchez, 2007
93	19860330	Marryat Creek	Australia	-26.18	132.07	5.7	reverse	2	10	bibliography		earthquake ESI-07 intensity assignation			20	13	onshore	King et al., 2019
94	19860913	Kalamata	Greece	37.039	22.112	6.1	normal	10	9	bibliography		earthquake ESI-07 intensity assignation + EEEs characterization	EMS	9	200	0	coastal	Fountoulis and Mavroulis, 2013
95	19880122	Tennant Creek	Australia	-19.84	133.99	6.6	reverse	5	10	bibliography		earthquake ESI-07 intensity assignation			160	16	onshore	King et al., 2019
96	19881016	Elia	Greece	37.92	20.99	6	normal	21	8	bibliography		earthquake ESI-07 intensity assignation + EEEs characterization	MM	8			coastal	Fokaefs and Papadopoulos, 2007
97	19920819	Suusamyr	Kyrgyzstan	42.142	53.575	7.3	reverse	14	10.5	bibliography	24	earthquake ESI-07 intensity assignation + map of EEEs + isoseismals	MM	10	2520	12	onshore	Grützner et al., 2019
98	19921018	Murindo	Colombia	7.0795	-76.862	7.2	strike-slip	10	11	bibliography	132	earthquake ESI-07 intensity assignation + isoseismals	MM	10	50000	75	onshore	Mosquera-Machado et al., 2009; Lalinde et al., 2007
99	19930326	Pyrgos	Greece	37.4	21.26	5.7	normal	15	7.5	bibliography	61	ESI-07 intensity assignation + EEEs characterization + isoseismals	EMS	8	145	0	coastal	Papanikolaou et al., 2009
100	19930721	Puerto Rondon	Colombia	6.47	-71.21	6	strike-slip	20.3	8	na		earthquake ESI-07 intensity assignation	MM	8			onshore	Lalinde and Sanchez, 2007
101	19940606	Paez	Colombia	2.917	-76.057	6.8	strike-slip	12	9	na		earthquake ESI-07 intensity assignation	MM				onshore	Lalinde and Sanchez, 2007
102	19950117	Kobe	Japan	34.214	135.015	6.9	strike-slip	16	10	bibliography		ESI-07 Scale map	JMA	7	600	24	coastal	Ota et al., 2009
103	19950513	Kozani-Grevena	Greece	40.13	21.67	6.5	normal	10	9	bibliography + remote sensing data		ESI-07 intensity assignation + EEEs characterization + isoseismals	MM	9.5	900	15	onshore	Papanikolaou and Melaki, 2017
104	19950527	Neftegorsk	Russia	52.63	142.83	7.4	strike-slip	11	10.5	bibliography		earthquake ESI-07 intensity assignation	EMS	8.5		46	onshore	Tatevossian et al., 2009
105	19970510	Ardekul-Ghaen	Iran	33.82	59.81	7.3	strike-slip	10	11	bibliography	19	earthquake ESI-07 intensity assignation	EMS	11		125	onshore	Amini et al., 2018
106	19970926	Colfiorito	Italy	43.014	12.853	6	normal	10	9	bibliography	109	earthquake ESI-07 intensity assignation + map of EEEs + isoseismals	MCS	9	800	12	onshore	Guerrieri et al., 2009
107	19980412	Julian Alps	Slovenia	46.194	13.407	5.6	strike-slip	8	7.5	bibliography	78	earthquake ESI-07 intensity assignation + map of EEEs + isoseismals	EMS	7.5	180	0	onshore	Gosar, 2012
108	19990125	Armenia	Colombia	4.44	-75.7	6.1	strike-slip	15	10	bibliography	123	earthquake ESI-07 intensity assignation + map of EEEs + isoseismals	MM	10	3000		coastal	Tovar & Sanchez, 2020

109	19990202	Murcia	Spain	38.19	-1.4	5	reverse		7	bibliography	3	ESI-07 intensity assignation + EEEs characterization	EMS	7	87	0	onshore	EEE catalogue
110	19990907	Athens	Greece	38.08	23.58	6	normal	17	8.5	bibliography		earthquake ESI-07 intensity assignation	MM	9		0.1	onshore	Fokaefs and Papadopoulos, 2007
111	19990921	Chichi	Taiwan	23.461	120.585	7.6	reverse	8	11	bibliography		ESI-07 Scale map	CWB	7	2650	100	onshore	Ota et al., 2009
112	20010126	Bhuj	India	23.4	70.28	7.7	reverse	25	11	reconnaissance field survey + bibliography	125	ESI-07 intensity assignation + EEEs characterization	MM	9.5	15000	1	onshore	Naik et al., 2020
113	20020806	Bullas	Spain	37.53	-1.51	5	strike-slip	1	6	bibliography	4	earthquake ESI-07 intensity assignation	EMS	6	5	0	onshore	Silva et al., 2014
114	20021103	Denali	United States	63.52	-147.57	7.9	strike-slip	12	12	bibliography	31	earthquake ESI-07 intensity assignation + map of EEEs + isoseismals	MM	11	40000	340	onshore	Comerci et al. 2015b
115	20030521	Boumerdes	Algeria	36.91	3.71	6.8	reverse	10	10	reconnaissance field survey + bibliography	10	Isoseismals	EMS	10	4500		coastal	Heddar et al., 2016
116	20030814	Lefkada	Greece	38.79	20.56	6.2	strike-slip	12	8.5	bibliography		earthquake ESI-07 intensity assignation + isoseismals	EMS	8		0	coastal	Papathanassiou and Pavlides, 2007
117	20030927	Altai	Russia	49.99	87.79	7.4	strike-slip	12	10	bibliography		earthquake ESI-07 intensity assignation	EMS	8	3000	70	onshore	Tatevossian et al., 2009
118	20041023	Chuetsu	Japan	37.32	138.264	6.6	reverse	13	9	bibliography		ESI-07 Scale map	JMA	7	900	1	onshore	Ota et al., 2009
119	20041226	Banda Aceh	Indonesia	3.4	95.48	9.1	reverse	30	12	bibliography	112	ESI-07 intensity assignation + EEEs characterization	MM	12			coastal	EEE catalogue
120	20050129	La Paca	Spain	37.51	-1.45	4.8	strike-slip	11	7	bibliography	6	earthquake ESI-07 intensity assignation	EMS	7	30	0	onshore	Silva et al., 2014
121	20051008	Muzaffarabad	Kashmir	34.42	73.52	7.6	reverse	13	11	bibliography		earthquake ESI-07 intensity assignation	MM	11	9400	112	onshore	Ali et al., 2009
122	20060108	Kythira	Greece	36.26	23.46	6.7	reverse	70	7.5	bibliography		ESI-07 intensity assignation + EEEs characterization + isoseismals	MM	7	15	0	coastal	Papanikolaou et al., 2009
123	20071010	Katanning	Australia	-33.95	117.51	4.7	reverse	1	8	bibliography		earthquake ESI-07 intensity assignation			0.2	0.5	onshore	King et al., 2019
124	20080512	Wenchuan	China	30.993	103.391	7.9	reverse	14	12	reconnaissance field survey		ESI-07 Intensity map	EMS	12	50000	220	onshore	Lekkas, 2010
125	20080608	Andravida	Greece	37.54	21.16	6.4	strike-slip	18	8.5	reconnaissance field survey	29	earthquake ESI-07 intensity assignation + map of EEEs + isoseismals	EMS	9	800	0	coastal	Mavroulis et al., 2013
126	20080827	South Baikal	Russia	51.716	103.666	6.3	strike-slip	24	7.5	reconnaissance field survey + bibliography	13	earthquake ESI-07 intensity assignation	MSK	7.5			onshore	Berzhinskii et al., 2010
127	20090406	L'Aquila	Italy	42.309	13.51	6.3	normal	8	9	bibliography	192	earthquake ESI-07 intensity assignation + EEEs characterization	MCS	9	2100	3	onshore	Huayong et al., 2019
128	20100227	Maule	Chile	-36.14	-76.3	8.8	reverse	23	11	na		earthquake ESI-07 intensity assignation	MSK	8	50000		coastal	EEE catalogue
129	20100903	Canterbury	New Zealand	-43.55	172.18	7.1	strike-slip	10	11	bibliography		ESI-07 intensity assignation + EEEs characterization + isoseismals	MM	8.5	1000	29	onshore	Sanchez and Maldonado, 2016
130	20110221	Christchurch	New Zealand	-43.49	172.71	6.3	strike-slip	5	10	bibliography		earthquake ESI-07 intensity assignation	EMS	10		0	coastal	Carydis et al., 2012; Quigey et al., 2016
131	20110311	Tohoku	Japan	38.32	142.37	9	reverse	20	12	bibliography		ESI-07 intensity assignation + EEEs characterization + isoseismals	JMA	7	85000		coastal	Sanchez and Maldonado, 2016
132	20110511	Lorca	Spain	37.43	-1.42	5.2	strike-slip	2	8	bibliography	72	ESI-07 intensity assignation + EEEs characterization	EMS	7	135	0	onshore	Silva et al., 2013
133	20111227	Tuva	Russia	51.83	95.96	6.6	strike-slip	17	9	reconnaissance field survey		ESI-07 Shock intensity map	MSK	7.5		3	onshore	Ovsyuchenko et al., 2017

134	20120220	Tuva	Russia	51.7	96	6.7	reverse	14	9	reconnaissance field survey		ESI-07 Shock intensity map	MSK	7	900	4	onshore	Ovsyuchenko et al., 2017
135	20120323	Pukatja	Australia	-26.12	132.12	5.2	reverse	2	9	bibliography		earthquake ESI-07 intensity assignation			1	1.3	onshore	King et al., 2019
136	20120520	Finale Emilia	Italy	44.895	11.263	6.1	reverse	9.5	8	reconnaissance field survey	45	earthquake ESI-07 intensity assignation + map of EEEs + isoseismals	MCS	7	350	0	onshore	Di Manna et al., 2012
137	20130420	Lushan	China	30.27	103.02	6.6	reverse	18	10	remote sensing data	25	earthquake ESI-07 intensity assignation	chinese	9	5200	0	onshore	Huayong et al., 2019
138	20131229	Matese	Italy	41.395	14.434	5.2	normal	20	7.5	reconnaissance field survey + bibliography		ESI-07 intensity assignation + EEEs characterization	MCS	7	90	0	onshore	Valente et al., 2017
139	20140203	Cephalonia	Greece	38.155	20.33	6	strike-slip	5	8	bibliography + remote sensing data	20	earthquake ESI-07 intensity assignation	EMS	8.5		0	coastal	Lekkas and Mavroulis, 2015; Papathanassiou et al., 2017
140	20151117	Lefkada	Greece	38.665	20.6	6.4	strike-slip	11	8	bibliography	128	ESI-07 intensity assignation + EEEs characterization + isoseismals	EMS	8	100	0	coastal	Papathanassiou et al., 2017
141	20160416	Pedernales	Ecuador	0.371	-79.94	7.8	reverse	21	9	reconnaissance field survey + bibliography		earthquake ESI-07 intensity assignation + map of EEEs + isoseismals	EMS	9	18000		coastal	Chunga et al., 2018
142	20160520	Peterman	Australia	-25.04	130.493	6.1	reverse	10	10	reconnaissance field survey	1000	earthquake ESI-07 intensity assignation + map of EEEs + isoseismals			300	21	onshore	King et al., 2018
143	20160824	Amatrice	Italy	42.698	13.233	6.2	normal	8	9	bibliography	3966	earthquake ESI-07 intensity assignation + EEEs characterization	EMS	10	2700	4.5	onshore	Huayong et al., 2019
144	20161030	Norcia	Italy	42.83	13.109	6.6	normal	10	10	bibliography	298	earthquake ESI-07 intensity assignation + EEEs characterization	EMS	11	3900	28	onshore	Huayong et al., 2019
145	20170720	Aegean Sea	Greece	36.97	27.42	6.5	normal	10	10	reconnaissance field survey	48	earthquake ESI-07 intensity assignation	EMS	7.5		0	coastal	Triantafyllou et al., 2020
146	20170808	Jiuzhaigou	China	33.2	103.88	6.3	reverse	9	9	remote sensing data		earthquake ESI-07 intensity assignation	chinese	9	1000	0	onshore	Huayong et al., 2019
147	20170821	Casamicciola Terme	Italy	40.738	13.897	3.9	normal	1.5	7	bibliography	47	earthquake ESI-07 intensity assignation + map of EEEs + isoseismals	EMS	8	2	2	onshore	Nappi et al., 2021
148	20170908	Gulf of Tehuantepec	Mexico	15.76	-94.11	8.2	normal	46	10	reconnaissance field survey + bibliography	256	earthquake ESI-07 intensity assignation + EEEs characterization + isoseismals	DYFI	9	200000		coastal	Velázquez-Bucio et al., 2022
149	20171115	Pohang	South Korea	36.065	129.269	5.4	reverse	5	8	reconnaissance field survey + bibliography		ESI-07 intensity assignation + EEEs characterization	KMA	8	200	0	onshore	Naik et al., 2020
150	20180225	Porgera	Papua New Guinea	-6.07	142.75	7.5	reverse	25	11	bibliography	2941	earthquake ESI-07 intensity assignation + EEEs characterization + grid analysis	DYFI	9		40	onshore	Sridharan et al., in prep
151	20180805	Lombok	Indonesia	-8.26	116.44	6.9	reverse	34	10	remote sensing data	7	earthquake ESI-07 intensity assignation	DYFI	8	1800		coastal	Ferrario, 2019
152	20180819	Lombok	Indonesia	-8.32	116.63	6.9	reverse	21	10	remote sensing data		earthquake ESI-07 intensity assignation	DYFI	7	1800		coastal	Ferrario, 2019
153	20181026	Zakynthos	Greece	37.52	20.55	6.8	Strike-slip	14	6.5	bibliography	428	earthquake ESI-07 intensity assignation					coastal	Mavroulis et al. (2019)
154	20181108	Lake Muir	Australia	-34.42	116.79	5.3	reverse	1	9	bibliography	400	earthquake ESI-07 intensity assignation				3	onshore	King et al., 2019
155	20191126	Durres	Albania	41.51	19.52	6.4	reverse	22	8.5	reconnaissance field survey	18	earthquake ESI-07 intensity assignation + EEEs characterization	EMS	9	800	0	coastal	Vittori et al., 2021

156	20200623	La Crucecita	Mexico	15.778	-96.12	7.4	reverse	23	10	reconnaissance field survey + bibliography	125	earthquake ESI-07 intensity assignation + EEEs characterization + isoseismals	DYFI	8	14000		coastal	Velázquez-Bucio et al., 2022
157	20201030	Samos	Greece	37.84	26.83	7	normal	19	9	reconnaissance field survey + remote sensing data	59	earthquake ESI-07 intensity assignation + EEEs characterization					coastal	Mavroulis et al., 2021
158	20180928	Sulawesi	Indonesia	-0.256	119.846	7.5	strike-slip	20	10-11	reconnaissance field survey + remote sensing data	7413	earthquake ESI-07 intensity assignation + ESI shakemaps	MM	11	3700	177	coastal	Naik et al., 2023
159	19960101	Sulawesi	Indonesia	0.83	120.01	7.7	reverse		8	bibliography	16	earthquake ESI-07 intensity assignation	MM	11			coastal	Naik et al., 2023
160	20181226	Etna, Sicily	Italy	37.63	15.1	4.9	strike-slip	0.3	10	reconnaissance field survey	4823	earthquake ESI-07 intensity assignation	EMS	8		5	onshore	Bella et al., 2019
161	20201229	Petrinja	Croatia	45.42	16.26	6.4	strike-slip	7.8	9	reconnaissance field survey + remote sensing data	770	EEEs characterization	EMS	8	600	13	onshore	Baize et al., 2022; Bjelotomic Oršulic et al., 2021
162	20210303	Thessaly	Greece	39.76	22.22	6.3			8-9	reconnaissance field survey		earthquake ESI-07 intensity assignation + EEEs characterization				0	onshore	Papathanassiou et al., 2022
163	20150604	Sabah	Malaysia	5.987	116.541	6	normal	10	9	remote sensing data	5198	ESI-07 intensity assignation + EEEs characterization	CDI	6.6	810	0	onshore	Ferrario, 2022
164	9580223	Ray-Taleghan/ Ruyan	Iran			7.7			11	reconnaissance field survey	1	earthquake ESI-07 intensity assignation + EEEs characterization	EMS	11	7850		onshore	Torabi et al., 2020
165	20211012	Sitia	Greece	35.07	26.47	6.3	normal - strike-slip	8.2	7-8	reconnaissance field survey + bibliography	1156	earthquake ESI-07 intensity assignation + isoseismals	MM	7			coastal	Dretaki et al., 2022
166	-426	Malian Gulf	Greece			6.9-7.5			9-10	bibliography	19	ESI-07 intensity assignation + EEEs characterization	MSK	11			coastal	Freitag K. and Reicherter K., 2019
167	20180206	Hualien	Taiwan	24.13	121.66	6.4	strike-slip	6.3	9	bibliography	9319	earthquake ESI-07 intensity assignation + EEEs characterization + ESI shake maps	CWB	7	100	15	coastal	Naik et al., 2022
168	19521022	Hualien	Taiwan	23.88	121.73	6.6	strike-slip		10	bibliography		earthquake ESI-07 intensity assignation	MM	7		10	coastal	Naik et al., 2022
169	20170720	Gökova Bay, SE Aegean Sea	Aegean Sea	36.962	27.405	6,6	normal	10	8	reconnaissance field survey + bibliography		EEEs characterization					coastal	Papathanassiou et al., 2019
170	19780916	Tabas-e-Golshan	Iran	33.49	56.94	7.1	reverse		9	bibliography		earthquake ESI-07 intensity assignation	EMS	9	100	100	onshore	Amini H., 2023
171	20210922	Woods Point, Victoria	Australia	-37.506	146.402	5.9	strike-slip	7	12.7	reconnaissance field survey	171	ESI-07 intensity assignation + EEEs characterization			88	5.69	onshore	La Greca et al., 2024
172	20210112	Khubsugul	Mongolia	51.281	100.438	6.9	strike-slip	8	8	bibliography		ESI-07 intensity assignation + EEEs characterization + isoseismals					onshore	Ovsyuchenkoa et al., 2023
173	20210118	San Juan	Argentina	-31.833	-68.799	6.5	strike-slip	20.8	8	reconnaissance field survey		ESI-07 intensity assignation + EEEs characterization + isoseismals	MMI	7	90		onshore	Palacios et al., 2024
174	20220919	Michoacán	Mexico	18.49	-102.89	7.6	reverse	16	10	reconnaissance field survey + bibliography + remote sensing data	8070	ESI-07 intensity assignation + EEEs characterization + isoseismals + Attenuation maps			450000		onshore	Velázquez-Bucio et al., 2024

175	20220905	Luding	China	29.59	102.08	6.6	strike-slip	16		remote sensing data	6233	ESI-07 intensity map			3545		onshore	Yang et al., (2023)
176	19760204	Guatemala	Guatemala	15.324	-89.101	7.5	strike-slip	5		remote sensing data	6224	ESI-07 intensity assignation + EEEs characterization + grid map			4687			Harp et al. (1981)
177	19800525	Mammoth Lakes	United States	37.696	-118.750	5.9	NDC	6		remote sensing data	4027	ESI-07 intensity assignation + EEEs characterization + grid map			2030			Harp et al. (1984)
178	19830502	Coalinga	United States	36.232	-120.312	6.5	reverse	9.6		remote sensing data	2980	ESI-07 intensity assignation + EEEs characterization + grid map			1547			Harp & Keefer (1990)
179	19910422	Valle de la Estrella	Costa Rica	9.685	-83.073	7.6	reverse	10		remote sensing data	1643	ESI-07 intensity assignation + EEEs characterization + grid map			1678			Marc et al. (2016)
180	19940117	Northridge	United States	34.213	-118.537	6.7	reverse	18.2		remote sensing data	11111	ESI-07 intensity assignation + EEEs characterization + grid map			4044			Harp & Jibson (1995)
181	19940117	Northridge	United States	34.213	-118.537	6.7	reverse	18.2		remote sensing data	5064	ESI-07 intensity assignation + EEEs characterization + grid map			293			Townsend et al. (2020)
182	19950116	Kobe	Japan	34.583	135.018	6.9	strike-slip	21.9		remote sensing data	2353	ESI-07 intensity assignation + EEEs characterization + grid map			175			Uchida et al. (2017)
183	19980717	Jueili	Taiwan	23.407	120.736	5.7	reverse	12.6		remote sensing data	847	ESI-07 intensity assignation + EEEs characterization + grid map			763			Huang (1999)
184	20021103	Denali	United States	63.517	-147.444	7.9	strike-slip	4.9		remote sensing data	1579	ESI-07 intensity assignation + EEEs characterization + grid map			14611			Gorum et al. (2014)
185	20030814	Lefkada	Greece	39.160	20.605	6.3	strike-slip	10		remote sensing data	274	ESI-07 intensity assignation + EEEs characterization + grid map			168			Papathanassiou et al. (2013)
186	20041023	Nigata-Chuetsu	Japan	37.226	138.779	6.6	reverse	16		remote sensing data	4862	ESI-07 intensity assignation + EEEs characterization + grid map			410			Sekiguchi & Sato (2006)
187	20051008	Kashmir	Pakistan	34.539	73.588	7.6	reverse	26		remote sensing data	2930	ESI-07 intensity assignation + EEEs characterization + grid map			3845			Basharat et al. (2016)
188	20051008	Kashmir	Pakistan	34.539	73.588	7.6	reverse	26		remote sensing data	2424	ESI-07 intensity assignation + EEEs characterization + grid map			2236			Sato et al. (2007)
189	20051008	Kashmir	Pakistan	34.539	73.588	7.6	reverse	26		remote sensing data	1453	ESI-07 intensity assignation + EEEs characterization + grid map			1453			Basharat et al. (2014)
190	20061015	Kiholo Bay	United States	19.878	-155.935	6.7	normal	38.9		remote sensing data	383	ESI-07 intensity assignation + EEEs characterization + grid map			146			Harp et al. (2014)
191	20070421	Aisen	Chile	-45.243	-72.648	6.2	strike-slip	36.7		remote sensing data	538	ESI-07 intensity assignation + EEEs characterization + grid map			1460			Sepulveda et al. (2010)
192	20070421	Aisen	Chile	-45.243	-72.648	6.2	strike-slip	36.7		remote sensing data	517	ESI-07 intensity assignation + EEEs characterization + grid map			1148			Gorum et al. (2017)
193	20080512	Wenchuan	China	31.002	103.322	7.9	reverse	19		remote sensing data	197481	ESI-07 intensity assignation + EEEs characterization + grid map			75459			Xu et al. (2014a)
194	20080512	Wenchuan	China	31.002	103.322	7.9	reverse	19		remote sensing data	69606	ESI-07 intensity assignation + EEEs characterization + grid map			37521			Li et al. (2014)
195	20080613	Eastern Honshu	Japan	39.030	140.881	6.9	reverse	7.8		remote sensing data	4164	ESI-07 intensity assignation + EEEs characterization + grid map			567			Yagi et al. (2009)
196	20090108	Cinchona	Costa Rica	10.165	-84.197	6.1	strike-slip	14		remote sensing data	4826	ESI-07 intensity assignation + EEEs characterization + grid map			470			Ruiz et al. (2019)
197	20100112	Haiti	Haiti	18.443	-72.571	7	strike-slip	13		remote sensing data	23567	ESI-07 intensity assignation + EEEs characterization + grid map			3748			Harp et al. (2016)
198	20100112	Haiti	Haiti	18.443	-72.571	7	strike-slip	13		remote sensing data	4490	ESI-07 intensity assignation + EEEs characterization + grid map			2756			Gorum et al. (2013)
199	20010311	Tohoku-Oki	Japan	38.297	142.373	9.1	reverse	29		remote sensing data	3475	ESI-07 intensity assignation + EEEs characterization + grid map			39014			Wartman et al. (2013)
200	20130721	Gansu	China	34.512	104.262	5.9	reverse	8		remote sensing data	2330	ESI-07 intensity assignation + EEEs characterization + grid map			195.92			Xu et al. (2014b)
201	20140803	Sichuan	China	27.189	103.409	6.2	strike-slip	12		remote sensing data	1024	ESI-07 intensity assignation + EEEs characterization + grid map			233			Xu et al. (2015)
202	20150425	Nepal	Nepal	28.231	84.731	7.8	reverse	8.2		remote sensing data	17638	ESI-07 intensity assignation + EEEs characterization + grid map			17568			Gnyawali & Adhikari (2017)
203	20150425	Nepal	Nepal	28.231	84.731	7.8	reverse	8.2		remote sensing data	2645	ESI-07 intensity assignation + EEEs characterization + grid map			18374			Zhang et al. (2016)
204	20150604	Sabah	Malaysia	5.987	116.541	6	normal	10		remote sensing data	5198	ESI-07 intensity assignation + EEEs characterization + grid map			811			Ferrario (2022)
205	20161130	Capellades	Costa Rica	9.949	-83.807	5.3	strike-slip	1.3		remote sensing data	52	ESI-07 intensity assignation + EEEs characterization + grid map			13			Ruiz et al. (2020)

206	20171117	Milin	China	29.833	94.984	6.4	reverse	8		remote sensing data	766	ESI-07 intensity assignation + EEEs characterization + grid map			1428			Hu et al. (2019)
207	20180225	Papua New Guinea	Papua New Guinea	-60.70	142.754	7.5	reverse	25.2		remote sensing data	11607	ESI-07 intensity assignation + EEEs characterization + grid map			24297			Tanyas et al. (2022)
208	20180805	Lombok	Indonesia	-8.258	116.438	6.9	reverse	34		remote sensing data	4823	ESI-07 intensity assignation + EEEs characterization + grid map			1798			Ferrario (2019)
209	20180819	Lombok	Indonesia	-8.319	116.627	6.9	reverse	21		remote sensing data	9319	ESI-07 intensity assignation + EEEs characterization + grid map			1798			Ferrario (2019)
210	20180928	Palu	Indonesia	-0.256	119.846	7.5	strike-slip	20		remote sensing data	7063	ESI-07 intensity assignation + EEEs characterization + grid map			3880			Zhao (2021)
211	20191016	Davao1	Philippines	6.715	125.007	6.4	strike-slip	16		remote sensing data	190	ESI-07 intensity assignation + EEEs characterization + grid map			653			Ferrario et al. (2024)
212	20191029	Davao2	Philippines	6.757	125.008	6.6	strike-slip	15		remote sensing data	4737	ESI-07 intensity assignation + EEEs characterization + grid map			1710			Ferrario et al. (2024)
213	20191215	Davao3	Philippines	6.697	125.174	6.8	strike-slip	22		remote sensing data	5666	ESI-07 intensity assignation + EEEs characterization + grid map			1710			Ferrario et al. (2024)
214	20191224	Mesetas	Colombia	3.450	-74.103	5.7	strike-slip	10		remote sensing data	838	ESI-07 intensity assignation + EEEs characterization + grid map			3102			Garcia-Delgado et al. (2021)
215	20200107	Puerto Rico	Puerto Rico	17.869	-66.827	6.4	strike-slip	9		remote sensing data	309	ESI-07 intensity assignation + EEEs characterization + grid map			741			Knoper et al. (2020)
216	20230206	Pazarcık	Turkey	37.226000	37.014000	7.8	strike-slip	10	9	reconnaissance field survey + bibliography + remote sensing data	5876	ESI-07 intensity assignation + EEEs characterization	MMI	9	35000	350	onshore	Boulton et al. (2025)
217	20230206	Elbistan	Turkey	38.011000	37.196000	7.5	strike-slip	7.4	10	reconnaissance field survey + bibliography + remote sensing data	5876	earthquake ESI-07 intensity assignation	MMI	8	35000	150	onshore	Boulton et al. (2025)
218	20240101	Noto	Japan	37.487000	137.271000	7.5	reverse	7.5	10	bibliography + remote sensing data	44535	ESI-07 intensity assignation + EEEs characterization + grid analysis			54733	100	onshore	Muccignato E., (2025)

CHAPTER 4

4.1 – ESI-07, LAP, LND GRID COMPLETE DATA SHEET

The complete data sheet containing all the 33 events investigated with ESI-07 grid methodologies are available online on:

Frontiers | Exploiting earthquake-induced landslide inventories for macroseismic assessment using the environmental seismic intensity (ESI-07) scale

CHAPTER 5

5.1 - EEES DESCRIPTIVE TABLES

For the Mw 7.5 Noto Peninsula earthquake case study, a total of 262 EEEs descriptive tables were compiled. Each entry includes the following attributes: site ID, upload date, geographic coordinates (latitude and longitude in decimal degrees), municipality, EEE type, EEE description, ESI-07 intensity value, photographic documentation, and bibliographic references.

For authors complete dataset, additional information is provided regarding the classification of each EEE type and the specific computational script adopted for the assignment of the corresponding ESI-07 intensity value.

The descriptive tables are available on Zenodo:
Mw 7.5 Noto Earthquake (Japan) ESI-07 Dataset and ESI-07 Intensity Grid Map

5.2 - EEES FINAL .XLS DATASET

For the Mw 7.5 Noto Peninsula earthquake an Excel spreadsheet containing 44 492 records was compiled. Each row in the dataset corresponds to a single EEE and includes the following fields: ID (unique identifier), Latitude and Longitude in decimal degrees, EEE type, ESI (Assigned ESI-07 Intensity value), Data Type (acquisition method) and Source.

The .xls daset is available on Zenodo:

Mw 7.5 Noto Earthquake (Japan) ESI-07 Dataset and ESI-07 Intensity Grid Map

AKNLOWLEDGEMENTS

Life is a constant journey of exploration and connection with oneself. Every path we choose brings greater awareness and understanding of both ourselves and the world around us. In this sense, the world, the Earth, and Nature are silent messengers, full of grace and magnificence, to which I will always remain devoted.

On this journey, I would first like to thank my supervisor, Dra. Francesca Ferrario, for her constant support, help, and guidance.

I am deeply grateful to Professor Alessandro Maria Michetti for his advice, supervision, and inspiration throughout this work.

I would also like to express my gratitude to Dr. Christoph Grützner and Dr. Luca Guerrieri for carefully reviewing this PhD thesis and for their valuable comments and suggestions.

I would like to thank the members and staff of the Geosciences-IR project, for offering me this opportunity for growth and training.

Thanks to the research team at the Department of Physical Geography and Geoinformatics at Comenius University in Bratislava, and in particular to Professors Jozef Minár and Juraj Procházka.

I am thankful to the entire Perigeo group, Professor Franz Livio, and my colleagues for providing such a stimulating and challenging environment. Special thanks go to Giorgio, Argelia, and Michela.

My heartfelt thanks to my parents, who taught me never to give up and to learn from my mistakes, and who ignited in me the fire and restlessness that have always driven me to do and to pretend more.

Thanks to my closest friends for their presence and affection throughout this path. In particular, a special thanks to Francesca, Martina, Alessia.

A heartfelt thanks to my sister Fabiana, who accompanied and supported me through moments of crisis and calm alike, and who gave me the gift of responsibility and caring for others.

The deepest gratitude and love goes to my stormy life partner, Baldo, for his unwavering dedication, loyalty, sincerity, and love, and for always being by my side, experiencing with me the challenges and gift of life.

And finally, thanks to everyone else: relatives, friends, acquaintances, people I have met, and even those I would rather not have met, each of whom has taught me something.

And, of course, to all my pets and my beloved cats faithful and constant companions in every moment